



Durham E-Theses

Growth and torque magnetometry of ferromagnetic single crystals

Paige, David Martin

How to cite:

Paige, David Martin (1983) *Growth and torque magnetometry of ferromagnetic single crystals*, Durham theses, Durham University. Available at Durham E-Theses Online: <http://etheses.dur.ac.uk/9328/>

Use policy

The full-text may be used and/or reproduced, and given to third parties in any format or medium, without prior permission or charge, for personal research or study, educational, or not-for-profit purposes provided that:

- a full bibliographic reference is made to the original source
- a [link](#) is made to the metadata record in Durham E-Theses
- the full-text is not changed in any way

The full-text must not be sold in any format or medium without the formal permission of the copyright holders.

Please consult the [full Durham E-Theses policy](#) for further details.

GROWTH AND TORQUE MAGNETOMETRY

OF

FERROMAGNETIC SINGLE CRYSTALS

DAVID MARTIN PAIGE, B.Sc. (DUNELM)

Thesis submitted to the University of Durham
in candidature for the Degree of Doctor of Philosophy,
February 1983.

The copyright of this thesis rests with the author.
No quotation from it should be published without
his prior written consent and information derived
from it should be acknowledged.





Thesis
1983/PA1

ABSTRACT

This thesis describes the development of an automatic diameter control system for a Czochralski crystal puller in which the torque on the crystal as it revolves in the melt is monitored and stabilised through changes in the melt temperature. The development of a torque magnetometer of new design having a high linearity and absolute accuracy is also described.

The on-line analysis of data produced by the torque magnetometer has yielded precise values for the magnetocrystalline anisotropy of cobalt (grown by Czochralski and other techniques). The magnetometer has also been used for investigations of the magnetocrystalline anisotropy of the terbium/gadolinium alloys. In both cases the compatibility of the observed temperature dependences of the anisotropy with particular models is investigated.

PREFACE

The work described in this thesis could be subdivided into two separate areas of study. The first was the development of a new automatic control system for a Czochralski crystal puller, the second was the development and application of a new torque magnetometer. The link between them is the fact that some of the cobalt samples used in the magnetometer experiments were grown by the author on an identical Czochralski crystal puller, though not under automatic control.

The development of the crystal growth controller is still at a very early stage. To date only copper crystals have been grown automatically. The torque magnetometer is more advanced; indicative of its simplicity and the availability of suitable off-the-shelf electronics. Both crystal puller and magnetometer could be improved and suggestions to this effect are described in the text.

The cobalt study was motivated by the need, pointed out by Szpunar and Lindgard (1979), for more accurate experimental data to test existing models for the magnetocrystalline anisotropy of both the pure element and the cobalt/rare-earth alloys; published results for the anisotropy were inconsistent. The possibility of a sample dependence in the anisotropy was explored and several crystals were tested. These were grown by differing techniques (float-zone, Bridgman and Czochralski). During this investigation the temperature dependences of both K_3

and K_4 were obtained for the first time.

The work on the terbium/gadolinium alloys was the continuation of a project which has been undertaken in the Physics Department at Durham over the past few years. This has involved magnetostriction studies (Joraide, 1980) as well as the present anisotropy measurements. The anisotropy work was done by the author in collaboration with Dr. R.D. Hawkins who subsequently achieved his doctorate. The data from this work has recently been re-analysed by the author since the torque curves were, in many cases, not obtained in the single-domain state as originally assumed (Hawkins, 1982), thus rendering some of the previous results invalid.

It was shown by Smith et al. that impurities in gadolinium could significantly alter its magnetic properties. By analogy to gadolinium it was suggested that existing measurements on the terbium/gadolinium alloys might also be affected by impurities. The terbium/gadolinium project was begun after very high purity samples had become available from the Centre for Materials Science, Birmingham University, since these motivated a fresh assessment of the alloys.

ACKNOWLEDGMENTS

Acknowledgment is made to the Science and Engineering Research Council whose financial support made this work possible.

I would also gratefully acknowledge the help of the following people:

Firstly I would like to thank Professor A.W. Wolfendale, F.R.S. for making available to me the facilities of the Physics Department at the University of Durham.

I would like also to thank Dr. B.K. Tanner for his excellent supervision.

I would like to thank Dr. W.D. Corner for many useful discussions on the work undertaken and for making available some unpublished data on the terbium/gadolinium alloys.

Thanks are also due to Mr. T. Brown of the Cavendish Laboratory, Cambridge, who assisted greatly in the growth of some of the cobalt crystals studied here and also to Dr. S. Takahashi of Iwate University, Japan, for providing additional crystals. The provision of terbium/gadolinium alloy samples by Dr. D. Fort of the Centre for Materials Science, Birmingham University, is also thankfully acknowledged.

I would like to thank Dr. R.D. Hawkins for the considerable work which he did in acquiring data in the terbium/gadolinium studies, a proportion of which was collected without any involvement on my behalf.

I wish to express my thanks to Mr. K.G. Moulson for expert advice in the construction of equipment and also to

Mr. D. Jobling and his staff for their workshop assistance.

I would like to thank Mr. P. Goddard for providing unpublished results for the c/a ratio for cobalt.

Finally I would like to thank Dr. B. Szpunar for discussions on the modelling of the cobalt anisotropy, for her computations of the temperature profiles predicted by the single-ion model and for a relevant paper, awaiting publication, which is summarised in Appendix B.

CONTENTS

Title	1
Abstract	2
Preface	3
Acknowledgements	5
Contents	7
List of figures	10
List of tables	19
CHAPTER ONE: BASIC MAGNETIC CONCEPTS	
1.1 Introduction	20
1.2 Ferromagnetism	22
1.3 Microscopic origins of ferromagnetism	24
1.4 Macroscopic ferromagnetism	26
CHAPTER TWO: MAGNETOCRYSTALLINE ANISOTROPY	
2.1 Introduction	29
2.2 Phenomenology	30
2.3 Atomic origins	33
2.3.1 The single-ion model	34
2.3.2 The two-ion model	37
2.3.3 The itinerant electron model	38
2.4 The variation of anisotropy with temperature	39
2.4.1 The single-ion model	41
2.4.2 The two-ion model	48
2.5 Magnetoelastic effects	48
2.6 Anisotropic magnetisation	50
CHAPTER THREE: CZOCHRALSKI CRYSTAL GROWTH AND AUTOMATION	
3.1 Introduction	53
3.2 Czochralski crystal growth	56
3.3 Automatic control of Czochralski growth	59
3.3.1 The bright-ring method	61
3.3.2 The laser reflection method	63
3.3.3 The optical TV imaging method	65
3.3.4 The X-ray shadow method	65
3.3.5 The weighing methods	67

3.3.6	The melt level method	68
3.3.7	Discussion of methods	68
CHAPTER FOUR: TORQUE MAGNETOMETRY		
4.1	Introduction	71
4.2	Analysis of data	72
4.2.1	The shear correction	72
4.2.2	Obtaining the anisotropy constants	74
4.2.3	Unsaturated samples	75
4.2.4	Extrapolation with respect to field	77
4.2.5	Non-intrinsic torque effects	80
4.3	Existing magnetometers	81
4.4	Suggested alternative designs	110
CHAPTER FIVE: A NEW METHOD OF AUTOMATIC CZOCHRALSKI CRYSTAL GROWTH		
5.1	Introduction	115
5.2	Advantages of viscous torque control	120
5.2.1	Of viscous torque control in general	120
5.2.2	Of the present design for achieving it	120
5.3	Disadvantages of viscous torque control	121
5.3.1	Of viscous torque control in general	121
5.3.2	Of the present design for achieving it	122
5.4	Mechanical details of the automatic puller	123
5.4.1	The unmodified puller	123
5.4.2	The growth conditions	126
5.4.3	The mechanical components of the control device	126
5.5	Electrical details of the automatic puller	140
5.5.1	Introduction	140
5.5.2	Details of the circuit operation	146
5.6	Operation	160
5.7	Results	163

5.7.1	General	163
5.7.2	The present equipment	166
5.8	Conclusion	171
CHAPTER SIX: A NEW TORQUE MAGNETOMETER		
6.1	Introduction	173
6.2	Advantages of the design	176
6.3	Disadvantages of the design	177
6.4	Mechanical details of the magnetometer	177
6.5	Electrical details of the magnetometer	185
6.6	Computer interface and hardware	190
6.6.1	Hardware	191
6.6.2	Software	192
6.7	Calibration	197
6.8	Performance	200
CHAPTER SEVEN: THE MAGNETOCRYSTALLINE ANISOTROPY OF COBALT		
7.1	Introduction	205
7.2	Previous work	205
7.3	The samples	212
7.4	Experimental technique	213
7.5	Results	217
7.6	Theoretical modelling of the anisotropy	245
7.7	Discussion	250
7.8	Conclusion	251
CHAPTER EIGHT: THE MAGNETOCRYSTALLINE ANISOTROPY OF TERBIUM/GADOLINIUM ALLOYS		
8.1	Introduction	253
8.2	Previous and subsequent work	255
8.2.1	On gadolinium	255
8.2.2	On terbium	255
8.2.3	On terbium/gadolinium alloys	257
8.3	The samples	263
8.4	Experimental technique	265
8.5	Results	273
8.6	Theoretical modelling of the anisotropy	285
8.7	Discussion	300
8.8	Conclusion	302

APPENDICES:

A	Relation between the anisotropy constants and coefficients	303
B	Single-ion calculations of the cobalt anisotropy after Szpünar	306
C	Torque curves for materials with uniaxial crystal anisotropy; unsaturated case	310
D	A data acquisition program for the new magnetometer	313
E	The sampling program for measuring the elastic-after-effect and time-constant of the new magnetometer	316
F	The program used in the cobalt experiment	318
G	The cobalt data	321
H	The magnetostrictive contribution to the measurements of the anisotropy of cobalt	324
I	The magnetometer program used during the work on terbium/gadolinium alloys	326
J	Data for the terbium/gadolinium alloys with programs for the temperature dependence analysis	330
K	Hyperbolic Bessel functions	338
	References	340

LIST OF FIGURES

2.1	Possible magnetocrystalline anisotropy energy surfaces; the uniaxial case.	29
3.1	Simplified diagram of a Bridgman crystal puller.	54
3.2	Zone refining.	54
3.3	Float-zone crystal growth.	54
3.4	Simplified diagram of a Czochralski crystal puller.	57
3.5	Optical pyrometer ("Bright ring") method of monitoring Czochralski growth.	62
3.6	Laser method for monitoring Czochralski growth.	62
3.7	Monitoring of Czochralski growth using a television camera.	64
3.8	X-ray shadow method of monitoring Czochralski crystal growth.	64
3.9	A weighing method of monitoring Czochralski crystal growth.	66
3.10	Monitoring Czochralski crystal growth using a melt level sensor.	66
3.11	Definition of the contact and meniscus angles.	69
4.1	The shear-correction.	73
4.2	Simplified diagram of the torque magnetometer of Weiss.	85
4.3	The torque magnetometer of Williams.	85
4.4	Simplified diagram of the torque magnetometer of Miller.	87
4.5	Simplified diagram of the torque magnetometer of Byrnes and Crawford.	87
4.6	A torque magnetometer showing in combination the features of those of Croft et al., Gerber and Vilim, Fletcher et al. and Wilson et al.	89
4.7	Simplified diagram of the torque magnetometer of Pearson.	89
4.8	Simplified diagram of the torque magnetometer of Aubert.	92
4.9	The torque magnetometer of Humphrey and Johnston.	92

4.10	Simplified diagram of the torque magnetometer of Penoyer.	94
4.11	Simplified diagram of the torque magnetometer of Maxim.	94
4.12	Simplified diagram of the torque magnetometer of Willey et al.	95
4.13	The torque magnetometer of Bransky et al.	95
4.14	Simplified diagram of the torque magnetometer of Westwood et al.	97
4.15	Simplified diagram of the torque magnetometer of Condon and Marcus.	97
4.16	Simplified diagram of the torque magnetometer of Vanderkooy.	99
4.17	Simplified diagram of the torque magnetometer of Verge et al.	99
4.18	Simplified diagram of the torque magnetometer of Voigt and Foner.	101
4.19	Simplified diagram of the torque magnetometer of Sato and Chandrasekhar.	101
4.20	The torque magnetometer of King et al.	102
4.21	Simplified diagram of the torque magnetometer of Neugebauer.	102
4.22	The torque magnetometer of Telesnin et al.	104
4.23	Simplified diagram of the torque magnetometer of Schelleng and Rado.	104
4.24	Simplified diagram of the torque magnetometer of Gengnagel et al.	106
4.25	The suspension of the torque magnetometer of Aldenkamp, Marks and Zijlstra.	106
4.26	Simplified diagram of the torque magnetometer of Griessen.	108
4.27	Simplified diagram of the torque magnetometer of Birss and Wallis.	108
4.28	Simplified diagram of the torque magnetometer of Tajima and Chikazumi and Kuntsevich and Palekhin.	109
4.29	Simplified diagram of the torque magnetometer of Warnock.	109
4.30	The torque meter of Fulinski and Grotowski.	112

5.1	Method of crystal torque measurement in the present Czochralski automation.	116
5.2	Suggestion for alternative torsional measurement method in Czochralski automation.	117
5.3	Simplified head of the Czochralski crystal puller.	124
5.4	Furnace region of the Czochralski crystal puller.	125
5.5	The head of the automatic crystal puller.	127
5.6	Cross-section of the head of the automatic crystal puller.	128
5.7	Details of the upper part of the automatic crystal puller.	130
5.8	Details of the lower suspension of the automatic crystal puller.	131
5.9	Principle of the eccentric motor drive and its effect on the movement of the suspension.	135
5.10	Diagram of the relationship necessary between the misalignment of the two drive axes and the position of the lamp and light detector.	136
5.11	Details of the lamp and detector of the automatic crystal puller.	138
5.12	Light-activated switch showing attachment to fibre-optic cable.	138
5.13	The power control potentiometer as housed in the control box.	139
5.14	Simplified diagram of the logic circuit for the automatic crystal puller.	142
5.15	More detailed diagram of the logic circuit for the automatic crystal puller.	143
5.16	The console of the control box for the automatic crystal puller.	145
5.17	Photoswitch circuit	148
5.18	Light activated switch	148
5.19	"Front end" pulse-chain generator and digital counter.	149
5.20	The ZN 1040 E count/display integrated circuit.	150
5.21	Reference pulse-chain generator.	151
5.22	Counter No 1.	152

5.23	Counter No 2.	152
5.24	Up/down control circuit.	154
5.25	Up/down control circuit logic levels for one operating cycle.	155
5.26	Low frequency discharge circuit.	154
5.27	Time delay circuit.	156
5.28	Time delay circuit logic levels for one operating cycle.	157
5.29	Clear circuit.	158
5.30	The complete logic circuit for the automatic crystal puller.	159
5.31	The complete growth apparatus.	161
5.32	The pulling region of the growth apparatus.	162
5.33	Plot of torque on a Czochralski grown copper crystal VS diameter.	164
5.34	Plot of torque on a 7mm diameter Czochralski grown copper crystal VS pull-rate.	164
5.35	Diagram showing schematically the change in melt shape with rise in freezing interface...	166
5.36	A control crystal grown without automation.	167
5.37	Crystal grown with an instability in the automatic feedback loop due to static friction in the support bearing.	167
5.38-5.40	Crystals grown with diameter control in the regions indicated using the new automation method.	169
5.41	Diagram showing the stepped crystal structure due to initial eccentricity of the crystal seed on a freely hanging suspension.	170
6.1	Simplified diagram of the magnetometer head.	174
6.2	Block diagram of the electronics of the torque magnetometer.	175
6.3	Detailed drawing of the magnetometer head.	178
6.4	The sample support rod.	180
6.5	The complete magnetometer.	182
6.6	The magnetometer on its support stand.	183
6.7	The magnetometer in situ with the electromagnet.	184

6.8	Torque curve for a 97mg c-plane disc of cobalt showing spasmodic induced torques from non-uniform field rotation.	188
6.9	Torque curve as for previous figure with elimination of induced torques.	189
6.10	Differentiator circuit for torque magnetometer.	190
6.11	Plot of modelled response of transducer in the absence of electronic smoothing.	195
6.12	Observed torque indicated by ADC; the modelled response plus electronic time-constant.	195
6.13	Log torque VS time as seen by the computer showing two regimes of linear decline from which the two time-constants and K can be constructed.	195
6.14	Calibration of the torque magnetometer.	198
6.15	Plot of log torque as read by the computer VS time for an instantaneous drop in torque.	201
6.16	Torque curve for a 97mg b-plane disc of cobalt at 293K and 1.7 T.	203
7.1	Previous data for K_1 VS temperature for cobalt.	208
7.2	Previous data for K_2 VS temperature for cobalt.	209
7.3	Change in the easy direction of cobalt with temperature.	211
7.4	Torque curves for a cobalt b-plane disc at 90K illustrating amplitude saturation.	218
7.5	Torque curves from 0 to π for a 97mg b-plane disc of cobalt showing inversion of the 2 nd harmonic at about 543K (1.612T).	219
7.6	Torque curves from 0 to π for a 97mg b-plane disc of cobalt in the region of the K_1 inversion at about 507K (1.612T).	220
7.7	K_1 VS temperature for cobalt sample No 1.	221
7.8 and 7.9	K_1 VS temperature for cobalt samples No 2 and No 3.	222
7.10	K_2 VS temperature for cobalt sample No 1.	223
7.11 and 7.12	K_2 VS temperature for cobalt samples No 2 and No 3.	224
7.13	K_3 VS temperature for cobalt sample No 1.	225

7.14 and 7.15	K_3 VS temperature for cobalt samples No 2 and No 3.	226
7.16	K_4 VS temperature for cobalt sample No 4.	227
7.17	Comparison of the suggested K_1 fits for the three cobalt samples.	229
7.18	Comparison of the suggested K_2 fits for the three cobalt samples.	230
7.19	Comparison of the suggested K_3 fits for the three cobalt samples.	231
7.20	Comparison of data for K_1 VS temperature for cobalt; old and new.	232
7.21	Comparison of data for K_2 VS temperature for cobalt; old and new.	234
7.22	Representation of one cycle of events showing annealing of the magnetocrystalline anisotropy.	235
7.23	Plot showing the effect on the K_1 temperature dependence for sample No 1 of excluding the third harmonic from the anisotropy derivation.	237
7.24	Plot showing the effect on the K_2 temperature dependence for sample No 1 of excluding the third harmonic from the anisotropy derivation.	238
7.25	Plot of magnetisation VS temperature for cobalt.	240
7.26	Plot of K_1 VS temperature for sample No 1 showing the effect of a systematic error of -1% in the shear-correction factor.	242
7.27	Plot of K_2 VS temperature for sample No 1 showing the effect of a systematic error of -1% in the shear-correction factor.	243
7.28	Plot of K_3 VS temperature for sample No 1 showing the effect of a systematic error of -1% in the shear-correction factor.	244
7.29	Plot of a possible single-ion fit to the temperature dependence of cobalt; the required c/a temperature dependence is given in figure 7.31.	247
7.30	Plot of a possible single-ion fit to the temperature dependence of cobalt; the required	

	c/a temperature dependence is given in figure 7.31.	248
7.31	Plot of the available c/a data with the predicted temperature dependence from a single-ion model of the anisotropy.	249
8.1	K_2^0 , K_4^0 and K_6^0 for $Tb_{0.018}Gd_{0.982}$ alloy (after Tajima).	259
8.2	K_2^0 VS temperature for terbium (after Féron).	259
8.3	K_4^0 VS temperature for terbium (after Féron).	259
8.4	Existing data for K_1 VS temperature for Tb_xGd_{1-x} alloys.	260
8.5	Existing data for K_4 VS temperature for Tb_xGd_{1-x} alloys.	261
8.6 and 8.7	Existing data for K_1 and K_4 VS temperature at OK for Tb_xGd_{1-x} alloys.	262
8.8	The ligament suspension torque magnetometer; simplified diagram of the electronics.	267
8.9	The torque magnetometer suspension.	268
8.10	The upper support of the torque magnetometer suspension.	269
8.11	Cross-section of the torque magnetometer vacuum system.	270
8.12	Typical torque curves produced by high uniaxial anisotropy in the disc plane.	274
8.13	Torque curves for a 171.7mg c-plane disc of terbium at 81K in fields of 1.16, 1.37, 1.58 and 1.85 Tesla.	275
8.14	K_1 VS temperature for Tb_xGd_{1-x} alloys (present values)	276
8.15	K_4 VS temperature for Tb_xGd_{1-x} alloys (present values)	278
8.16 and 8.17	K_1 and K_4 VS composition for Tb_xGd_{1-x} alloys at 80K; comparison of present and existing data.	280
8.18 and 8.19	K_1 and K_4 VS composition at OK for Tb_xGd_{1-x} alloys; comparison of present extrapolations to OK and existing data.	281
8.20	K_1 VS temperature for Tb_xGd_{1-x} alloys; comparison of present and existing data.	282

8.21	K_4 VS temperature for Tb_xGd_{1-x} alloys; comparison of present and existing data.	283
8.22	Anomalous torque curves produced by a 26.5mg a-plane disc of $Tb_{0.05}Gd_{0.95}$ at 181K in fields of 1.16, 1.45, 1.70 and 1.85 Tesla.	284
8.23	Theoretical fits for K_1 VS temperature for $Tb_{0.05}Gd_{0.95}$ alloy.	289
8.24	Theoretical fits for K_1 VS temperature for $Tb_{0.1}Gd_{0.9}$ alloy.	290
8.25	Theoretical fits for K_1 VS temperature for $Tb_{0.2}Gd_{0.8}$ alloy.	291
8.26	Theoretical fits for K_1 VS temperature for $Tb_{0.3}Gd_{0.7}$ alloy.	292
8.27	Theoretical fits for K_4 VS temperature for $Tb_{0.05}Gd_{0.95}$ alloy.	293
8.28	Theoretical fits for K_4 VS temperature for $Tb_{0.1}Gd_{0.9}$ alloy.	294
8.29	Theoretical fits for K_4 VS temperature for $Tb_{0.3}Gd_{0.7}$ alloy.	295
8.30	Theoretical fits for K_4 VS temperature for $Tb_{0.5}Gd_{0.5}$ alloy.	296
8.31	Theoretical fits for K_4 VS temperature for $Tb_{0.75}Gd_{0.25}$ alloy.	297
C.1	The domain phases in a uniaxial crystal	310

LIST OF TABLES

4.1	Examples of the main types of torque magnetometer described in the literature.	83-84
5.1	Examples of the viscosities of metals at their respective melting points.	172
7.1	Details of the cobalt samples.	212
8.1	Values of the anisotropy coefficients of terbium.	256
8.2	Details of the Tb_xGd_{1-x} alloy samples.	264
8.3	K_1 and K_4 temperature dependences for Tb_xGd_{1-x} alloys.	287
E.1	Output from the torque magnetometer at intervals after an instantaneous relaxation of the torque.	317
G.1	Anisotropy data for cobalt sample No 4 .	321
G.2	Anisotropy data for cobalt sample No 1.	322
G.3	Anisotropy data for cobalt samples No 2 and No 3.	323
J.1	K_1 torque data for Tb_xGd_{1-x} alloys.	331
J.2	K_1 data for Tb_xGd_{1-x} alloys.	332
J.3	Interpolated K_4 data for Tb_xGd_{1-x} alloys.	333
J.4	Extrapolated K_4 data for Tb_xGd_{1-x} alloys.	334

CHAPTER ONE

BASIC MAGNETIC CONCEPTS

1.1 Introduction

Two excellent texts have been written on general magnetism by Chikazumi (1964) and Morrish (1965).

If a pair of opposite magnetic poles or a circulating "Amperian" current causes a magnetic force to manifest itself, when observed from a sufficient distance both appear to be equivalent magnetically. The common properties are therefore described by a common name; both are said to have a magnetic moment. In practice a magnetic material demonstrates properties readily explainable if it is regarded as having a magnetic moment or being composed of particles with such moments, the particles being either whole atoms or electrons. The magnetic moment per unit volume of a material is termed the magnetisation.

From either description of the origin of the magnetic moment (poles vs Amperian currents) it is apparent that it is directional in nature having, by analogy to the Earth's moment, a north and south direction. Under the influence of a magnetic body an object having a magnetic moment will orientate preferentially along a certain direction. The behaviour of the moment can be described mathematically in terms of a vector field and the effect of the magnetic body on the moment termed a magnetic field. Each point of the field is characterised by a north direction and a magnitude indicative of the forces on the moment.



The strength of a magnetic field, H , can be compared to that inside a long solenoid of N turns per unit length carrying a current I ;

$$\underline{H} = NI\underline{n} \quad \dots(1.1)$$

where \underline{n} is a unit vector along the solenoid axis. The unit of \underline{H} is therefore the ampere per metre (Am^{-1}) in the S.I. system.

The size of a magnetic moment, $\underline{\mu}$, can be quantified by comparing it to that produced by a current loop. The moment of a circulating current, I , of area a is given by;

$$\underline{\mu} = I a \underline{n} \quad \dots(1.2)$$

where \underline{n} is the unit vector perpendicular to the area. Magnetic moment can therefore be measured in ampere metre² in the S.I. system. Magnetisation, $\underline{\mathcal{Q}}$, which is magnetic moment per unit volume, has units of ampere per metre.

Macroscopically field, \underline{H} , and magnetisation, $\underline{\mathcal{Q}}$, are the most basic quantities in magnetism. Other quantities definable in terms of these (according to the S.I. system) are;

- 1) Flux density, \underline{B} ;

$$\underline{B} = \mu_0(\underline{H} + \underline{\mathcal{Q}}) \quad \dots(1.3)$$

where B is in units of tesla and μ_0 is a constant called the permeability of free space;

- 2) Susceptibility, χ ;

$$\chi = \frac{\mu_0 |\underline{M}|}{|\underline{B}|} \quad \dots(1.4)$$

Susceptibility may be defined in other ways, for instance as the differential of magnetisation with respect to flux density rather than as the ratio.

Classically magnetisation cannot occur in a material in thermal equilibrium, not even in an applied field; magnetisation can only be explained by a quantum mechanical theory. In such a theory the magnetic moment of an atom arises from three sources; the (quantised) electron spin, the (quantised) orbital angular momentum of the electron and the change in the orbital moment induced by a magnetic field. The first two effects produce paramagnetism in which finite atomic moments independently orientate in an applied field to create a positive susceptibility. The last effect produces what is called diamagnetism contributing a negative susceptibility irrespective of whether the atomic moment is normally finite. In certain materials spontaneous ordering of finite atomic moments occurs; a material then has a magnetisation in zero applied field and an undefined susceptibility; these are ferromagnets and related materials. All three types of magnetism are discussed in detail by Kittel (1971).

1.2 Ferromagnetism

Materials demonstrating a spontaneous magnetic order may be categorised as follows:

1) They can be ferromagnetic; all internal moments are aligned with each other (subject to thermal agitation).

2) They can be antiferromagnetic; the moments order in such a way as to produce no net magnetisation.

3) They can be ferrimagnetic; the ordering is not in a

single direction but a net magnetisation results.

The materials studied in the present work are all ferromagnetic. An excellent text on ferromagnetism has been written by Bozorth (1951).

For every ferromagnet there is a temperature above which thermal agitation destroys the spontaneous order; this is the Curie temperature T_c . Above the Curie temperature ferromagnets become paramagnetic.

The alignment of the atomic moments in ferromagnets can be likened to the paramagnetic alignment of independent moments in a magnetic field, called the Weiss molecular field (Weiss, 1907). The degree of alignment indicates that the Weiss field is of the order of 10^3 teslas for a typical ferromagnet which is much greater than the aligned moments themselves. The Weiss field can only be explained quantum mechanically; it is a classical analogy to the result of what is known as the exchange interaction (see next section) in which an effective coupling occurs between the electron spins of adjacent atoms and hence the moments associated with those atoms. In ferromagnets the coupling is such that mutual alignment of adjacent moments is energetically favourable, thus simulating the presence of an applied field.

Ferromagnetism may result from an indirect coupling of the atomic moments in which exchange forces are mediated by local conduction electrons. The moments, by exerting their effect simultaneously on nearby electrons, effect in consequence each other. This is thought to be the alignment mechanism in the ferromagnetic rare-earths and this mechanism will be contrasted with direct coupling in the next section.

1.3 Microscopic origins of ferromagnetism

Pauli's exclusion principle states that any wavefunction involving several identical particles must be antisymmetric (must change sign) when the coordinates, including the spin coordinates, of any identical pair are interchanged. Thus for two electrons having the same spin state, the exclusion principle dictates that for overall antisymmetry the spatial part of the wavefunction must be antisymmetric. The only possible combination of spatial wave functions representing the system of two electrons is;

$$\psi_a = \psi_a(1)\psi_b(2) - \psi_a(2)\psi_b(1) \quad \dots(1.5)$$

where $\psi_a(1)$ is the single spatial wavefunction for an electron labelled "a" at coordinate (1). As the electrons approach each other, that is coordinates (1) and (2) approach, the wavefunction tends to zero and the probability of finding the electrons close to each other therefore small. The classical analog is that a force of repulsion exists between the electrons. For electrons of opposite spin state the spatial wavefunction is symmetric and an apparent attraction exists. Thus the exclusion principle produces what is called the "exchange interaction"; it is not electrostatic.

For two electrons experiencing a potential due to an atomic nucleus or, more generally, several nuclei, a Hamiltonian, \mathcal{H} , may be written for the electron-electron interaction and an exchange integral defined;

$$J = \frac{1}{2} \iint \psi_a(1)^* \psi_b(2)^* \mathcal{H} \psi_b(1) \psi_a(2) d\tau_1 d\tau_2 \quad \dots(1.6)$$

The energy of the electron-electron interaction may

then be written as the following simplification due to Heisenberg (1928);

$$U = -2J_{ij} \underline{S}_i \cdot \underline{S}_j \quad \dots(1.6)$$

where S_i is the spin (complete with moment) of the i^{th} atom.

Heisenberg's equation relates to the direct interaction of electrons in a common potential. If the exchange integral is positive the energy with which the spins align is negative and ferromagnetism occurs. Ferromagnetism in the transition metals occurs as a result of the direct interaction between the electron spins of adjacent atoms since for some of these metals the interatomic spacing is such that J is positive. In the rare-earth elements the ferromagnetic mechanism is an indirect one called the RKKY interaction (after Rudermann and Kittel, 1954 ; Kasuya, 1956; and Yosida, 1957).

In the simple RKKY theory, free conduction electrons interact with individual ions with a Hamiltonian having some functional dependence on the electron spin and the ionic spin. This gives rise to a polarisation of the conduction electrons whereby their spins tend to align parallel with the spin of the nearby ion. The polarisation due to one ion may be written;

$$P_i(r) = \frac{9 Z^2 r}{4V^2 E_f} S_i F(2K_f r) \quad \dots(1.7)$$

where Z is the atomic density of conduction electrons, V the atomic volume, K_f and E_f the Fermi wavevector and energy respectively and $F(x)$ is an oscillatory function dying away rapidly with respect to x ;

$$F(x) = \frac{\text{Sin}x - x\text{Cos}x}{x^4} \quad \dots(1.8)$$

The Hamiltonian for the interaction of this polarisation with a second ion of spin S_j is then simply;

$$H = -r S_j P_i(r_j) \quad \dots(1.9)$$

giving an overall indirect exchange interaction which reduces to;

$$U = - \frac{g Z^2 r^2}{4V^2 E_f} F(2K_f r) \underline{S}_i \cdot \underline{S}_j \quad \dots(1.10)$$

which is of the same form as the Heisenberg expression.

Hence for appropriate lattice conditions ferromagnetism will result.

1.4 Macroscopic ferromagnetism

The spontaneous magnetisation of a ferromagnetic material predicted by the microscopic theory is not always observed macroscopically. This occurs because the magnetisation breaks down within the solid into regions within which a coherent magnetisation exists but which together cancel if observed from a point outside the sample. The size and magnetic orientation of these regions, called domains, depend on the various energies associated with their formation within a material (Landau and Lifshitz, 1935):

- 1) Magnetostatic; the energy change which occurs simply due to the work done by the forces between magnetic moments. Moments tend to align antiparallel with each other or parallel to the surface of a magnetised solid for this reason.
- 2) Magnetocrystalline; the energy associated with the interaction of atomic moments with assymetry in the local crystalline environment. It results in energetically favourable directions for the magnetisation within the crystal

(see chapter 2).

3) Magnetostrictive; the energy due to the elastic deformation of the crystal lattice as the local magnetisation direction changes, which as well as tending to produce favoured magnetisation directions also affects the ease with which the differing regions of strain associated with each domain fit together.

Domain structures are usually complex and modified by defects and impurities in the material in that these can present an energy barrier to the motion of the "Bloch" walls between domains as they move to establish the configuration which would have otherwise given a minimum in the overall energy.

The macroscopic magnetisation of a ferromagnetic substance, assuming free domain wall movement, occurs through the growth in number and size of those domains which are favoured by a prevailing field. Above a certain field, only one domain will be left, with a magnetisation which will tend to follow the applied field if it is rotated. The approach to saturation of the magnetisation, its subsequent behaviour during reversal of the field, and the energy losses associated with these processes are critical properties in defining the engineering applications of a material.

Energy lost during field-cycling is transferred to heat by driving domain walls through defects or impurities in the crystal lattice, and the magnitude of the loss, large or small, defines whether a material is magnetically "hard" or "soft" respectively. The average macroscopic magnetisation of a sample if removed from a saturating field is known as the remanence. The reverse field required to reduce the average

magnetisation to zero is the coercivity.

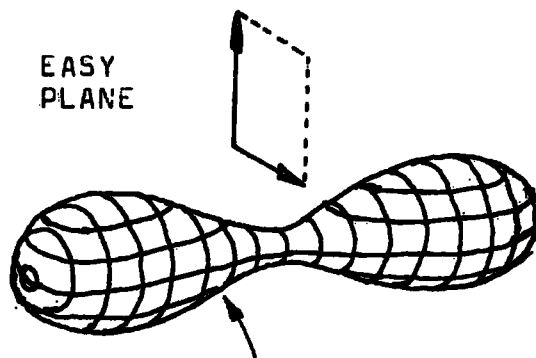
CHAPTER TWO

MAGNETOCRYSTALLINE ANISOTROPY

2.1 Introduction

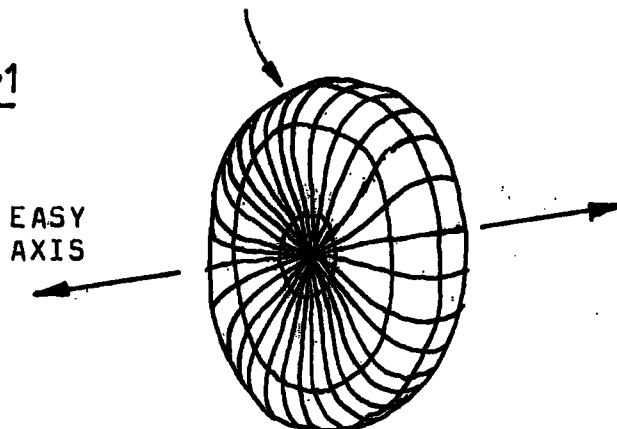
The energy required to magnetise an unstressed spherical ferromagnetic crystal is dependent on the direction of magnetisation; a phenomenon called magnetocrystalline anisotropy.

The surface traced by a vector of magnitude equal to the energy required to magnetise a crystal to saturation along a given direction is exemplified in figure 2.1:



MAGNETISATION ENERGY SURFACES WITH
RESPECT TO CRYSTALLOGRAPHIC DIRECTION

Fig 2.1



POSSIBLE MAGNETOCRYSTALLINE ANISOTROPY
ENERGY SURFACES; THE UNIAXIAL CASE

A direction for which magnetisation occurs readily is called an easy-axis. Anisotropy yielding cylindrically symmetric energy surfaces of the type illustrated is termed uniaxial. Easy axes, cones or planes are closely related to crystal structure; for instance cubic materials like iron often have three cartesian easy-axes whilst hexagonal materials like cobalt are often uniaxial.

Magnetocrystalline anisotropy shows a very dramatic temperature dependence falling away quickly with increasing temperature disproportionately to the drop in saturation magnetisation itself.

The simplest physical consequence of magnetocrystalline anisotropy is that materials experience a torque within a magnetic field proportional to the differential of the anisotropy energy with respect to the angle of induced magnetisation referred to the crystal axes. Torque magnetometry, described in chapter 4, utilises this phenomenon to determine the form of the anisotropy, which is parameterised as described in the next section.

This chapter introduces the conventions by which magnetocrystalline anisotropy (sometimes abbreviated herein to anisotropy) is described, indicates simply its atomic origins and describes the theoretical temperature dependences suggested by particular anisotropy models.

2.2 Phenomenology

The energy required to magnetise a crystal in a specific direction at constant strain and temperature is given by;

$$E/V = \int_0^{\alpha_s} B_z \cdot d\alpha \quad \dots(2.1)$$

where E/V is the energy per unit volume, \underline{d} is the magnetisation vector and \underline{B}_i is the internal field vector.

The directional dependence of the energy for a saturated sample can be parameterised in several ways of which only a few have become conventional. Taking the hexagonal structure as an example, the energy surface is often expressed as in equation 2.2; tailored to reflect the crystal symmetries to which the surface is related;

$$E/V = K_0 + K_1 \sin^2 \theta + K_2 \sin^4 \theta + K_3 \sin^6 \theta + K_4 \sin^6 \theta \cdot \cos 6\phi + \dots \quad \dots(2.2)$$

where θ is the angle between the magnetisation vector and the c-axis and ϕ the angle between an a-axis and the projection of the magnetisation vector on the basal plane. The K_n are the anisotropy constants. Analogous expressions for the anisotropy energy for each of the 32 crystallographic point groups have been derived by Doring (1958).

A systematic expansion for the anisotropy energy would be;

$$E/V = \sum_{L=0}^{\infty} \sum_{m=-L}^{+L} K_L^m \cdot Y_L^m \quad \dots(2.3)$$

where the Y_L^m are surface spherical harmonics and the K_L^m suitable constants, in some cases irrelevant due to crystal symmetry. The hexagonal expression would be;

$$E/V = K_0^0 + K_2^0 \cdot Y_2^0(\theta) + K_4^0 \cdot Y_4^0(\theta) + K_6^0 \cdot Y_6^0(\theta) + K_6^6 \cdot Y_6^6(\theta, \phi) + \dots \quad \dots(2.4)$$

More common however are expressions using the Legendre polynomials, $P(\theta)$, abstracted from the above harmonics, the hexagonal expression being;

$$E/V = K_0^0 + K_2^0 \cdot P_2(\cos\theta) + K_4^0 \cdot P_4(\cos\theta) + K_6^0 \cdot P_6(\cos\theta) \\ + K_6^6 \sin^6\theta \cos 6\phi + \dots \quad \dots(2.5)$$

with analogies for other structures. The definition of the spherical harmonics and Legendre polynomials are given in Appendix A along with the relationships between the constants of equation 2.2 and 2.5.

Birss and Keeler (1974) point out that spherical harmonic formalism facilitates the comparison of derived constants with theoretical predictions and, due to the orthogonality of the individual harmonics, produces values of the anisotropy constants which are independent of the number of higher terms in the experimental fit. However direct comparison with existing experimental data may require the use of the alternative convention, as was the case with the cobalt measurements in chapter 7. Consistency suggested the use of the alternative convention in chapter 8.

Another convention for the anisotropy energy expansion is given by Volkov et al. (1981) who considered reduction as well as transformational symmetries for the lattice to tailor expressions similar to equation 2.2 to produce in the hexagonal case;

$$E/V = \hat{K}_1(3\cos^2\theta - 1) + \hat{K}_2(35\cos^4\theta - 30\cos^2\theta + 3) \\ + \hat{K}_3(231\cos^6\theta - 315\cos^4\theta + 105\cos^2\theta - 5) \\ + \hat{K}_4 \sin^6\theta \cdot \cos 6\phi + \dots \quad \dots(2.6)$$

where the terms are orthogonal and involve constants \hat{K}_n . The latter convention has not yet been established, having appeared very recently.

2.3 Atomic origins

The exchange potential between the spins of neighbouring ions in a ferromagnetic material is of the form;

$$H_{ex} = J_{ij} \underline{S}_i \cdot \underline{S}_j \quad \dots(2.7)$$

which is invariant with respect to sympathetic rotation of the spins relative to the line of the ionic centres; it does not give rise to anisotropy. Anisotropic spin orientation occurs in order to accommodate within the lattice the distortions of the electronic charge clouds associated with the ionic spins due to the spin-orbit interaction. Two important mechanisms by which the charge clouds tend to align in the lattice give rise to the single- and two-ion model of magneto-crystalline anisotropy respectively.

In the single-ion model, the electronic charge cloud of an ion, distorted by the spin associated with it, couples to the crystalline electrostatic field, hence creating the necessary energetic link between magnetisation and the lattice symmetry. In the two-ion model, anisotropy occurs because of the dependence of the interaction energy on the shape of adjacent electronic charge clouds; an energy which changes with respect to the angle between the spin-orbit distortion and the line of the ionic centres. The two models are not exclusive.

Single- and two-ion models apply to magnetic ions

with localised moments and are not wholly applicable to the iron transition metals in which the active electrons are itinerant. In the latter case the spatial dependence of the itinerant electron wave functions, each distributed throughout the lattice and dependent on the crystal symmetry, is modified, again by the spin-orbit interaction, in such a way that there exist energetically favourable orientations for the spins.

The three cases of single-ion, two-ion and itinerant electron anisotropies will be discussed briefly.

2.3.1. The single-ion model

Single-ion anisotropy is found to be dominant in magnetic materials in which the sets of magnetic electrons associated with each ion are isolated. Examples include magnetic insulators, in which the isolation of the metallic ions is indicated by the absence of electronic conduction bands. Another example is that of the rare-earths where the magnetic 4f orbitals are much smaller than the lattice spacing and overlap very little.

For a system of non-interacting ions in which the spins are aligned by the effect of the electrostatic crystalline field on the distortion of individual ionic charge clouds due to the spin-orbit interaction, the Hamiltonian for the electronic states can be written;

$$\mathcal{H} = g\mu_B \underline{B}_m \cdot \underline{S} + \mu_B \underline{B}_0 \cdot (\underline{L} + 2\underline{S}) + \mathcal{H}_C \quad \dots(2.8)$$

where \underline{B}_m is an effective molecular field which simulates the effect of the exchange interaction with neighbouring

ions on the electron spin orientations, B_0 is the applied magnetic field and \mathcal{H}_c is the Hamiltonian due to the effect of the crystal field and spin-orbit interaction on the electrons. The first and second terms are isotropic, being the exchange and Zeeman interactions respectively. \mathcal{H}_c creates the anisotropy.

The detailed calculation of electronic energies from equation 2.8 depends on the relative magnitudes of the contributions of the spin-orbit and crystalline field effects.

The crystalline field, $V_c(\underline{r})$, experienced by an electron at position \underline{r} , can be expressed as an expansion of spherical harmonics restricted to suit the symmetry of the crystal;

$$V_c(r, \theta, \phi) = \sum_{L, m} r^L \cdot A_L^m \cdot Y_L^m(\theta, \phi) \quad \dots(2.9)$$

where θ and ϕ are referred to the crystallographic axes.

The coefficients of the expansion, A_L^m , are frequently derived experimentally by electron spin resonance (eg Abraham and Bleaney, 1970), and depend on the radial distance to neighbouring ions, screening and covalency effects. It is useful in deriving the energies of the electronic states to write the crystalline field as a series of operator equivalents, O_L^m , similar to the Y_L^m , which are polynomials in L or J called Stevens factors (after Stevens, 1952);

$$V_c = \sum_{L, m} B_L^m \cdot O_L^m \quad \dots(2.10)$$

where the coefficients, B_L^m , are given by

$$B_L^m = r^L A_L^m \cdot \alpha_L \quad \dots(2.11)$$

where α_L are constants.

The other part of the anisotropic Hamiltonian, due to the spin-orbit interaction, has the form;

$$\mathcal{H}_{SL} = \sum_i \rho(\underline{r}_i) \underline{S}_i \cdot \underline{L}_i \quad \dots(2.12)$$

where;

$$\rho(\underline{r}_i) = \frac{\hbar^2}{2m^2c^2} \frac{1}{r_i} \frac{dU}{dr_i} \quad \dots(2.13)$$

and U is the central ionic potential.

The electronic energies, E_i , of the multiplet states associated with each ion, can be calculated treating the two parts of \mathcal{H}_c as a perturbation on the exchange and Zeeman interactions; though the latter is normally negligible. The quantisation axis is usually taken to be that of the effective molecular field \underline{B}_m . The energies, E_i , are found by virtue of the anisotropy to be dependent on the alignment of \underline{B}_m in the crystal, that is the magnetisation angle in cases of negligible Zeeman energy, and are a function of this angle (θ, ϕ) . A partition function for the electronic states can then be written;

$$Z(\theta, \phi) = \sum_i \text{Exp}(-E_i(\theta, \phi)/(k_B T)) \quad \dots(2.14)$$

yielding a free energy per ion of;

$$E(\theta, \phi) = -k_B T \text{Log}_e Z(\theta, \phi) \quad \dots(2.15)$$

which for a collection of such ions is the free energy which features in the phenomenological expressions of the magnetocrystalline anisotropy.

Darby and Isaac (1974) give examples of detailed derivations for the anisotropy of several classes of materials using the single-ion model. Aubert (1980)

also gives specific examples. Both these papers are relevant reviews on the magnetocrystalline anisotropy of ferro- and ferrimagnets.

2.3.2. The two-ion model

The two-ion model is sometimes found to be important in magnetic insulators and the rare-earths as contributing with the single-ion model to the overall anisotropy.

The classical electromagnetic coupling between two ionic spins;

$$\frac{\mu_0 g^2 m_B^2}{4\pi r_{ij}} (\underline{S}_i \cdot \underline{S}_j - \frac{3(\underline{S}_i \cdot \underline{r}_{ij})(\underline{S}_j \cdot \underline{r}_{ij})}{r_{ij}^2}) \quad \dots(2.16)$$

though anisotropic with respect to the angle between spins and the line of the ionic centres, is too small to yield the anisotropies manifest by real materials. However Van Vleck (1937) found that by superimposing the spin-orbit coupling on the exchange energy between neighbouring spins in a second order perturbation calculation, an interaction of the same form as the electromagnetic dipole interaction is obtained, scaled by a function, $C_{ij}(\underline{r}_{ij})$, which dies away rapidly with respect to separation of the ions;

$$C_{ij}(\underline{r}_{ij}) (\underline{S}_i \cdot \underline{S}_j - \frac{3(\underline{S}_i \cdot \underline{r}_{ij})(\underline{S}_j \cdot \underline{r}_{ij})}{r_{ij}^2}) \quad \dots(2.17)$$

For typical nearest neighbour separations the interaction, called the pseudo-dipolar interaction, is often too strong to account for observed anisotropies. However, a fourth order perturbation calculation gives a pseudo-quadrupole interaction which is of the right magnitude to explain anisotropy in cubic materials for which the pseudo-

dipolar interaction averages to zero. The form of the pseudo-quadrupole interaction is;

$$D_{ij}(\underline{S}_i \cdot \underline{r}_{ij})^2 (\underline{S}_j \cdot \underline{r}_{ij})^2 \quad \dots(2.18)$$

and can only occur if the total ionic spin is greater than unity. Exact calculations are difficult on this model; only qualitative explanations are possible.

2.3.3. The itinerant electron model

The spatial dependences of the itinerant electron wave functions are determined by the atomic symmetry of the lattice and have allowed energies, $E_n(k)$, where k labels the states and n is a band index. The effect of the spin-orbit interaction on the electronic states is to introduce a directional dependence in their energies. The total free energy of the crystal is then;

$$E(\underline{\alpha}) = \sum_{\substack{n,k \\ \text{OCCUPIED STATES}}} E_n(k, \underline{\alpha}) \quad \dots(2.19)$$

where $\underline{\alpha}$ is the magnetisation direction. The details of the calculation of the crystal free energy depend on the particular simplifying assumptions which can be made to facilitate it.

The crystal potential can be written;

$$V_c(\underline{r}) = \sum_{\underline{R}_n} U(\underline{r} - \underline{R}_n) \quad \dots(2.20)$$

where \underline{R}_n is a lattice vector and U is a central potential associated with each ion. By comparison with equation 2.12, the spin-orbit interaction for Bloch states can be written;

$$\mathcal{H}_{SL} = \sum_{\underline{R}_n} \rho(\underline{r} - \underline{R}_n) \underline{S} \cdot \underline{L}(\underline{r} - \underline{R}_n) \quad \dots(2.21)$$

and this is usually regarded as a perturbation on the unmodified electronic states of which, for simplicity, only a few are considered. Furey (1967) has analysed the case for nickel and found that electrons having wavevectors near the symmetry point X of the Brillouin zone are particularly important and that in this region the different, closely spaced bands create energies which in some cases favour $\langle 100 \rangle$ spin alignment, in others dis-favour it, and that the sharp temperature dependence of the anisotropy occurs as the occupation of these bands changes through the smearing of the Fermi surface. Iron has been analysed by Franse (1971) who found that bands were not as closely spaced at the Fermi energy and that their difference in contribution to the anisotropy was less significant to the overall temperature dependence. Cobalt has been analysed by Mori et al. (1974) who found electrons having wavevectors near symmetry point A (along the $\langle 1000 \rangle$ direction) were very important.

Calculations are imprecise in analyses of the type described and predictions of, for example, temperature dependences for the anisotropy constants are poor. It seems that the itinerant electron model for the anisotropy describes only one mechanism among others, notably the single-ion model, by which anisotropy can occur in the 3d transition metals.

2.4 The variation of anisotropy with temperature

The Landé g factor of an ion, denoting the ratio of the total angular momentum, J , to the magnetic moment, is

an indicator of the degree to which the magnetic moment is either orbital or electronic. A value of 2 indicates electronic moment only and complete quenching of the orbital angular momentum.

It is found that magnetocrystalline anisotropy falls rapidly with respect to temperature, much more quickly than the strength of the spin-orbit interaction indicated by the Landé g factor and much faster than the magnetisation and therefore cannot be due to a weakening of the microscopic mechanism causing anisotropy.

The cause of the temperature dependence of the anisotropy is now generally recognised, with the exception of effects specific to the itinerant electron model, to be loss of parallelism between individual spins due to thermal excitation (Akulov, 1936). Thus for saturation along a hard direction thermal effects tend to direct the spins toward an easy-axis and lower the energy associated with them, whilst for saturation along an easy-axis the misalignment due to temperature promotes the ionic energies since they are excited toward a hard direction. The effect of this sampling of the anisotropy energy over an angle is therefore to reduce the energy difference between easy and hard magnetisations, that is to reduce the observed anisotropy. The elementary moment, whether single ions or ions in pairs or clusters, will in all cases be subject to this mechanism whereby anisotropy is thermally degraded. Even in the itinerant electron model, some of the temperature dependence will occur for this reason.

To determine the effect of the temperature on anisotropy

the average energy of all the spins must be obtained. Since the macroscopic magnetisation is the average of the projection of the distributed spins onto the magnetisation vector, the ratio of the magnetisation $\sigma_s(T)$ to that produced for coherent spins $\sigma_s(0)$ (at 0 K), is a useful parameter to describe the spin distribution;

$$m(T) = \frac{\sigma_s(T)}{\sigma_s(0)}$$

≡ The reduced magnetisation ... (2.22)

Callen and Callen (1966) report a history of the calculations of the spin distribution and anisotropy change with respect to temperature and Birss (1964) gives a rigorous mathematical background. The predicted temperature dependences are as follows:

2.4.1. The single-ion model

At absolute zero the ionic spins are supposedly aligned and, for a density of the spins of N per unit volume, the anisotropy energy associated with each can be written;

$$e(s) = \frac{1}{N} \sum_L K_L(0) \mathcal{Y}_L(s) \quad \dots (2.23)$$

where $K_L(0)$ is the L^{th} order anisotropy constant at 0 K, and, after Callen and Callen (1966), $\mathcal{Y}_L(s)$ is a normalised polynomial in either the spin operators or a unit vector along the spin axis and expressible as a series of spherical harmonics restricted to suit the crystal symmetry. For a single-ion model, this equation continues to apply to individual spins under the effects of the fixed crystalline potential when reoriented by thermal agitation.

Thus the anisotropy energy for a spin distribution per unit volume may be written;

$$E/V = \sum_L K_L(0) \sum_m a_L^m \langle Y_L^m(S) \rangle \quad \dots(2.24)$$

where $\langle Y_L^m(S) \rangle$ is an average value computed assuming magnetisation to be isotropic in magnitude. By a change in coordinates to the magnetisation frame rather than lattice frame, Callen and Callen obtained;

$$E/V = \sum_L K_L(0) \langle Y_L^0(\underline{s}') \rangle Y_L(\underline{\alpha}) \quad \dots(2.25)$$

where $\underline{\alpha}$ is a unit vector parallel to the magnetisation and \underline{s}' is the spin unit vector referred to this direction. Comparing with equation 2.23, the quantity;

$$K_L(0) \langle Y_L^0(\underline{s}') \rangle \quad \dots(2.26)$$

can be seen to be the temperature dependent anisotropy and therefore the coefficient $K_L(T)$ is given by;

$$\frac{K_L(T)}{K_L(0)} = \frac{\langle Y_L^0(\underline{s}') \rangle_T}{\langle Y_L^0(\underline{s}') \rangle_0} \quad \dots(2.27)$$

Thus Callen and Callen expressed the temperature profile of the anisotropy in terms of the average of the spin components in the magnetisation direction and, using the fact that;

$$\frac{\langle Y_L^0(\underline{s}') \rangle_T}{\langle Y_L^0(\underline{s}') \rangle_0} = m(T) \quad \dots(2.28)$$

obtained in a quantum mechanical treatment at low temperature;

$$\frac{K_L^0(T)}{K_L^0(0)} = (m(T))^{L(L+1)/2} \quad \dots(2.29)$$

At arbitrary temperatures this yielded;

$$\frac{K_L^0(T)}{K_L^0(0)} = \hat{I}_{L+\frac{1}{2}}(x) \quad \dots(2.30)$$

where $\hat{I}_{L+\frac{1}{2}}(x)$ is the reduced hyperbolic Bessel function of order $L + \frac{1}{2}$ and x is a parameter describing the spin distribution and which can be eliminated using the fact that;

$$m(T) = \langle \cos \theta \rangle = \mathcal{L}(x) = \hat{I}_{3/2}(x) \quad \dots(2.31)$$

where $\mathcal{L}(x)$ is the familiar Langevin function equal to the reduced hyperbolic Bessel function of order $3/2$. Hence in general;

$$\frac{K_L^0(T)}{K_L^0(0)} = I_{L+\frac{1}{2}}(\mathcal{L}^{-1}(m(T))) \quad \dots(2.32)$$

The definitions of these functions are given in Appendix K. Equation 2.32 reduces to the required $L(L+1)/2$ power law at low temperatures for which $x \rightarrow \infty$.

The $L(L+1)/2$ power law has been derived classically by Zener (1954) who assumed that spins deviated from alignment according to a random-walk function.

Brenner (1957), commenting on Zener's model, considered a Boltzman distribution to be more suitable than a random-walk function since the Boltzman distribution implied a field causing alignment of the moments, and derived an equation in the cubic case for the reduced K_4^0 in terms of the reduced temperature, t_r (reduced with respect to the Curie temperature). By inserting the expression for magnetisation given by the Langevin-Weiss formula;

$$m(T) = \coth(3m(T)/t_r) - t_r/(3m(T)) \quad \dots(2.33)$$

he found that at low temperatures this approximated to a 10th power law but an increased power at higher temperatures. The 10th power law was required by the L(L+1)/2 rule. Carr (1958) developed the ideas of Brenner and showed for hexagonal materials;

$$\frac{K_1(T)}{K_1(0)} = (K_1(0) + 8/7 K_2(0))(m(T))^3 - 8/7 K_2(0)(m(T))^{10} + \dots \dots (2.34)$$

in the convention of equation 2.2 for K_n.

However, this could not explain the change in sign of K₁ for cobalt. Consequently Carr extended his theory to account for thermal expansions along different crystallographic axes and showed that change in the lattice parameter ratio of cobalt with respect to temperature was of just the right size to cause the necessary change in the anisotropy constants through a change in the crystalline field.

Carr's calculation of the additional factor in the equation relied on determinations of the dependence of the crystal field on lattice parameter for hexagonal materials made by McKeehan (1933 and 1937), room temperature values of c/a for cobalt from Owen and Jones (1954) and thermal expansion data at room temperature for cobalt, which he assumed to be uniform over a wide temperature range (American Institute of Physics handbook, 1957). The calculation also relied on the 0 K value of K₂(0)/K₁(0) taken then to be 0.28.

The K₁ anisotropy equation then became;

$$\frac{K_1(T)}{K_1(0)} = (1 - 3t)(m(T))^3 \dots (2.35)$$

explaining the inversion at approximately 500 K and generally fitting the cobalt data well. However information

particularly the c/a ratio measurements, was inaccurate and some uncertainty still remains in the form the scaling factor should take, which must be known to test the theory properly. Takahashi et al. (1978) recalculated using \dot{c}/a and $d(c/a)/dT$ values from "Thermo physical properties of matter" (1975) and got a value of 1.3 rather than 3 in the scaling factor giving a poor correlation to experiment. It is not known therefore to what extent Carr's work is valid.

Szpunar (to be published) has very recently worked specifically on the problem of cobalt in which, as in Carr's work, the single-ion model was assumed, and repeated the anisotropy calculation using the relationships between the anisotropy constants, the crystal field parameters and Stevens factors for the hexagonal case as given by Lindgard and Danielsen (1975). The assumption that the Stevens factors followed the single-ion temperature dependence law;

$$\langle O_L^0 \rangle = C(m(T))^{L(L+1)/2} \quad \dots(2.36)$$

was made and using the c/a dependence of the crystal field parameters, B_L^m , as given by Dixon (1972), a relationship was established between anisotropy and temperature. However again the uncertainty in experimental c/a measurements prevented an accurate assessment of the theory and, as indicated in chapter 7, all that could be shown was that a reverse calculation of the c/a ratio from the anisotropy data gave values within the experimental error over the temperature range for which the ratios were available. These comparisons are original to the present thesis. A detailed derivation of the anisotropy dependence on temperature following Szpunar

is given in Appendix C. Ono (1981) has also considered the temperature dependence of the anisotropy of cobalt including the effects of c/a changes but obtains poor correlation with experimental values above room temperature.

Formulae derived from spin-wave considerations have been given by Pal (1954), Keffer (1955) and by Hausmann (1970) showing specifically, in the case of K_4^0 for cubic materials, the standard 10^{th} power law or approximately (Turov and Mitsek, 1960) the 10^{th} power law. These theories treat the mis-orientation of single spins in proximity to others as part of a corporate excitation called a spin wave having thermally excitable energy quanta called magnons. The effect of temperature on anisotropy and magnetisation can therefore be analysed but no real change in the theoretical predictions is found. Cooper (1968, b) reviews these spin-wave calculations.

Brooks (1969) pointed out that the enormous anisotropy in some rare-earths must have an effect on the axial symmetry of the spin distribution for an arbitrary magnetisation direction. For instance, in terbium the spin precession must be compressed into the easy basal-plane increasing the power fall-off of the basal-plane anisotropy and reducing the uniaxial fall-off. Egami (1972) and Brooks and Egami (1973 a,b, 1974), using a spin-wave analysis, showed that the normal $L(L+1)/2$ power law had to be modified by a term including the distortion of the symmetry of the spin distribution parameterised by $b(T)$. They showed;

$$\frac{K_L^0(T)}{K_L^0(0)} = (m(T))^{L(L+1)/2} / (1 - b(T))^{(L(L+1)-4)/2} \dots(2.37)$$

and;

$$\frac{K_L^0(T)}{K_L^0(0)} = (m(T))^{L(L+1)/2} / (1 + b(T))^{L(L-1)/2} \quad \dots(2.38)$$

They also showed, for low temperatures, $(1-b(T))$ is proportional to reduced magnetisation and that the initial power laws for K_2^0 and K_6^6 in terbium would therefore be 2nd and 36th changing rapidly as the ellipticity parameter fell to zero with respect to temperature to approach the normal power dependence. The parameter $b(T)$ was related simply to the difference between the transverse spin components as follows;

$$b(T) = \frac{(S_y^2 - S_x^2)}{2S^2} \quad \dots(2.39)$$

where S_y and S_x are components of the spin distribution perpendicular to the operative molecular field. There is no definitive experimental evidence for these laws (Coqblin, 1977).

Cooper (1968, a) considered, in a single-ion model, magnetoelastic effects in the anisotropy to derive a basal-plane temperature contribution given by;

$$\frac{K_6^6(T)}{K_6^6(0)} \propto I_{9/2} \cdot I_{5/2} \quad \dots(2.40)$$

to be added to the normal $I_{13/2}$ dependence. Generally speaking, magnetostrictive effects are excluded from the theoretical analyses, which makes experimental data difficult to correlate with theory since the actual measurements involve magnetostrictive contributions. The general effect of magnetostriction on the observed anisotropies is dealt with separately in section 2.5.

2.4.2. The two-ion model

The two-ion temperature dependence of the K_1 anisotropy constant was shown by Callen and Callen (1965) to be described by an $(m(T))^2$ law in a cluster-theory calculation in which the influence of nearest and next-nearest neighbours on the discrete ions were taken into account. They showed that generally;

$$\frac{K_L^0(T)}{K_L^0(0)} = (m(T))^L \quad \dots(2.41)$$

is applicable at high temperatures (Callen and Callen, 1966).

Van Vleck (1937) showed that the pseudo-dipole interaction gave a variation in K_2^0 having a power dependence on $m(T)$ varying from 2 to 4 as temperature increases and that the pseudo-quadrupole interaction for cubic materials gave a K_4^0 power of 6 decreasing to 5 at higher temperatures. By introducing an improved model in which the pseudo-quadrupole interaction between pairs of ions was considered, the effect of the other ions being treated as a molecular field, Van Vleck obtained a power law of 10 decreasing to about 5 at higher temperatures which is initially in accord with the $L(L+1)/2$ power law. These results pertain to a theory which is known to be qualitative at best and difficult to treat mathematically.

2.5 Magnetoelastic effects

Magnetostriction is a term used for the change in dimensions of a magnetic material with respect to the

orientation of the magnetisation vector in the crystal lattice. The energy change associated with the re-orientation of the magnetisation due to work done against the elasticity of the lattice is called variously magnetostrictive or magnetoelastic energy and contributes to the magnetocrystalline anisotropy observed experimentally.

The magnetostrictive distortion is usually represented as a power series of the direction cosines of the magnetisation, α_i , and the direction along which the distortion is measured β_i , relative to the crystal axes. For hexagonal crystals, one particular convention to second order is;

$$\begin{aligned} \frac{\Delta L}{L} = & (\lambda_1^{\alpha,0} + \lambda_1^{\alpha,2}(\alpha_3^2 - 1/3))(\beta_1^2 + \beta_2^2) \\ & + (\lambda_2^{\alpha,0} + \lambda_2^{\alpha,2}(\alpha_3^2 - 1/3))\beta_3^2 \\ & + 1/2 \lambda^{\delta,2}((\alpha_1\beta_1 + \alpha_2\beta_2)^2 - \\ & \quad (\alpha_1\beta_2 - \alpha_2\beta_1)^2) \\ & + 2 \lambda^{\epsilon,2}(\alpha_1\beta_1 + \alpha_2\beta_2)\alpha_3\beta_3 \quad \dots(2.42) \end{aligned}$$

where the λ_L^{mn} are magnetostrictive parameters of which the $\lambda_1^{\alpha,0}$ and $\lambda_2^{\alpha,0}$ do not describe a shape dependence on magnetisation direction, but rather a distortion with respect to magnetisation intensity. Clearly a knowledge of the elasticity of the lattice along the various crystal axes, for the several ways strain can be applied, would allow an energy to be associated with the magnetostrictive deformation and this could be expressed in terms of the

magnetisation direction. The elasticity is in fact described by up to 36 elastic stiffness constants in a material obeying Hooke's law and these are labelled $C_{n,m}$ where n and m vary independently between 1 and 6. Detailed calculations will not be given but relevant solutions include, for the HCP structure as given by Birss (1964);

$$\Delta K_1 = -2C_{44} (\lambda \epsilon, 2)^2 \quad \dots(2.43)$$

where K_1 follows the convention of equation 2.2 and ΔK_1 is the magnetostrictive contribution to the K_1 anisotropy constant. The contribution of magnetostrictive energy to the anisotropy will be discussed for particular materials in chapters 7 and 8.

2.6 Anisotropic magnetisation

Callen and Callen (1960) point out that the anisotropy in the magnetisation energy must produce a directional dependence in the value of the magnetisation itself to yield 'anisotropic magnetisation'. This is a generalisation of the idea mentioned in section 2.4 where a distortion of the thermal spin distribution in terbium with respect to crystal direction was postulated, being the effect of the anisotropy on the spread of the spins. Although not stated explicitly this implied an anisotropy in the local spontaneous magnetisation. Aubert (1968) successfully measured anisotropy in the magnetisation of nickel to find a proportional variation of 0.06% with respect to orientation. The effects of the magnetisation anisotropy on measured magnetocrystalline

anisotropies is usually very small.

Callen and Callen showed that the magnetisation can be described by spherical harmonics;

$$\sigma(T, \theta, \phi) = \sum_{L=0}^{\infty} \sum_{m=-L}^{+L} \sigma_L(T) Y_L^m(\theta, \phi) \quad \dots(2.44)$$

parameterised by the $\sigma_L(T)$ where $\sigma_0(T)$ is the main isotropic component. They proceeded to show that the relationship between the $\sigma_L(T)$ and the zero temperature anisotropy coefficients $K_L^0(0)$ (in the convention of equation 2.5) is;

$$\sigma_L(T) = \frac{L(L+1)}{2\sigma_0(0)} K_L^m(0) \chi_0(T) \quad \text{for } L > 0 \quad \dots(2.45)$$

where $\chi_0(T)$ is the isotropic susceptibility;

$$\chi_0(T) = \mu_0 \frac{d(\sigma_0(T))}{dB_0} \quad \dots(2.46)$$

and where the normal $m(T)^{L(L+1)/2}$ power law has been assumed for the temperature dependence of the $K_L^m(T)$. By inspection, the anisotropic magnetisation coefficients, $m_L(T)$, can be thought of as the magnetisation induced by an anisotropy field due to the coefficients subscripted by L .

The magnetocrystalline anisotropy energy measured experimentally will include the Zeeman energy between the applied field and the non-isotropic components of magnetisation, that is the $\sigma_L(T)$ for $L > 0$. Hence;

$$K_L^m(T)_{\text{experiment}} = K_L^m(T)_{\text{magnetocrystalline}} - \mu_0 \sigma_L(T) B_0 \quad \dots(2.47)$$

Assuming constant χ_0 over the field range employed, the

supplementary energy term in the anisotropy can, in principle, be eliminated by extrapolating measured anisotropies to zero field to yield constants free from the effects of the anisotropic magnetisation.

Callen and Callen calculate a relative anisotropy in the magnetisation of cobalt of 0.1% contributing negligibly to the experimental anisotropy constants.

High anisotropy and low exchange energy is a combination for which the contribution of anisotropic magnetisation to the anisotropy is large. The gadolinium/terbium alloys of chapter 8, particularly as they approach their Curie temperatures, manifest this combination, though no quantitative information has ever been obtained on the directional dependence of their spontaneous magnetisations.

Papers have appeared qualifying the initial work of Callen and Callen, notably those of Charap (eg Charap, 1961) who analysed the phenomenon of anisotropic magnetisation more extensively using a spin-wave theory. However, the general results elucidated here have remained unchanged.

CHAPTER THREE

CZOCHELSKI CRYSTAL GROWTH AND AUTOMATION

3.1 Introduction

The properties of a crystalline materials often differ significantly from those of the non-crystalline state giving them applications in which the distinct property is sought. For instance the conductivity and mobility requirements for integrated circuit semiconductors dictate the use of single crystals.

Crystal growth by liquid-solid equilibrium, of which the principal techniques are Bridgman, float-zone and Czochralski, is the most widely practised commercial method for single crystal growth. In all of these, crystals are propagated as material solidifies from the melt at a controlled interface. The three techniques are illustrated schematically in figures 3.1, 3.3 and 3.4.

The Bridgman technique, first used by Bridgman (1925), consists of traversing the solid-liquid interface along a volume of molten material contained within an elongated crucible by passing a cooling wavefront down the melt. The cooling may be achieved by lowering the power of a furnace having a natural thermal gradient or by physically transporting the crucible out of the heated zone (fig. 3.1). The nucleation end of the crucible is usually pointed so that solidification begins at a single point; multiple nucleation would produce a polycrystal. Vertical cylindrical crucibles or horizontal open boats are

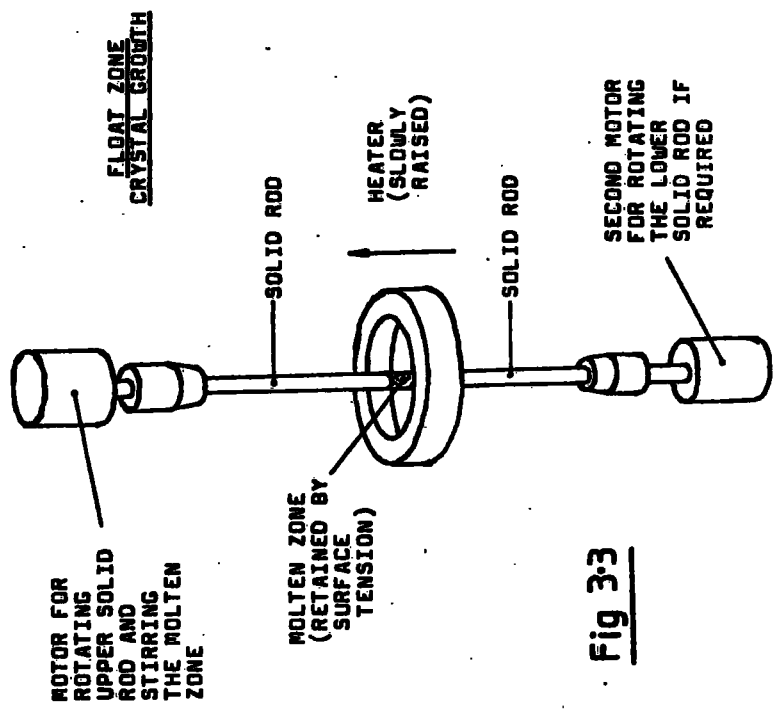
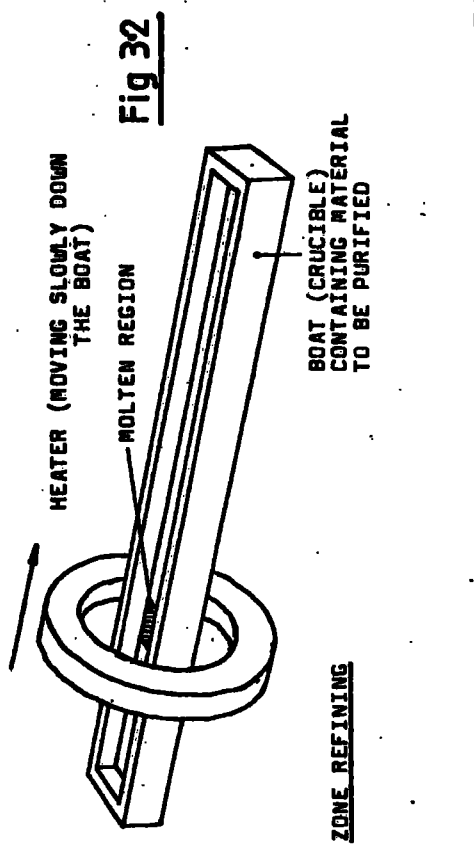
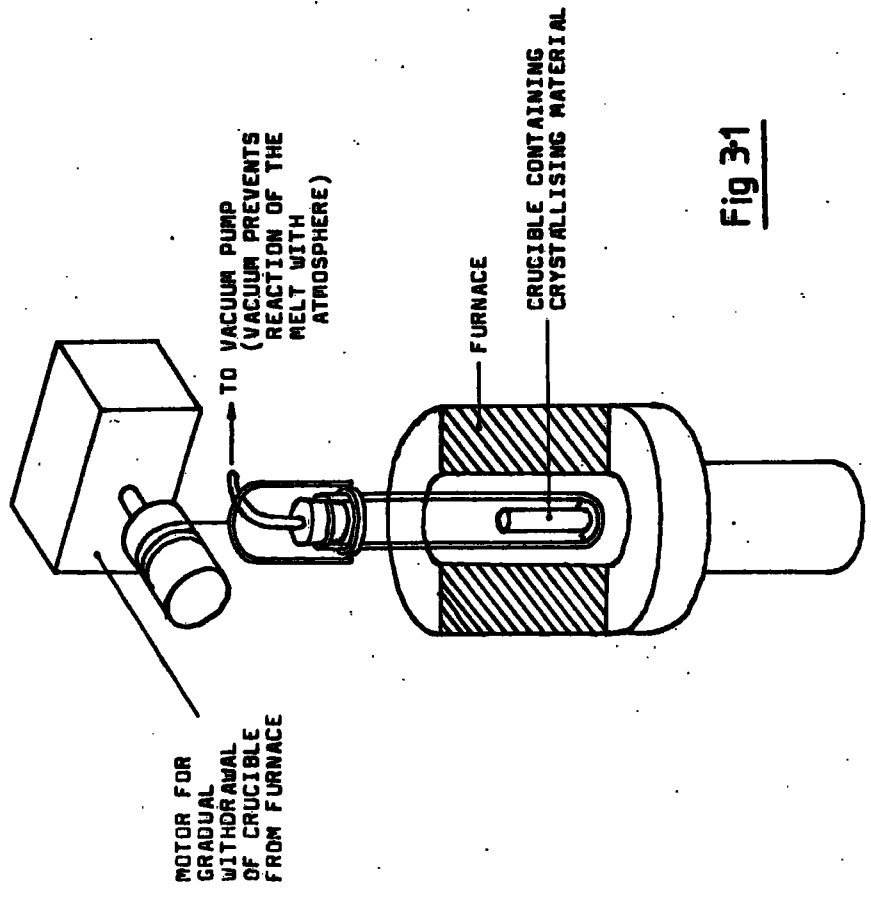


Fig 33



SIMPLIFIED DIAGRAM OF A BRIDGEMAN CRYSTAL GROWER

THE ESSENTIAL PROCESS IN THE BRIDGEMAN TECHNIQUE IS TO CAUSE A SINGLE FREEZING INTERFACE TO PASS ALONG THE MATERIAL IN THE CRUCIBLE; ACHIEVED USUALLY BY WITHDRAWING THE CRUCIBLE SLOWLY FROM THE FURNACE. THE CRYSTALLINE SOLID MAY PROPAGATE IF PRESENT INITIALLY.

common and usually heated in a vacuum or inert gas to prevent reaction with the atmosphere. Enclosed crucibles are sometimes used for particularly volatile materials for which Czochralski or float-zone growth are unsuited. The Bridgman technique is sometimes called the Bridgman-Stockbarger technique due to the extensive use of it by Stockbarger (eg Stockbarger, 1936).

Zone refining, shown schematically in figure 3.2, is a purification technique in which a molten zone is swept repeatedly in a single direction through the solid. A predisposition for impurities to occupy the liquid rather than the solid at the freezing interface ensures that they are systematically driven to one end of the sample which may then be partially removed leaving a purged remainder. Single crystals are sometimes produced by this procedure by analogy to the Bridgman technique.

Float-zone growth is a crucible-free technique with the consequent advantage of low melt contamination from the walls of a container. It involves the passage of a localised molten zone along a vertical rod of material, the zone being held between the adjacent solid regions by the surface tension of the melt (fig. 3.3). Rotation of the growing or diminishing rod tends to create symmetry in the zone which helps stabilisation and also homogenises impurities in the growing crystal. Float-zone growth requires a seed crystal to nucleate the solidifying interface, the zone being initiated in the seed. Float-zone equipment tends to be more complex than Bridgman, partly because

heating a very small zone remotely can be problematical, sometimes requiring electron beam melting or the focusing of a radiant source.

3.2 Czochralski growth

One of the most important growth techniques is that named after Czochralski who in 1917 grew rod shaped crystals from the melt. The rods solidified at the melt surface as they were withdrawn and the crystalline state propagated through the bulk of the rod if initially present in the seed. It was using this technique that Teal and Little (1950) grew the first single crystals of silicon and germanium and this technique remains today the chief method of production for the semiconductor industry.

The normal requirements for a Czochralski crystal puller are;

- 1) a mechanism for rotating the crystalline rod while withdrawing it from the melt;
- 2) a means of containing and heating the melt, usually by a resistive or radio-frequency furnace;
- 3) a means, if necessary, of preventing the melt from reacting with the atmosphere by surrounding the growth region by vacuum or inert gas.

Figure 3.4 shows a schematic Czochralski crystal puller, minus gas/vacuum system. Detailed diagrams of a particular Czochralski crystal puller are given in chapter 5, see for example figures 5.3 and 5.4.

Czochralski technique has advantages over Bridgman because it imposes no mechanical constraint on the

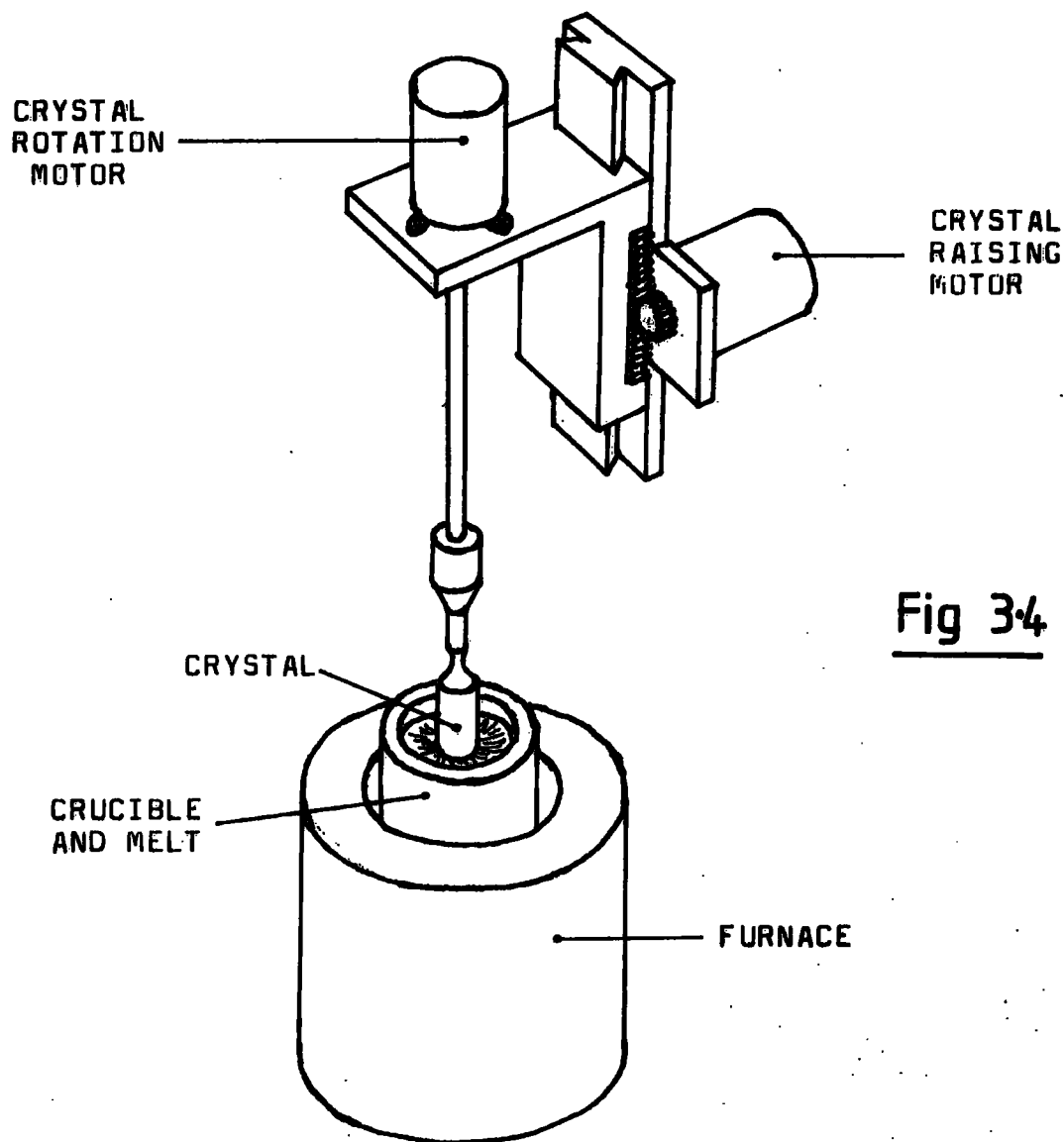


Fig 34

SIMPLIFIED DIAGRAM OF A CZOCHRALSKI CRYSTAL PULLER

THE ESSENTIAL PROCESS IN CZOCHRALSKI GROWTH IS TO WITHDRAW MATERIAL FROM THE MELT AT A RATE WHICH ALLOWS THE BUILD UP OF SOLIDIFYING MATERIAL TO BE SUSTAINED AND THE CRYSTALLINE STATE TO BE PROPAGATED IF INITIALLY PRESENT.

freezing interface. In Bridgman technique, the forces which materials create on the crucible if they expand on freezing (a few percent in the case of silicon) distort the crystal introducing dislocations and even low angle grain boundaries. No such problem arises in Czochralski growth. Furthermore, for the growth of large crystals, Czochralski technique can be scaled whereas float-zone growth is limited to small crystals for which a practical cross-sectional zone can be retained by surface tension (or, to some extent, radio frequency levitation), diameters of about 1 cm being typical.

The physical characteristics of a material may exclude growth by the Czochralski technique or indeed any other liquid-solid method. Properties preventing growth are;

- 1) the material decomposes before it melts or melts incongruously;
- 2) the material sublimes before it melts or its vapour pressure is too high at the melting point;
- 3) structural change during cooling (eg FCC \rightarrow HCP for Co at \approx 700 K) adversely affects crystal perfection;
- 4) the melting point is impractically high;
- 5) the growth conditions are not suited to a desired dopant eg due to its volatility.

The most critical experimental parameter in Czochralski growth is the melt temperature which, during typical growth, must be regulated to about 0.5% just above the melting point. Control of the pull-rate is not as critical. For high crystal perfection, however, all parameters are important including rotation-rate, transverse and

longitudinal thermal gradients at the growing tip and, if relevant, the flow rate of the inert gas.

Rotating the crystal during growth is necessary to preserve rotational symmetry of the crystal and distribute impurities. Rotation rates are limited to a few hundred RPM since above this, melt agitation adversely affects the growing interface and thereby crystal perfection, 60 RPM being typical.

The crystal can be initiated by using a polycrystalline starting rod and growing a thin neck in which a single crystallite propagates to the exclusion of others. Thereafter the crystal can be grown out to the desired diameter. However for a required orientation of the crystal lattice a well characterised seed crystal must be used.

An excellent text on Czochralski and crystal growth techniques in general is R.A. Laudise "The Growth of Single Crystals" (1970).

3.3 Automatic control of Czochralski growth

Automatic control of Czochralski growth is defined here to be the automatic stabilisation of crystal diameter during growth.

Automatic diameter control systems for Czochralski growth were patented in 1959 (Levinson 1959), first reported in the literature in 1966 (Apilat et al., 1966) and were available commercially in the West by 1971. As indicated by Lorenzini et al. (1974) the effect of these systems on the silicon materials industry was significant allowing

many pullers to be run simultaneously by fewer, less skilled operators to produce crystals for which subsequent grinding was minimal. Furthermore the increased control allowed consistency in the shape of the growing interface, with its influence on crystal perfection, so as to realise reproducibly the special growth conditions whereby zero dislocation crystals are produced.

There are six basic methods of control which have so far been applied to Czochralski growth, each characterised by the method of determining the diameter of the crystal. In all cases deviations from the required diameter are translated to corrective changes in the melt temperature or pull-rate completing a feedback-loop in which crystal diameter is stabilised. The control electronics will not be discussed in detail here. An alternative method of making corrective changes to the crystal diameter was reported by Vojdani et al. (1974) who used the Peltier effect to remove heat at the growing interface by passing current down the crystal. This method is only appropriate to small and medium band-gap semiconductors, these having the necessary Peltier coefficient, and has never been used in the closed-loop control of crystal diameter.

The six methods of control, excluding the viscous torque method reported for the first time in chapter 5, are shown schematically in figures 3.5 to 3.10. A review article by Hurle (1977) on this subject is excellent but does not mention the use of melt depth sensors.

Bachmann et al. (1970) reported Czochralski growth

in which the growth conditions were changed sequentially by a programmer. No in-progress diameter measurements were made but limited automation was achieved including the control of neck-down. This was an open-loop method relying on the reproducibility of the furnace conditions from one run of the puller to the next and did not constitute automation as defined here.

One method of producing Czochralski crystals with a fixed cross-section is to use a die floating on the melt surface containing a hole through which the crystal is pulled. This technique has found its principal application in the growth of ribbons rather than cylindrical rods and again is not an automatic technique in the sense defined.

The six automation methods are described in the following sections.

3.3.1. The 'bright-ring' method

Historically the 'bright-ring' method was one of the earliest forms of automatic control (Patzner et al. 1967) and used an optical pyrometer focused on the melt surface adjacent to the crystal (fig. 3.5). Changes in the crystal diameter were detected as the luminous meniscus region, that is the 'bright-ring', advanced or retreated across the view of the pyrometer increasing or decreasing its output. Stabilising the pyrometer output by adjusting the growth conditions constrained the diameter of the crystal as required. The bright-ring, as shown by Digges et al. (1975) and independently by Turovskii et al. (1977), was due to the reflection of light from hot

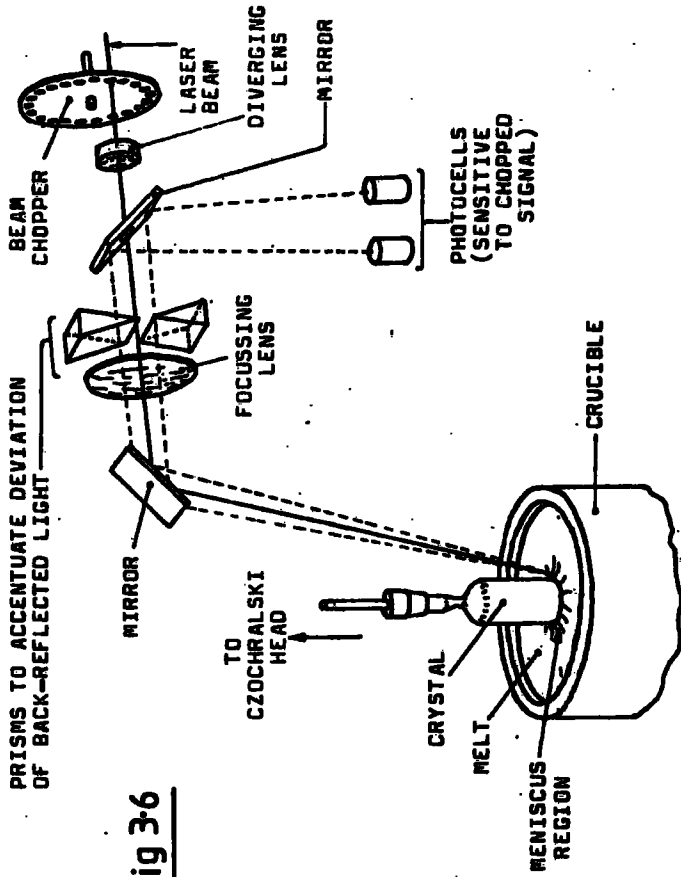


Fig 3-6

MENISCUS SENSITIVE OPTICAL METHOD FOR MONITORING CZOCHRALSKI GROWTH (C.F. "BRIGHT RING" METHOD)

THE RETREAT OR ADVANCE OF THE MENISCUS (WITH REDUCTION OR GROWTH OF THE CRYSTAL) DEVIATES THE REFLECTED LASER BEAM PRODUCING AN OUT-OF-BALANCE SIGNAL AT THE PHOTOCELLS RELATED TO CRYSTAL DIAMETER.

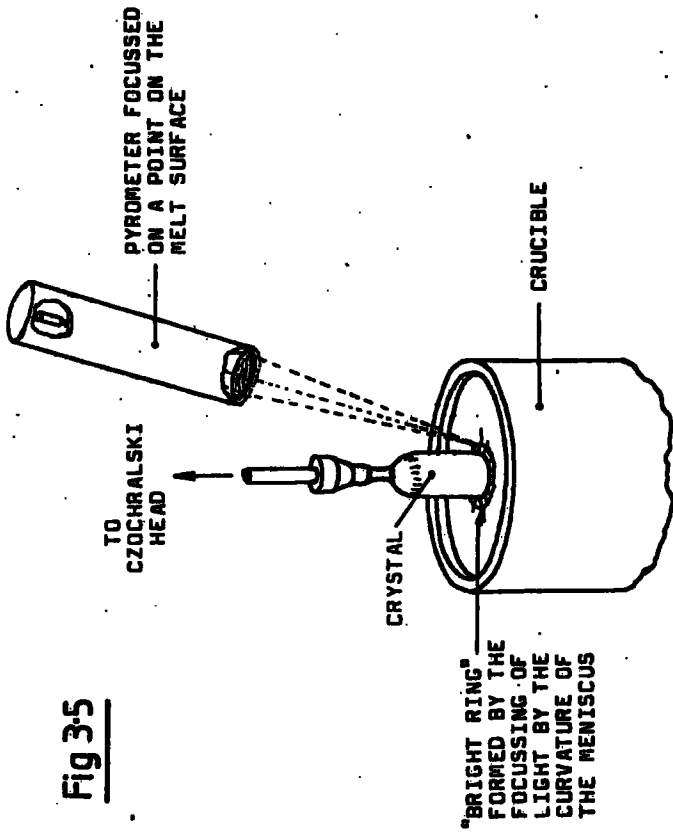


Fig 3-5

OPTICAL PYROMETER ("BRIGHT RING") METHOD OF MONITORING CZOCHRALSKI GROWTH

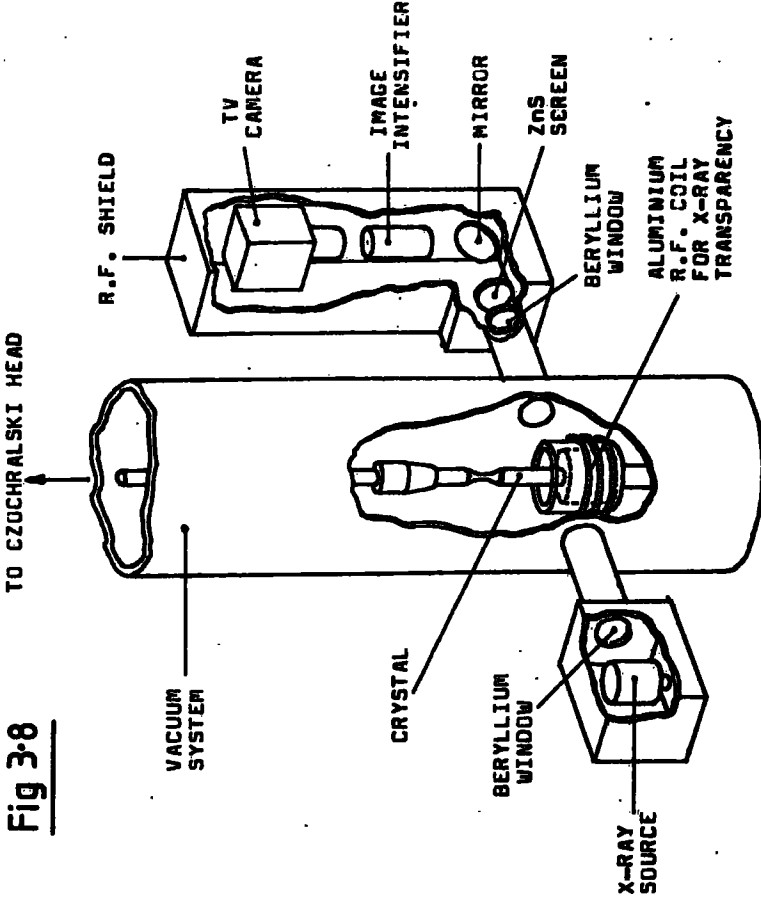
THE APPARENT INTENSIFICATION OF THE MELT LUMINESCENCE IN THE REGION OF THE MENISCUS ENABLES THE MENISCUS ADVANCE OR RETREAT TO BE MONITORED AND WITH IT THE CRYSTAL DIAMETER.

areas of the growth system by the curved meniscus. Domey et al. (1971) reported a development of the technique using a computer in the feedback process with control of both melt temperature and pull-rate rather than solely pull-rate. Van Dijk et al. (1974) and Turovskii et al. (1977) report further developments of this method. All bright-ring methods require the crucible to be lifted to keep the melt level constant in order to prevent apparent movement of the bright-ring with respect to melt depletion as viewed off the crystal axis. Bright-ring control has achieved $\pm 1\%$ diameter regulation in silicon (Turovskii et al. 1977) and a similar accuracy in apatite (Steinbrugge et al. 1972) and is therefore one of the best available techniques in this respect.

3.3.2. The laser reflection method

Closely related to the 'bright-ring' method is the laser reflection method described by Gross and Kersten (1972) and Van Dijk et al. (1974). The meniscus position was sensed optically but in this case using a chopped He-Ne laser to vertically illuminate the melt surface near the growing interface (fig. 3.6). Change in the position of the meniscus curvature deviated the reflected laser beam, detected by twin photodiodes tuned to the chopping frequency. The out-of-balance signal initiated appropriate changes in the melt temperature. Control of the crystal diameter was $\pm 1\%$ for 2 cm diameter

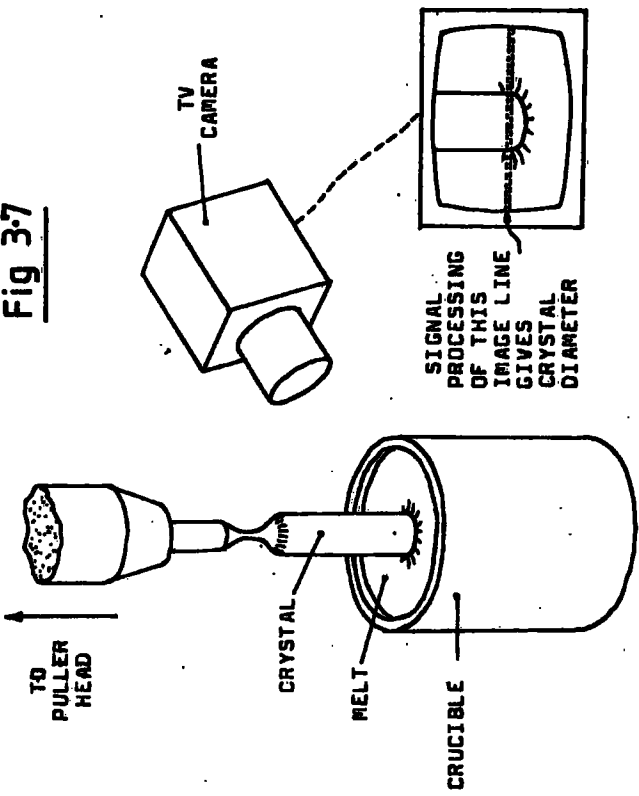
Fig 3-8



X-RAY SHADOW METHOD OF MONITORING CZOCHRALSKI GROWTH

AS IN FIGURE 3.7 INFORMATION FROM A PARTICULAR LINE IN THE VIDEO IMAGE YIELDS THE CRYSTAL DIAMETER. THE EQUIPMENT SHOWN IS A SCHEMATIC DIAGRAM OF THAT OF PRUETT AND LIEN(1974)

Fig 3-7



MONITORING OF CZOCHRALSKI GROWTH USING A TELEVISION CAMERA

A PARTICULAR LINE IN THE VIDEO IMAGE YIELDS THE ELECTRONIC SIGNAL FROM WHICH CRYSTAL DIAMETER CAN BE INFERRED.

crystals of the KCl and $\text{Bi}_{12}\text{GeO}_{20}$ (Gross and Kersten, 1972) comparable to the previous method.

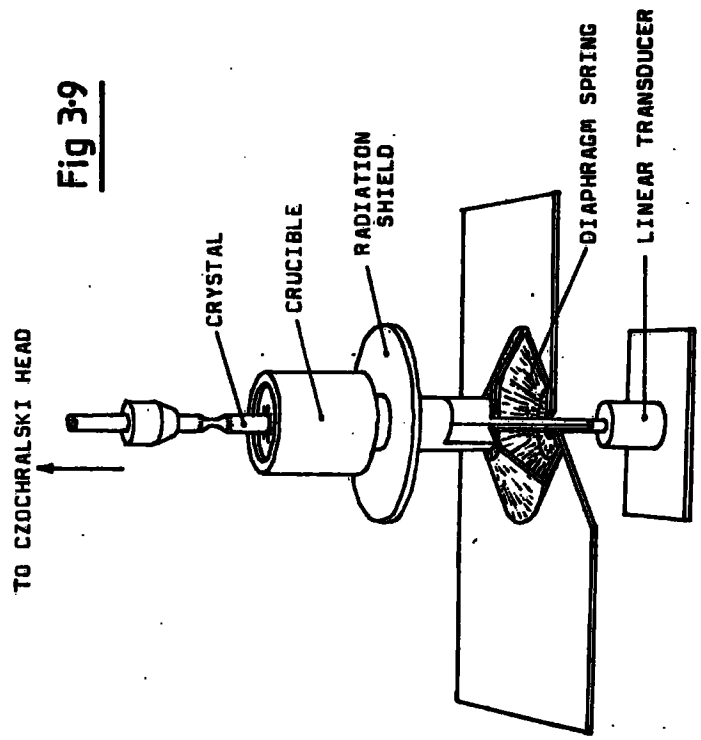
3.3.3. The optical TV imaging method

Gartner et al. (1972), O'Kane et al. (1972) and Kim et al. (1982) describe control by imaging the crystal with a television camera and deriving the diameter from the intensity profile of a line in the video image cutting the interface region (fig. 3.7). Viewing the crystal out-of-normal due to the crucible wall, produced an ellipsoidal image of the meniscus having an ill-defined boundary with the crystal yielding low interface definition and reducing control accuracy. A conventional black and white vidicon and infra-red TV camera were used respectively. Stabilisation of diameter to within $\pm 5\%$ was possible by feedback to the melt temperature. This control method has not been widely adopted presumably due to its inaccuracy.

3.3.4. The X-ray shadow method

Pruett and Lien (1974) and Van Dijk et al. (1974) report the inspection of crystal X-ray shadows using a television monitor. (fig. 3.8). Resolution was hampered by the finite source size causing blur in the silhouette detected using a ZnS screen. As in the previous method, the duration of the traverse of a raster over the darkened part of an appropriate line in the video image yielded crystal diameter. The method is particularly suited to liquid encapsulation Czochralski growth in which,

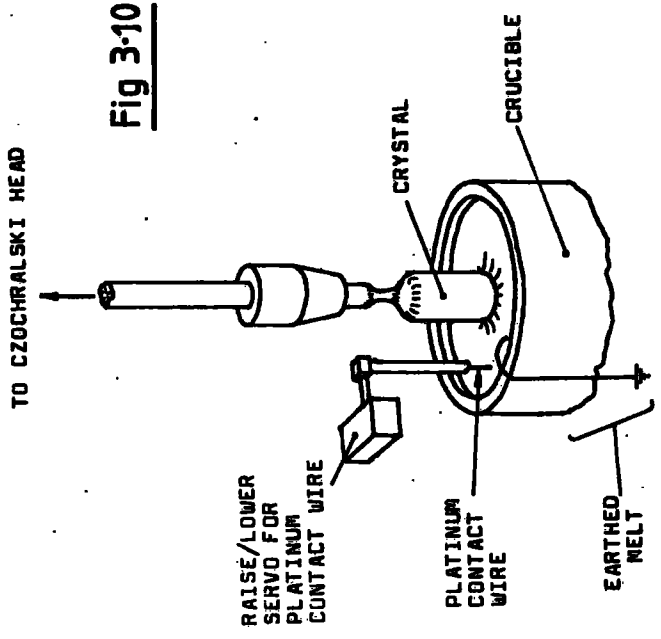
Fig 3-9



A WEIGHING METHOD OF MONITORING CZOCHRALSKI GROWTH (IN THIS CASE THE CRUCIBLE RATHER THAN THE CRYSTAL IS WEIGHED)

THE DIFFERENTIAL OF THE WEIGHT WITH RESPECT TO PULL RATE GIVES THE CRYSTAL DIAMETER.

Fig 3-10



MONITORING OF CZOCHRALSKI GROWTH USING A MELT LEVEL SENSOR

THE DIFFERENTIAL OF THE MELT HEIGHT WITH RESPECT TO THE PULL RATE GIVES THE CRYSTAL DIAMETER.

to prevent volatilisation of the melt, an immiscible non-volatile material is floated on the surface (after Metz et al., 1962) obscuring the interface region to optical analysis and complicating the use of the next two methods of diameter measurement. X-ray imaging can however, for some material combinations, show the submerged crystal tip, as in the case for GaP encapsulated by B_2O_3 . Van Dijk et al. (1974) used this technique to automate growth via the melt temperature and achieved $\pm 2.5\%$ diameter stabilisation. Pruett and Lien used the technique to complement manual control of the furnace. However, X-ray imaging has not been mentioned in the literature since 1974.

3.3.5. The weighing methods

By far the most important method for automatic control of the Czochralski technique is the weighing method (fig. 3.9). Though envisaged in a patent as early as 1959 (Levinson) and again in 1966 (Rummel) the first working version was reported as recently as 1972 (Bardsley et al.) and described subsequently by Zinnes et al. (1973), Kyle and Zydzik (1973), Reinert and Yatsko (1974), Valentino and Brandle (1974), Satoh et al. (1976), Garabedian et al. (1976), Mateika et al. (1977), Bardsley et al. (1977) and Fukuda et al. (1982). In this method, the weight of the crystal or crucible for constant pull-rate can be compared directly to a linearly increasing datum to provide a signal indicative of the average diameter error over the preceding crystal profile. Conversely the differential of the weight with respect

to pull-rate yields the diameter of the crystal (Valentino and Brandle, 1974; Bardsley et al. 1977). To achieve this method of control the modification necessary to a standard crystal puller need not be extensive; all that is required is a load cell within the gas/vacuum system. Garabedian et al. (1976) quote control accuracy of $\pm 0.4\%$ in gadolinium-gallium-garnet using the weighing method; the most precise for any automation method.

3.3.6. The melt level method

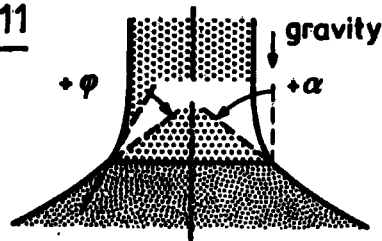
In the melt level method, the decrease in the melt level is compared to crystal length or pull-rate to yield an error signal in the diameter (fig. 3.10). Though preceded by patents on the weighing method, this seems to have been the earliest working automation method for Czochralski growth, all the development being carried out in the U.S.S.R. Introduced by Apilat et al. (1966) continuous improvement followed, notably by Belgurov et al. (1970) who reported a specialised platinum contact melt-level transducer and by Burachas and co-workers subsequently. Timan and Burachas (1981) and Goriletsky et al. (1981) achieved diameter control of $\pm 1.5\%$ by this method.

3.3.7. Discussion of methods

Both Hurle (1977) and Jozsef (1979) in review articles on the automation of Czochralski growth conclude that methods which measure not only crystal diameter but also the shape of the meniscus at the growing interface are the best means of stabilising crystal diameter. One reason for this is that the meniscus angle, α , defined in figure 3.11, is

dependent on the inclination of the crystal walls to the melt at the growing interface.

Fig 3-11



Definition of the contact angle φ and the meniscus angle α in a schematic cross section through the axis of a Czochralski growth arrangement with axial symmetry. The crystal is indicated by an ordered, the melt by a disordered arrangement of dots.

(AFTER WENZL ET AL., 1978)

This means that meniscus angle is dependent on the derivative of crystal diameter with respect to distance pulled and the sensing of the meniscus angle can therefore indicate impending diameter changes prior to their occurrence. In particular it has been shown (eg. Wenzl et al. 1978) that the contact angle φ of the surface of the melt with respect to the crystal surface is a constant for a given material, being zero only for those materials for which the liquid completely wets the solid. Maintaining a meniscus angle of φ therefore produces parallel-sided crystals. However, a meniscus angle of φ defines a size and shape for the meniscus column held above melt-level by the surface tension. Thus the deviation from this column geometry anticipates the ensuing diameter changes of the crystal. A general paper on the relationship between the meniscus geometry and the shape of growing crystals has been written by Surek et al. (1980).

Clearly the 'bright-ring' and laser methods measure not just crystal diameter but depend also on the state of the meniscus, since reflections from the meniscus region in both cases produce the signal by which control is accomplished. Likewise, though not as critically, the weighing and melt level methods are meniscus sensitive because the volume of fluid supported above the melt surface by the meniscus is accredited to the crystal rather than the melt in both cases. Television methods (optical, infra-red or X-ray shadow) are simply diameter sensitive since meniscus profiles are beyond the resolution of any realistic equipment. The control of diameter for these methods is accordingly poor.

Two methods which have been applied to the automation of float-zone growth but not Czochralski growth involve in the first case γ -ray attenuation through the molten zone (Autenshlyus et al. 1975) and in the second case viscous torque measurement (Quenisset et al. 1980). Both methods could be applied to Czochralski growth and the latter is described in chapter 5. It would be difficult to collimate and detect γ -rays in a method whereby the small meniscus region just above the melt in Czochralski growth is resolved accurately and therefore the γ -ray method would be insensitive to the meniscus shape. Viscous torque measurements would, on the other hand, be sensitive to the shearing of the fluid between crystal and melt surface, that is the latter would be meniscus sensitive and, at least in this respect, a promising method of automation.

CHAPTER FOUR

TORQUE MAGNETOMETRY

4.1 Introduction

The magnetocrystalline anisotropy of a material may be determined by several methods, including the analysis of magnetisation curves, by ferromagnetic resonance, electron diffraction, inelastic neutron scattering and magnetostrictive measurements. A further method is that of torque magnetometry in which the differential of the anisotropy energy surface with respect to angle is inferred directly from the torque experienced by a material in a magnetic field.

A torque magnetometer is basically a device which measures the torque on a sample normal to the plane of relative rotation between the sample and an applied magnetic field to determine plots of torque versus field angle. Related devices, such as the torque pendulum first used by Rathenau and Snoek (1941), the rotating sample magnetometer devised by Ingerson and Beck (1938) and the ripple-field magnetometer of Birss et al. (1976), which all measure magnetocrystalline anisotropy directly, will not be discussed here.

The following chapter deals firstly with obtaining anisotropy values from torque curves (section 4.2) and then describes existing torque magnetometers, which can be compared with the magnetometer of chapter 6. The anisotropy

constants measured by a torque magnetometer include the effects of magnetostriction and anisotropic magnetisation and in neither case can these be eliminated satisfactorily without independent measurements of the spurious property.

The review of Pearson (1979) is an excellent text on the experimental aspects of torque magnetometry. A brief introduction to torque magnetometry is given by Zijlstra (1960).

4.2. Analysis of data

4.2.1. The shear-correction

It has been mentioned earlier (chapter 2) that the torque on a saturated material in a magnetic field can be found by differentiating the anisotropy energy with respect to angle. A problem arises however, when obtaining the anisotropy energy from the torque measured experimentally, because the energy is conventionally expressed in terms of the angle of magnetisation within the lattice, rather than the angle of the external applied field, and it is dependence on the latter that produces the observed torque. The solution is to correct the experimental torque curve to one with magnetisation angle along the abscissa by applying a 'shear-correction', since the torque value, field value and magnetisation value, for any point on the curve, define an angle by which the field vector and magnetisation vector must differ (see fig. 4.1). Each point on an experimental torque curve must therefore be slid or 'sheared' by an appropriate amount to yield torque with respect to magnetisation

THE SHEAR-CORRECTION

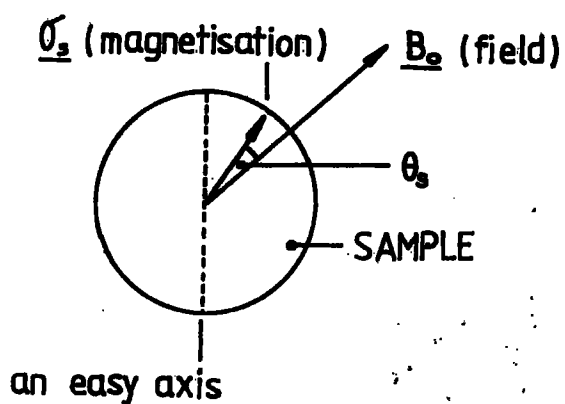
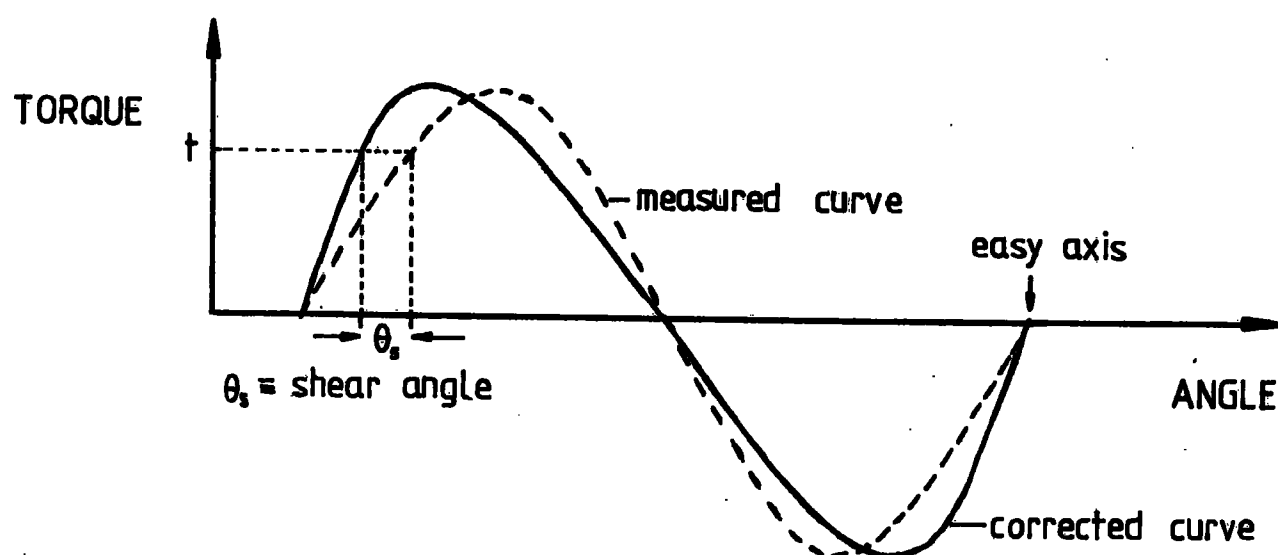


Fig 4.1

angle from which the anisotropy constants can then be obtained.

4.2.2. Obtaining the anisotropy constants

A common method of deriving the anisotropy constants from a shear-corrected torque curve is to Fourier analyse the curve and to use certain established relationships between the constants and the harmonic content. For example, the hexagonal anisotropy energy expression (eqn. 2.2) differentiates with respect to θ to give;

$$\begin{aligned} \frac{\partial(E/V)}{\partial\theta} = \tau_b = & K_0 + 2K_1 \sin\theta \cdot \cos\theta + 4K_2 \sin^3\theta \cdot \cos\theta \\ & + 6(K_3 + K_4 \cos 6\phi) \sin^5\theta \cdot \cos\theta + \dots \end{aligned} \quad \dots(4.1)$$

which is the shear-corrected torque per unit volume for field rotation about the 'b'-axis. If expressed as a series of harmonics, in phase with the easy-axis, parameterised by the Fourier coefficients $A_2, A_4, A_6 \dots$, that is;

$$\tau_b = A_2 \sin 2\theta + A_4 \sin 4\theta + A_6 \sin 6\theta + \dots \quad \dots(4.2)$$

then the anisotropy constants are given by;

$$K_n = (-1)^{n+1} \frac{4^{n-1}}{n} \sum_{j=n}^{\infty} \binom{j+n-1}{j-n} A_{2n} \quad \dots(4.3)$$

In particular;

$$K_1 = A_2 + 2A_4 + 3A_6 + 4A_8 + \dots \quad \dots(4.4)$$

$$K_2 = -2A_4 - 8A_6 - 20A_8 + \dots \quad \dots(4.5)$$

$$K_3 = -16/3 A_6 + 32A_8 + \dots \quad \dots(4.6)$$

Note that care must be taken in the definition of K_4 and higher order uniaxial constants since conventionally K_4 is taken to be the first basal-plane anisotropy constant (the case throughout this thesis). There is no report of a uniaxial K_4 , as defined in equation 4.3., being measured experimentally so there is no confusion in practice. The basal-plane torque is given by;

$$\tau_c = B_6 \sin 6\phi + B_{12} \sin 12\phi + \dots \quad \dots(4.7)$$

whence;

$$K_4 = 6B_6 + \dots \quad \dots(4.8)$$

Relationships between torque Fourier coefficients and anisotropy constants for other crystal structures can be derived fairly easily for a given phenomenological convention. The Fourier analysis is usually done numerically by measuring discrete values of torque at specified field angles and, after shear-correction, calculating the coefficients using an integration technique suited to the unequal angular spacing of the data due to shear.

4.2.3. Unsaturated samples

Torque measurements can be made on samples which are not saturated, that is not in the single domain state. Under these circumstances the anisotropy constants can only be retrieved by assuming a model for domain behaviour and deriving the torque in a given field from it.

The simplest theory for domain behaviour, from which torque values in a given field can be obtained, is what is called 'phase theory', first described in detail by

Néel (1944). In phase theory no analysis is made of the microscopic behaviour of the domains; they are simply assumed to be made up of a few distinct types having a characteristic magnetic orientation. Each domain type is called a phase, and the theory involves only the volume proportion and magnetisation direction for each phase. The domains are assumed to be mobile, corresponding to a magnetically soft material, and the internal magnetisation of each is assumed to be constant; the saturation magnetisation. The volume proportion and direction of the phases are established by assuming a state of minimum energy in the sum of the magnetostatic and magnetocrystalline contributions, where the former is calculated by assuming a macroscopic magnetisation which is uniform and a vectorial average of the phases. A derivation of the torque created by an unsaturated uniaxial disc is given in Appendix C. A few papers have appeared which describe in detail phase theory treatment of the magnetisation process in crystalline materials, particularly Néel (1944), Néel et al. (1960), Birss and Hegarty (1966), Polivanov and Kalugin (1968), Jahn and Müller (1969), Voigt and Pelster (1973), Burd et al. (1977) and most comprehensively Birss and Martin (1975). Of these, Polivanov and Kalugin, Jahn and Müller, Voigt and Pelster treat the resultant torque in a magnetic field.

In the case of partial saturation of the torque curves, in an interval around the easy-axis, anisotropies can be derived using the conventional method by fitting a harmonic series to the available shear-corrected curve

and then assuming its continuation into the undefined region. The accuracy of the derivation suffers because the shear corrections are necessarily gross if the applied field could not wholly saturate the sample and the angular interval for which the corrected torque curve is available is therefore invariably small. One simplification is to assume a leading term only in the anisotropy, which can then be derived by interpreting the corrected easy-axis gradient as the beginning of a sinusoidal plot. The K_1 data for the terbium/gadolinium alloys was determined in this way in chapter 8.

4.2.4. Extrapolation with respect to field

Torque curves taken in the non-saturated state demonstrate a shape and amplitude which is critically dependent on the size of the applied field. For saturation at all field angles, the torque curve amplitudes of most materials remain virtually constant (eg for Co in the 1.4 - 1.9 T field range in figure 7.4) and the change that occurs to the torque curve with increasing field is in the shape as the shear-error reduces. A rough value of the anisotropy constants can therefore be obtained from saturated torque curves since, for an appropriate shear-correction, they are largely independent of the applied field. However, it was realised as long ago as 1939 (Tarasov), that torque curve amplitudes failed to show a limiting value and that an extrapolation was necessary; a reciprocal-field plot continued to $1/H=0$ being suggested. Later, Kouvel and Graham (1956 and 1957) suggested a $1/\sqrt{H}$ plot. However, it has now become clear that there is no correct

means of making the extrapolation.

The first difficulty in making an extrapolation is the lack of a definitive theory which describes the anisotropy field dependence parameterised by constants which could be experimentally determined. Sievert and Zehler (1970) pointed out that anisotropy constants measured by torque curves include components which are dependent on the anisotropy of the magnetisation, that is, its magnitude variation with respect to crystallographic orientation described by Callen and Callen (1960) and Aubert (1968), multiplied by the applied field. They concluded that an extrapolation to zero field is required to retrieve anisotropies since only then would the anisotropies truly reflect the change in the free energy of the crystal with respect to magnetisation direction. They also concluded that, in a simple theory, the extrapolation ought to use a best fitting quadratic and demonstrated a good quadratic fit between saturated shear-corrected anisotropies with respect to field in the case of cobalt. What they did not know is that their cobalt anisotropies at finite field are at variance with better recent measurements indicating that a wrong shear-correction parameter, $1/(\sigma_s V B_0)$, was used which creates a quadratic error in the anisotropy with respect to field in a second order expansion. It is impossible, therefore, to say that there is a quadratic component in the field dependence of the anisotropy. Indeed Phillips and Shepherd (1970) suggest a quadratic with respect to $1/B$ rather than B . Interestingly enough, independently of Sievert and

Zehler, another detailed study of the field dependence of the anisotropy constants of cobalt has been done. Ono and Yamada (1979) and Ono (1981) showed cobalt anisotropy field dependences which were much smaller than those of Sievert and Zehler (confirming the possibility of shear errors in the former work) and of a form which fitted a theory in which the effect of the Fermi surface movement in the applied field was taken into account using an itinerant-electron model for the anisotropy. The field dependence of the magnetisation value was also considered. This was evidently a theory giving a complex field dependence; it gave only qualitative predictions. Generally speaking, therefore, the complexity of the field dependence rules out the possibility of an extrapolation by a simple functional form.

The second difficulty in making the extrapolation is that, to obtain accurate anisotropies using torque magnetometry, the samples need to be saturated. This necessarily means high fields and therefore a very long projection of the theoretical fit for the field dependence to the zero field value. The extrapolation is therefore inherently inaccurate.

In chapter 7 an extrapolation technique was not applied to the cobalt data, nor to the K_1 values for the alloys in Chapter 6. However, the K_4 values for the alloys showed such a sharp field dependence that an extrapolation was carried out using the form;

$$K_4 \Big|_{B=B_0} = K_4 \Big|_{B=\infty} (1 - C/(B_0^n)) \quad \dots(4.9)$$

where the power index, n , was adjusted to give a least-squares fit to the data. In fact a value of $n=1$ was optimum; in agreement with early measurements of the field dependence by Tarasov (1939) on silicon-iron.

4.2.5. Non-intrinsic torque effects

Phillips and Shepherd (1970) analysed the anisotropic torque produced by several non-intrinsic effects in torque magnetometry. Excluded from these are magnetostrictive terms in the anisotropy (intrinsic), ferromagnetic impurities in the sample support mechanism and the effect of stray magnetic field on the electrical components of the magnetometer. Included are the non-horizontal mounting of a sample disc, the ellipticity of a disc and the eccentricity of a specimen with respect to the magnetometer movement.

A non-horizontal disc tilted to a small angle α_0 from the plane of field rotation will generate a torque

$$\Gamma = -VB_0\sigma_s \rho (1 - \cos\alpha_0)\sin 2\theta \quad \dots(4.10)$$

assuming that the disc is thin and saturated to σ_s .

Typically, for a field of 1 tesla, magnetisation of 10^2 emu/g and density of 10^4 kg/m³, the contribution to the anisotropy constants (principally in the uniaxial case to K_1) would be about 10^3 J/m³ for a misalignment of 2° in the disc.

A slightly elliptical disc of fractional diameter variation, δ , and small thickness to diameter ratio, R , will produce a torque of;

$$\Gamma = \frac{3\mu_0(\sigma_s \rho)^2 \pi R \delta V}{16} \sin 2\theta \quad \dots(4.11)$$

which for $\delta=0.01$, $R=0.2$, $\rho=10^4 \text{ kg/m}^3$ and $\sigma_s=10^2 \text{ emu/g}$ gives an anisotropic energy contribution of about 10^3 J/m^3 , again principally to K_1 in the uniaxial case.

An eccentrically mounted specimen, in a uniform field gradient which rotates with the applied field, produces a resolved torque of;

$$\Gamma = v\sigma_s \rho \left(\frac{dB_0}{dx}\right) r \sin 2\theta \quad \dots(4.12)$$

where r is the distance between the centre of mass of the specimen and the rotation axis of the magnetometer. For $r=10^{-3} \text{ m}$, $\rho=10^4 \text{ kg/m}^3$, $\sigma_s=10^2 \text{ emu/g}$ and field gradient= 1 T/m , the contribution to anisotropy energy, again principally to K_1 , would be about 10^3 J/m^3 .

4.3. Existing magnetometers

The literature available reporting in detail the construction of torque magnetometers is extensive. Torque magnetometry as a technique was reported in 1905 by Weiss, and torque magnetometers have been described since then. The present survey concentrates mainly on equipment devised since 1950. Torsion susceptibility balances for fluids (eg Splittgerber and Gill, 1971) are excluded. Where possible, papers quoted refer to the initial reports of a type of instrument or an improvement made, rather than its use subsequently. Detail will be kept to a minimum and diagrams are schematic only. The purpose of this section is to indicate the background against which the mechanically simple yet effective magnetometer of chapter 6 was constructed.

Four aspects of the design of a torque magnetometer by which it can be conveniently classified are:

1) The support method by which the necessary rotations of the sample can take place (suspension fibre, leaf springs, air bearings, etc).

2) The method of detecting the position of the magnetometer movement if electrical feed-back is employed (photocells, inductance methods, capacitative methods, etc.).

3) The method of producing counter-torque on the sample (field coil, passive elastic, controlled elastic, quadrant electrometer, etc).

4) The method of reading the torque produced by the sample (light lever and scale, capacitative, inductive or resistive transducers, etc.)

Table 4.1 gives the specification of several magnetometers according to this scheme against the authors reporting them (full references appear at the back of this thesis). Sensitivity ranges are quoted where available, the most sensitive extreme corresponding to experimental noise. Cross-references are given to relevant illustrations (figures 4.2 - 4.29).

Historically the first torque magnetometer was that of Weiss (1905) who measured the anisotropy of pyrrhotite. The design is perhaps the simplest possible and illustrated in figure 4.2. Sevastyanov (1960), using a 5 μ m quartz fibre, achieved sensitivities of 5×10^{-12} Nm using essentially this method. The misorientation of a suspension fibre, twisted so as to maintain a fixed sample alignment in a rotating field, indicated the torque on the sample.

TABLE 4-1

<u>AUTHORS</u>	<u>SUPPORT</u>	<u>DETECTION OF MOVEMENT</u>	<u>COUNTER- TORSION</u>	<u>QUANTITY READ</u>	<u>SENSITIVITY</u>	<u>FIG. NO.</u>
WEISS (1905)	SINGLE FIBRE	LIGHT LEVER AND SCALE	MANUAL TWIST OF FIBRE	OVERALL FIBRE TWIST	-	4.2
SEVAST'YANOV (1960)	SINGLE FIBRE	LIGHT LEVER AND SCALE	MANUAL TWIST OF FIBRE	OVERALL FIBRE TWIST	$5 \cdot 10^{-12}$ Nm (MOST SENSITIVE)	-
WILLIAMS (1938)	TWIN JEWEL BEARINGS	POINTERS ON TORSION WIRE	MANUAL TWIST OF FIBRE	MISALIGN- MENT OF POINTERS	-	4.3
TARASOV AND BITTER (1937)	HORIZONTAL KNIFE EDGES ON SAMPLE AXIS	POINTER AND SCALE	WEIGHTS ON A LEVER	WEIGHT APPLIED	-	-
MILLER (1950)	TWIN JEWEL BEARINGS	STRAIN- GAUGE	STRAIN- GAUGE ELASTICITY	STRAIN- GAUGE OUTPUT	$5 \cdot 10^{-3}$ Nm (LEAST SENSITIVE)	4.4
BYRNES AND CRAWFORD (1958)	TWIN PIVOT BEARINGS	STRAIN- GAUGE	STRAIN- GAUGE ELASTICITY	STRAIN- GAUGE OUTPUT	$7 \cdot 10^{-3}$ (LEAST SENSITIVE)	4.5
CROFT ET AL (1955)	SINGLE FIBRE	LIGHT LEVER AND PHOTOCELLS	COIL IN AUXILLIARY FIELD	RESTORING CURRENT IN COIL	-	4.6
PEARSON (1956)	DOUBLE FIBRE	LIGHT LEVER AND PHOTOCELLS	COIL IN AUXILLIARY FIELD	RESTORING CURRENT IN COIL	10^{-7} - $5 \cdot 10^{-5}$ Nm	4.7
GERGER AND VILIM (1968)	DOUBLE FIBRE	LIGHT LEVER AND PHOTOCELLS	COIL IN AUXILLIARY FIELD	RESTORING CURRENT IN COIL	10^{-6} - 10^{-3} Nm	4.6
AUBERT (1966)	SINGLE FIBRE AND CENTRING WEIGHT	LIGHT LEVER AND PHOTOCELLS	COIL IN AUXILLIARY FIELD	RESTORING CURRENT IN COIL	10^{-7} - 10^{-2} Nm	4.8
HUMPHREY AND JOHNSTON (1963)	DOUBLE FIBRE	LIGHT MASK AND PHOTOCELLS	CONDUCTOR IN AUXILLIARY FIELD	RESTORING CURRENT IN CONDUCTOR	10^{-13} Nm (MOST SENSITIVE)	4.9
PENGYER (1959)	JEWEL AND AIR- BEARING	LIGHT LEVER AND PHOTOCELLS	COIL IN AUXILLIARY FIELD	RESTORING CURRENT IN COIL	10^{-7} - 10^{-2} Nm	4.10
KAXIM (1968)	JEWEL AND MAGNETIC BEARING	LIGHT LEVER AND PHOTOCELLS	COIL IN AUXILLIARY FIELD	RESTORING CURRENT IN COIL	10^{-9} - $2 \cdot 10^{-3}$ Nm	4.11
WILLEY ET AL (1972)	DOUBLE AIR- BEARINGS	LIGHT LEVER AND PHOTOCELLS	COIL IN AUXILLIARY FIELD	RESTORING CURRENT IN COIL	10^{-5} - 10^{-3} Nm	4.12
ABE AND CHIKAZUMI (1978)	TRIPLE LEAF- SPRINGS	LIGHT LEVER AND PHOTOCELLS	COIL IN AUXILLIARY FIELD	RESTORING CURRENT IN COIL	10^{-6} 10^{-2} Nm	-
BRANSKY ET AL (1968)	DOUBLE RIBBON AND JEWEL BEARING	LIGHT MASK AND PHOTOCELLS	COIL IN AUXILLIARY FIELD	RESTORING CURRENT IN COIL	$2 \cdot 10^{-11}$ Nm (MOST SENSITIVE)	4.13
WESTWOOD ET AL (1970)	JEWEL AND PLAIN BEARING	LIGHT MASK AND PHOTOCELLS	COIL IN AUXILLIARY FIELD	RESTORING CURRENT IN COIL	$5 \cdot 10^{-9}$ Nm (MOST SENSITIVE)	4.14

TABLE 4-1 cont.

<u>AUTHORS</u>	<u>SUPPORT</u>	<u>DETECTION OF MOVEMENT</u>	<u>COUNTER- TORQUE</u>	<u>QUANTITY READ</u>	<u>SENSITIVITY</u>	<u>FIG. No.</u>
CONDON AND NARCUS (1964)	SINGLE FIBRE	A.C. INDUCTION INTO COIL	D.C. CURRENT TO SAME COIL IN A FIELD	D.C. CURRENT RESTORING COIL	10^{-11} - 10^{-7} Nm	4.15
VANDERKOOY (1969)	DOUBLE FIBRE	A.C. INDUCTION INTO COIL	D.C. CURRENT TO SAME COIL IN A FIELD	D.C. CURRENT RESTORING COIL	10^{-9} Nm (MOST SENSITIVE)	4.16
VERGE ET AL (1976)	DOUBLE JEWEL BEARINGS	A.C. INDUCTION INTO COIL(S)	D.C. CURRENT TO SAME COIL IN A FIELD	D.C. CURRENT RESTORING COIL(S)	$5 \cdot 10^{-9}$ - 10^{-3} Nm	4.17
VOIGT AND FOWER (1972)	DOUBLE FIBRE	VARIABLE CAPACITOR	COIL IN MAIN FIELD	RESTORING CURRENT IN COIL	10^{-7} - 10^{-3} Nm	4.18
SATO AND CHANDRASEKHAR (1957)	SINGLE FIBRE	LIGHT LEVER AND PHOTOCELLS	MOTORIZED TWIST OF FIBRE	FIBRE TWIST SCALE AND MICROSCOPE	-	4.19
KING ET AL (1964)	SINGLE FIBRE	LIGHT LEVER AND PHOTOCELLS	QUADRANT ELECTROMETER	RESTORING VOLTAGE OF ELECTROMETER	10^{-11} Nm (MOST SENSITIVE)	4.20
REUGEBAUER (1959)	SINGLE FIBRE	LIGHT LEVER AND SCALE	HANDUAL TWIST OF FIBRE	FIBRE TWIST READ ON LIGHT SCALE	-	4.21
TELESNIA ET AL (1964)	SINGLE FIBRE	LIGHT LEVER AND SCALE	HANDUAL TWIST OF FIBRE	OVERALL FIBRE TWIST	10^{-11} Nm (MOST SENSITIVE)	4.22
SHELLENG AND RADC (1969)	TWIN JEWEL BEARINGS	SCALE AND MICROSCOPE	HANDUAL TWIST OF FIBRE	AS READ ON SCALE	-	4.23
GENGAGEL ET AL (1963)	DOUBLE FIBRE	LIGHT LEVER AND PHOTOCELLS	PASSIVE FIBRE	MOVEMENT OF TRACKED PHOTOCELLS	10^{-7} - $5 \cdot 10^{-3}$ Nm	4.24
ALDENKAMP ET AL (1960)	TRIPLE LEAF- SPRINGS	A.C. INDUCTION INTO COIL	PASSIVE LEAF- SPRINGS	INDUCED A.C.	10^{-6} - 10^{-3} Nm	4.25
BURD ET AL (1977)	TRIPLE LEAF- SPRINGS	LIGHT LEVER AND SCALE	PASSIVE LEAF- SPRINGS	AS READ ON SCALE	-	4.25
BIRSS AND SHEPHERD (1978)	TRIPLE LEAF- SPRINGS	VARIABLE CAPACITOR	PASSIVE LEAF- SPRINGS	CAPACITANCE MEASUREMENT	-	4.25
GRIESEN (1973)	QUADRUPLE LEAF- SPRINGS	VARIABLE CAPACITOR	PASSIVE LEAF- SPRINGS	CAPACITANCE MEASUREMENT	-	4.26
BIRSS AND WALLIS (1983)	FIBRE AND WIRE CRADLE	RESISTIVE CHANGE IN WIRE CRADLE	STRETCH OF CRADLE WIRES	RESISTANCE OF STRAINED WIRES	$3 \cdot 10^{-7}$ - $5 \cdot 10^{-4}$ Nm	4.27
TAJIMA AND CHIKAZUMI (1967)	PHOSPHOR- BRONZE CAGE	STRAIN- GAUGES ON CAGE	DISTORTION OF CAGE	STRAIN- GAUGE OUTPUTS	$5 \cdot 10^{-4}$ - 10^{-2} Nm	4.28
WARNOCK (1965)	RADIAL LEAF- SPRINGS	STRAIN- GAUGES ON LEAF- SPRINGS	PASSIVE LEAF- SPRINGS	STRAIN- GAUGE OUTPUTS	10^{-5} - 10^{-1} Nm	4.29

SIMPLIFIED DIAGRAM OF THE TORQUE MAGNETOMETER OF WEISS

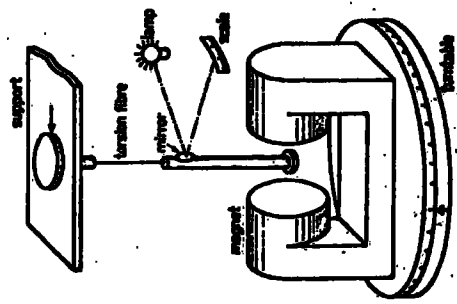


Fig 4.2

Torque meter with reversible magnet. When rotating the magnet the torsion balance is held in its null position (indicated by a light beam on the scale) by adjusting the twist of the torsion fibre.

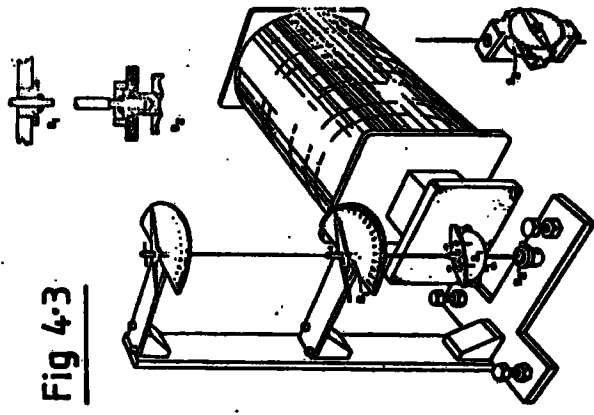


Fig 4.3

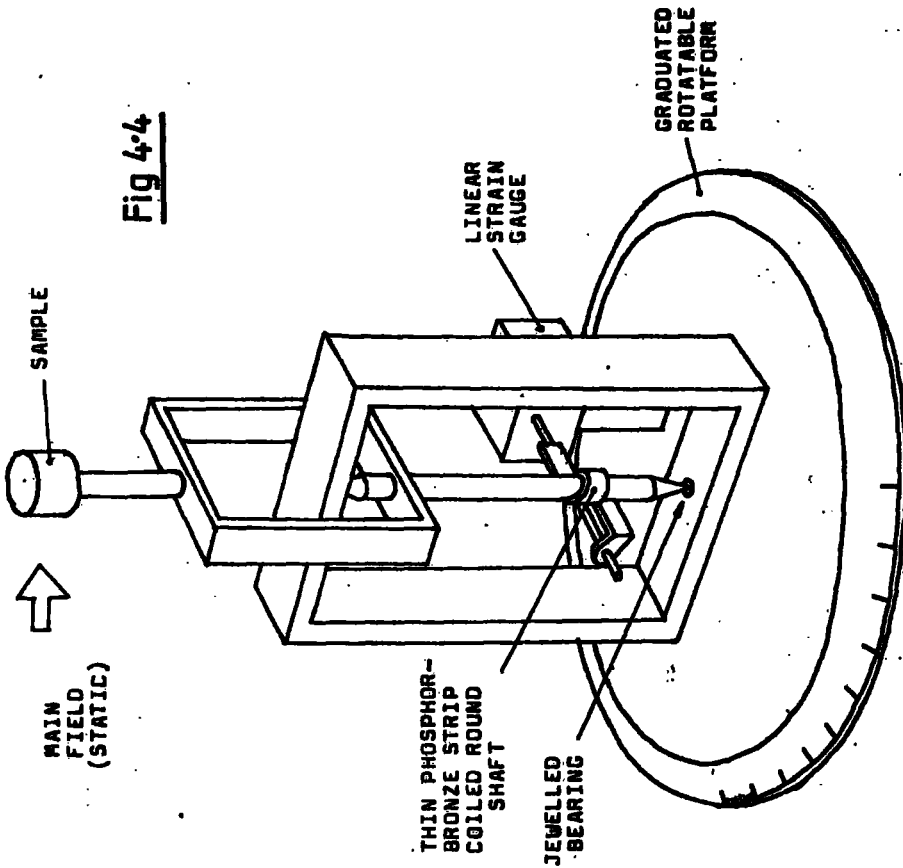
The torsion magnetometer with half of the electromagnet removed.

THE TORQUE MAGNETOMETER OF WILLIAMS

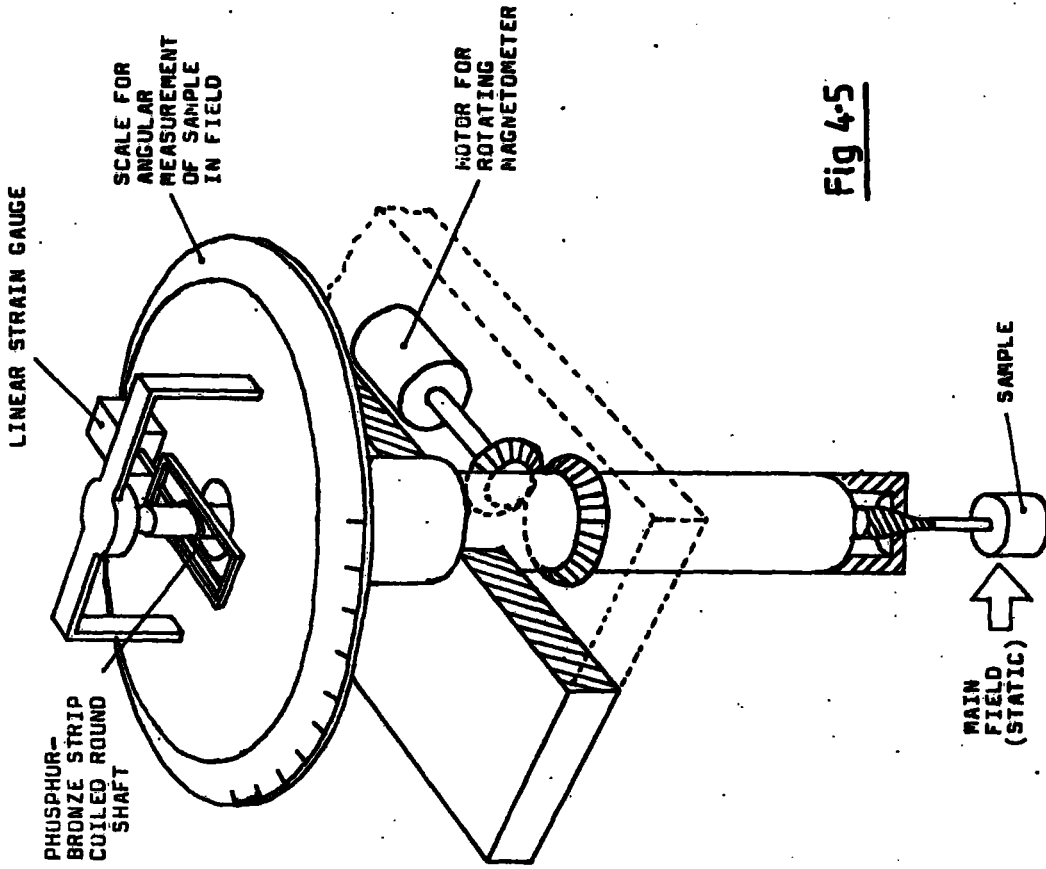
The arrangement is still used in paleomagnetic devices (eg Stacey, 1960, and Stacey and Banerjee, 1967) However Harrison (1955) has shown that a fibre suspension of this kind can be unstable for low torsional constants and large twists, in that the sum of the anisotropy and torsional energies may be a maximum at a point of torsional balance, rather than a minimum. Consequently, there has been only limited adoption of this technique where accurate relative torque measurements are required.

Two notable early magnetometers were those of Williams (1936) and Tarasov and Bitter (1937) of which the former is illustrated in figure 4.3. Williams used a calibrated phosphor-bronze torsion fibre in a version of the Weiss magnetometer having a movement guided in jewel bearings. The misalignment of the two pointers, at the top and bottom of the fibre, indicated torque. The latter used a modified commercial balance acted upon by the torque of the sample fixed coaxially to the axis of the horizontal bar of the balance to achieve a relative torque accuracy of about 0.2%. The field necessarily rotated in a vertical plane; a configuration never reported subsequently.

The first torque magnetometer to drive a pen recorder, to produce continuous torque curves automatically, was that of Miller (1950). A shaft held between jewel bearings was coupled to a linear strain transducer by a phosphor-bronze strip coiled once round the shaft (fig. 4.4). Shaft motion, due to the torque on the sample, winched the strip so as to move the transducer. The whole was carried on a rotating table between magnet pole pieces. A position



SIMPLIFIED DIAGRAM OF THE TORQUE MAGNETOMETER OF MILLER



SIMPLIFIED DIAGRAM OF THE TORQUE MAGNETOMETER OF BYRNES AND CRAWFORD

THIS MAGNETOMETER IS SIMILAR IN OPERATION TO THAT OF MILLER AND REPRESENTS A DEVELOPMENT OF IT.

potentiometer relayed a voltage, proportional to magnetometer angle, to an X-Y recorder fed simultaneously by the transducer to produce torque curves. A development of this design was reported by Byrnes and Crawford (1957 and fig. 4.5). This type of head fell into disuse, but automatic recording of torque curves is now almost standard. Apart from the previous two magnetometers, those devised after 1950 are generally still in use in some form today.

1955 brought the development of a torque magnetometer featuring a fibre suspension with automatic electrical feedback in which the torque on a sample in the main field was counteracted by a current-carrying coil in an auxiliary field controlled by electro-optical measurement of the twist of the suspension from equilibrium (Croft et al. 1955). The coil current required to prevent appreciable movement of the suspension indicated torque and was fed to a pen recorder. The suspension was oil-damped using a circular conduit and paddles shown in figure 4.6 (minus the lower suspension fibre). A high sensitivity duplicate made by Boyd (1960) could detect torques of 10^{-10} Nm. A variation on these magnetometers was that of Pearson (1956) and recent high sensitivity developments of it (eg Jayaraman and Dutta-Roy, 1976), in which a lower fibre tensioned the movement to improve lateral stability. A magnetometer of this type was used in the K_4 analysis of the terbium/gadolinium alloys of chapter 8. Gerber and Vilim (1968) also held the movement between two fibres with the lower fibre a carefully optimised distance down

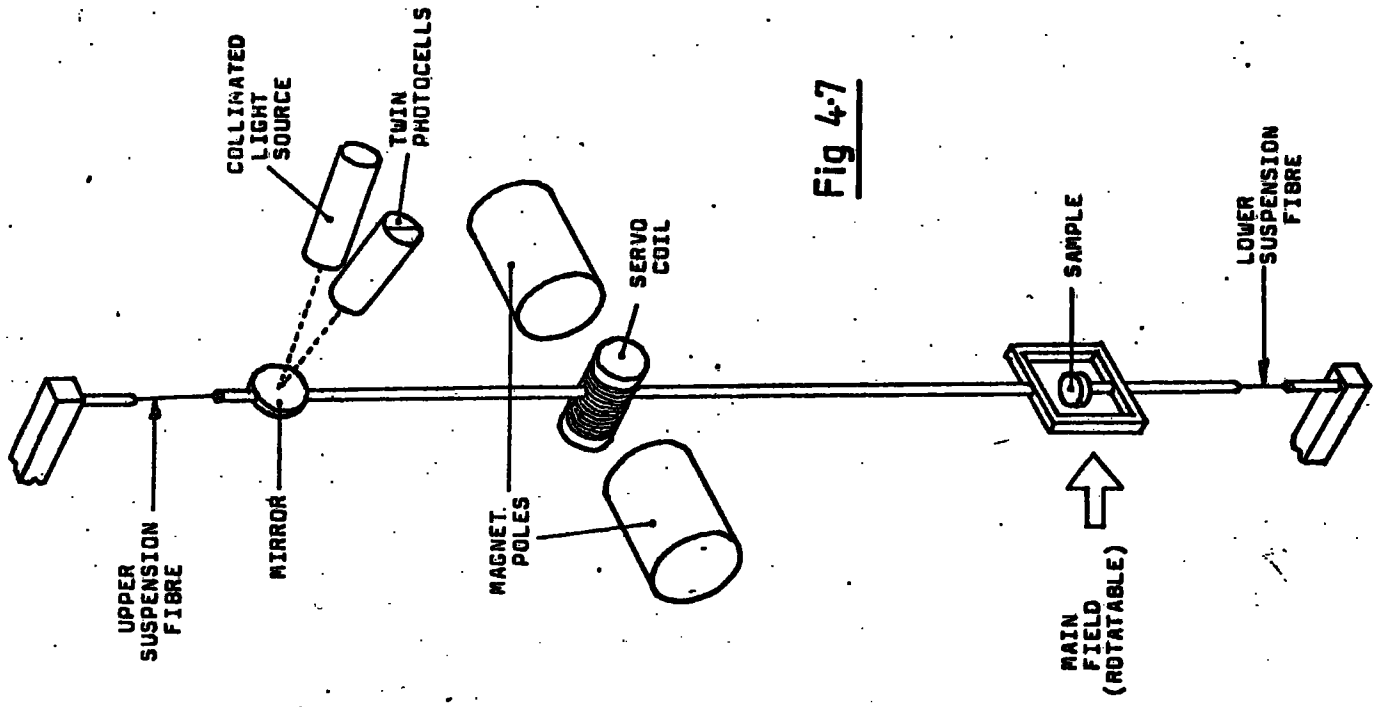


Fig 4-7

SIMPLIFIED DIAGRAM OF THE TORQUE MAGNETOMETER OF PEARSON

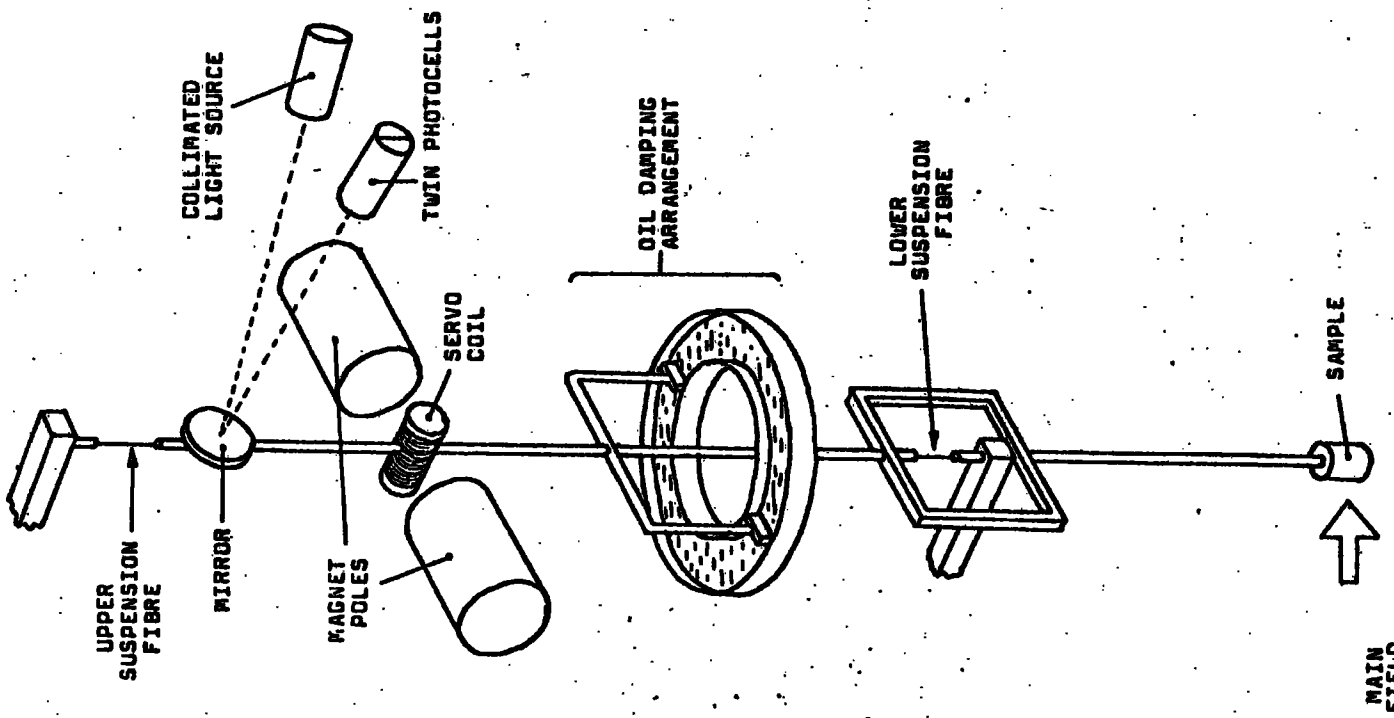


Fig 4-6

OF THOSE OF CROFT ET AL., GENSER AND O'LEARY, FLETCHER ET AL., WILSON ET AL.

the movement in a frame accomodating it giving a compromise between lateral stability and thermal isolation of the sample at the tip. This magnetometer had all the features of figure 4.6. Wilson et al. (1977) reported on-line torque analysis from such a device (without the oil-damping) with the whole magnetometer driven round in a fixed field by a stepper-motor controlled by the computer. Commercial galvanometer coils were inevitably used in this kind of design when small torques were being measured. The magnetometer of Croft et al. was enclosed in a vacuum system and operated in conjunction with a cryostat to allow measurements of the temperature dependence of the anisotropy. Low temperature facilities were common thereafter.

The magnetometer of Fletcher et al. (1969) was a simple high sensitivity device (10^{-8} - 10^{-4} Nm) of the Croft type (as in figure 4.6 minus lower suspension fibre and oil-damping) for use up to 1000 K with a readily interchangeable fibre allowing several sensitivity ranges. Larsen and Livesay (1979) described a similar device for use in a pressurised hydrogen environment up to about 200 atm. Interchangeable balancing coils gave a torque range of 10^{-11} - 10^{-4} Nm. An L.E.D. light source was used to survive the pressures since the optical parts were contained within the pressure vessel. Data was collected and processed on-line by a computer.

Escudier (1975) reported a double fibre suspension like that of Gerber and Vilim with the interposed member fixed and having a large mobile surrounding frame continuing

down to the sample. This instrument could measure relative torque changes of 10^{-5} by particularly accurate current measurements through the balancing coil. Of similar relative accuracy was the magnetometer of Aubert, constructed at the same institution, in which the lateral stability of the sample was maintained by a large weight on the fibre suspension (fig. 4.8) and the usual photocells and balancing coil enabled torsional feedback.

A high sensitivity magnetometer using a simple current-carrying wire in a field to create the balancing torque, rather than a coil, was reported by Humphrey and Johnston (1963) and is illustrated in figure 4.9. The conducting element was fed through the gold coating on the double quartz suspension fibres, the element also forming a mask which occluded twin photocells in the feedback process.

The use of torsional feedback by a balancing coil in an auxiliary magnetic field was also a common feature in torque magnetometers partially or entirely without suspension fibres. Furthermore, as will be seen, instruments appeared in which the method of determining the movement of the suspension in the feedback process involved entirely electrical methods (usually inductive).

Of the magnetometers that depart from the Croft et al. tradition in the support of the suspension, notable are those of Penoyer (1959), Maxim (1968), Willey et al. (1972) and Abe and Chikazumi (1976). Penoyer achieved support of the suspension using a jewel, on the undersurface of the balancing coil frame, resting on a steel point, and lateral stability was provided at the lower end by an

air-bearing in which an air cushion isolated the moving surfaces (fig. 4.10). Maxim used the upper jewel bearing design of Penoyer but used a main field with an intentional inhomogeneity of a form which attracted the sample to the centre of the pole-piece gap providing lateral stability. The pole-piece faces were indented in order to achieve this (fig. 4.11). Willey et al. used opposing conical air-bearings to support the suspension and achieve a robust and sensitive magnetometer (fig. 4.12). Abe and Chikazumi used a triple leaf-spring cage in which the lower end of the vertical radial leaf-springs were fixed in an inverted version of figure 4.25 where the weight of the movement attached to the upper disc virtually counteracted the torsional restraint of the springs by its tendency to cause rotational collapse. The geometry of the springs constrained the suspension to rotate about a single axis with inherent lateral stability. However the counter-torque was still provided mainly by a coil rather than elastically. The Abe and Chikazumi suspended body was complex, and involved twin stepper-motors to control a sample support-platform in three dimensions under computer control. It provided automatic sample orientation, without X-ray analysis, by inspection of the torque curves.

Two magnetometers of further note which involved balancing coils in auxiliary fields were those of Bransky et al. (1968) and Westwood et al. (1970). The former magnetometer (fig. 4.13) utilised a commercial electrobalance turned through 90° with the counter torque

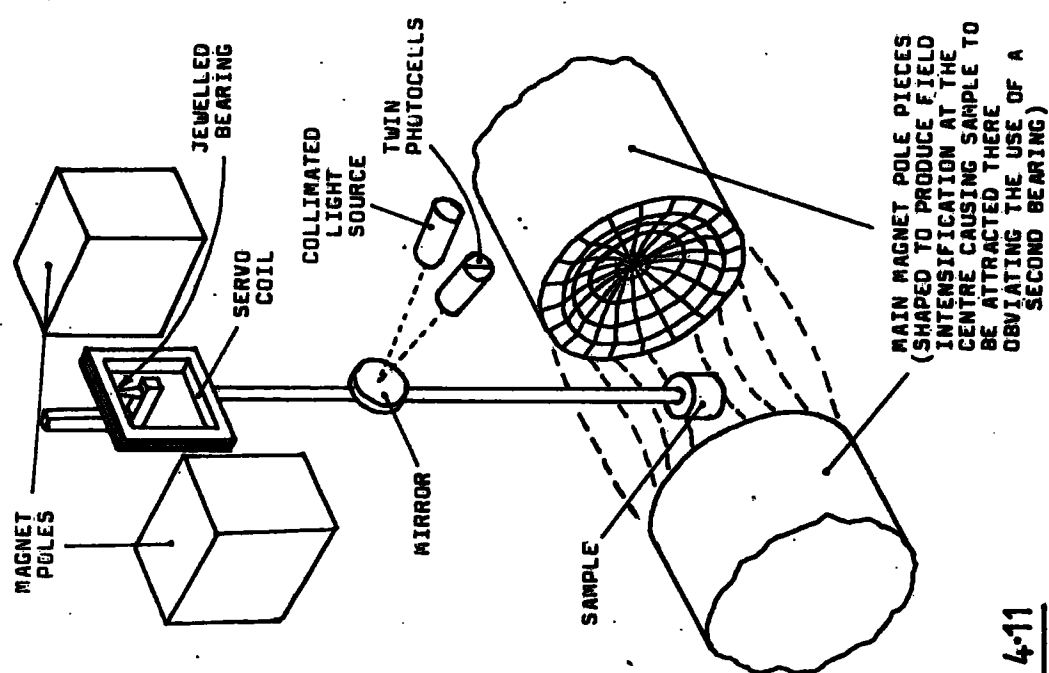


Fig 4-11

SIMPLIFIED DIAGRAM OF THE TORQUE MAGNETOMETER OF MAXIM

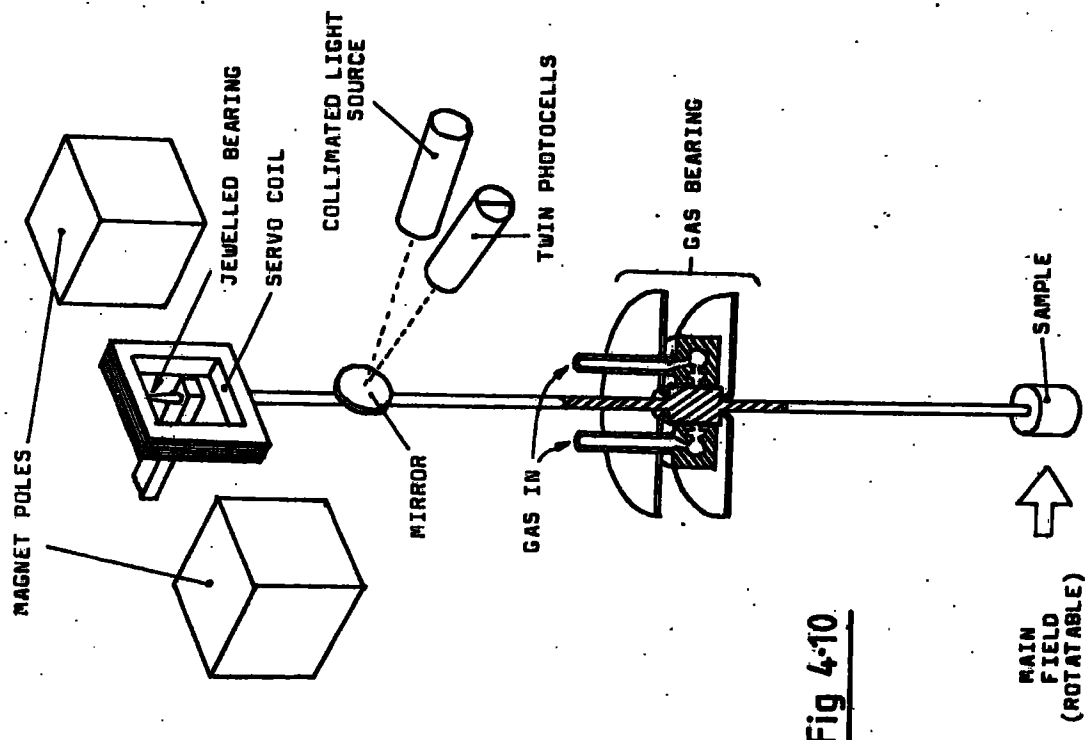


Fig 4-10

SIMPLIFIED DIAGRAM OF THE TORQUE MAGNETOMETER OF PENOYER

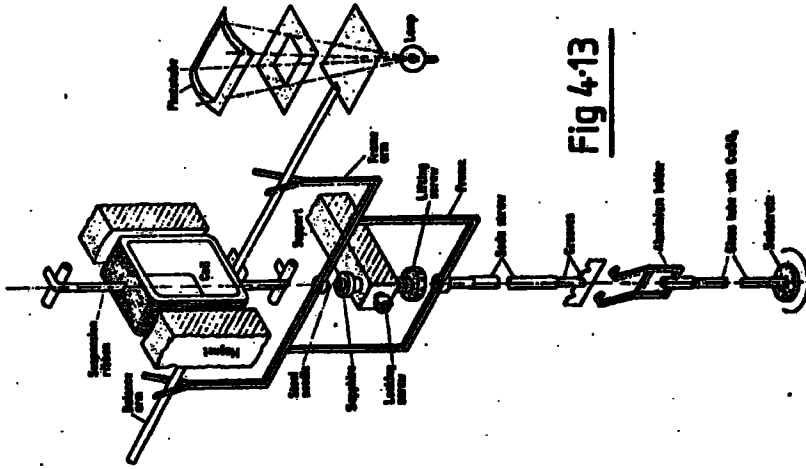


Fig 4-13

THE TORQUE MAGNETOMETER
OF BRANSKY ET AL.

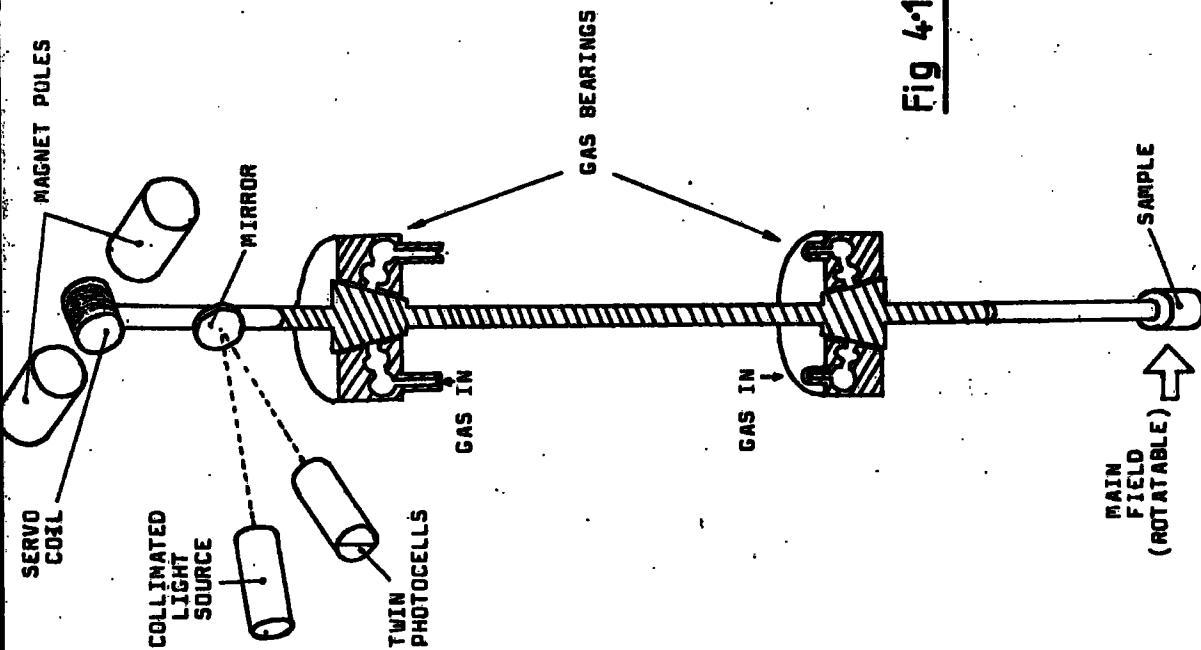


Fig 4-12

SIMPLIFIED DIAGRAM OF THE TORQUE MAGNETOMETER OF WILLEY ET AL
TWIN GAS BEARINGS REPRESENT THE NOVELTY.

coil from the original balance supported by double suspension ribbons. The coil was jointed through a double fork and bar arrangement to turn the rest of the movement, which rested on a jewel bearing. The sensing of the suspension orientation was by an eccentric mask and photocells. The instrument of Westwood was essentially a low sensitivity device for use in an undergraduate laboratory. A jewel bearing took the suspension weight and a plain bearing centred the lower end (fig. 4.14), with a mask and photocells controlling the balancing coil current.

A magnetometer using a balancing coil in an auxiliary field was constructed by Condon and Marcus (1964). It differed from those discussed previously in that two supplementary Helmholtz-like coils were attached to the poles of the balancing coil magnet to induce a high frequency a.c. voltage in the balancing coil in proportion to its deviation with respect to the coil-pair perpendicular. The induced signal was fed to a phase-sensitive amplifier which controlled a d.c. current, running simultaneously through the balancing coil, in such a way as to provide the necessary counter torque to fix the balancing coil at 90° to the pair. D.c. current indicated torque as usual. Following the very simple method of Rhyne and McGuire (1967), who used a balancing coil in the main field along side the sample to counteract the anisotropy torque, Vanderkooy (1969) and Verge et al. (1976) produced two very simple magnetometers adopting the Condon and Marcus position sensing method.

The magnetometers of Vanderkooy and Verge were both

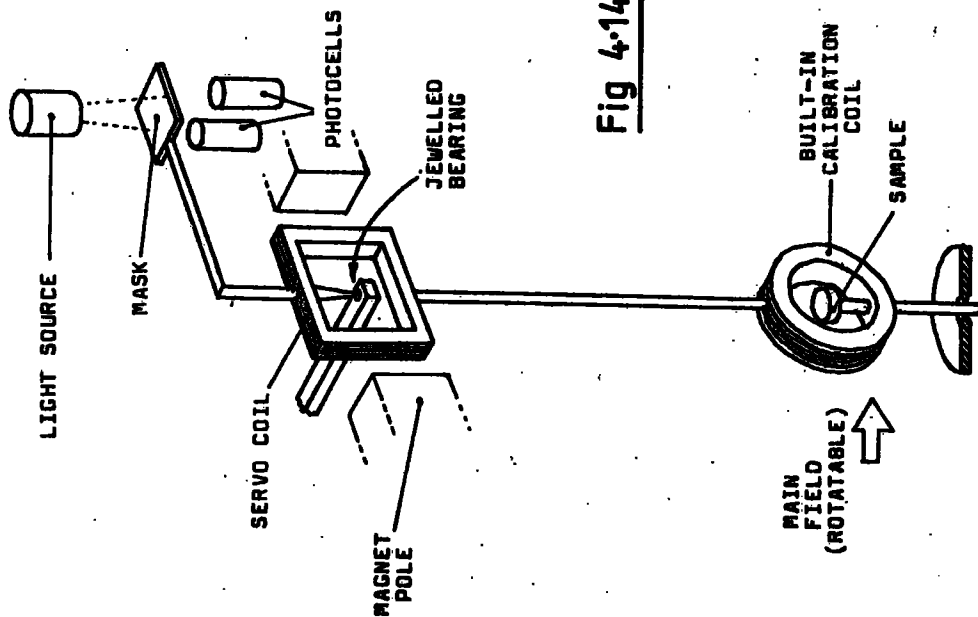


Fig 4-14

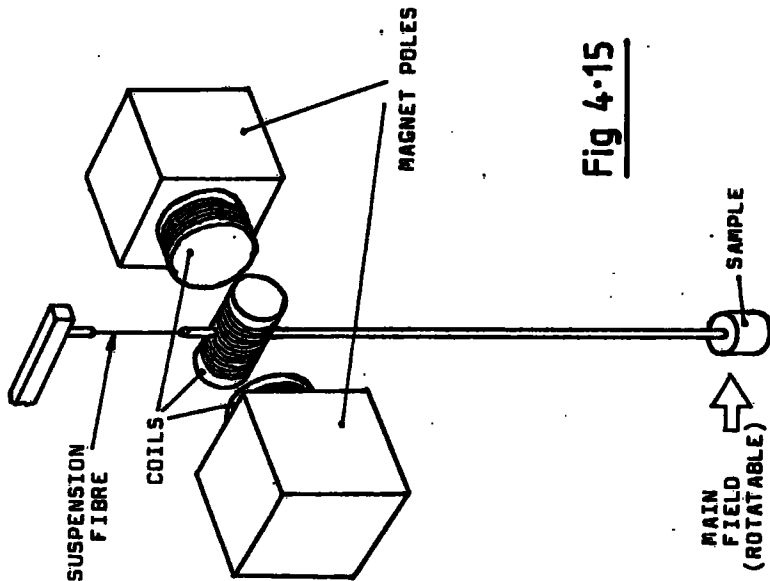


Fig 4-15

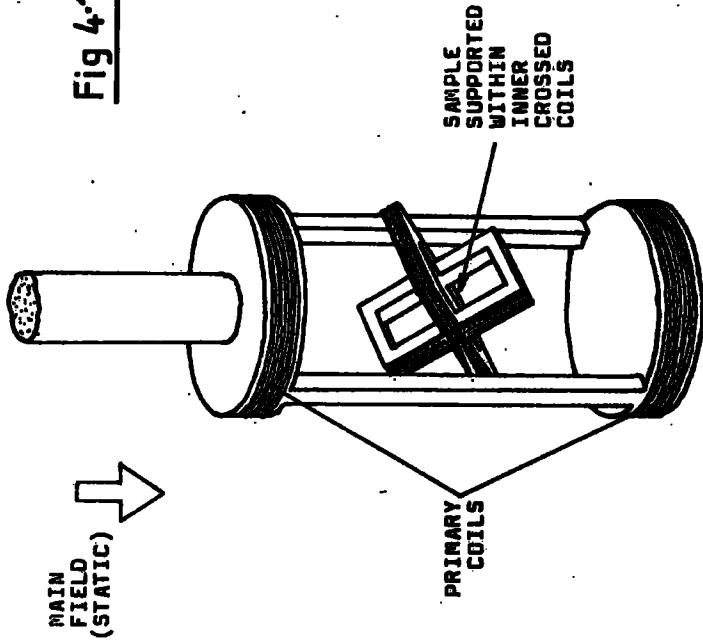
SIMPLIFIED DIAGRAM OF THE TORQUE MAGNETOMETER OF CONDON AND MARCUS

SIMPLIFIED DIAGRAM OF THE TORQUE MAGNETOMETER OF WESTWOOD ET AL

suitable for use in the bores of solenoids, with sample rotation occurring on an axis perpendicular to the bore. The magnetometer of Vanderkooy is illustrated in figure 4.16. Using the solenoid field itself to create the counter-torque, the d.c. field of the balancing coil stabilised the sample orientation at an angle where the a.c. signal induced in the balancing coil from the static coil pair was minimised at the input of the phase sensitive amplifier supplying the d.c. current. The necessary adaptation to the Condon and Marcus method was to add an artificial signal to the a.c. output of the balancing coil so that the phase sensitive amplifier minimised the sum of the signals to produce an equilibrium balancing coil position deviating from 90° to the static pair by an amount depending on the phase and amplitude of the added signal. Vanderkooy found the $\pm 60^\circ$ movement of balancing coil and sample were practical with the constraints of the coil leads and the diminishing efficiency of the balancing coil as it approached parallelism with the solenoid field. Verge et al. improved the magnetometer of Vanderkooy by introducing two balancing coils, set at 90° (fig. 4.17), and summing the a.c. outputs so as to produce a positional signal of changing phase rather than amplitude (c.f. the synchro-resolver in machine servo systems). Direct current was fed to the two coils in such a proportion as to produce a positional stability of constant compliance with respect to sample orientation. Verge achieved a $\pm 100^\circ$ rotation.

Voigt and Foner (1972) have reported a magnetometer suitable for use in a solenoid, in which a balancing coil

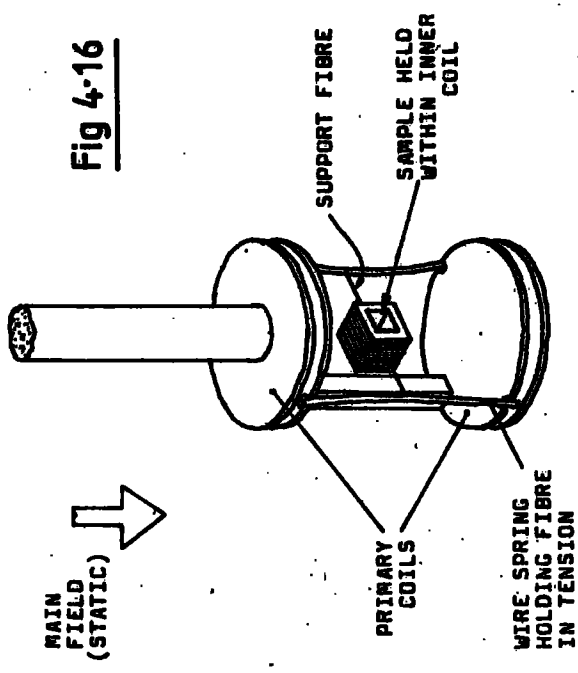
Fig 4-17



SIMPLIFIED DIAGRAM OF THE TORQUE MAGNETOMETER OF VERGE ET AL

SUITABLE FOR WORK IN THE BORE OF A SOLENOID.

Fig 4-16



SIMPLIFIED DIAGRAM OF THE TORQUE MAGNETOMETER OF VANDERKOOIJ

SUITABLE FOR INSERTION INTO THE BORE OF A SOLENOID.

like that of Vanderkooy was rotated physically in a small cage by a worm gear with the coil current controlled so as to stabilise the capacitance between a semicircular plate on the coil and a semicircular plate on the cage (fig. 4.18).

In the category of magnetometers of the type suited to a normal iron-yoke electromagnet and using a fibre suspension, was the magnetometer of Sato and Chandrasekhar (1957) who achieved torsional feedback using a motor driven support which twisted the top of the suspension fibre so as to counteract the torque (fig. 4.19). Barron and Hoffman (1970) reported a similar instrument with the motor drive passing through magnetic linkages into a high vacuum enclosure around the magnetometer.

Again, of those magnetometers suited to the normal iron-yoke electromagnet and using fibre suspensions, were three notable high sensitivity torque magnetometers using the restoring force of a quadrant electrometer. A general paper on the use of quadrant electrometers to measure small torsional movements is given by de Boer et al. (1980). King et al. (1964) produced an instrument with electro-optical position sensing to establish feedback through the electrometer potential (fig. 4.20), and two similar instruments were devised subsequently; Dey (1972) and Gradmann et al. (1976). These instruments were suited to anisotropy measurements on thin films and have a sensitivity greater than those of the coil feedback magnetometers, that is typically 10^{-11} Nm.

Three magnetometers have been devised for specialised work on thin films, deposited on a substrate within the

**SIMPLIFIED DIAGRAM OF THE TORQUE MAGNETOMETER
OF SATO AND CHANDRASEKAR**

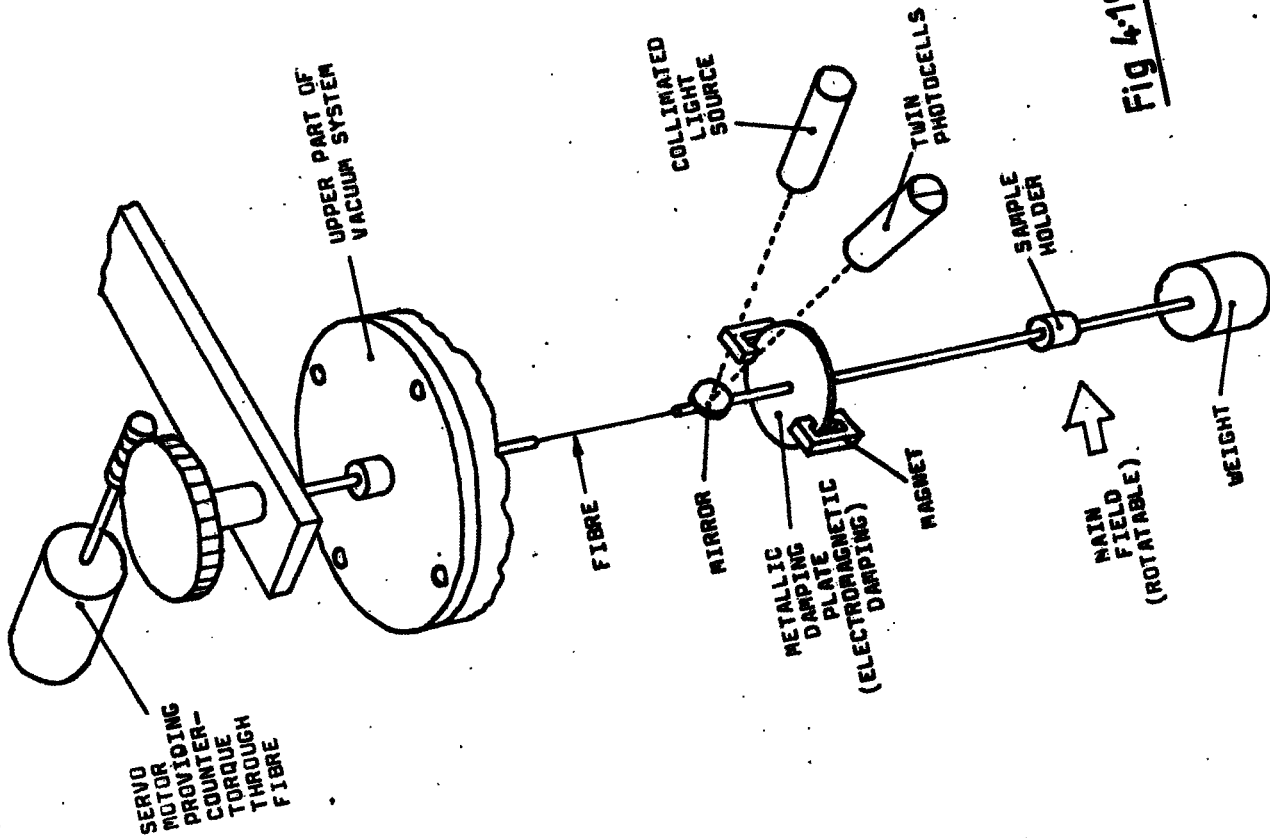
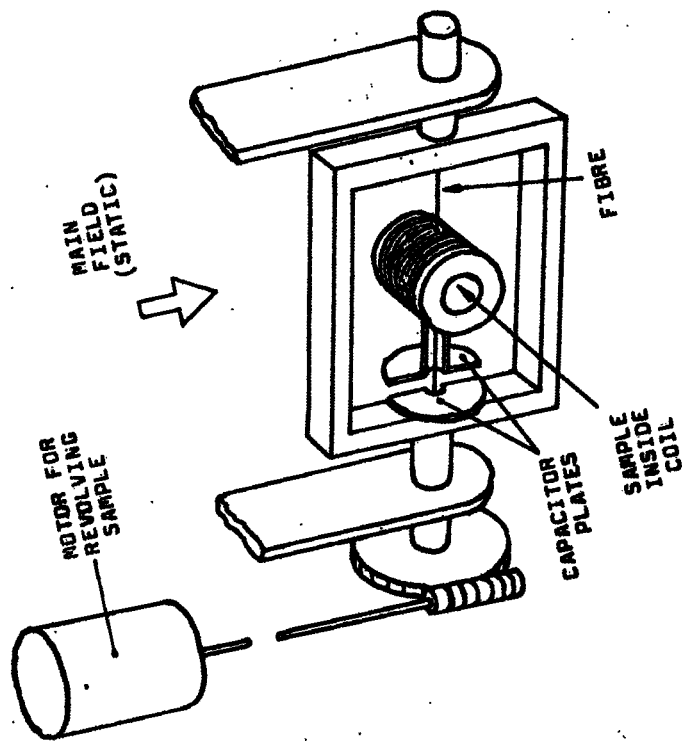


Fig 4-19

Fig 4-18



**SIMPLIFIED DIAGRAM OF THE TORQUE MAGNETOMETER
OF VOIGT AND TONER**

SUITABLE FOR INSERTION INTO THE BORE OF A SOLENOID.

MAGNETIC COUPLING FOR RAISING AND LOWERING SUBSTRATE VIA PULLEY

Fig 4:21

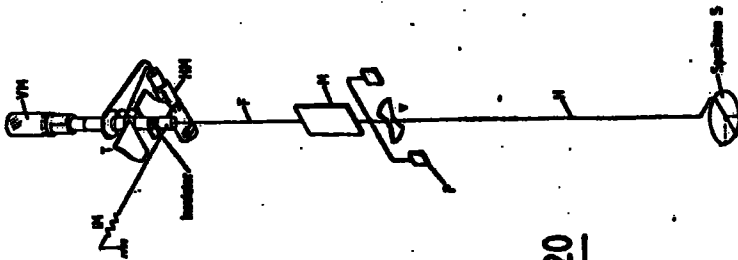
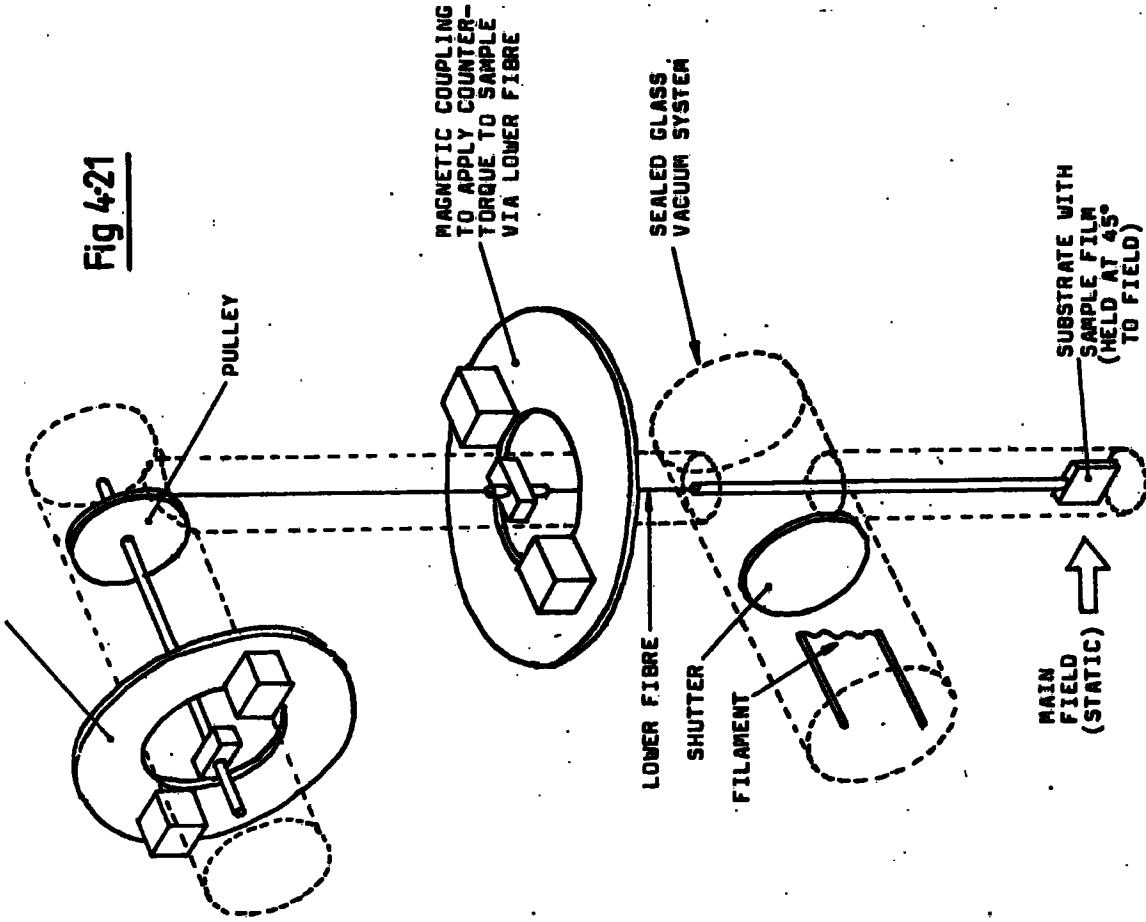


Fig 4:20

Schematic diagram of suspended system.
 F, phosphor bronze fibre; M, mirror; P, parallel; V, suspended vanes; H, specimen holder; VM, vertical micrometer; HM, horizontal micrometer; T, torsion bar.

THE TORQUE MAGNETOMETER
OF KYNG ET AL

magnetometer in high vacuum, using the simple Weiss fibre. In the design of Neugebauer (1959 and fig. 4.21) the substrate was lifted, by a pulley operated by magnets external to the vacuum system, into the main field after deposition of the film. The devices of Graham and Lommel (1962) and Telesnin (1964) deposited the film with the substrate in situ. The benefit of the fibre was that it could be conveniently twisted by the magnetic linkages (Neugebauer, Graham and Lommel) or by a shaft rotating in an 'O'-ring seal (Telesnin and fig. 4.22) to produce a simple magnetometer having very few parts within the (high) vacuum system.

An adaptation of the simple manually twisted fibre design for use in the bore of a solenoid was that of Schelleng and Rado (1969) in which the sample was supported transversely on a shaft, held between jewel bearings in the solenoid bore, driven by a cotton thread around a coaxial pulley. A similar pulley, supported on jewel bearings above the solenoid, tensioned the thread and was acted upon by a phosphor-bronze fibre. A micrometer read the misalignment between the ends of the fibre to yield torque (fig. 5.23).

Gengnagel et al. (1963) reported a magnetometer in which two thick fibres were used to support the magnetometer movement without electrical feedback to the suspension. An automated output was provided by tapping the control voltage of a servo motor which moved twin photocells on rails transversely to a light lever reflected from a mirror on the suspension. The torsion fibre was interchangeable, providing different sensitivities, and the instrument had the usual vacuum jacket and heating facilities. The magnetometer

THE TORQUE MAGNETOMETER OF IELESNIN ET AL

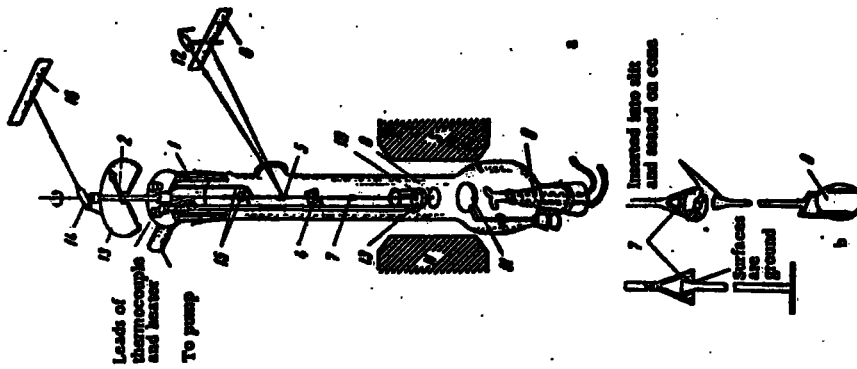
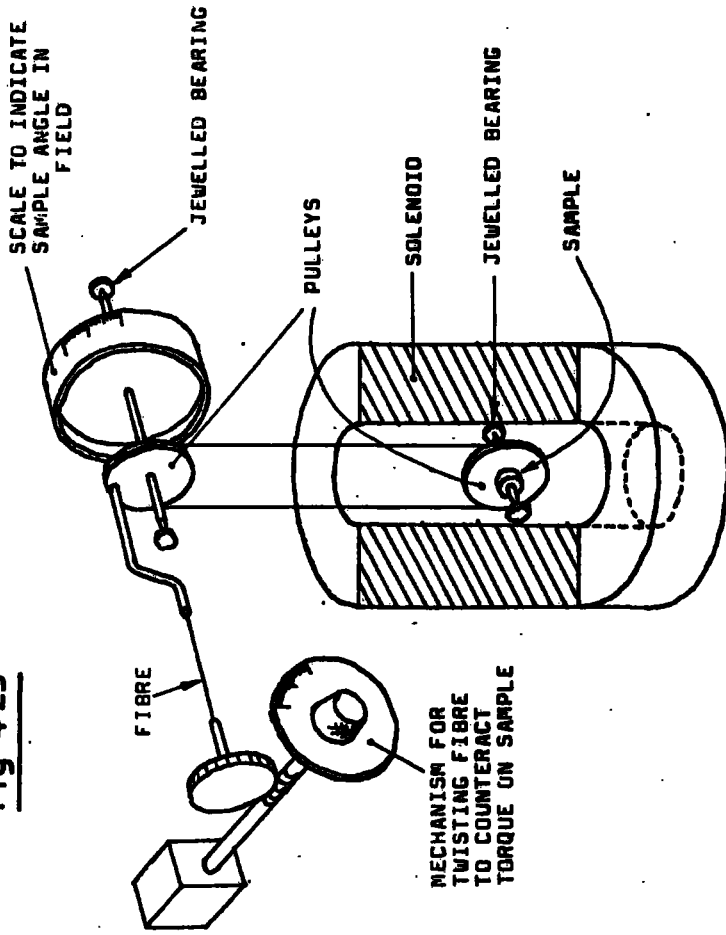


Fig 4-22

- a) Magnetometer. 1) Quartz fiber; 2) ground-glass joint with indication; 3) dial; 4) damper; 5) mirror scale; 6) mirror scale; 7) cone with slit; 8) backing; 9) ground-glass joint with spacers; 10) backing heater; 11) shield; 12) illumination; 13) thermocouple; 14) optical device for accurate reading of angle of torsion of fiber; 15) stop; 16) mirror scale.
- b) Connection of object holder to suspension system of magnetometer.

Fig 4-23



SIMPLIFIED DIAGRAM OF THE TORQUE MAGNETOMETER OF SCHELLENG AND RADO

of Gengnagel was of a type in which the torsional feedback was purely elastic with no adjustment, either manual or automatic, of the restoring system to minimise sample movement. It had a very rigid head on which were made positional measurements of high angular sensitivity, and in this respect was akin to the generation of magnetometers classically illustrated by that of Aldenkamp et al.

In 1960 Aldenkamp et al. described a magnetometer having three symmetrically disposed leaf-springs (fig. 4.25) suspending the sample with good lateral stability and the necessary susceptibility to twist. They used an inductive linear displacement transducer, eccentrically placed from the axis of the magnetometer with components attached appropriately to the upper and lower discs, to establish a changing signal with respect to rotation of the suspension. The magnetometer of chapter 6 (Paige and Tanner, 1982) is similar to this, but for a directly angularly sensitive coaxial transducer (fig. 6.1). The Aldenkamp et al. magnetometer was essentially frictionless and revolved as a whole in a stationary magnetic field.

The triple leaf-spring configuration of figure 4.25 has been used in conjunction with capacitative displacement measurement (Alberts and Alberts, 1971, Birss and Shepherd 1978) and with a simple optical lever and scale (Burd et al, 1977). The design of Birss and Shepherd involved two capacitor plates secured so as to face each other on the perimeter of the suspension down the line of relative movement between their individual support posts attached separately to the two discs. The whole was in miniature.

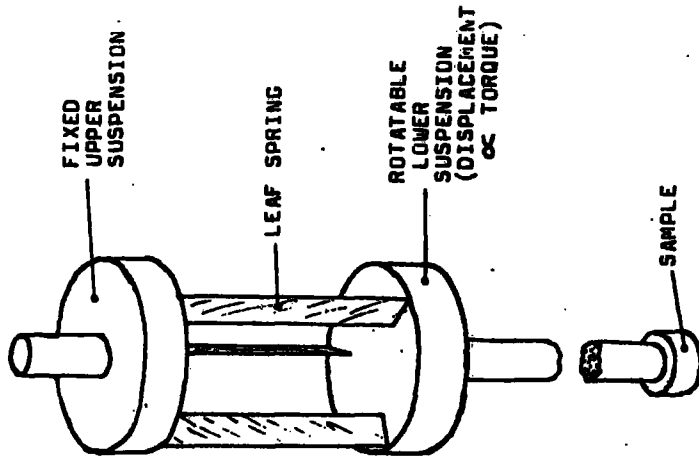


Fig 4-25

TORQUE MAGNETOMETER AFTER ALDENKAMP, MARKS AND ZILSTRA

SEVERAL VARIANTS OF THIS TRIPLE LEAF SPRING CONFIGURATION HAVE APPEARED. THE DIFFERENCES LIE IN THE DETECTION METHOD, WHEREBY THE MOVEMENT OF THE LOWER DISC IS MONITORED. THE USE OF A MUTUAL INDUCTANCE METHOD IS DESCRIBED IN THE CHAPTER 6.

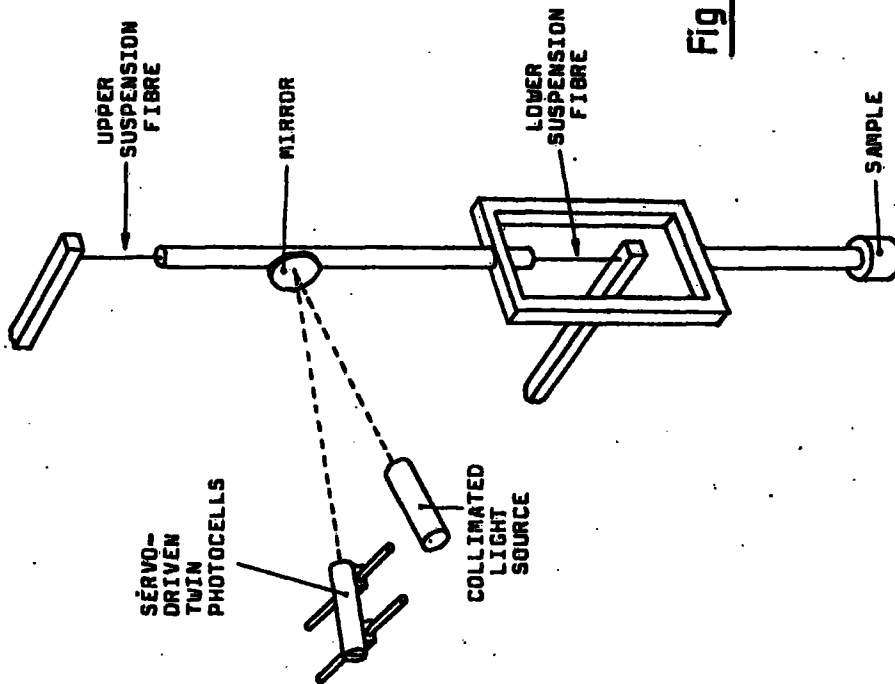


Fig 4-24

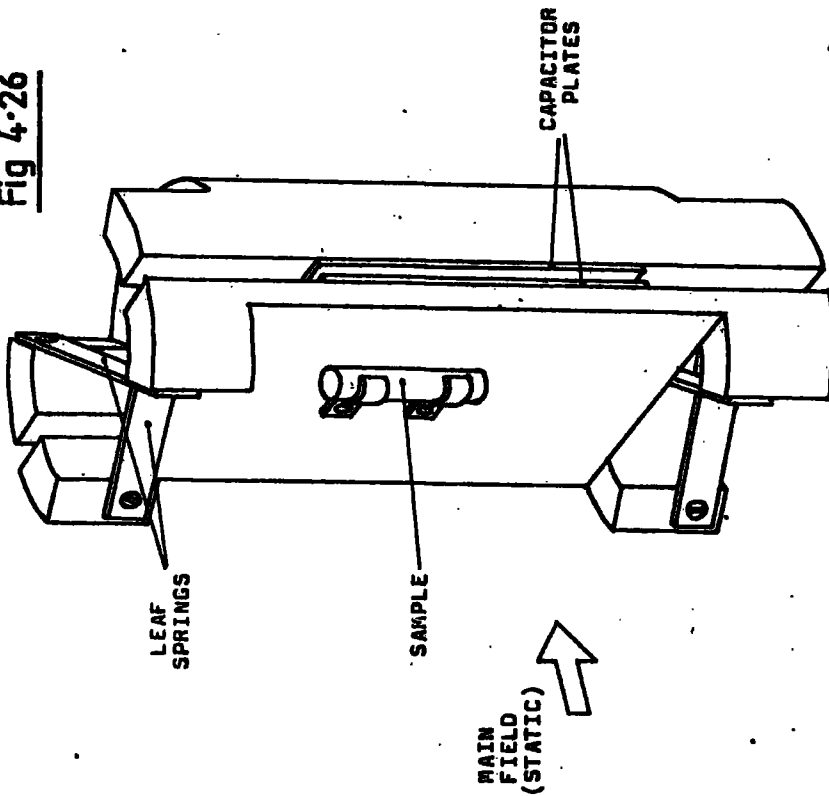
SIMPLIFIED DIAGRAM OF THE TORQUE MAGNETOMETER OF GENGNAGEL ET AL

and was contained within the cryostat region inside the main field.

A magnetometer like that of Birss and Shepherd, using a different leaf-spring configuration, was that of Griessen (1973). Sample torques were detected by capacitance measurement using opposing plates, as illustrated in figure 4.26, on a movement with different geometry but similar constraints to that of the leaf-spring arrangement of Aldenkamp et al.

A particularly innovative magnetometer was reported by Birss and Wallis (1963) again having passive elastic restraint, in this case produced by a wire cradle (fig. 4.27). Two further papers indicating developments of it followed; by Birss and Wallis (1965) and Birss and Hegarty (1967). A fibre provided some support of the sample to keep it on the magnetometer axis. The ingenuity lay firstly in the use of the cradle wires as strain-gauge elements, and secondly in using a configuration which gave the associated electrical bridge natural immunity to magnetoresistive, translational and thermal changes in the wires. The torque on the inner two pegs (fig. 4.27) caused one of the two wires, strung in 'Z' configuration from two outer diagonally opposing fixed pegs, to relax, and the other, strung from a different pair of fixed diagonally opposing pegs, to stretch. Opposite torques had the opposite effect on each nichrome wire in the miniature assembly. The out-of-balance voltage signal, created by the changing resistance of the wires due to strain gave the torque magnitude and sense. The voltage changes were monitored using a Wheatstone bridge.

Fig 4-26



SIMPLIFIED DIAGRAM OF THE TORQUE MAGNETOMETER OF GRIESSEN
THE MECHANISM IS SUPPORTED ON A ROTATING SHAFT COAXIAL WITH SAMPLE.

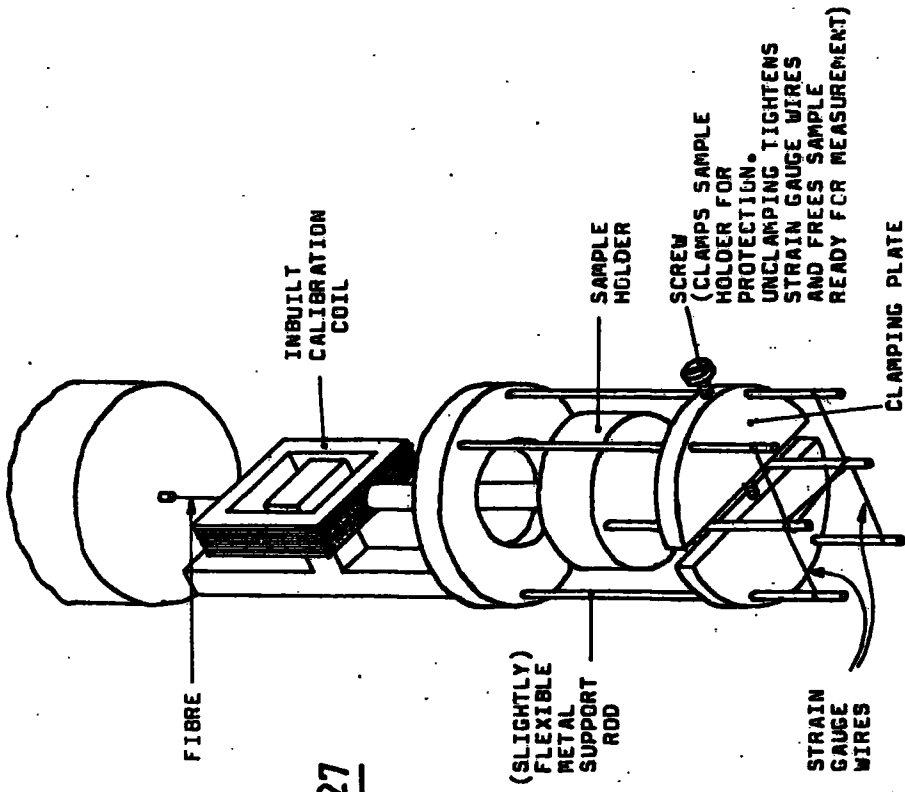
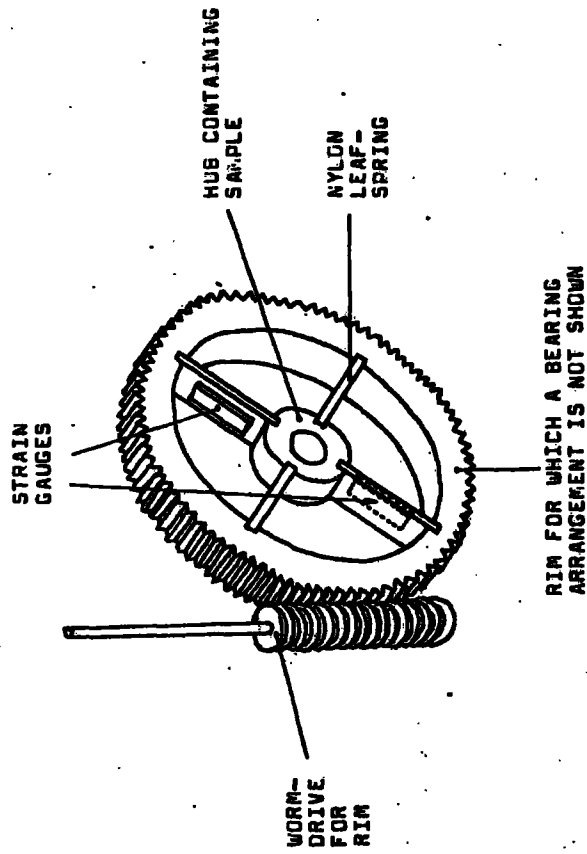


Fig 4-27

SIMPLIFIED DIAGRAM OF THE TORQUE MAGNETOMETER OF BIRSS AND WALLIS

THIS IS ONE OF THREE ESSENTIALLY SIMILAR DESIGNS INVOLVING BIRSS. THE CONFIGURATION OF THE STRAIN GAUGE WIRES AND CLAMP ARE INNOVATIVE.

Fig 4-29



SIMPLIFIED DIAGRAM OF THE TORQUE MAGNETOMETER OF WARNOCK

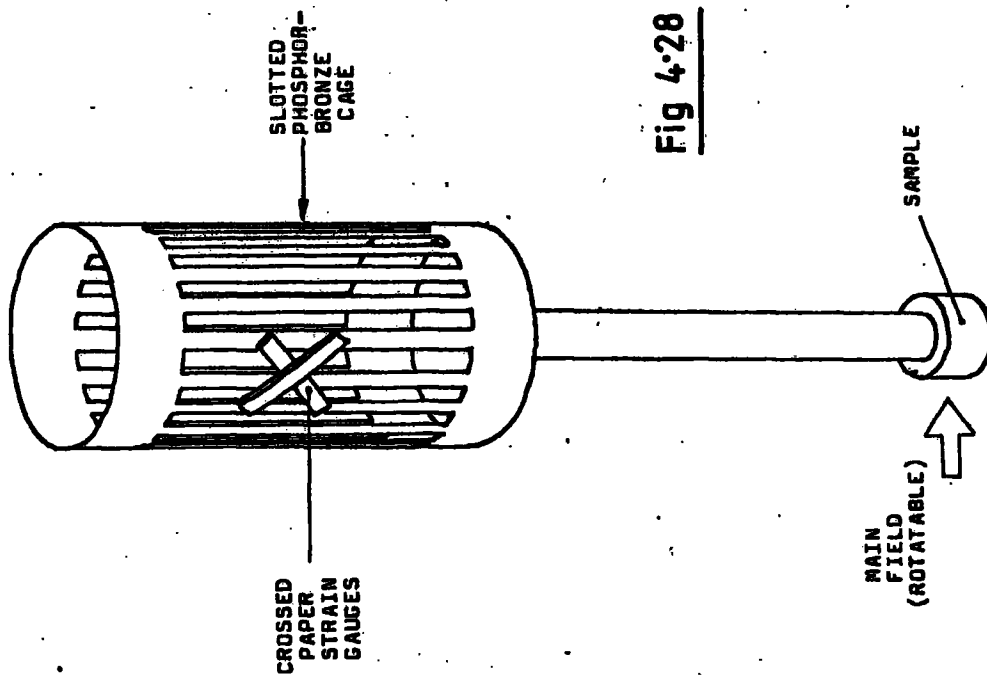


Fig 4-28

SIMPLIFIED DIAGRAM OF THE TORQUE MAGNETOMETER OF TAJIMA AND CHIKAZUMI AND ALSO KUNTSEVICH AND PALEKHIN

Another magnetometer arrangement having passive elastic restraint was reported by Tajima and Chikazumi (1967) and seemingly independently by Kuntsevich and Palekhin (1973), and is shown in figure 4.28. A torsion cage was constructed from a thin-walled slotted, phosphore bronze tube, and movement was detected by two crossed paper strain-gauges on the surface. The strain-gauges were included in a bridge circuit sensitive to torsion on the cage but insensitive to deflection. The cage did not have the same preferential tendency to twist as that of Aldenkamp et al., and was appropriate for the measurement of large torques.

Another strain-gauge arrangement was that of Warnock (1975) shown in figure 4.29. Four radial nylon leaf-springs converging from a circular rim to a hub carrying the sample were monitored by two strain-gauges on opposing 'spokes' while the whole was rotated in a solenoid bore. The device was particularly ^{suited to} high anisotropy materials.

Finally, chapter 6 describes a computerised magnetometer based on the Aldenkamp et al. design featuring readily available off-the-shelf electronics and comprehensive on-line data correction to account for non-ideal magnetometer behaviour (eg non-linearity in the electrical position monitoring, time-constant effects in the electronics etc.). The device achieves a high absolute accuracy in torque measurements.

4.4. Suggested alternative designs

Reviewing the literature, it is evident that torque measurements are carried out in several analysis techniques,

and in particular industrial research has gone into devices which measure torque. In this category is a torque meter devised for general use by Fulinski and Grotowski (1977). Suggested applications were the measurement of torques created by moving-coil meters, the calibration of small rotational springs, the measurement of static or dynamic friction in small bearings and the measurement of the drive torques in fractional horsepower motors. A working version produced by them had a sensitivity range of about 10^{-8} to 10^{-3} Nm (lower limit corresponding to noise value). The design was very similar to several of the torque magnetometers described previously in that a movement, retained in this case between jewel bearings, was held in check by a balancing coil between the pole-pieces of a small magnet. The method of determining the deviation from the null position was, however, unusual in that a Meissener generator was used. This device consisted of an oscillator featuring two coils in a position of strong flux linkage with a small air-gap between them (see fig. 4.30). The oscillations were sustained by positive feedback relying, at one stage, on the mutual inductance between the two coils. An aluminium flag, attached to a lever on the movement, swung into the air-gap, reducing the oscillation amplitude by an amount depending on the penetration of the flag into the gap. An amplifier with a d.c. output, offset to zero for a standard detected signal from the oscillator, fed the balancing coil so as to drive the flag to a point limiting the Meissener oscillations to the standard amplitude and thereby establishing a torsional feedback in the meter movement. Clearly a torque magnetometer

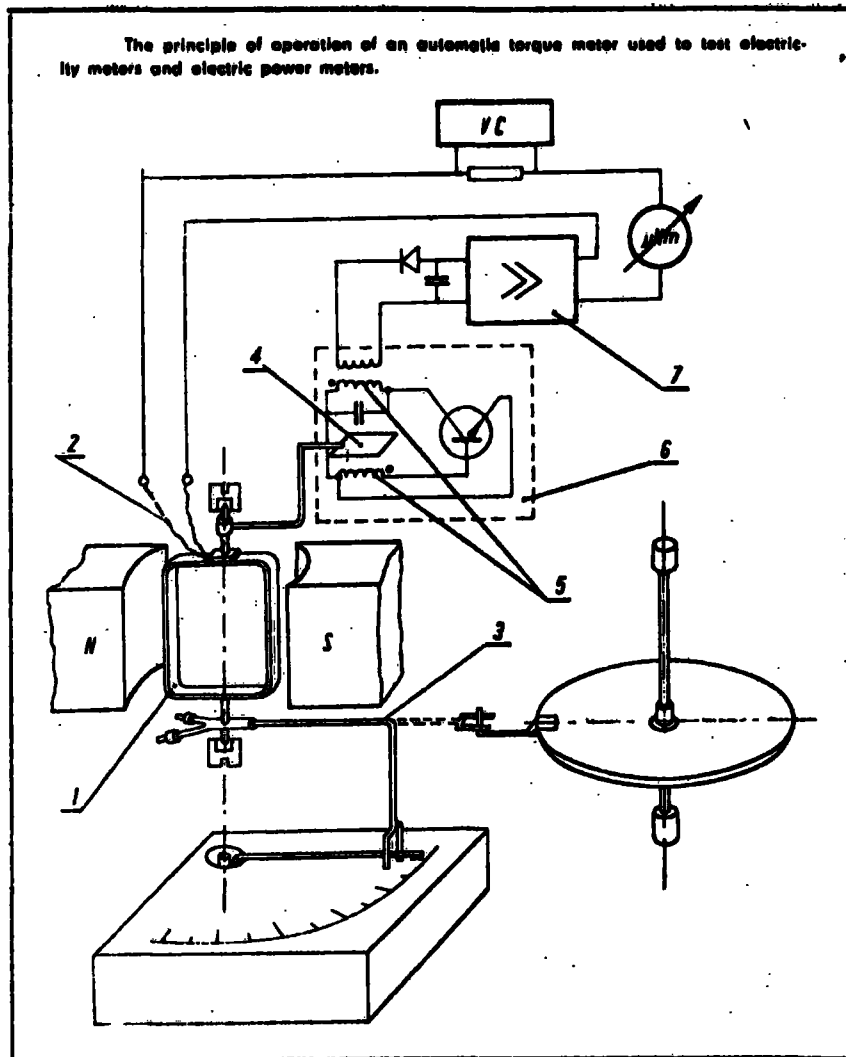


Fig 4-30

The moving-coil final control mechanism 1 generating a compensating torque to counteract the torque being tested, is fed from the "control" system of the Meissner generator 6 via amplifier 7. The shaft of the moving element mounts an aluminium flag (screen) 4 that moves in the air gap between the coils 5 of the feedback circuit of the Meissner generator 6. The pointer of the movable element 3 terminates in a fork, the former engaging the pointer of the instrument being tested during the measurement.

THE TORQUE METER OF FULINSKI AND GROTUWSKI

THE USE OF A MEISSNER GENERATOR TO SENSE THE POSITION OF THE METER MOVEMENT COULD CLEARLY BE ADOPTED IN THE DESIGN OF A TORQUE MAGNETOMETER.

could be built with this method of stabilisation. An advantage would be the simplicity of the electronics.

Techniques obviously exist in industry for measuring torques produced by machinery, but these are usually heavy duty devices and irrelevant to torque magnetometry.

Taking the scientific literature, many experiments have been reported in which torsion balances are used. The gravitational experiments of Cavendish or Eötvös are examples. In particular, static measurements of very small torsional movements are carried out in the Eötvös experiment, and photoelectric autocollimators have measured the angular deflection of mirrors to about 10^{-8} radians (Hakner, 1969). However, Kantor et al. (1972) describe a method of determining the deflection to a sensitivity of 10^{-9} radians; by using the mirror to project an image of a laser-illuminated pin-hole to a pair of remote twin photocells. For a $100 \mu\text{m}$ quartz fibre suspension of length 10 cm, torques of 10^{-15} Nm would be detected, but such extreme sensitivity is seldom required in torque magnetometry.

Makheyen and Gogolev (1972) have described a method of measuring torsional angles using twin reflecting diffraction gratings of which one is attached to the movement. It is a valuable technique when the view of the moving suspension is so restricted that information on a limited angular change must be conveyed, not by a simple optical lever, but by the frequency of the emerging light. Applications to torque magnetometry are not obvious, nor is the similar technique involving the extinction of appropriately polarised light reflected from a tilting surface on a moving body.

It has come to the attention of the author that the cross-coil transducer of the magnetometer reported in chapter 6 bears a resemblance to the internal windings of a certain servo transducer, called a magslip, manufactured in this country by Muirhead and Co. Ltd. The standard 'transmitter' magslip consists of a stator, similar to that of a three-phase induction motor, energised by three in-phase or in-antiphase supply voltages producing a non-rotating alternating field across a single-coil armature. The function of the magslip as a servo element will not be described here, but there exists a null-orientation for the armature at which no voltage is induced. In this situation the magslips functions in the same way as the transducer of chapter 6. Modification of the magslip to leaf-spring support, rather than plain bearings, would be easy, yielding a device with a high voltage output for a given deflection of the ready-made, very accurate coil-system. Furthermore, fine adjustment of the angle of the primary field would be possible by a change in the amplitude ratio of the three primary coil voltages using a potentiometer, eliminating the phase-shift network (see chapter 6, section 6) which would otherwise be required to offset the induced a.c. signal to produce a quiescent equilibrium output. The construction of a torque magnetometer around such a device seems therefore to be an interesting possibility.

CHAPTER FIVE

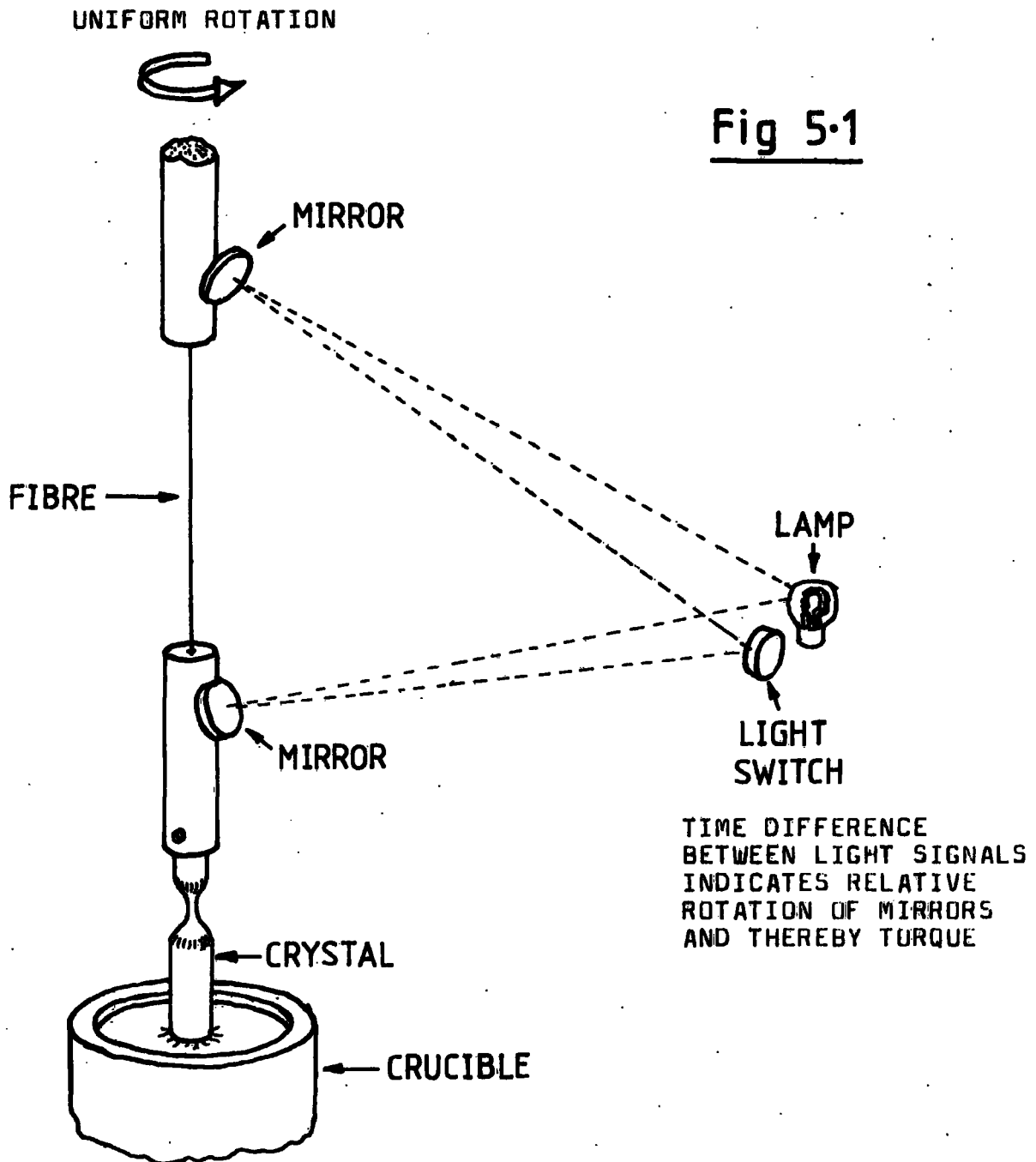
A NEW METHOD OF AUTOMATING CZOCHELSKI CRYSTAL GROWTH

5.1 Introduction

This chapter describes the early development of a system for automating Czochralski crystal growth. The innovation lies chiefly in the measurement of the viscous torque on the growing crystal as it is rotated in the melt to determine the size of the crystal. The crystal diameter is stabilised by control of the melt temperature. Float-zone growth has been monitored by a viscous torque method by Quenisset et al. (1980) but the Czochralski technique has never been treated in this way.

Only one particular design for accomplishing control has been looked into in the present work. It is a design incorporating a suspension fibre which carries the crystal, whereby torque is derived from twist in the fibre (fig. 5.1). Mirrors at the top and bottom of the fibre reflect light signals to a light switch as the whole suspension rotates, the interval between pulses indicating torque. The simple on/off pulses created by the light-switch trigger the timing part of a logic circuit which subsequently controls the crystal grower R.F. furnace via a potentiometer driven by a stepper-motor. The attraction of this design lay in its simplicity.

An alternative system would be that of measuring the torque created by the crystal on the crucible using a torsion



METHOD OF CRYSTAL TORQUE MEASUREMENT IN
PRESENT CZOCHRALSKI AUTOMATION

head like that of the torque magnetometer of chapter 8.

The arrangement could be as shown in figure 5.2 with a long rod allowing isolation of the pick-up coil, connected through

SUGGESTION FOR ALTERNATIVE TORSIONAL MEASUREMENT METHOD
IN CZOCHRALSKI AUTOMATION

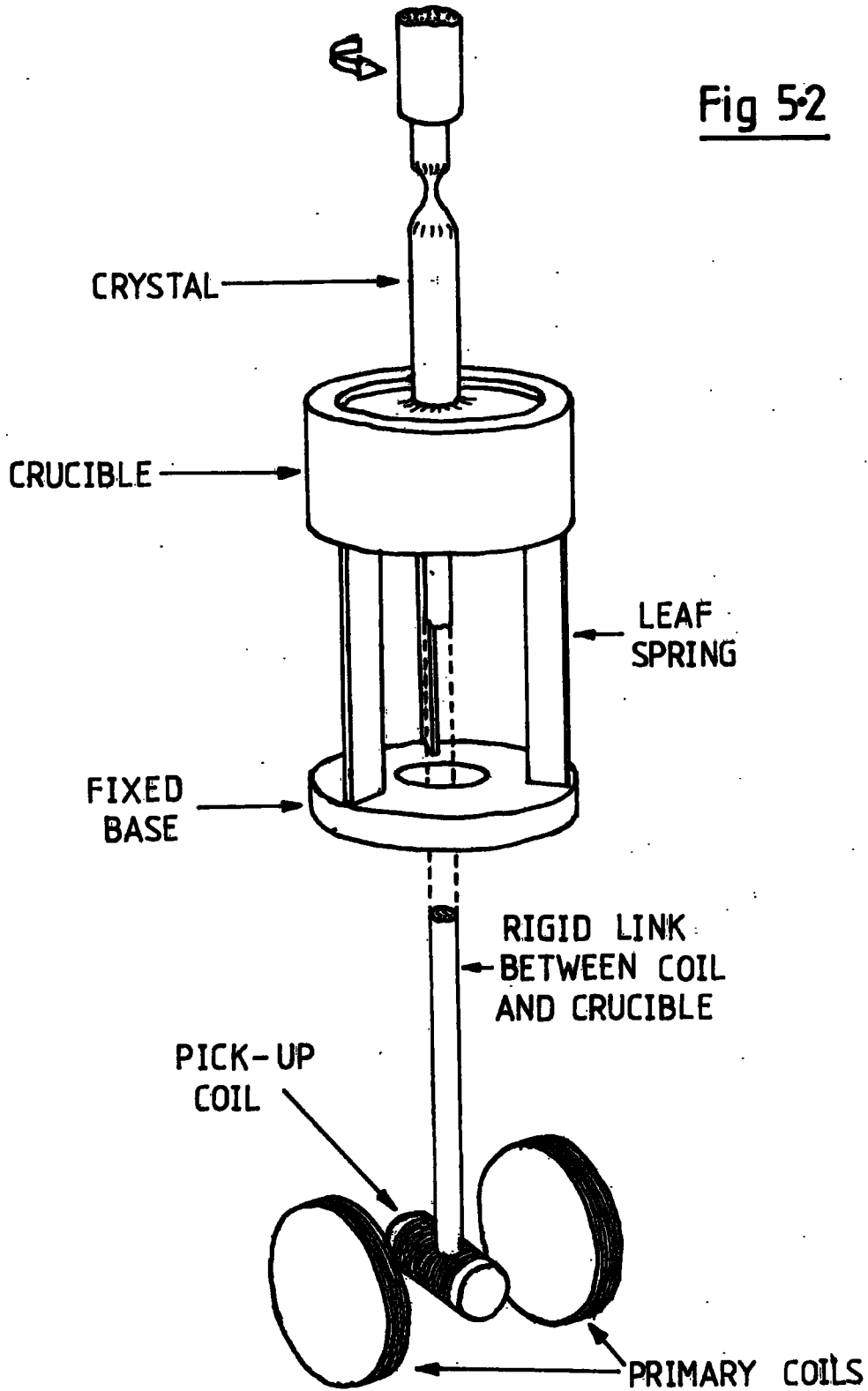


Fig 5-2

the rod to the crucible, from the R.F. heater field. Microcomputer control of the potentiometer stepper-motor using available hardware for the Minicam interface (see page 191) would be fairly straight forward. However commercial interest had been shown in a fairly inexpensive method of control so the former design was selected having a cheaper custom built "hard" controller.

The growth control was accomplished by changing the melt temperature; the alternative of changing the crystal pull-rate did not have as significant an effect on the crystal diameter. Furthermore the R.F. furnace power controller had a facility for attaching a remote potentiometer so a stepper-motor controlled potentiometer could therefore readily be attached in such a way as to change the melt temperature.

It was anticipated, and indeed proved to be the case, that a given torque value would fail to define a particular diameter of crystal at growth equilibrium without some knowledge of the combination of pull-rate and melt temperature creating the torque. Torque, as expected, was found to be a function of diameter, temperature and pull-rate. However the three variables are at growth equilibrium functionally inter-related and therefore either of the latter two could in principle be eliminated. Therefore at equilibrium for torque to depend simply on diameter, a remaining variable, either pull-rate or temperature, must be fixed. The control process is therefore necessarily simple in that only one parameter can be adjusted, and it was decided that the parameter liable to drift in a way that would most affect the crystal would be changed and the other assumed to be stable and left

untouched. Therefore temperature adjustment was again indicated.

In using viscous torque control it is assumed that for stable growth conditions, that is when for the prevailing conditions of fixed pull-rate and melt temperature the growing crystal has reached an equilibrium diameter, the torque so required to rotate the crystal in the melt (at a fixed rate) monotonically increases with respect to crystal size. Additionally it is assumed that any physical change in the melt as its temperature is changed in order to affect the diameter of the crystal, particularly viscosity and surface tension effects, do not, prior to re-establishing a stable diameter, cause the torque to change in the opposite sense to the change which would occur ultimately at the new equilibrium. Since crystal diameter decreases with respect to melt temperature during Czochralski growth, the above conditions are fulfilled for most materials, the requirement being that viscosity and surface tension decrease monotonically with respect to temperature over the relevant temperature range. The complex flows established in the melt due to convective and magnetohydrodynamic stirring change with temperature but were found in retrospect, for the present equipment and materials, not to interfere with this well-behaved relationship between crystal diameter and torque. The use of a graphite susceptor to heat the copper crystals grown here reduced the magnetohydrodynamic stirring considerably.

5.2 Advantages of viscous torque control

5.2.1 Of viscous torque control in general

Perhaps the most important advantage, which was not fully appreciated until after testing the equipment and which is inherent to the method of viscous torque control, is that the torque on the crystal is very sensitive to the conditions of the meniscus region around the growing interface and changes drastically depending on the height of the solid/liquid interface above the melt surface, that is the torque depends on the size of the small liquid column between the crystal and the melt surface retained by surface tension (see fig. 5.35). The dependence is intuitively obvious, the magnitude of the effect is not, as is detailed later. Sensitivity to the state of the meniscus marks out viscous torque control as superior to some other methods, for instance the imaging techniques mentioned in chapter 3, section 3.3.2 and 3.3.3, in that changes in crystal diameter can be anticipated. For example if crystal torque is monitored during an increment in the melt temperature during growth, the melting back of the crystal along its length would be detected almost immediately, as a reduction in the torque, before narrowing of the crystal had begun. Corrective measures could then be implemented before significant change in the crystal diameter had occurred.

5.2.2 Of the present design for achieving it

Viscous torque control is in principle simple, as is the present equipment. The fact that there are no electrical

components within the vacuum system eliminates lead-throughs.

The essential elements of the internal mechanism are two mirrors and a fibre.

Related to simplicity is the fact that the cost of automation was low, that is of the order of £200 for components.

An indirect advantage of the present crystal suspension is that the thermal gradients at the growing interface are reduced due to the thermal insulation of the crystal by the fibre. The reduced temperature gradients reduce the number of dislocations formed during growth to produce more perfect crystals (Zasimchuk et al., 1979).

5.3 Disadvantages of viscous torque control

5.3.1 Of viscous torque control in general

A disadvantage of the method of viscous torque control is that torques on the crystal are small, and accurate measurement of them by a mechanism robust enough to support the crystal (or crucible if the counter-torque is measured) is difficult. It might be possible under certain circumstances to float a thin layer of viscous fluid on the melt surface to increase the torque on the crystal to produce a diameter sensitive (but not meniscus sensitive) torque reading of more manageable size (c.f. liquid encapsulation methods for Czochralski growth devised by Metz et al., 1962) but generally the problem of measuring very small torques remains. A preliminary experiment whereby the end of a right 12 mm cylinder was rotated concentrically in contact with a water surface at 20°C (viscosity = 1.005 centipoise) at 50 RPM

(water 3 cm deep in a beaker 8 cm diameter concentric with the cylinder) gave a torque of 4×10^{-8} Nm. Faster rotation rates would promote torque but be unsuitable for quality Czochralski growth. The viscosity of copper is about 5 centipoise at its melting point so the expected torques for copper crystals up to 12 mm diameter were at most 2×10^{-7} Nm.

Another disadvantage is that the viscous torque on a crystal is dependent on the level of the melt during the pulling process since as the melt level lowers, the shearing of the fluid increases. However most of the fluid shearing occurs locally at the growth interface and therefore the torque is not significantly changed by remote changes in the fluid boundaries and is thus not critically dependent on melt depth. Furthermore attempts can be made to use crucibles of sufficient size, or even automatically replenished crucibles, such that the melt dimensions do not alter notably during growth.

5.3.2 Of the present design for achieving it

One disadvantage of using a suspension fibre is that in the simplest arrangement where all the crystal weight is carried by the fibre without a secondary support bearing (one of these was ultimately employed) strength and torsional sensitivity tend to be exclusive. If it is assumed that the torque on the crystal is proportional to its cross-sectional area and that the strength of the fibre and its torsional rigidity per unit length are proportional to the fibre cross-sectional area and that a given angular deflection is required for successful torque measurement, it can be shown that, for a specific set of fibre and crystal materials, the length of

fibre required to monitor the torque is proportional to the maximum length of crystal to be pulled. Furthermore, for a 10° torsional deflection, the proportionality might be about one metre of fibre per centimetre of crystal; wherein lies the disadvantage since commercially grown crystals might therefore require a 10 to 100 metre fibre suspension. Consequently, in the very simple form outlined in the introduction, the automatic control device is only suitable for growing small crystals. In fact a jewel support bearing was added even in the present version of the device due to repeated breakage of the fibre.

5.4 Mechanical details of the automatic puller

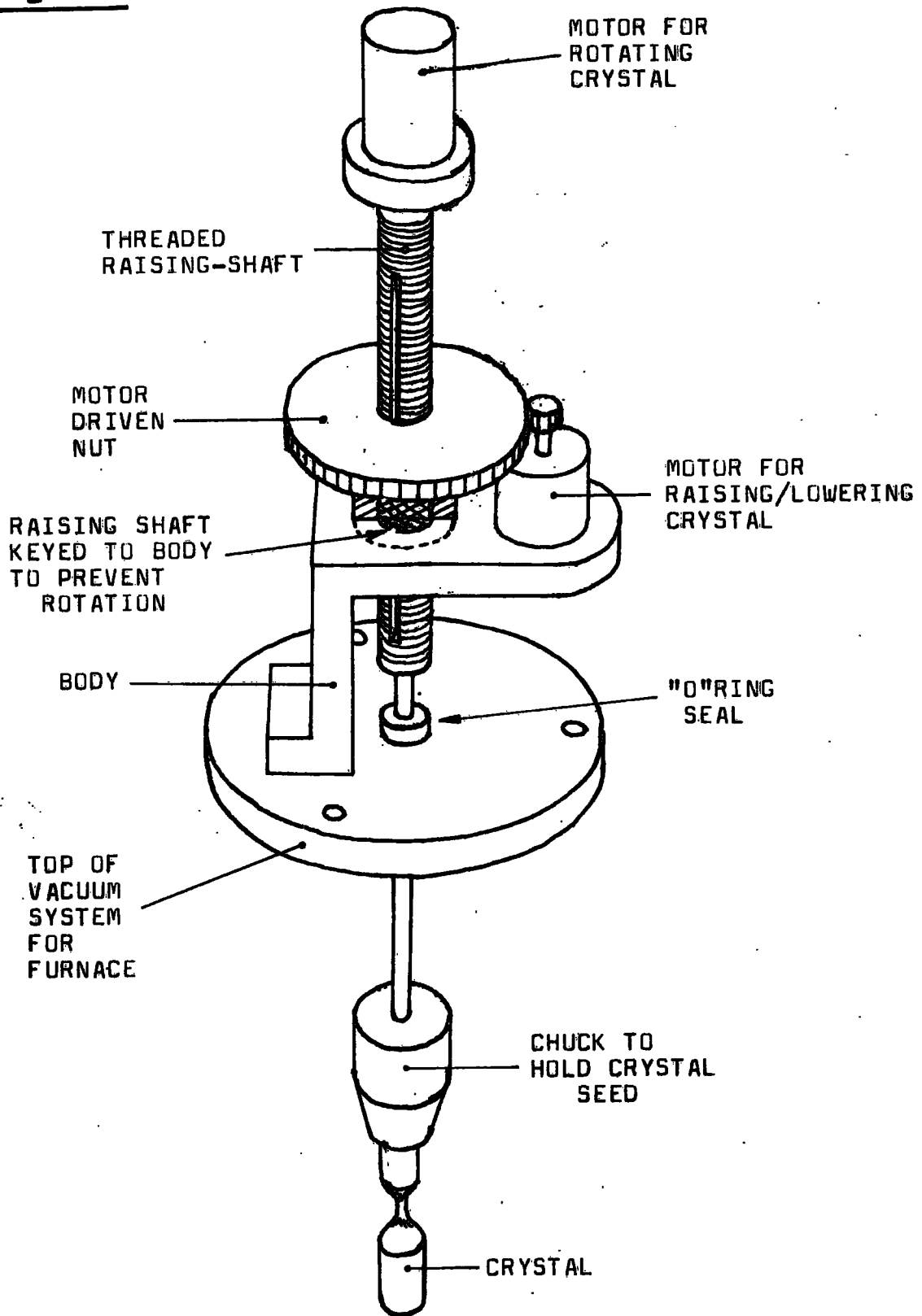
5.4.1 The unmodified puller

The unmodified head of the present commercial Czochralski puller is shown in simplified form in figure 5.3. The machine used as the basis for the modification was a Metals Research BCG 365 crystal puller.

The essential requirements of lifting and rotating were performed by the puller head using two independent motors. The pulling distance was about 12 cm covered at rates of up to 1 mm per minute. The rate of the pull motor was uniform enough for the present work (stable to within about 5%) but the rotating motor was replaced (see section 5.4.3). The flange on the bottom of the head formed the upper wall of a vacuum system surrounding the furnace, the rotating part of the puller penetrating the flange through a double "O"-ring seal.

The furnace part of the crystal puller was essentially a vertical double-walled vacuum system with the inter-spacing

Fig 5-3



SIMPLIFIED HEAD OF A CZOCHRALSKI CRYSTAL PULLER

THE AUTOMATIC CRYSTAL PULLER REPORTED HERE HAS A HEAD BASED ON THIS DESIGN.

FURNACE REGION OF THE CZOCHRALSKI CRYSTAL PULLER

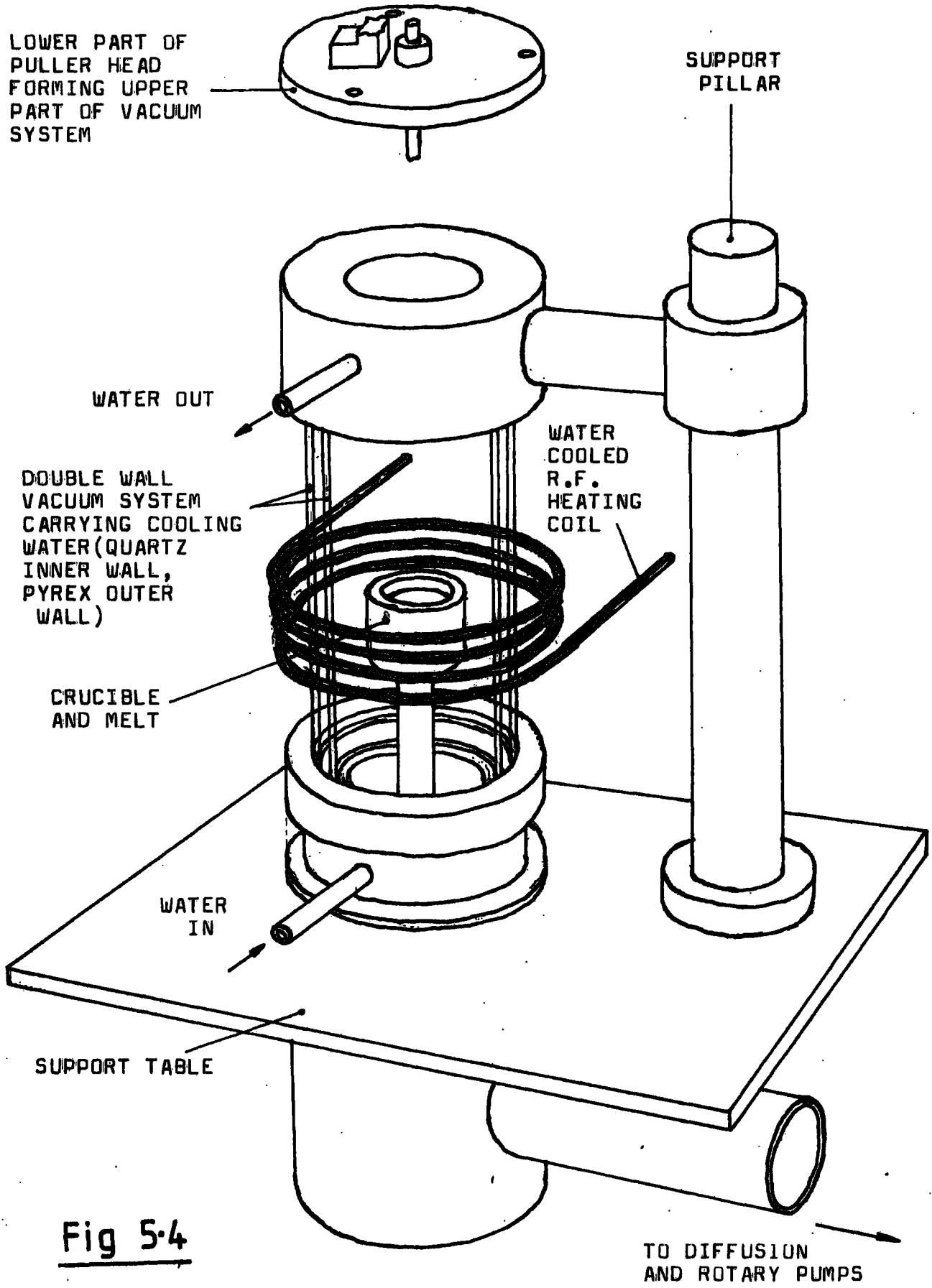


Fig 5.4

forming a conduit for cooling water (see fig. 5.4). An inner wall of quartz and outer wall of pyrex ensured good visibility of the central crucible. Since an inert gas atmosphere was not used, rotary and diffusion pumps in tandem provided the vacuum necessary to prevent melt oxidation during growth. The crucible was heated using a 25 KW Stanelco Thermatron radio frequency furnace operating at 480 KHz.

5.4.2 Growth conditions

The automatic control device was developed by growing copper crystals in vacuum in a graphite susceptor (to reduce magnetohydrodynamic stirring). An inert gas atmosphere was not used in case of convective disturbance to the crystal suspension. The crucible was approximately 2.5 cm in diameter and 3 cm deep and almost full when crystal pulling began. Crystals in excess of 1 cm in diameter were grown for less than the full 10 cm distance due to the appreciable loss of melt that full growth would incur. Melt loss could have detrimental effects on the automation by altering crystal torque and also by changing the thermal response of the melt and hence the feedback process.

5.4.3 The mechanical components of the control device

A detailed diagram of the modified Czochralski head is given in figure 5.5 and a cross-section is given in figure 5.6. The components were as follows:

1) The suspension fibre:

As originally envisaged the fibre was to have supported the weight of the crystal as well as provide the drive torque. The physical requirements for these two roles were however

THE HEAD OF THE AUTOMATIC CRYSTAL PULLER

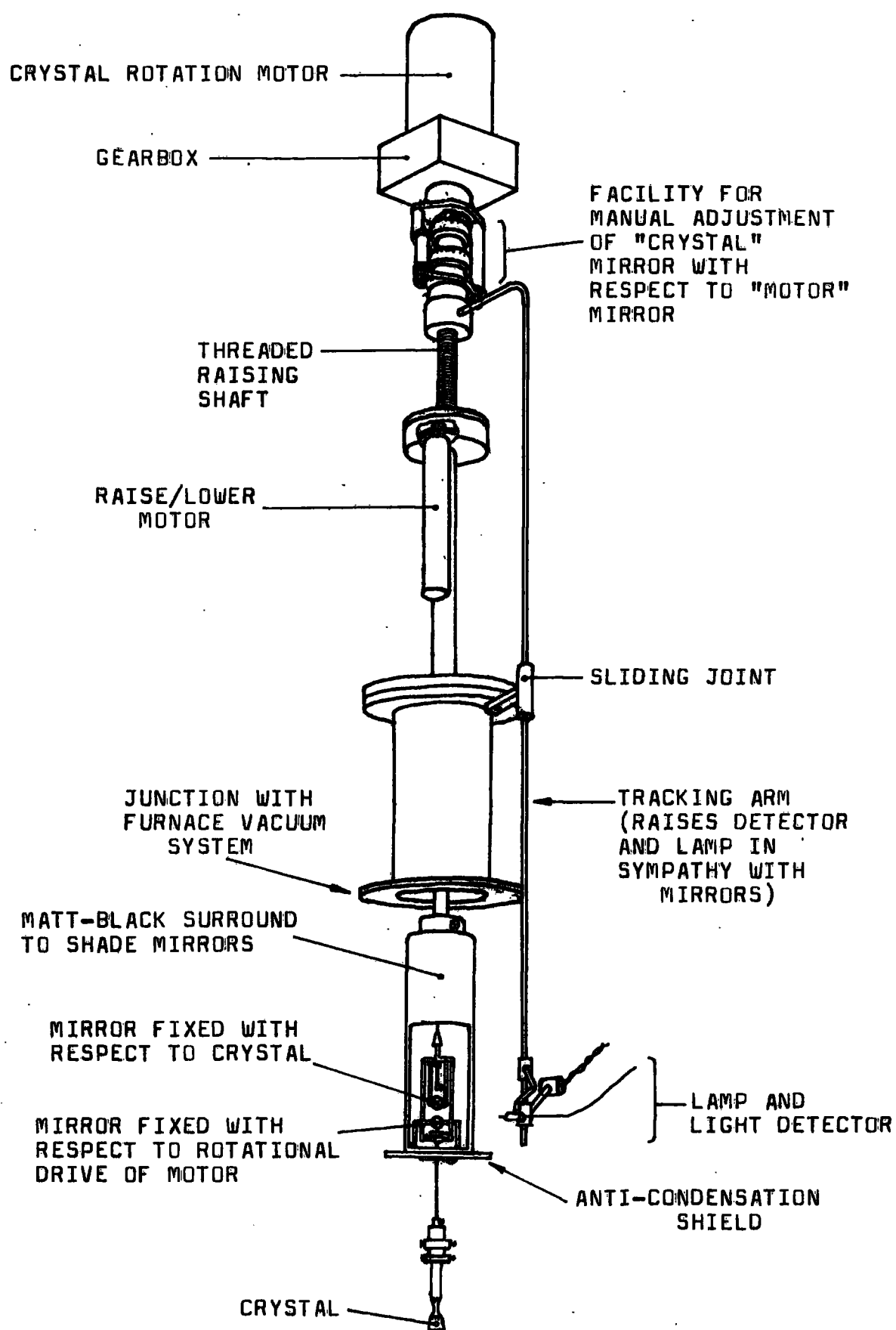


Fig 5-5

CROSS-SECTION OF THE HEAD OF THE AUTOMATIC CRYSTAL PULLER

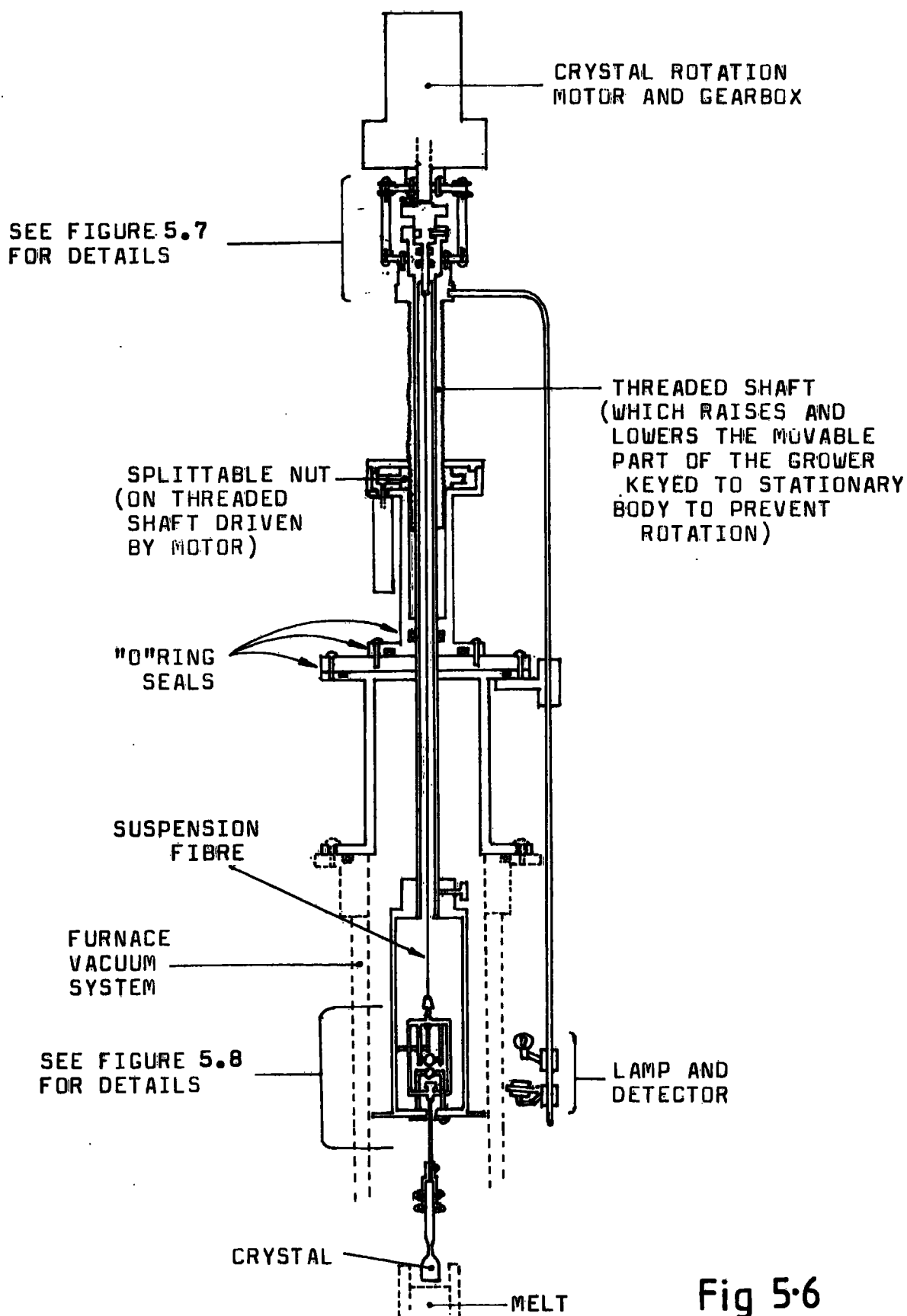
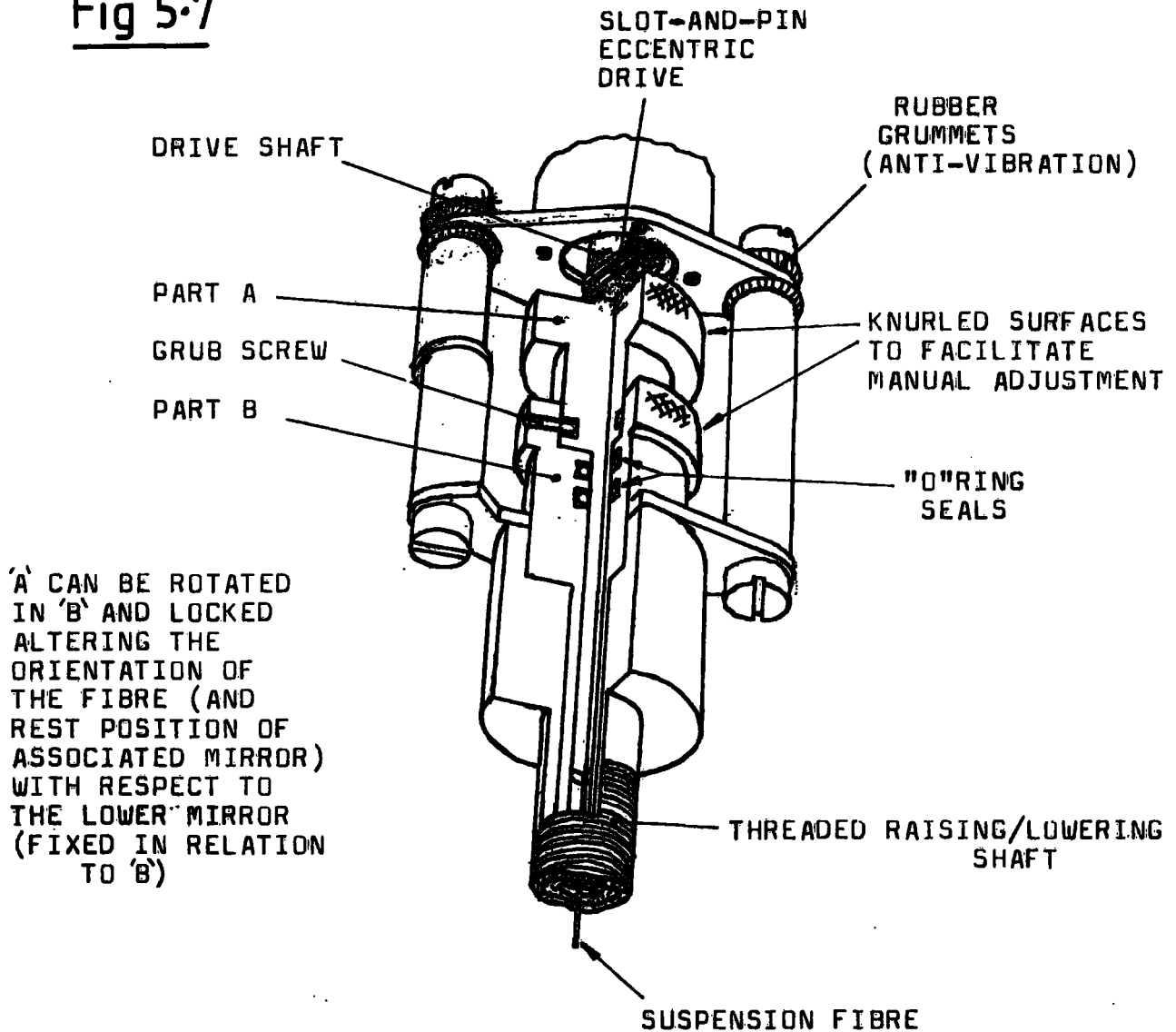


Fig 5.6

competitive and its dual function was eventually rejected; a jewel bearing was incorporated to take the crystal weight. Metal fibres were found to be too liable to rotational creep, even under the small torques applied. For a 44 SWG copper wire a rotation of 30° per hour was observed at a temperature varying between 200°C and 30°C along a 50 cm length under torques of approximately 10^{-7} Nm, this hourly rotation being typical of the legitimate torsional rotation created by a crystal. Metal fibres were also inconvenient because they formed, if not properly insulated from the body of the puller, an electrical earth route for the melt. The earthing currents were produced by R.F. induction and large enough to instantly fuse the wires. Borosilicate glass fibre was used as a simple alternative and the creep was reduced to a satisfactory level. The borosilicate fibre was 49 cm long of thickness between 80 and $100\ \mu\text{m}$ having a torsional constant of about 1.5×10^{-7} Nm per radian.

Attachment of the fibre was with Araldite at its upper point and with a pin-chuck to the lower suspension. In order to prevent the pin-chuck from breaking the fibre, a jacket of Araldite was applied to about 1 cm of its length at the lowest point. The maximum possible length of fibre was incorporated into the head, the central stem being replaced by tubing in order to achieve this, the sensitivity of the suspension to torque being thereby promoted.

Manual adjustment of the fibre and hence the equilibrium orientation of the suspension could be made externally when the puller was under vacuum by the mechanism illustrated in detail in figure 5.7.

DETAILS OF UPPER PART OF AUTOMATIC CRYSTAL PULLERFig 5-7

2) The intermeshing frames:

The two intermeshing frames (fig. 5.8) had several purposes. The upper frame supported the mirror and was fixed with respect to the crystal. The upper frame and mirror were free to rotate on the jewel bearing under the restoring force of the suspension fibre. The interleaving of the upper frame

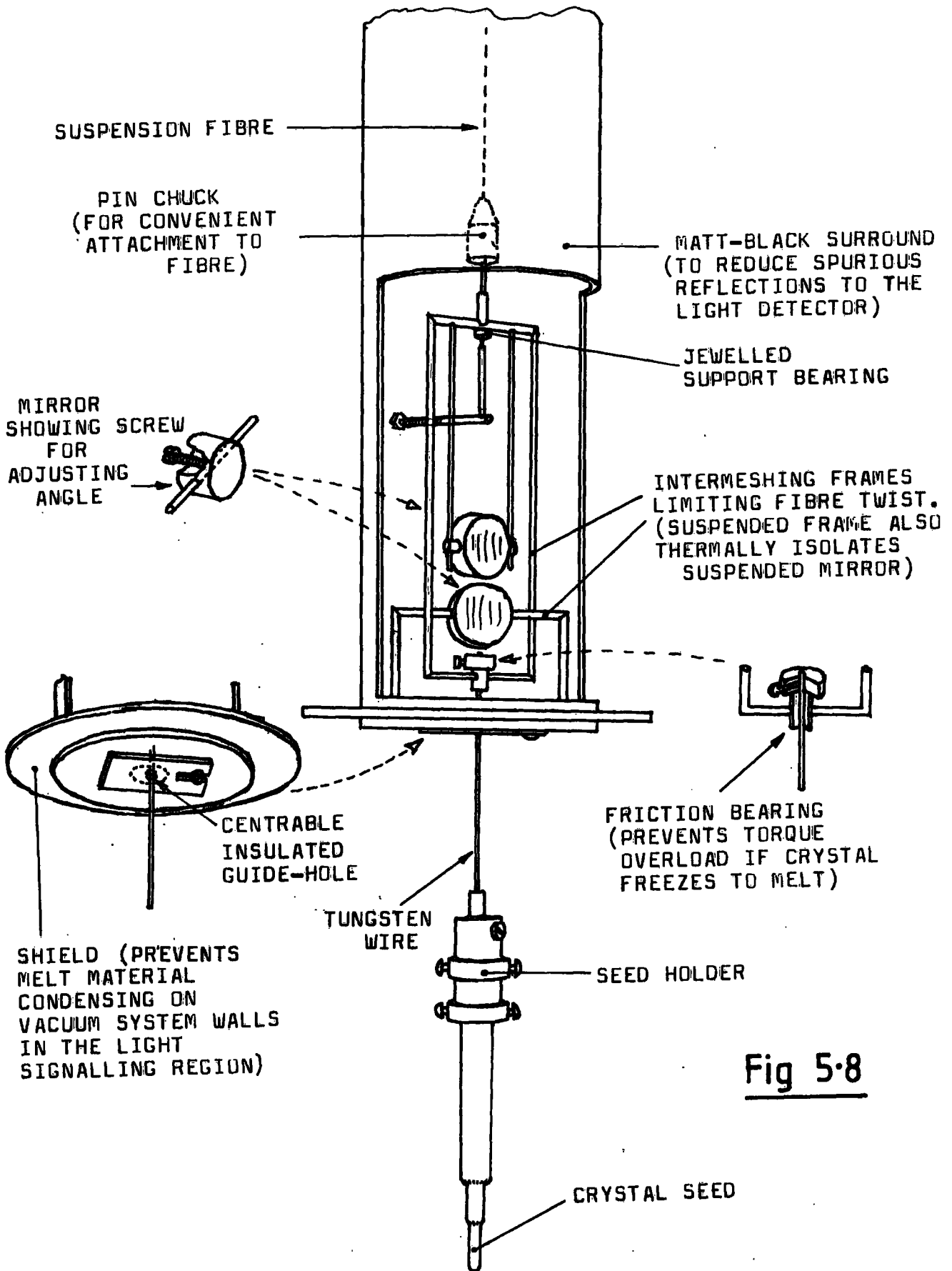


Fig 5.8

DETAILS OF LOWER SUSPENSION OF AUTOMATIC CRYSTAL PULLER

with the lower frame prevented excessive twisting of the fibre. The upper frame was shaped so as to produce maximum thermal isolation of the mirror from the heat conducted up the suspension from the crystal. The lower frame, fixed with respect to the motor drive, carried the remaining mirror which was thermally isolated by the cooling effect of the brass surround. At points on the frames likely to clash together, Araldite was applied as insulation to prevent the arcing of earth currents. The shape of the frames prevented alignment of the mirrors with each other, making superposition of the reflected light signals impossible, as was necessary to the operation of the circuitry.

The upper frame provided a useful point to attach the jewel bearing, which was electrically insulated by securing it with Araldite thereby preventing accidental earthing from the pin to the brass jewel holder. At the bottom of the upper frame was another bearing, operative only if the torques on the crystal exceeded significantly those encountered in typical growth. The latter bearing prevented the mechanism being damaged if the melt froze while the crystal was immersed.

The lower frame and mirror were positioned close to the lower part of the upper frame to resist any small upward thrusts which would unhitch the jewel bearing.

3) Mirrors:

The mirrors (fig 5.8) were made from $\frac{1}{2}$ " aluminium rod. They were crudely formed on a lathe then polished with Dialap 6 μm polish. Their focal length was approximately 4 cm. The mirrors fulfilled the requirement that more light was reflected by them from the lamp to the detector than

any other revolving surface. The mirrors could be tilted and secured with single screws so as to enable light from the lamp to reach the detector via either mirror as the whole mechanism rotated.

4) Matt-black surround and attachments:

The matt-black surround (fig 5.8) reduced stray light on the detector. The blacking was achieved using a normal commercial paint outgassed for one week. The surround provided protection to the suspension, and support for four related attachments; the condensation shield, the support-pin, the lower frame and the centrable guide hole.

The circular condensation shield prevented material from the melt condensing on the quartz inner tube in the signalling region. A 5 mm tolerance was left between the shield and tube to prevent contact, little condensation filtering through. A full complement of reflected light was always, in this way, available to the photoswitch.

The vertical section of the support-pin carried a hardened steel point resting in the jewel bearing. The horizontal part of the support-pin was made of threaded brass, two nuts clamping it to the wall of the matt-black surround. The shape and method of attachment of the pin allowed flexibility of the position of the tip in two directions, given that limited tilting was permissible. Adjustment of the pin position allowed it to be accurately centred on the rotation axis to minimise swaying of the suspension as it revolved.

The centrable guide hole constrained the suspension to afford limited protection against sideways forces.

The hole was insulated around its perimeter with Araldite to prevent arcing of earth currents, though it did not ordinarily come into contact with any part of the suspension. The 6 mm hole could be aligned with the rotation axis by moving the small steel plate secured through a slot by one screw. A 1 mm tungsten wire (fig 5.8) on the suspension ensured against fusing in the event of electrical contact with the guide hole should the insulation have worn.

Precautions had to be taken to make sure that the head of the crystal puller was vertical so that the suspension did not rub on the guide hole and, equally as important, that the tungsten support wire, the jewel bearing and the centre of gravity of suspended mass were sufficiently collinear to avoid rubbing of the tungsten wire in the hole.

5) The brass spacer:

In order to accommodate the lengthened part of the puller head (between the crystal and the top of the vacuum system), a tubular brass spacer approximately 16 cm long was inserted, flanged ends were suitable for mating with the existing surfaces of the head and furnace unit.

6) The motor drive:

The original motor for rotating the crystal in the melt was replaced by a squirrel-cage motor since a stable revolution rate was essential for stability in the viscous torques generated. Drift in the revolution rate was of the order of 1% during use.

The rotation of the motor was transferred via a reduction gearbox to the crystal puller to give a final drive of 50 RPM. The drive was transmitted through a

mechanism which produced a well defined non-uniform rotation over each each revolution, giving an angular velocity with a sinusoidal component (see fig 5.9).

PRINCIPLE OF THE ECCENTRIC MOTOR DRIVE
AND ITS EFFECT ON THE MOVEMENT OF THE SUSPENSION

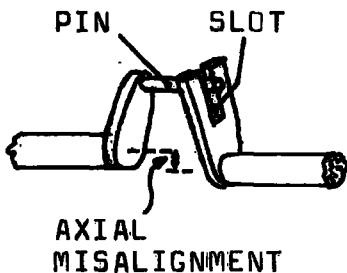
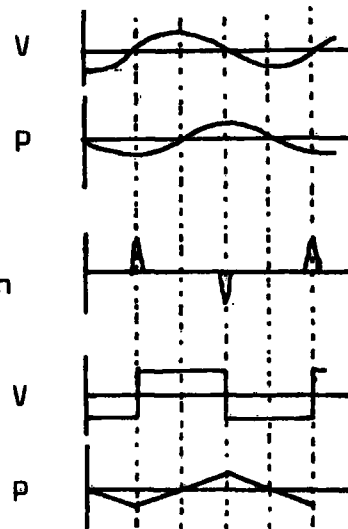


Fig 5-9

Velocity and position of main drive W.R.T. a 50 RPM rotating reference frame

Torque on suspension due to static friction in the bearing

Velocity and position of suspension W.R.T. a 50 RPM rotating reference frame



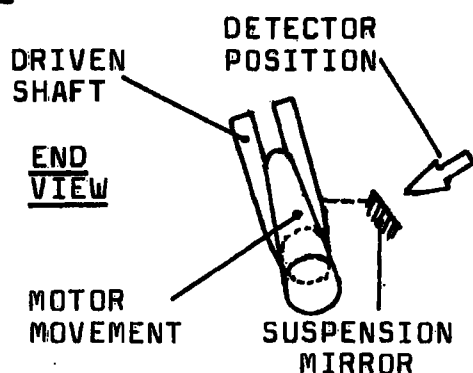
This procedure was introduced so that the rotational rocking of the support-pin, within the rotating frame of reference of the motor drive, prevented sticking of the jewel bearing due to static friction, the actual suspension and jewel having too great an inertia and too tenuous a coupling with the drive to follow the rocking action. Hence the jewel bearing was operated in a continuous state of slip giving sufficient mobility for the crystal torques to act consistently on the suspension fibre.

One important detail about the use of the rocking bearing was that care had to be taken so that the suspension deflection was sampled at an appropriate phase in the execution of the rocking action. The crystal, observed in

a 50 RPM rotating frame, was, in practice, forced into a slight rotational rock by the pin with an amplitude dependent on the mass of the crystal, hence invalidating the assumption that the crystal itself maintained continuous or at least reproducible rotation. The best solution was to make sure that the light from the suspension mirror, for a position of approximate torsional equilibrium during growth, was reflected when the support pin was at a position of maximum or minimum velocity, this corresponding in a very simple picture, where static friction only is considered, to the point in time when the forced rocking of the crystal was at zero displacement. Thus the configuration of the eccentric drive mechanism and detector was as indicated in figure 5.10.

DIAGRAM OF THE RELATIONSHIP NECESSARY
BETWEEN THE MISALIGNMENT OF THE TWO DRIVE
AXES AND THE POSITION OF THE LAMP AND
LIGHT DETECTOR

Fig 5-10



The detector must be positioned so as to collect light from the suspension mirror at the point of maximum (or minimum) velocity of the main drive (see text).

Driven shaft carries suspension mirror following at an arbitrary but fairly constant angle for a given crystal torque.

Static tests whereby the drive mechanism was rocked in the lab frame with an amplitude comparable to that experienced during normal running, that is about 20° , and frequency of 50 cycles per minute, showed that the forced rocking of a typical crystal on the fibre support

had an amplitude of only two or three degrees. Assuming a 30° twist on the suspension fibre (7×10^{-8} Nm) as being typical and a rocking of the crystal of 3° amplitude observed by proper detector positioning as a $1\frac{1}{2}^\circ$ error in the crystal angle, and taking into account the fact that the forced rocking is counteracted to some extent by viscous damping from the melt, the typical relative error in the torque is $<5\%$ due to this effect.

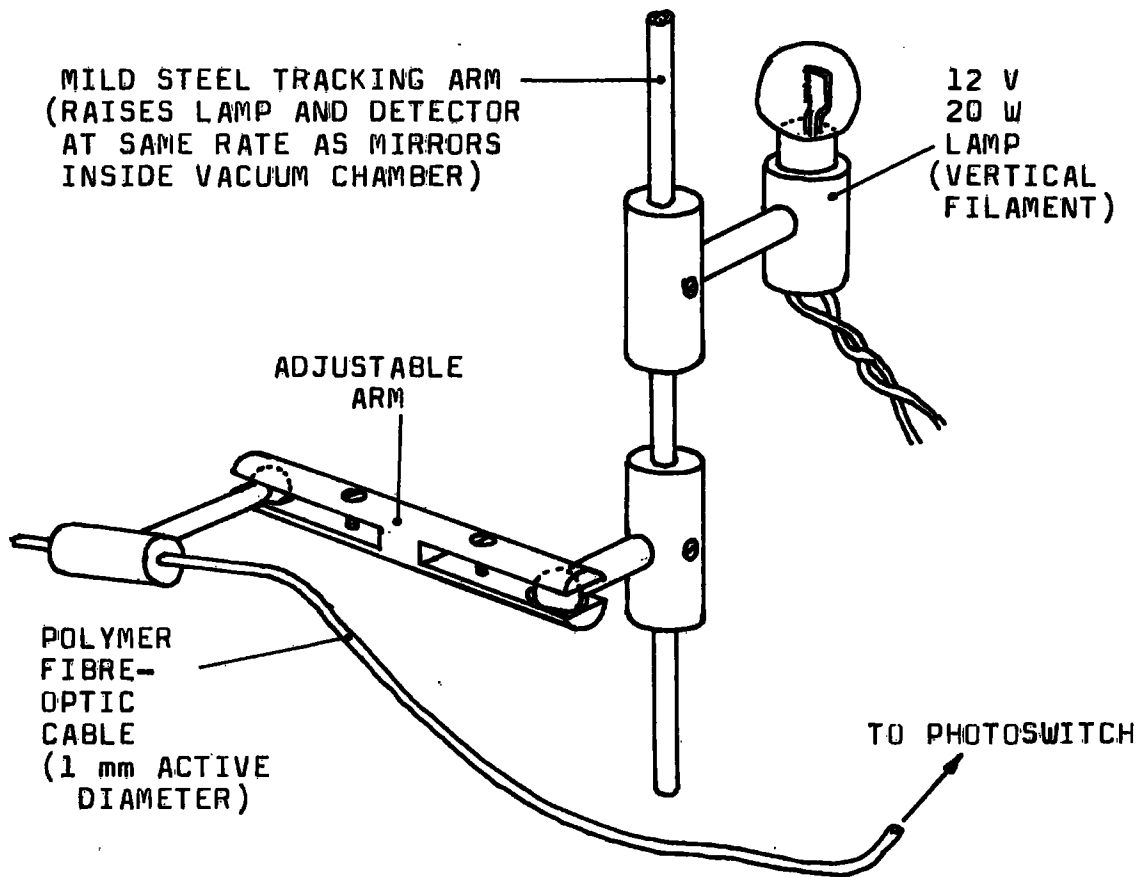
The motor drive and gear box were vibrationally insulated from the crystal puller in a limited way by rubber grommet supports to reduce disturbance to the melt during growth of the crystals (see fig.5.7).

7) The lamp and detector:

The lamp was a single uncollimated 24 watt, 12 V bulb having a vertical filament. The filament produced vertical reflected strips of light in the image plane producing, as they were swung horizontally over the detector, a sharp signal. The elongation of the reflection allowed a convenient tolerance in the vertical position of the detector and lamp, which were adjustable as illustrated in figure 5.11 on two independent slides and, in the case of the detector, on two ball and socket articulations.

The detector was a single-strand polymer fibre-optic cable of 1 mm optical diameter carrying light to a TTL-compatible photoswitch in the main control box (see section on electrical details). The fibre-optic cable was necessary because R.F. interference disturbed the photoswitch if placed near the furnace. The method of attachment of the fibre to the detector in the control box

Fig 5-11



DETAILS OF LAMP AND DETECTOR OF AUTOMATIC CRYSTAL PULLER

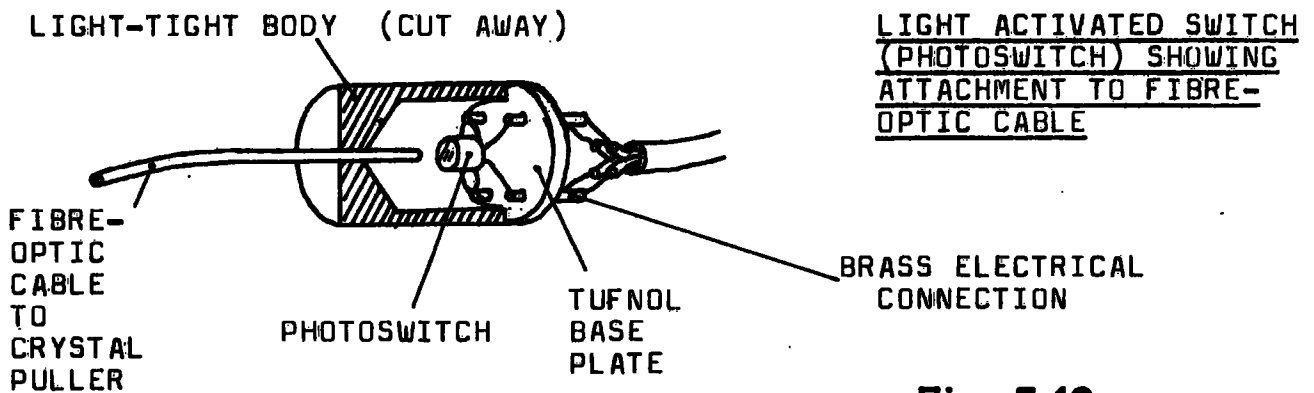


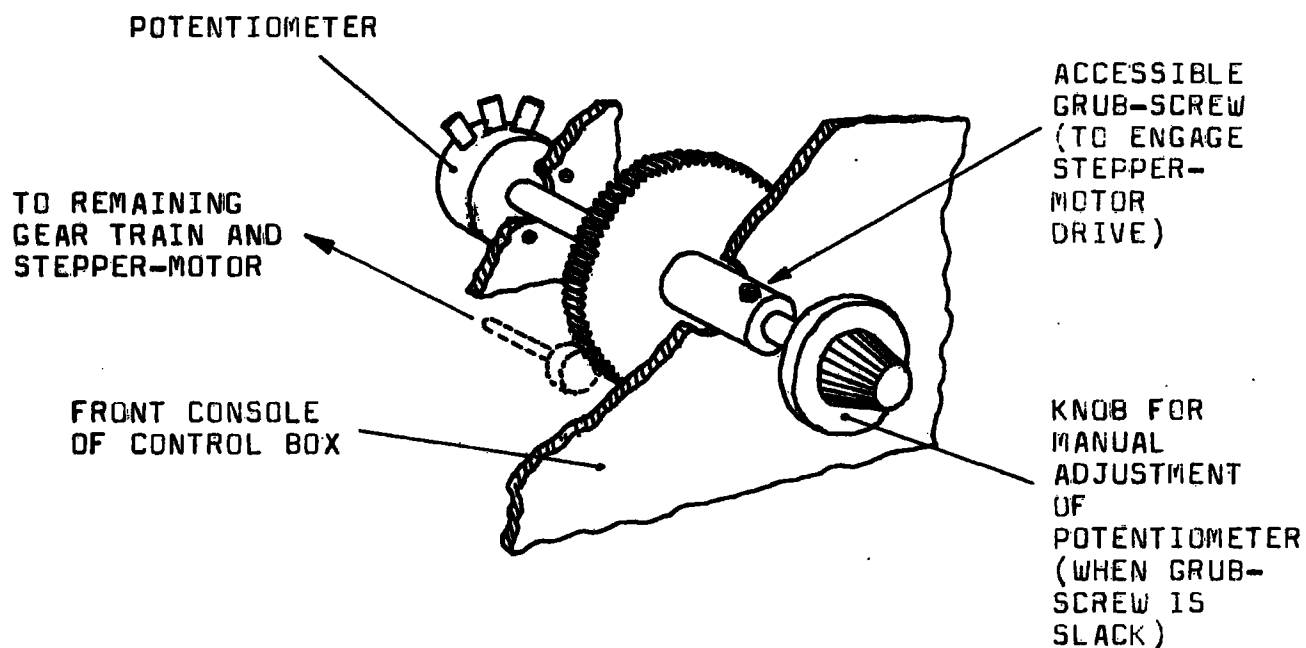
Fig 5-12

is shown in figure 5.12.

The lamp and detector, mounted externally to the vacuum system, were tracked vertically in sympathy with the internal components of the crystal puller by a rod attached to the threaded raising shaft and running in a sliding bearing (fig 5.5 and 5.6).

8) The stepper-motor and potentiometer

The stepper-motor for adjusting the R.F. furnace power was geared to a 100.Ω linear potentiometer with a reduction ratio of 120:1



THE POWER CONTROL POTENTIOMETER AS HOUSED IN THE CONTROL BOX

Fig 5-13

The normal running speed of the stepper-motor was about 90 RPM giving a resistance slew-rate of about $1.5 \Omega/\text{second}$. As set up during the growth of copper, the full range of the resistance would change the melt temperature by about 100°C in an interval that covered the melting point, giving the temperature required for stable growth over a wide range of crystal diameters. Manual adjustment of the potentiometer could be achieved by slackening the locking screw, securing the final tubular drive of the gear train to the potentiometer spindle, and retightening after movement of the spindle (see fig 5.13). The whole assembly was housed with the logic circuitry in a control box with only the potentiometer dial and locking screw accessible.

5.5 Electrical details of the automatic puller

5.5.1. Introduction

The circuitry for the control device (excluding the R.F. regulation circuit operated by the power potentiometer) had to perform the following functions:

- 1) Determine the time delay between pairs of light pulses arriving from the crystal suspension

- 2) Draw a comparison between the observed delay and a datum, representing the delay consistent with the desired growth conditions, and create an error signal.

- 3) Use the error signal to control the stepper-motor so as to turn it by an amount and in a direction which would drive the furnace power and subsequently the growth process toward the desired equilibrium.

A grossly simplified schematic diagram of the circuit

used is shown in figure 5.14. The circuit works in two stages : In the first, the light-pulse pair is converted to a single pulse by a bistable which triggers, for the duration of that pulse, a signal generator, the pulse chain being fed into a counter stack. In the second stage the stack is counted down by a reference pulse-chain. Extra pulses required to restore the counter to zero indicate the error, the up/down count control during restoration indicating the error sign. The error pulse is fed, during the zeroing of the counter, to the stepper-motor to produce the required control of the furnace. Once the motor action is complete, the circuit returns to the light detection mode to re-cycle.

A more detailed schematic version of the circuit appears in figure 5.15. Additional details include;

- 1) a means of suppressing the bistable output for a period proportional to the relaxed misalignment of the mirrors to allow an offset in the torque signal so that zero signal can represent zero torque;

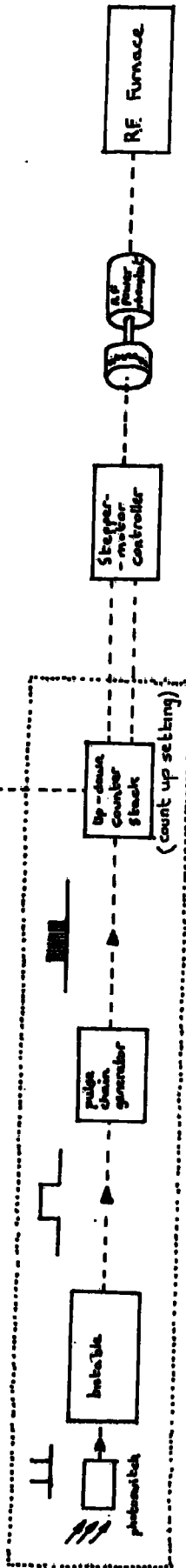
- 2) an independent digital counter to indicate to the operator the number of pulses initiated by the bistable thereby manifesting the torque;

- 3) a time delay circuit and third counter enabling the corrective movement of the stepper-motor to occur in two opposing unequal stages with intervening delay.

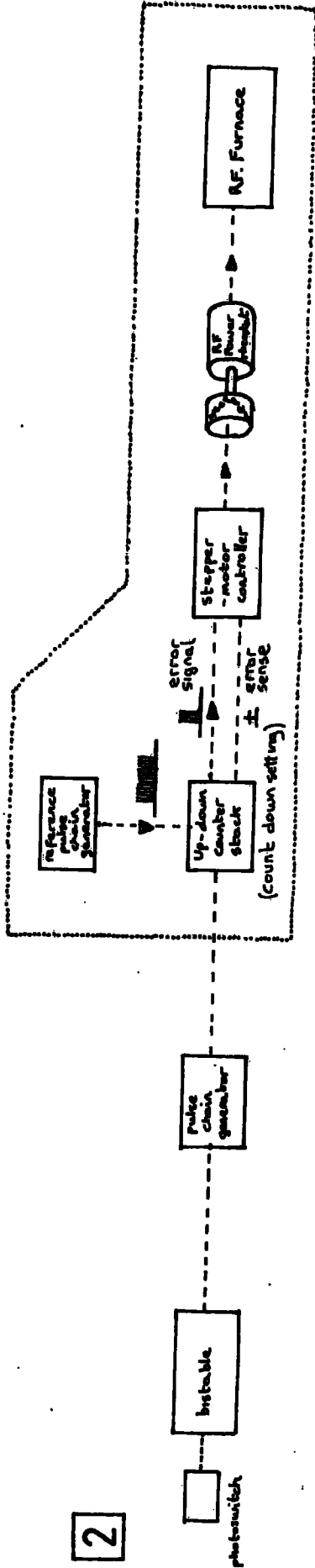
The flexibility in the stepper-motor action mentioned in 3 above was included in case long asymptotic approaches of the diameter of the crystal to equilibrium were observed, in which case deliberate overshoot and return of the power

Fig 5.14

1



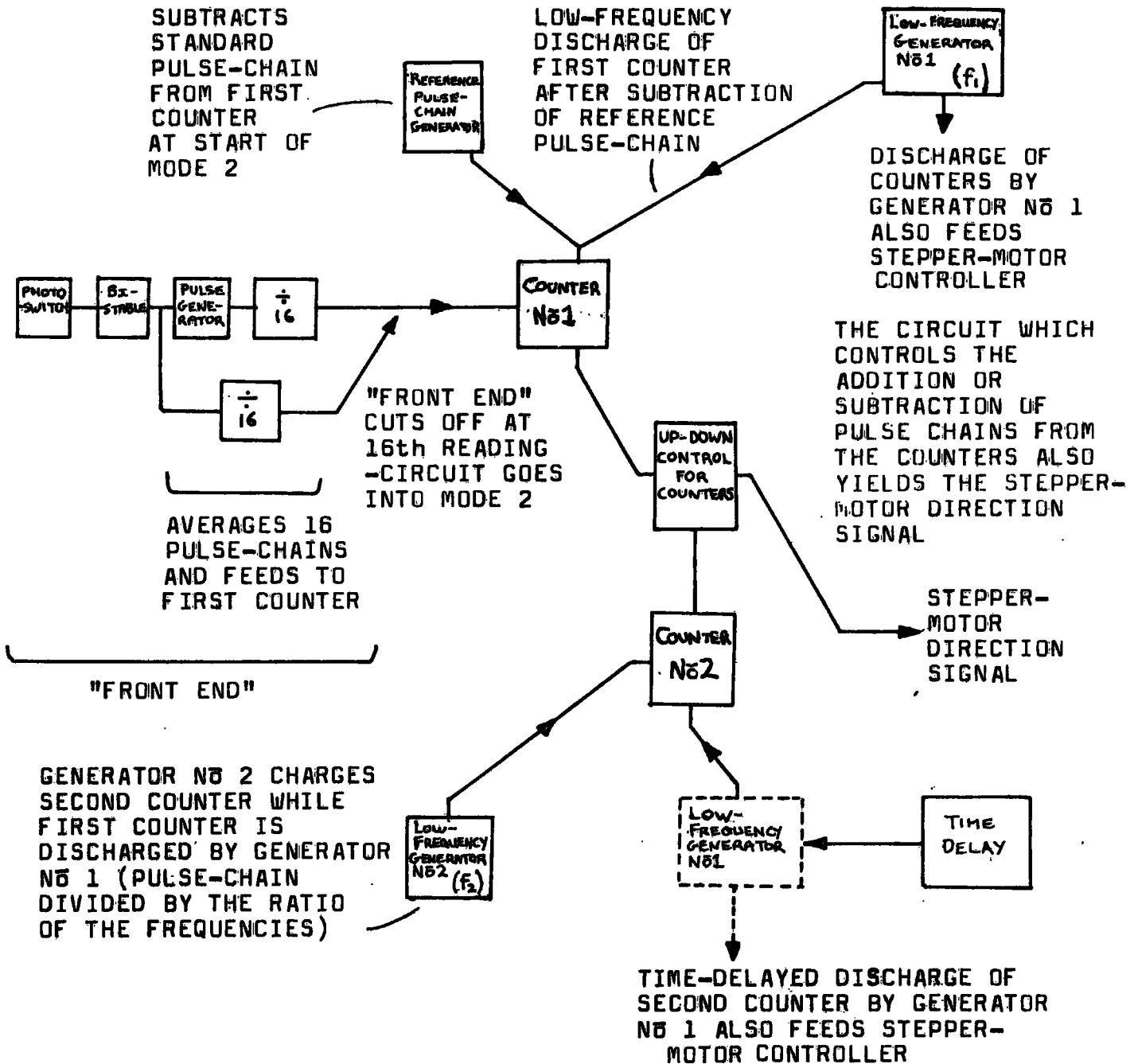
2



SIMPLIFIED BLOCK DIAGRAM OF THE LOGIC CIRCUIT FOR THE AUTOMATIC CRYSTAL PULLER

THE CIRCUIT OPERATES IN A LIGHT DETECTION MODE INITIALLY, THEN SWITCHES TO CONTROL MODE. THE OPERATIVE ELEMENTS IN THE TWO MODES ARE SHOWN ENCLOSED IN DOTTED LINES. THE REAL CIRCUIT IS MORE COMPLEX (SEE NEXT FIGURE).

MORE DETAILED DIAGRAM OF THE LOGIC
CIRCUIT FOR THE AUTOMATIC CRYSTAL PULLER
(STEPPER-MOTOR CONTROLLER NOT SHOWN)



A MORE COMPREHENSIVE DESCRIPTION OF THE ORDER OF EVENTS OCCURRING DURING ONE OPERATING CYCLE OF THE CIRCUIT IS GIVEN IN THE TEXT. THE FULL DETAILS OF THE CIRCUIT ARE GIVEN IN FIGURES 5.17 to 5.30.

Fig 5-15

setting would improve the feedback response.

The console for the control box is shown in figure 5.16. The adjustments available are;

- 1) The photoswitch light threshold.
- 2) The dead-time (offset) by which part of the torque signal is suppressed.
- 3) The torque datum
- 4) The total movement of the stepper-motor for a given detected error in the crystal torque, abbreviated to T.S.C.; total stepper change.
- 5) The delay between the two stepper-motor movements per operating cycle.
- 6) The ratio of the first to the second movement of the stepper-motor.
- 7) A coarse manual adjustment to the power setting of the furnace.
- 8) A fine adjustment to the power setting of the furnace which can be controlled by the stepper-motor.
- 9) A revolving shaft making any stepper-motor action obvious (geared 1:10 with motor).
- 10) A switch to interrupt the feedback process and display, on the digital counter, discrete torque values for each rotation of the crystal puller.

The simple application of 74121 and 555 monostable/astable integrated circuits as control elements in the logic circuit allowed adjustments to the circuit to be made through the R.C. networks associated with them; hence the possibility of potentiometer controls on the front console. The 74121 and 555 integrated circuits are quoted as having a time

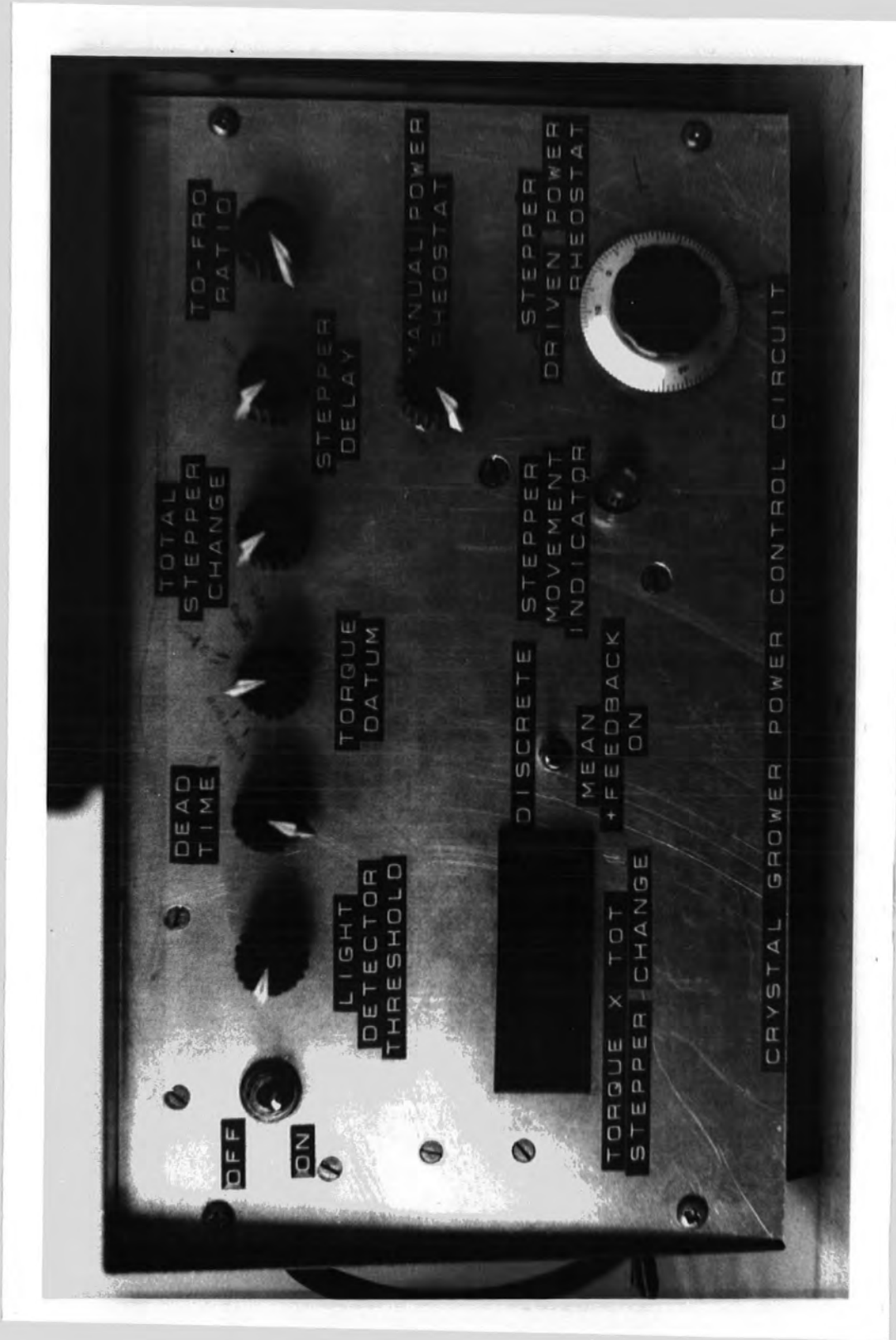


Fig 5-16

THE CONSOLE OF THE CONTROL BOX

delay reproducible to about 1% at a given temperature, which was adequate for the accuracy desired here.

The details of some of the logic gating was influenced by the availability of integrated circuits; alternative solutions could be devised.

5.5.2. Details of the circuit operation

Referring to figure 5.15, the order of events in the control circuit during normal operation is as follows:

- 1) The bistable triggered by the photoswitch sends successive bursts of pulses from the generator (frequency adjustable using T.S.C. control) through a divide-by-16 integrated circuit (a 7493 using the last bit of the fourth bistable as output) to counter No 1. After 16 bursts, counter No 1 is isolated and is left containing an average over 16 values of the torque in units dependent on the pulse generator frequency. At this stage, the digital counter (not shown) is latched to display the torque permanently until the same point in the next operating cycle.

- 2) Upon isolation from the torque signal, that is at the beginning of mode 2, the reference pulse chain generator delivers a standard number of pulses, controlled by the datum setting, to the counter, reset to count down rather than up. Monitoring the counter for the empty condition allows a signal to be produced defining the polarity of the remaining contents. The number left in the counter is proportional to the deviation of the crystal torque from the present datum.

- 3) A low frequency (approximately 50 Hz) generator

discharges the contents of counter No 1 to the stepper-motor, the error polarity signal defining whether a count reversal is necessary and also indicating the required direction of motor revolution. Simultaneously to the discharge a second counter is charged at a lower frequency to accumulate a reduced error signal with a scaling factor equal to the ratio of the two low frequencies.

4) After the first movement of the stepper-motor, a time delay operates which inhibits all circuitry for a short period.

5) At the end of the delay, the counting direction of the second counter is reversed and the counter discharged at the higher low frequency to the stepper-motor after its directional control has been reversed.

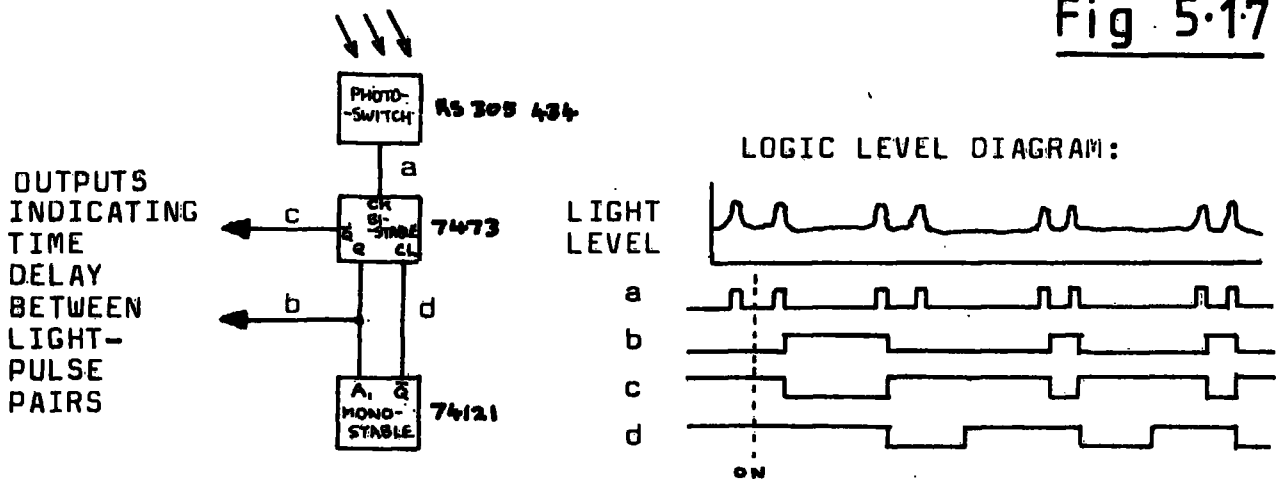
6) When both counters are empty a signal initiates mode 1 and a full cycle of the circuit has been completed.

To facilitate a detailed description of the logic circuitry, it will be discussed as the sum of the smaller circuit elements shown in figures 5.17 to 5.29.

The photoswtich circuit (fig 5.17) was based on an RS 305 434 T.T.L. compatible integrated circuit using a silicon photodiode (fig 5.18). In order to produce distinct triggering of the switch, it was found necessary to isolate the photoswtich from the power supply of the rest of the circuit. The voltage regulators used to power the rest of the circuit were loaded to an extent that caused greater voltage instability than was permissible for the critically sensitive photoswitch, the symptom being that as the light level rose through threshold the

PHOTOSWITCH CIRCUIT
 (OPERATES CONTINUOUSLY IN BOTH CIRCUIT MODES)

Fig 5.17



THE DIAGRAM INDICATES THE AUTOMATIC ADJUSTMENT OF THE BISTABLE OUTPUT INTO PHASE WITH THE PULSE PAIRS FROM THE PHOTOSWITCH GIVEN THAT THE MONOSTABLE RUNS FOR A PERIOD OF HALF THE REPEAT TIME FOR THE PULSE PAIRS.

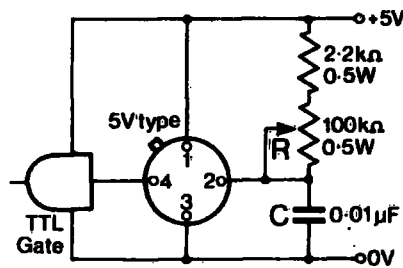


Fig 5.18

LIGHT ACTIVATED SWITCH (RS 305-434)

THIS DEVICE IS A TTL COMPATIBLE SWITCH WITH A LIGHT THRESHOLD SET BY AN EXTERNAL RC NETWORK. SUCH A DEVICE PERFORMED THE LIGHT DETECTION ON THE AUTOMATIC CRYSTAL PULLER.

switching action would tremble and upset the circuit logic. A third 7805 voltage regulator for the photoswitch alone solved the problem.

Since the light-pulse pairs could be timed in two possible ways, namely the short interval or the long interval,

when torsional information was not required. The signal from line C activated the 74121 monostable via the negative-triggered input to prevent the astable (signal generator) passing pulses to line g and the digital counter (based on the ZN 1040 E shown in fig 5.20).

ZN1040E COUNT DISPLAY INTEGRATED CIRCUIT (RS 306-285)

A ZN1040E WAS USED TO PROVIDE A DIGITAL DISPLAY OF THE TORQUE SIGNAL (THE "FRONT END" COUNTER).

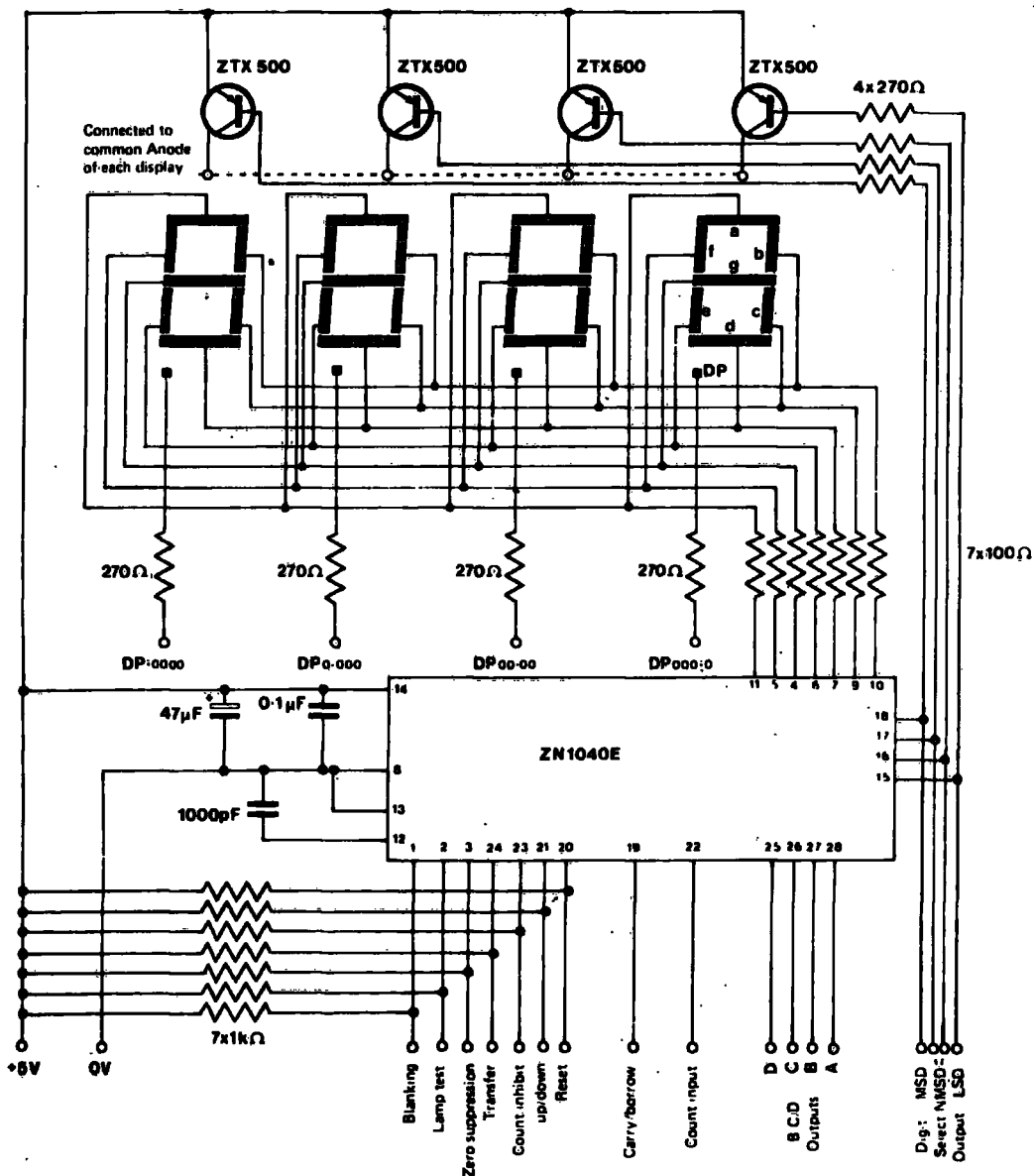
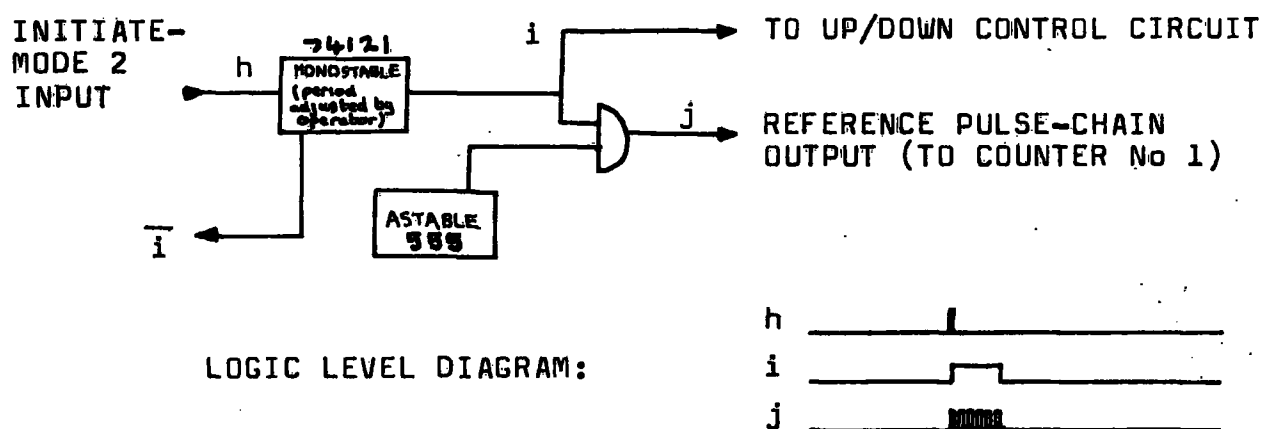


Fig 5.20

After briefly suppressing the astable signal (frequency approximately 10 KHz) the remaining signal continued until interrupted by the end of the bistable pulse, this process occurring 16 times before the front-end was inhibited. On the 16th bistable pulse a negative going signal from a divide-by-16 integrated circuit triggered a monostable which latched the digital counter so as to display the accumulated signal that had arrived along line g (also via a divide-by-16 integrated circuit). The latching pulse was sent out via line h to trigger the reference pulse-chain generator circuit which in turn, via the up/down control circuit, inhibited the front-end leaving the circuit in mode 2.

REFERENCE PULSE-CHAIN GENERATOR

Fig 5.21



The reference pulse-chain generator circuit (fig 5.21) operated once, very briefly, during a normal working cycle of the whole circuit.

Counters number 1 and 2 (figures 5.22 and 5.23) were

similar, both consisting basically of a stack of bistables each having three 74193 counter integrated circuits.

Counter No 1 was charged during mode 1 by the torque signal, then discharged by the reference signal followed by a low frequency signal. The counting direction of the 74193 stack was set by the particular input used, but two nand gates altered this to control by the logic state of a pair of inputs (1,0 or 0,1), a third input taking the pulse chain. The counting directions of both counters were set simultaneously by the up/down control circuit. Using three four-input nor gates feeding a three-input nand gate, a counter-empty signal was produced by a zero count in either circuit (0=empty). For the first counter this signal was relayed to the up/down count control as indicating whether a count reversal was necessary before low frequency discharge. For the second counter it served only to indicate that a new operating cycle of the circuit as a whole could begin. Clearing of the first counter when the circuit is switched on was accomplished using a capacitative voltage transient on the clear input. The second counter was provided with a similar clearing pulse originating in the clear circuit.

The up/down control circuit (fig 5.24) altered the count direction of the two counters, treated together by the circuit, on the basis of four inputs. The logic level diagram for the possible cases of positive and negative torque error is given in figure 5.25. The four inputs are labelled h, i, k and n.

The low frequency discharge circuit (fig 5.26) was a more complex version of the reference pulse-chain circuit.

UP/DOWN CONTROL CIRCUIT

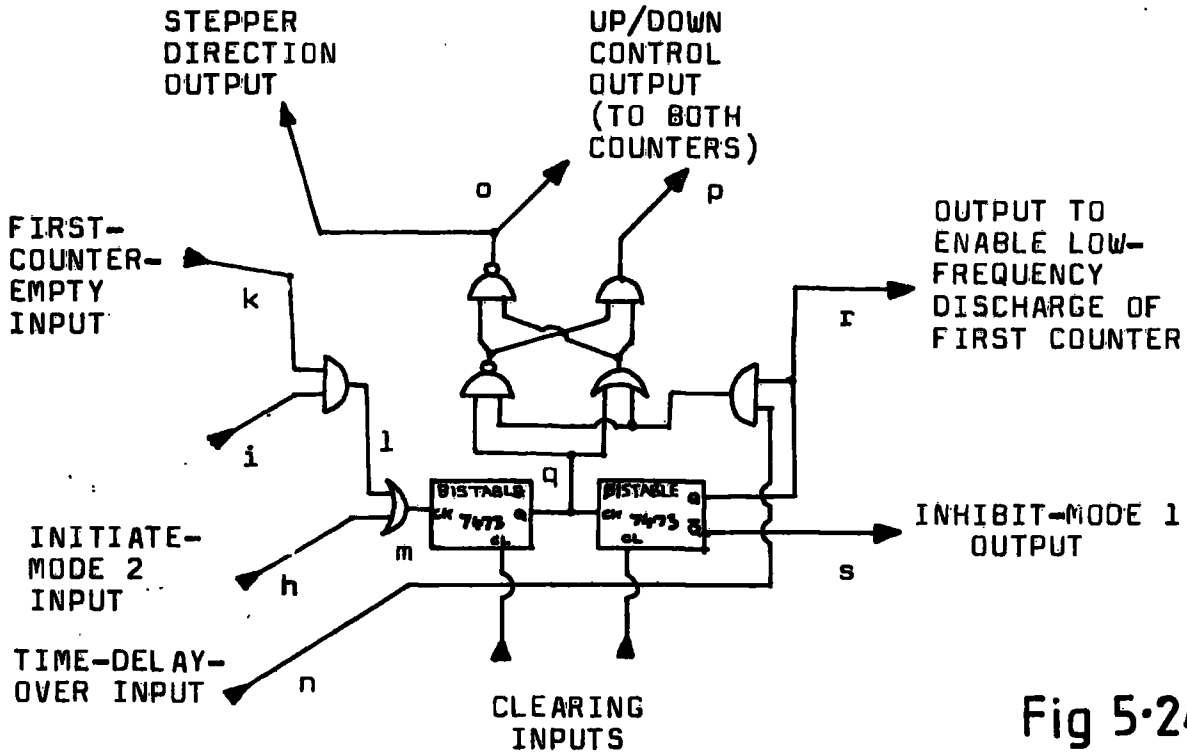


Fig 5-24

THIS CIRCUIT CONTROLS THE DIRECTION IN WHICH THE STEPPER-MOTOR TURNS SINCE THIS IS INDICATED BY THE COUNTING SENSE REQUIRED BY THE TWO COUNTERS AS THEY DISCHARGE THE TORQUE-ERROR PULSE CHAIN (OR THE DIVISION OF IT).

LOW-FREQUENCY CHARGE AND DISCHARGE CIRCUIT

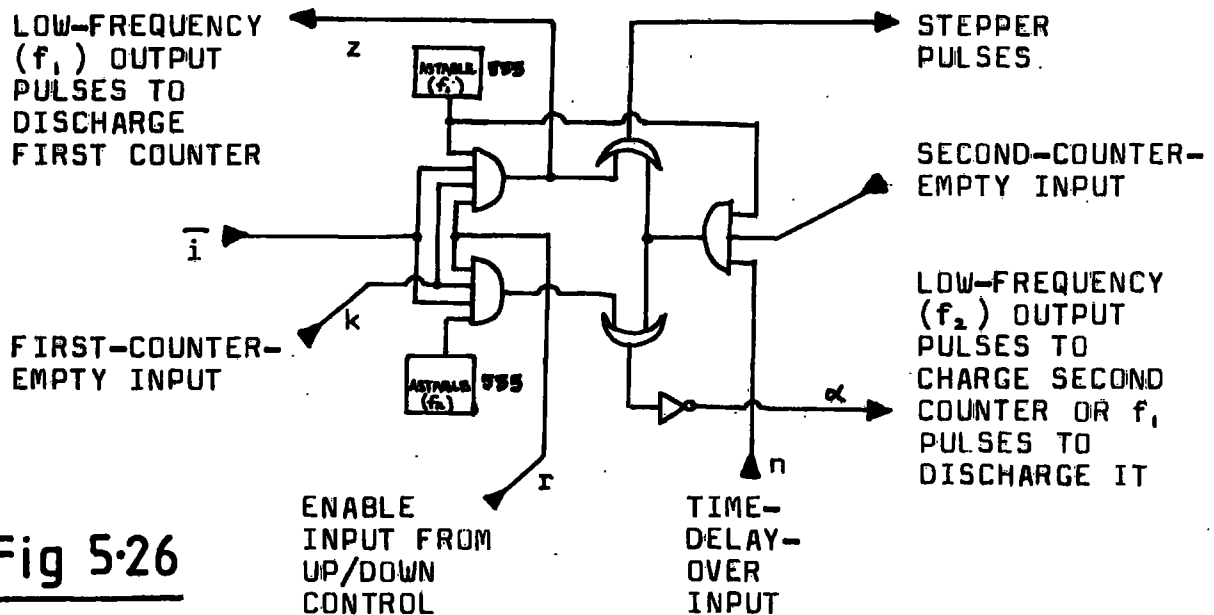


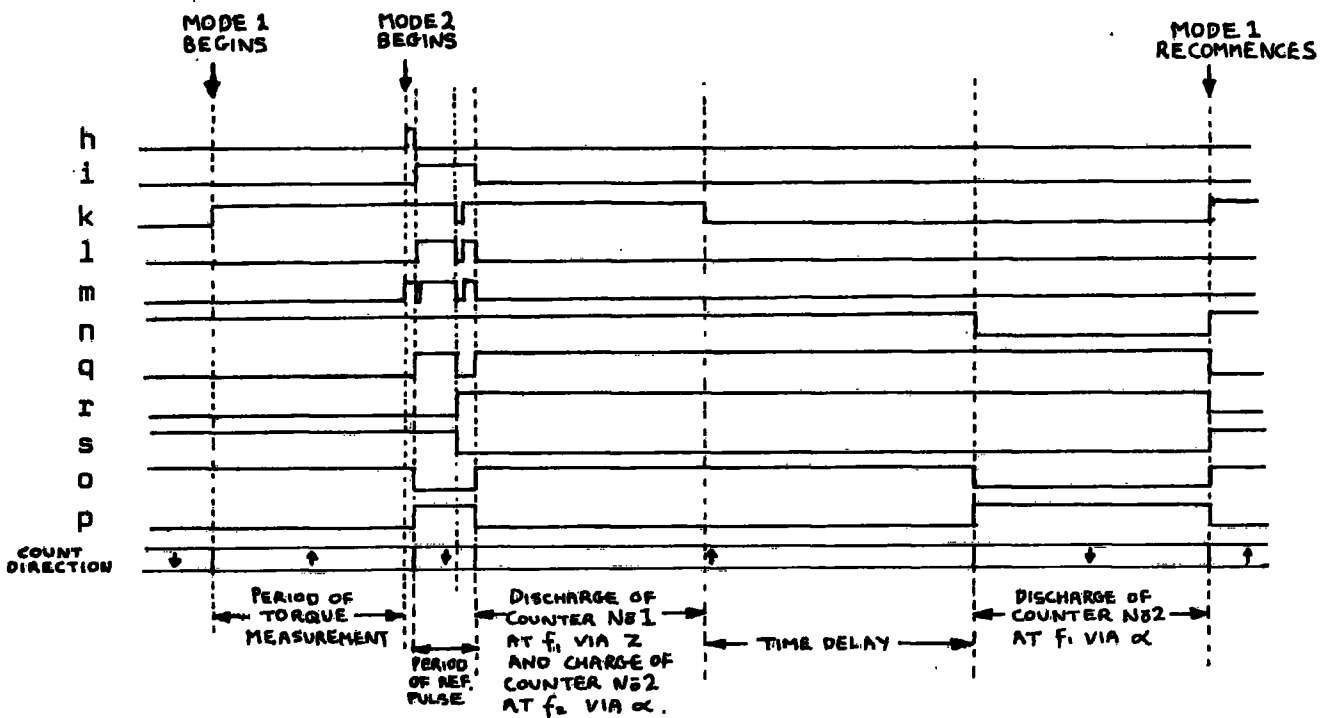
Fig 5-26

THIS CIRCUIT OPERATES ON COUNTERS 1 AND 2 PRODUCING AS IT DOES SO THE PULSES WHICH DRIVE THE STEPPER-MOTOR LOGIC.

UP/DOWN CONTROL CIRCUIT LOGIC LEVELS
FOR ONE OPERATING CYCLE:
(TWO POSSIBLE CASES)

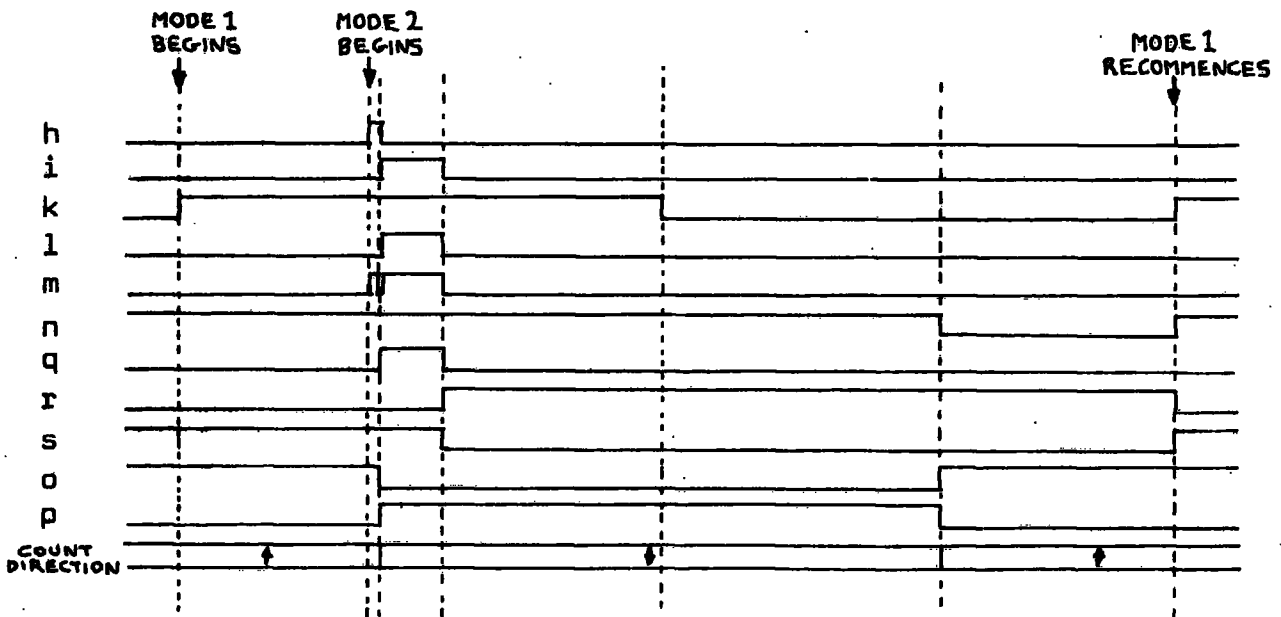
CASE 1

REFERENCE PULSE EMPTIES COUNTER No1 AND OVERRUNS TO GIVE A NEGATIVE TORQUE ERROR IN COUNTER.



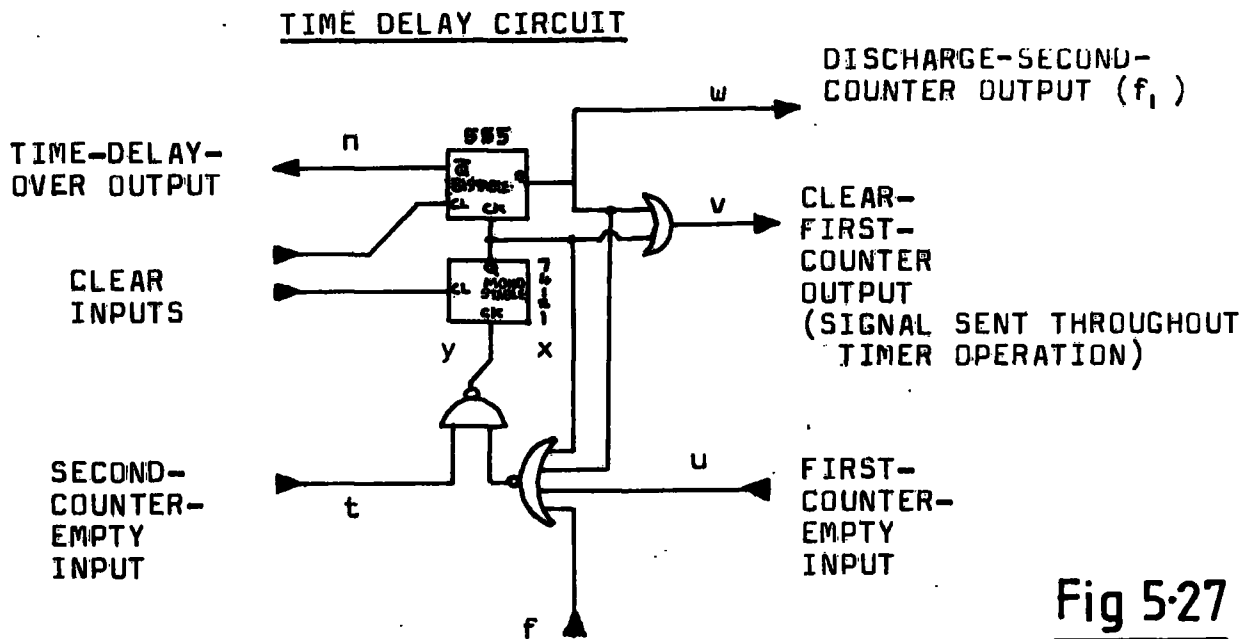
CASE 2

REFERENCE PULSE LEAVES COUNTER No1 CONTAINING A POSITIVE TORQUE ERROR.



The differences were that the low frequency circuit had the capability of providing two signals of differing frequency and that there were five control inputs. The logic level diagram of figure 5.25 indicates the activities of the low frequency circuit.

The time delay circuit (fig 5.27) had a range of 8 to 160 seconds.

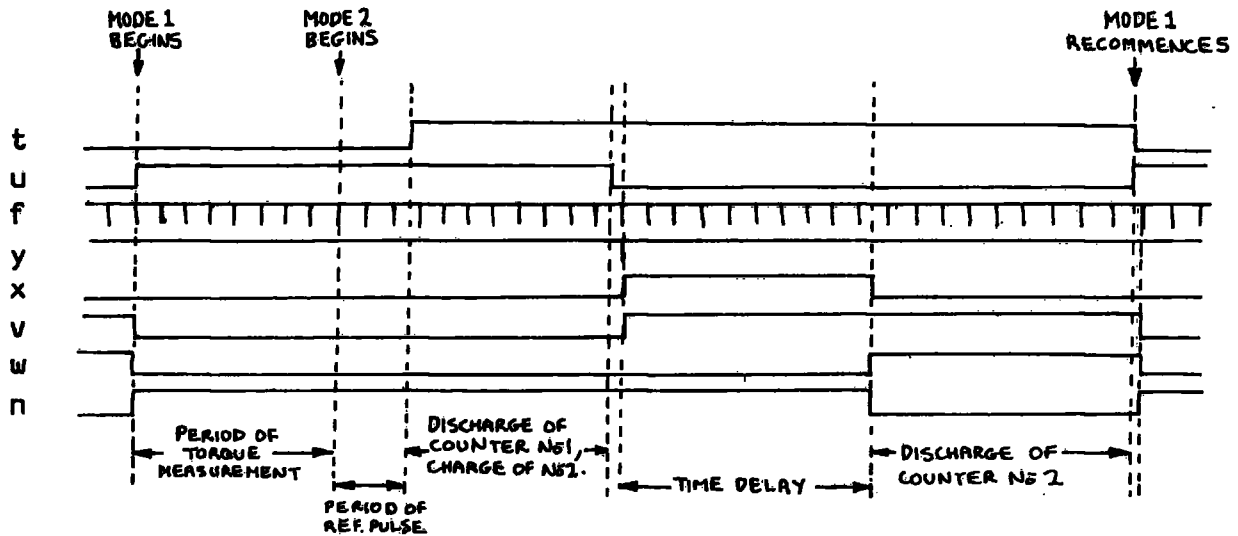


THIS CIRCUIT CONTROLS THE DELAY BETWEEN THE FORWARD AND BACKWARD CORRECTIVE MOVEMENTS OF THE STEPPER-MOTOR.

Two inputs monitored for an appropriate condition of the counters, namely that the first was zero and the second non-zero, while the third input provided a distinct triggering pulse from part of the front-end circuitry. Logic levels during operation are indicated in figure 5.28. A clearing pulse was sent to counter No 1 from the beginning

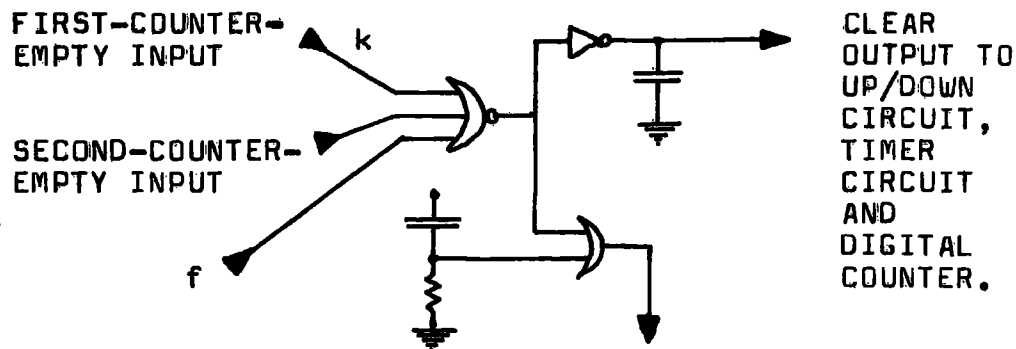
TIME-DELAY CIRCUIT LOGIC LEVELS
FOR ONE OPERATING CYCLE

Fig 5-28



of the time-delay to the recommencement of mode 1 because changing the count direction at the end of the delay, using lines O and P, injected a pulse in counter No 1 causing the loss of the empty-signal if clearing was not maintained. Loss of the empty-signal at that stage would prevent the circuit as a whole working. For the same reason, at the commencement of mode 1, a clearing pulse was supplied to counter No 2 simultaneously to the final change in counting direction, so that it would be zero as required at the beginning of the operating cycle.

The clear circuit (fig 5.29) reset (cleared) all counters and bistables at the end of mode 2 for each operating cycle. It also produced transient clearing pulses at switch-on. The clearing pulses at the beginning of mode 1, were triggered by pulses from the front-end

CLEAR CIRCUITFig 5-29

CLEAR-SECOND-COUNTER OUTPUT
(COUNTERS MUST BE HELD CLEAR DURING THE
CLEARING OF THE UP/DOWN CIRCUIT)

THIS CIRCUIT CLEARS THE UP/DOWN CONTROL CIRCUIT WHICH IN TURN SENDS THE "FRONT END" INTO MODE 1. THE CIRCUIT ALSO CLEARS THE TIMER WHICH IN TURN PRIMES THE FIRST COUNTER. THE CIRCUIT ALSO RESETS THE DIGITAL COUNTER IN THE "FRONT END". NOTE THAT CLEARING PULSES ARE PRODUCED TRANSIENTLY BY THE CAPACITORS ON SWITCH-ON.

along line f in order that mode 1 synchronised with the incoming torque signals, preventing truncation of the first torque signal.

The complete circuit, minus the circuitry for the stepper-motor, is given in figure 5.30. All switches were incorporated into one four-pole, four-throw toggle switch allowing display of the torque for every revolution of the puller without mode 2 operating.

The Impex 4-pole stepper-motor (type ID0 4) was controlled by a commercially available TTL-compatible circuit requiring only a direction input (1 or 0) and a clock input to step the motor. These were coupled to R and T respectively in figure 5.30. As is normal, the earth

(MINUS THE COMMERCIAL STEPPER MOTOR CIRCUITRY COUPLED TO "R" AND "T")

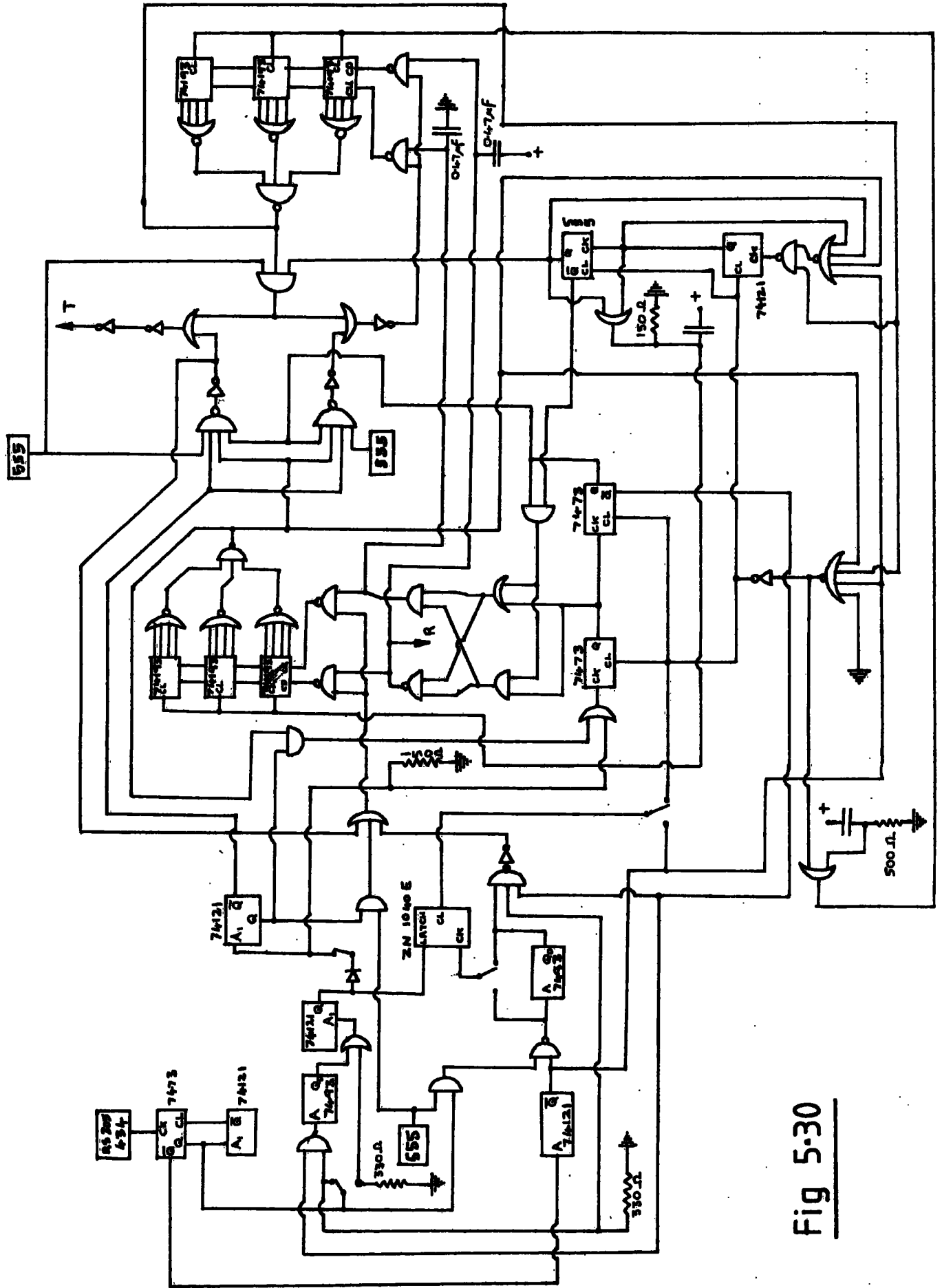


Fig 5-30

line of the motor was isolated as far as possible from the logic circuitry to prevent inductive noise disturbing the latter. (A standard RS 238 514 mains filter was also incorporated to protect the logic circuitry).

A typical digital read-out from the circuit was 500 units for a 10° mismatch of the suspension mirrors, corresponding to a torque of about 3×10^{-8} Nm. Thus the sensitivity was typically about 6×10^{-11} Nm per bit though instabilities gave a standard deviation of about 50 bits in the torque signal, averaged over 16 readings, under normal running conditions.

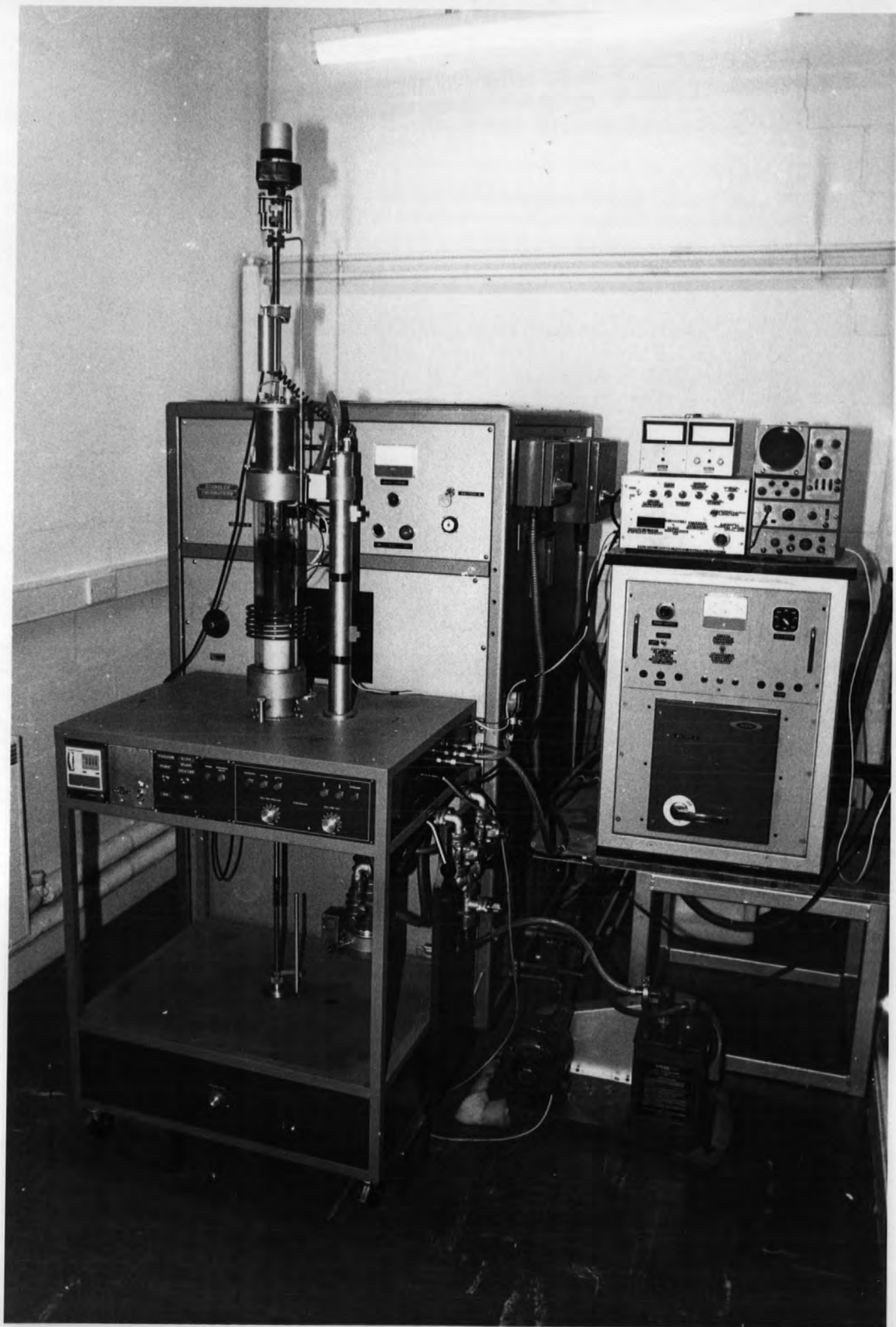
5.6 Operation

In operation it was found important to;

1) manually adjust the suspension fibre to give sufficient rotational clearance between suspended frame and lower frame (fig 5.8) to ensure that the relative rotational rocking of the lower frame did not cause it to strike the upper over the anticipated torque range. Striking of the frames was manifest as a gross instability in the apparent torque;

2) adjust the photoswitch threshold to about the middle of the range over which the two distinct light pulses were observed, the photoswitch output being displayed on an oscilloscope. An initially clean quartz tube was used so that there was no light intensity change with respect to tracking of the detector;

3) switch into full control (from discrete torque measurement) while the rotating mirrors of the suspension





were well away from the detector, that is whilst no torque signal was being sent, thereby eliminating the possibility that the first signal was truncated resulting in a small error in the first averaged torque reading in the new status.

Adjustment of the remaining electrical controls was dependent on the desired crystal size and growth rate.

Figures 5.31 and 5.32 show the whole equipment and the pulling region respectively.

5.7. Results

On the basis of the work done, certain observations can be made, some relevant to viscous torque control in principle, others to the present means of achieving it.

5.7.1. General

A plot of torque VS diameter is given in figure 5.33 for copper under typical conditions of pull-rate and rotation rate, for the melt dimensions mentioned in 5.4.2. The monotonic increase is as required, but the torque is smaller than anticipated by about a factor of 3 (see comment on pull-rate).

The melting point viscosities for a number of metals are as given in table 5.1 from Cavalier (1960) and Ofte (1967) with copper having a value of about 5 centipoise. Assuming that the torque is proportional to viscosity, then most pure metals will give torques of the order shown in figure 5.33. Table 5.1 is on page 172.

A plot of torque VS pull-rate for copper at a

PLOT OF TORQUE ON A CZOCHRALSKI GROWN COPPER
CRYSTAL VS DIAMETER (CRYSTAL TURNING AT 50 RPM
AT A PULL-RATE OF 0.6 mm/min)

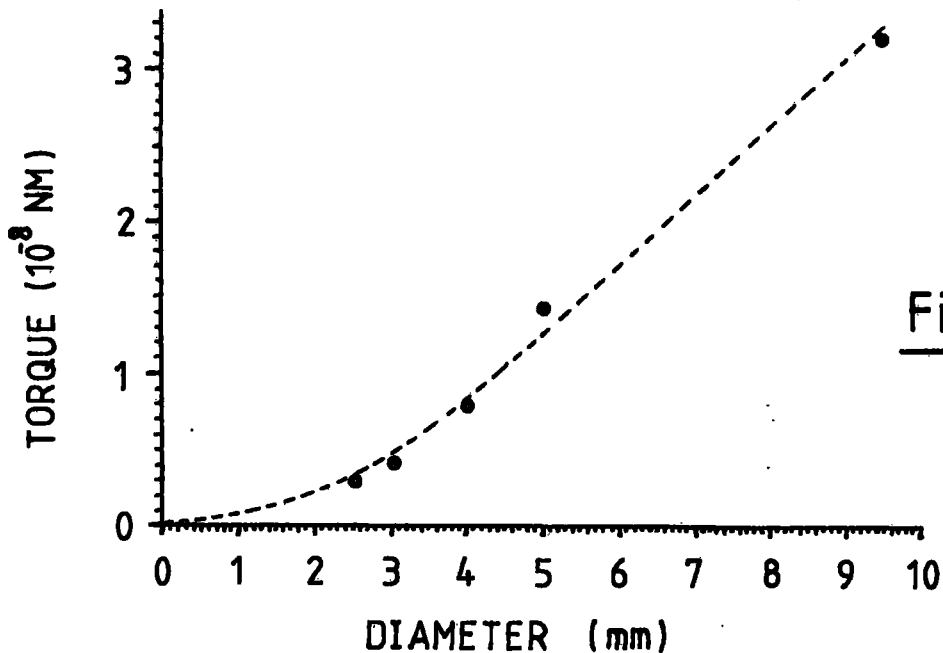
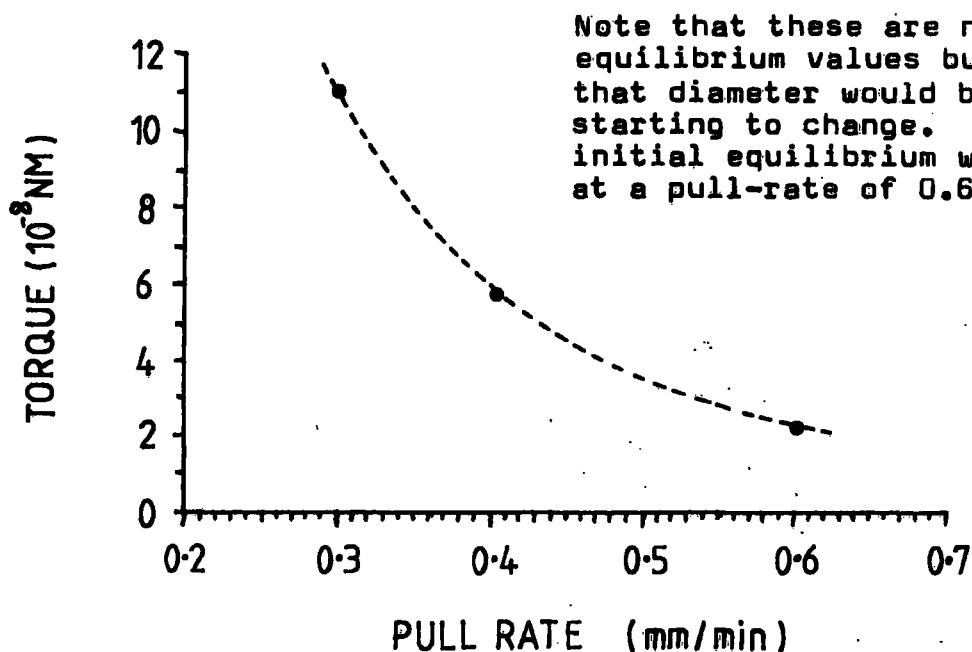


Fig 5-33

PLOT OF TORQUE ON A 7mm DIAMETER CZOCHRALSKI
GROWN COPPER CRYSTAL VS PULL-RATE (CRYSTAL
TURNING AT 50 RPM)



Note that these are not equilibrium values but that diameter would be starting to change. The initial equilibrium was at a pull-rate of 0.6 mm/min

Fig-5 34

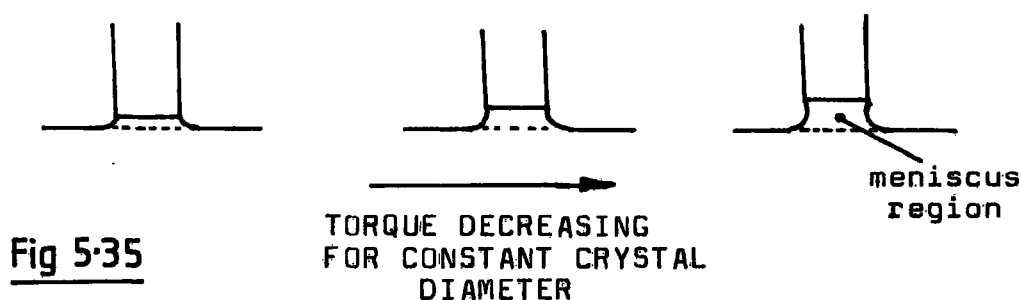
diameter of 7 mm, for a melt temperature which stabilises growth at that diameter at a pull-rate 0.3 mm/min, is shown in figure 5.34. The extraordinary sensitivity of the torque measurements to the conditions of the meniscus at the growing interface is apparent, indeed a change in the pull-rate by a factor of 2 changes the torque by a factor of 5. For a very slow pull, the torque approaches the anticipated values deduced from the early trials with water for which no meniscus column was present.

Higher pull-rates give lower torques prior to the reduction in crystal diameter that the change in the pull-rate subsequently causes. Higher pull-rates were observed to give relatively more stable (albeit smaller) torque readings, the increased meniscus column between growth interface and melt surface presumably decoupling the crystal from stirring effects in the bulk of the melt, the majority of the torque then being due to shearing of the fluid in the meniscus region (see fig 5.35). The torque on larger diameter crystals will be less critically dependent on the (relatively) smaller meniscus region.

The torque on the growing crystal is dependent on the concentricity of the crystal tip in the melt. An eccentrically rotating crystal requires a torque dependent on its diameter but also on any concentricity change during growth. Furthermore, instability in the torque reading develops for eccentric rotation. Centring of the crystal on its rotation axis is therefore vital for effective automatic control.

The torque on the crystal can be altered significantly by impurities in the melt, particularly those manifested on the melt surface, which interfere with the normal rotational shear of the fluid. Impurities of a type visible on the melt surface shortly after liquification but subsequently lost by adhesion to the crucible or by evaporation (or perhaps 'lost' by dissolution into the melt) were observed to cause torque increases of a factor of two.

DIAGRAM SHOWING SCHEMATICALLY THE CHANGE IN THE MELT SHAPE WITH RISE IN THE FREEZING INTERFACE (ASSUMED PLANAR) DUE TO SUDDEN INCREASE IN THE MELT TEMPERATURE OR CRYSTAL PULL-RATE; THE MENISCUS REGION INCREASING AND CRYSTAL TORQUE DECREASING



5.7.2. The present equipment

A control crystal was grown without any torsional feedback to illustrate the drift in the crystal diameter occurring under conditions of nominal temperature stability. The crystal (fig. 5.36) shows a gradual increase in diameter (typical of other crystals not shown) with an absence of fluctuations associated with the power adjustments made during the growth of later automated crystals. This crystal shows a 100% increase in diameter over a 6 cm length grown in 1 hour and 40 minutes.

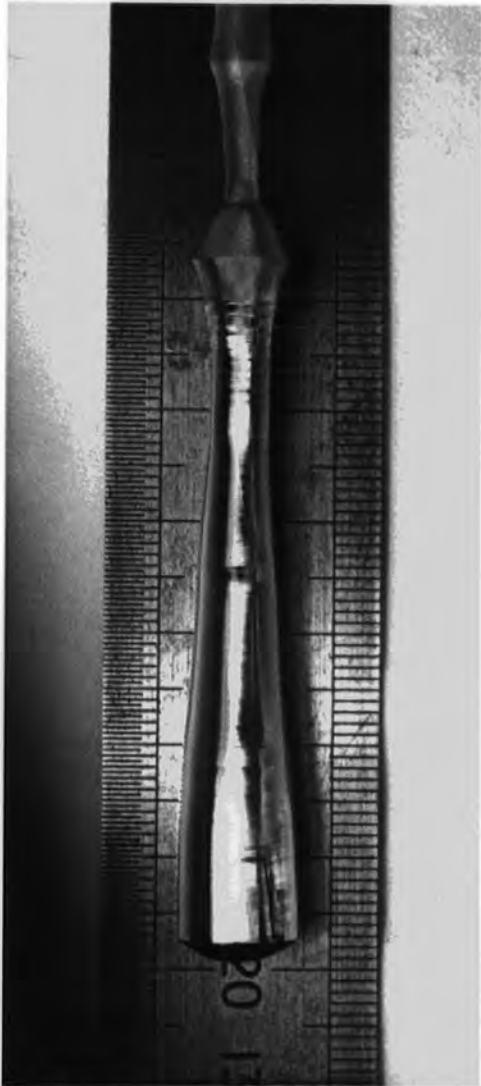
Feed-back sensitivity is the change in equilibrium diameter (rather than observed diameter which is usually in a state of transition) correlating to the overall change in the furnace power (after forward and reverse adjustments) per given detected torque deviation. The time-constant refers to the response of the crystal diameter to an alteration of the power controller of the furnace.

Fig 5.37

Pull-rate = 0.4 mm/min
 Feed-back sensitivity = $2.5 \times 10^5 \text{ N}^{-1}$
 Time-constant = 160 secs
 Time delay = 120 secs
 To:fro ratio = 2:1

Fig 5 36

A 'control' crystal



Three lengths of crystal grown under automatic control are illustrated in figures 5.38-5.40. The crystals were not necked down since testing of the equipment did not require this. The regions over which control took place are indicated. These crystals show a poor level of control having a diameter variation of approximately $\pm 10\%$, the torsional measurement being too insensitive and unstable in the present equipment for more accurate work. The system is however workable and further development could improve the control by the factor of 10 necessary to compete with existing commercial methods. The principal problem at the moment is friction in the jewel support bearing (which could be replaced by a floating bearing using silicone oil).

At a given diameter of crystal, a certain small change in the R.F. power potentiometer produces a well defined change in crystal diameter once equilibrium in the growth has been re-established. Since the control circuit changes the power by an amount dependent on the torque error signal, the feedback can be measured in millimeters (of crystal diameter) per newton metre (of torque error) for the prevailing mean diameter. A time-constant can usually be defined for a given crystal diameter (by which profile changes occur to the crystal for a step in R.F. power), though the speed of response of the crystal may in some cases be dependent on the changing thermal mass of the melt. Other feedback parameters, more readily measured, are the delay time between forward and reverse movements of the power potentiometer by the stepper-motor and the ratio of these movements. The control conditions are summarised by these parameters in figures 5.37-5.40 with each crystal shown.

Pull-rate = 0.7 mm/min
 Sensitivity = $2.5 \times 10^5 \text{ N}^{-1}$
 Time-constant = 160 secs
 Time delay = 165 secs
 To:fro ratio = 2:1

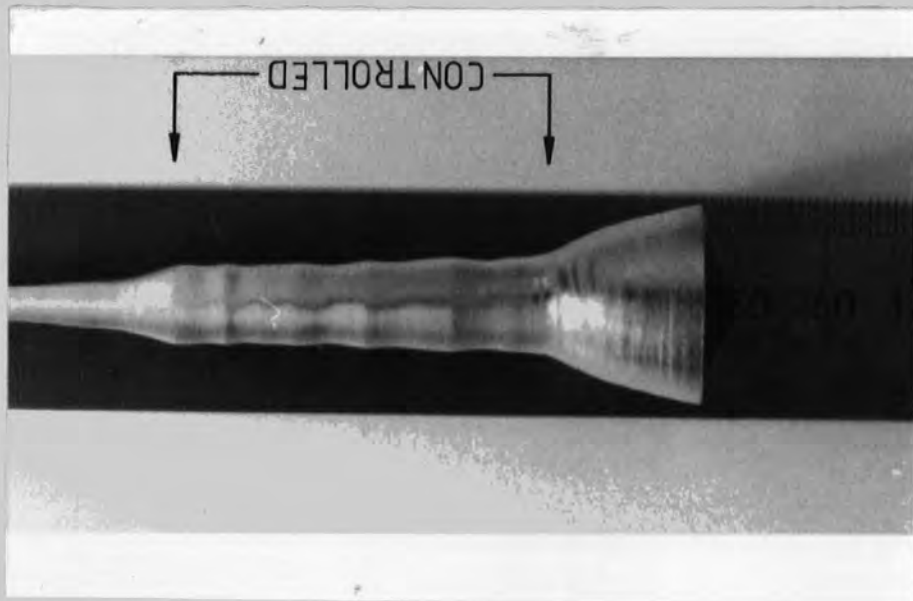


Fig 5.38

Pull-rate = 0.4 mm/min
 Sensitivity = $2.5 \times 10^5 \text{ N}^{-1}$
 Time-constant = 160 secs
 Time delay = 100 secs
 To:fro ratio = 2:1

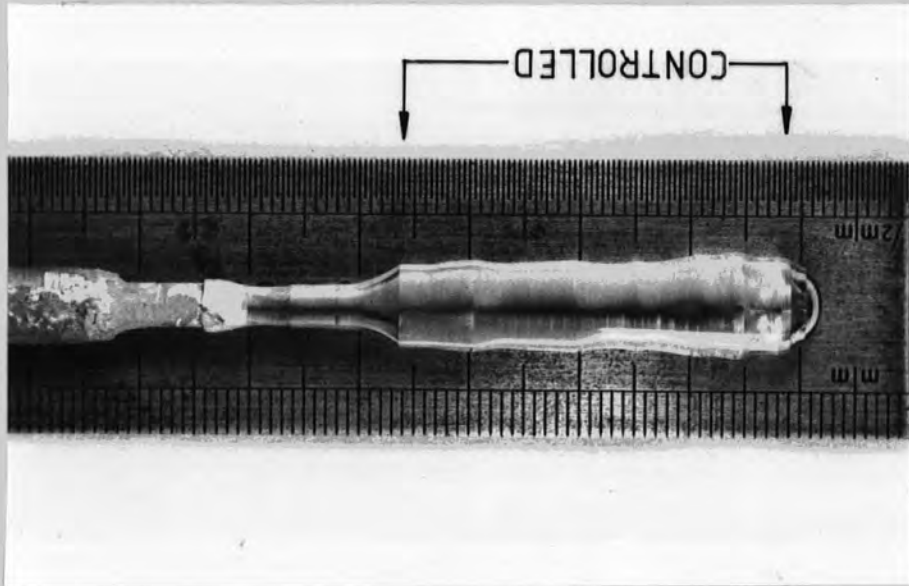


Fig 5.39

Pull-rate = 0.6 mm/min
 Sensitivity = $2.5 \times 10^5 \text{ N}^{-1}$
 Time-constant = 160 secs
 Time delay = 100 secs
 To:fro ratio = 2:1

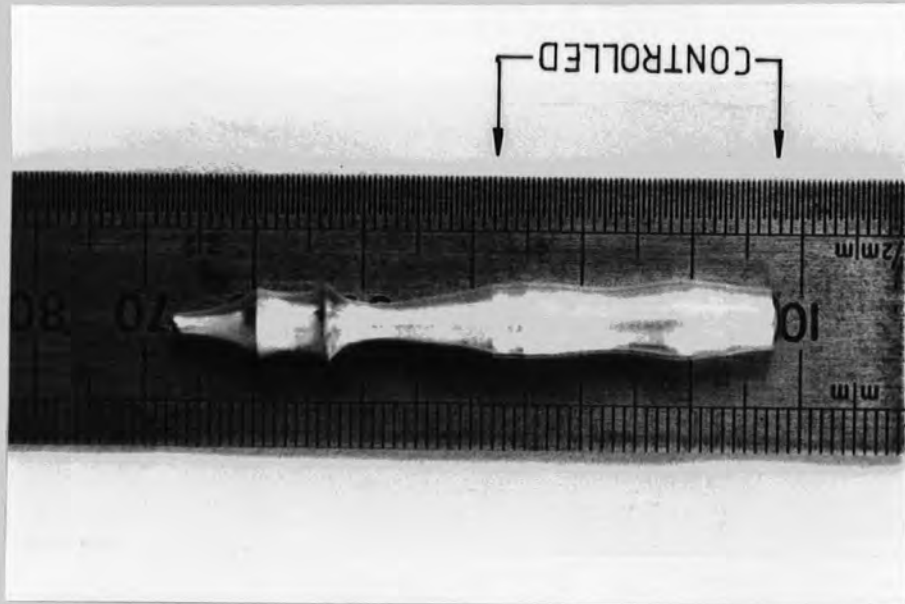


Fig 5.40

The consequence of not rocking the jewel bearing supporting the suspension is shown in figure 5.37 ; the shape of the crystal is due to a positive feedback whereby the crystal orientation sticks at opposite extremes on the jewel bearing due to static friction, and overcorrective measures to the diameter (about an average value) are required to establish a crystal-torque/fibre-torque difference capable of dislodging the bearing.

DIAGRAM SHOWING THE STEPPED CRYSTAL
STRUCTURE DUE TO INITIAL ECCENTRICITY
OF THE CRYSTAL SEED ON A FREELY
HANGING SUSPENSION

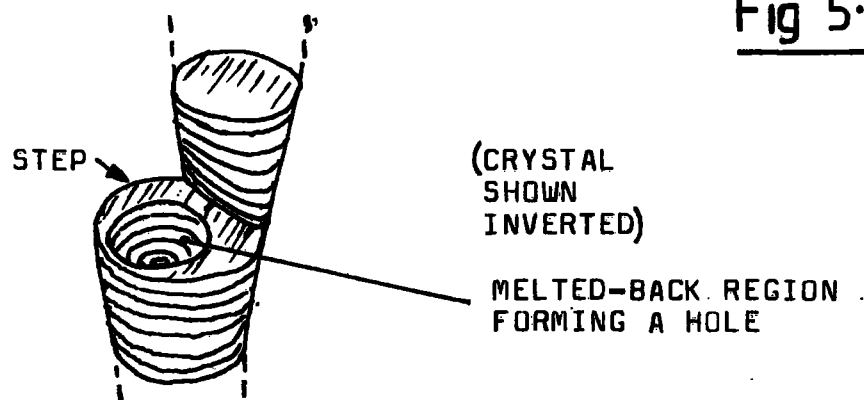


Fig 5.41

It has been found, very conveniently, that poorly centred crystals automatically centre themselves in the present equipment aided by the fact that the weight added to a growing tip will always move the centre of gravity of the whole crystal in such a way as to bring greater collinearity between the hanging point, the centre of gravity (these two define the rotation axis) and the tip of the crystal. However, this centring mechanism can be catastrophic if the crystal tip is misaligned by more than a few millimeters since high points on the growing interface can become fresh seeding points causing disjointed growth of the kind

illustrated in figure 5.41.

5.8 Conclusion

A new form of automatic control for Czochralski growth has been explored. The method relies on difficult measurements of the very small viscous torques associated with crystal rotation.

A very simple mechanism for achieving control has been described and, while failing to match the precision of commercial systems, demonstrates the viability of the technique.

It has been found that viscous torque control has advantages over some other techniques since it is meniscus sensitive, indeed extremely so. The magnitude of the observed meniscus effect is significant ; viscous torque control may well in principle be better than present commercial methods for control of smaller diameter crystals (up to say 3 cm) under certain common conditions, primarily that the surface tension, like that of silicon, is high enough to create an adequate meniscus column between crystal and melt. Under these conditions the torque on the crystal has a component which is proportional to the differential of the crystal diameter with respect to axial distance. This differential component is present to a much greater degree in torque measurements than any other measuring technique and is the property that reviewers (Hurle, 1977 and Jozsef, 1979) have singled out as the basis for a successful automation method.

EXAMPLES OF VISCOSITIES OF METALS
AT THEIR RESPECTIVE MELTING POINTS

METAL	MELTING POINT °C	VISCOSITY (CENTIPOISE)
LEAD	337	2.47
GOLD	1063	4.84
URANIUM	1133	6.5
COBALT	1495	5.5
NICKEL	1452	5.8
IRON	1536	5.9
BISMUTH	271	2.0
TIN	232	2.6

INFORMATION TAKE FROM OFTE (1967) AND CAVALIER (1960)

TABLE 5-1

CHAPTER SIX

A NEW TORQUE MAGNETOMETER

6.1. Introduction

The new torque magnetometer described here is based on the design due to Aldenkamp, Marks and Zijlstra (1960). It is innovative in the use of a mutual inductance of direct angular sensitivity to detect the movement of the magnetometer head. A wide dynamic range and on-line data processing using a microcomputer render the device particularly suitable for the rapid analysis of a large number of samples and, due to its rigidity, for accurate measurement on materials of large magnetocrystalline anisotropy.

A simplified diagram of the magnetometer head is shown in figure 6.1. The suspension employs two horizontal discs connected by three symmetrically placed leaf-springs which are highly sensitive to small twists but very rigid with respect to sideways displacement. The specimen is mounted on a support attached to the lower disc while the upper disc is rigidly clamped. For small displacements, the movement of the lower disc indicates torque proportionally.

In the original design, Aldenkamp et al. rotated the magnetometer itself in a fixed magnetic field and used an eccentrically placed linear position transducer to measure angular displacement. In the present design the magnetometer is fixed in a rotating field and an angularly sensitive transducer is used.

A block diagram of the electronics is given in

SIMPLIFIED DRAWING OF MAGNETOMETER HEAD

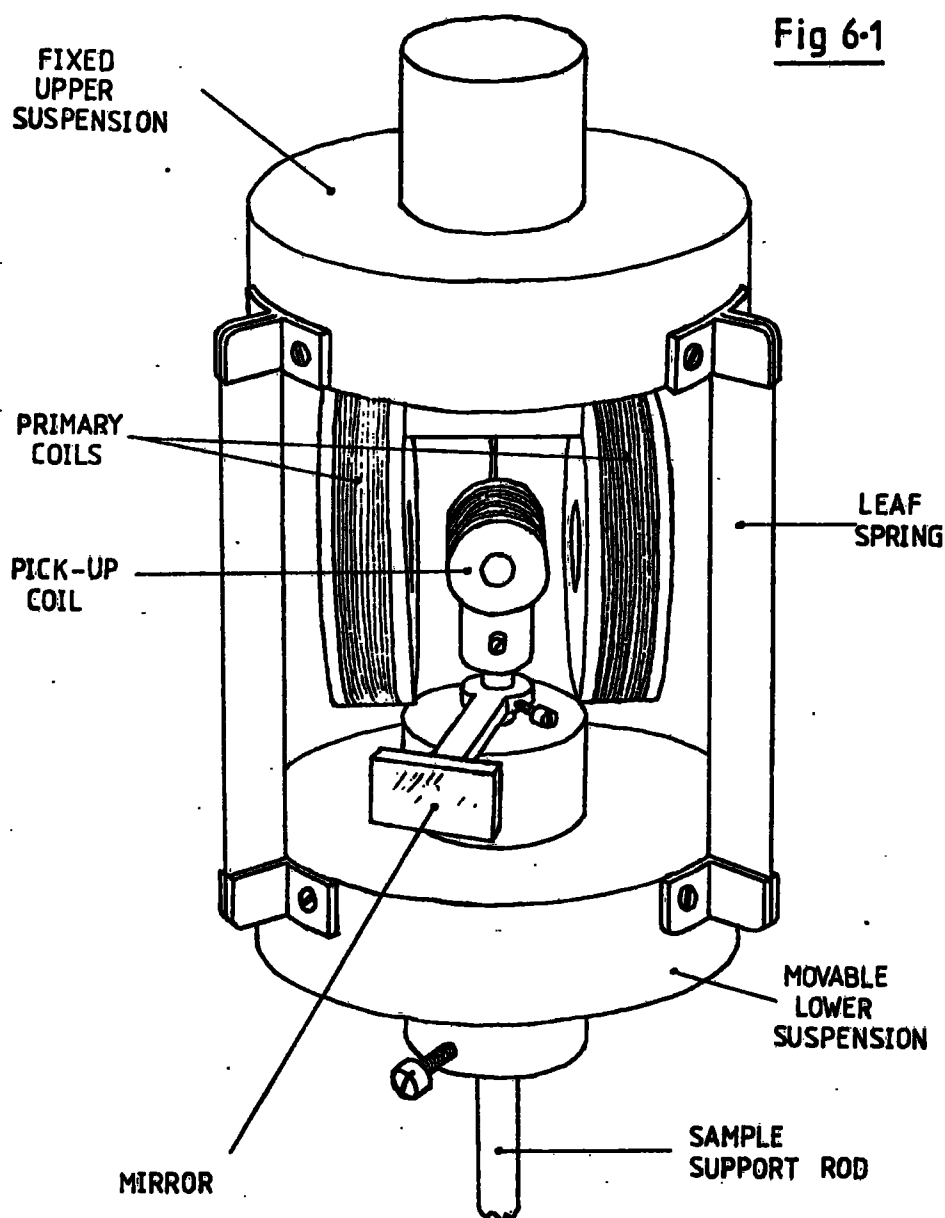
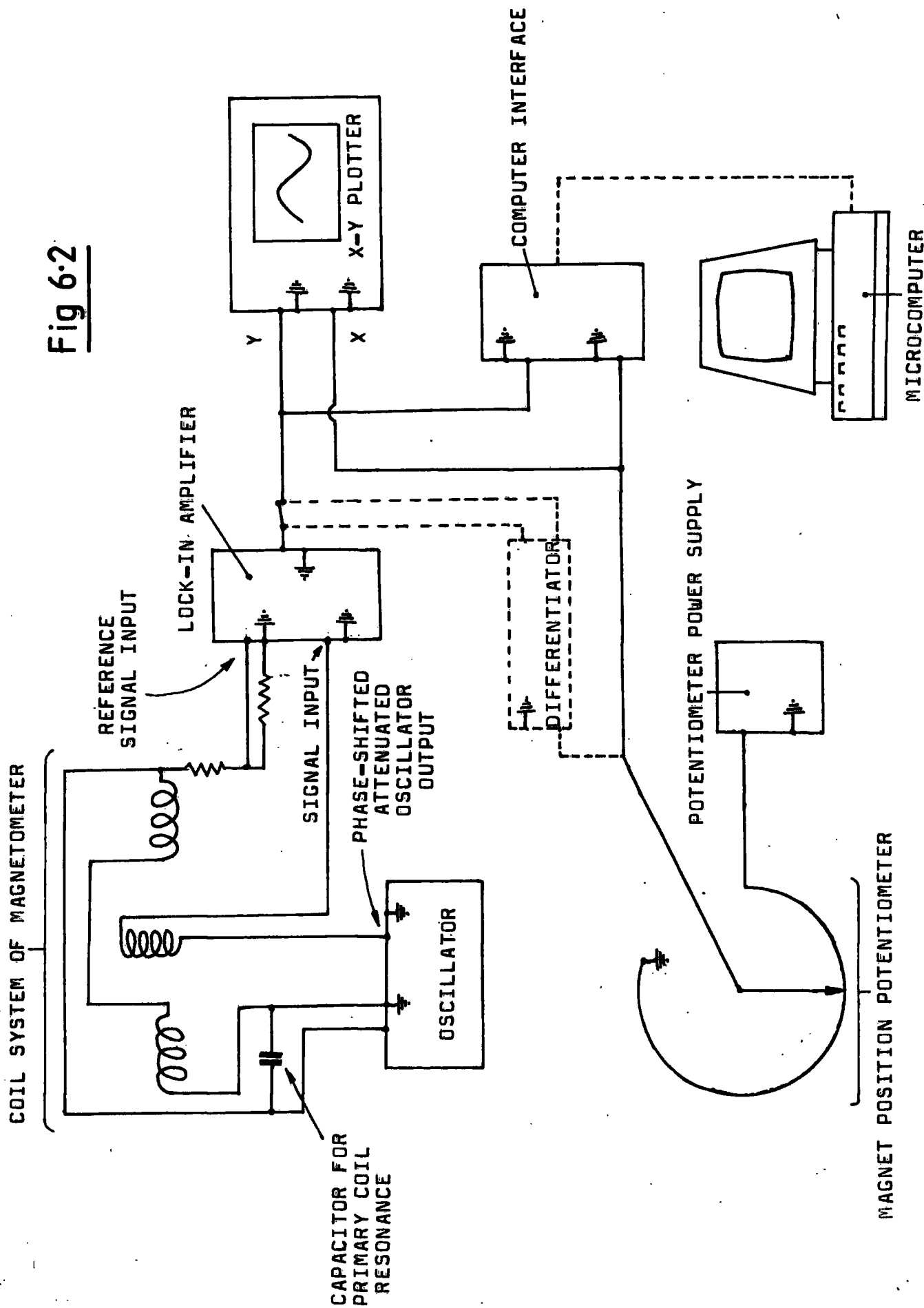


figure 6.2. Indicated on this is the cross-coil transducer, driven by an oscillator and mounted on the magnetometer head, which produces a signal having a phase and amplitude indicating the applied torque. A lock-in amplifier interprets the signal for the 'Y' input of an X-Y plotter with 'X' input linked to a position potentiometer on the magnet base. Hand rotation of the magnet traces out a torque curve on the plotter, the graphical information also being recorded by an

BLOCK DIAGRAM OF THE ELECTRONICS OF THE TORQUE MAGNETOMETER

Fig 6.2



on-line computer. Subsequent analysis of the data to yield anisotropy constants can take as little as one minute. Further details of the electronics and computer are given in sections 6.5 and 6.6.

The torsional constant of the magnetometer is measured once, thereafter torque can be inferred from the deflection of a light beam from a mirror on the moving part of the head and the electrical output calibrated with respect to this.

6.2 Advantages of the design

The normal advantages of the triple leaf-spring design over alternatives apply (see chapter 4), namely robustness, cheapness and, due to the particular calibration method, accuracy. Furthermore, since the sample is attached to the end of a rod rather than within an enclosure forming part of a more complex suspension, rapid sample changing is facilitated. The established advantages of an on-line microcomputer also apply, chiefly the rapidity in obtaining and processing experimental data.

Advantages specific to the present design are principally that the cross - coil mutual inductance is easy to construct, uses a readily available off-the-shelf phase sensitive detector and provides a very wide ranging, very positionally sensitive means of monitoring the head with all the advantages that, in turn, accrue to this. Indeed, overall rigidity and relatively high sensitivity are both obtained simultaneously in that 10^6 Nm sensitivity is available on a suspension capable of withstanding nearly 1 Nm.

The large working range allows, therefore, a range of samples to be investigated which differ in anisotropy by an amount normally excluding the use of a single unmodified instrument.

6.3 Disadvantages of the design

One disadvantage of the present design is that the sideways restraint of the sample by the magnetometer compares unfavourably to that of a (double) ligament suspension magnetometer of the same torsional constant. Thus the forces produced by a particular sample magnetisation and field inhomogeneity may require the use of ligaments to obtain the necessary combination of both lateral support and freedom for sample rotations of the magnitude necessary in any measurement of torque. Furthermore, in any attempt to increase the mechanical sensitivity of the present design, which has a large moment of inertia due to the lower disc, the natural frequency of angular vibration becomes inacceptably low in that sufficient damping of the vibrations interferes with the dynamic response of the magnetometer during torque curve acquisition. This moment of inertia limits the practicable sensitivity of the leaf-spring arrangement and favours again the ligament suspension.

6.4 Mechanical details of the magnetometer

The primary coils of the transducer were mounted on a rotatable cross-slide combination (fig 6.3) to allow the coils to be centred accurately and orthogonally around the pick-up coil. This procedure minimised the spurious signal produced by the pick-up coil when the magnetometer was relaxed

DETAILED DRAWING OF MAGNETOMETER HEAD

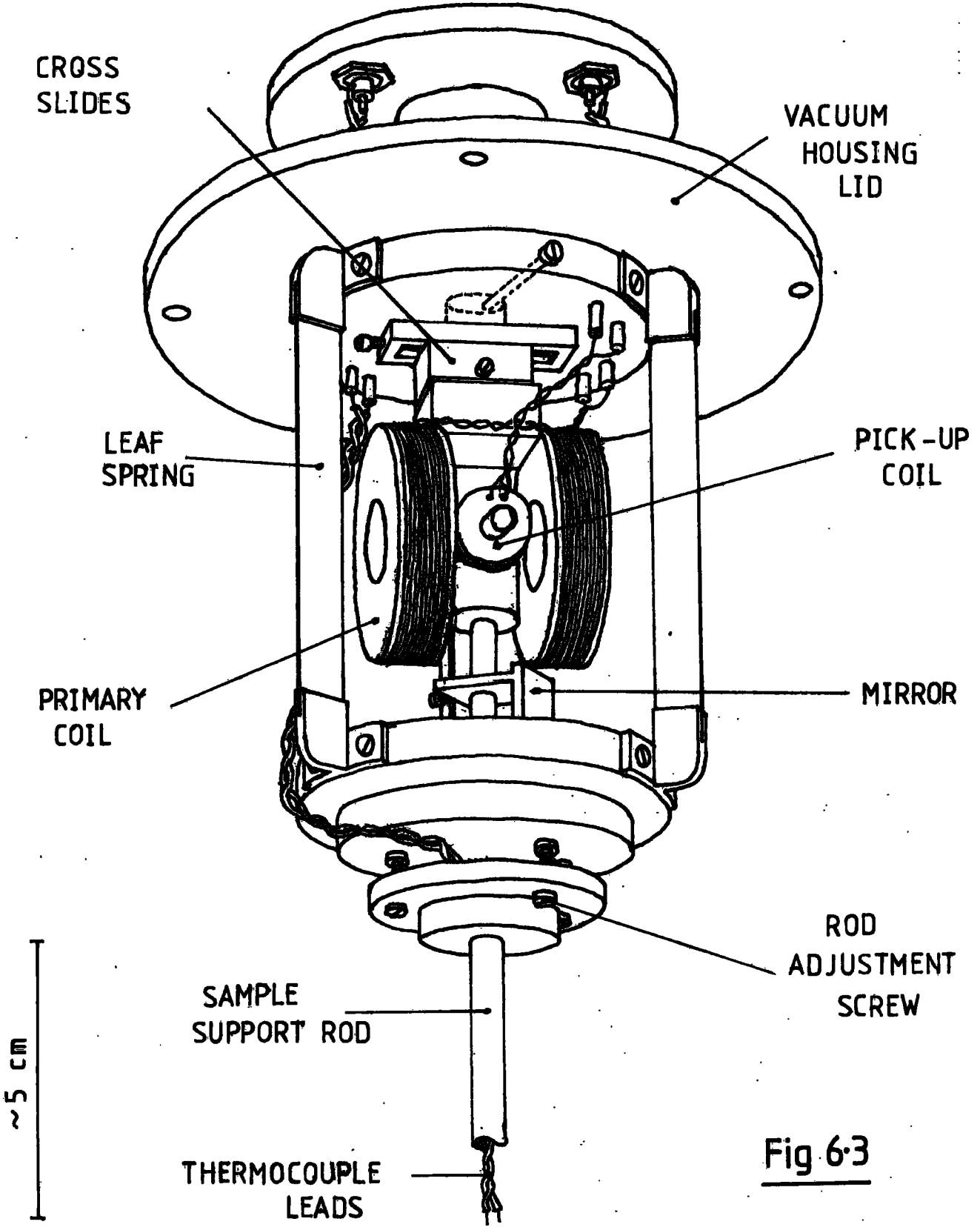


Fig 6.3

and in turn reduced the amount of electrical back-off necessary to produce the quiescent state (see section 6.5).

The leaf-springs were made of stainless steel and of dimensions 10 mm x 75 mm x 0.54 mm which attached to a 7 cm diameter lower disc producing a torsional constant of 0.1474 rad/Nm. Thus, even in the case of the cobalt crystal analysed in figure 6.16, the maximum sample rotation was only 4 arc minutes. Ordinarily no correction to the torque curve due to magnetometer rotation was therefore necessary. Conventional ligament suspension feedback instruments of the 'null deflection' type (eg Croft et al., 1955) turn a similar amount to produce the out-of-balance opto-electronic signal. The leaf-springs enabled a maximum working load of between 0.1 and 1 Nm. A general equation for the torsional constant of the triple leaf-spring suspension, due to Birss and Shepherd (1978) is given below;

$$\frac{\theta}{\Gamma} = \frac{I_e^3}{6EAb^2R^2} + \frac{I_e}{M_s A(a^2 + b^2)} \quad \dots(6.1)$$

where E is Young's modulus, M_s the shear modulus, A the cross-sectional area of the springs, $2a$ their width, $2b$ their thickness, I_e their effective length, and R the distance of their centres from the axis of suspension.

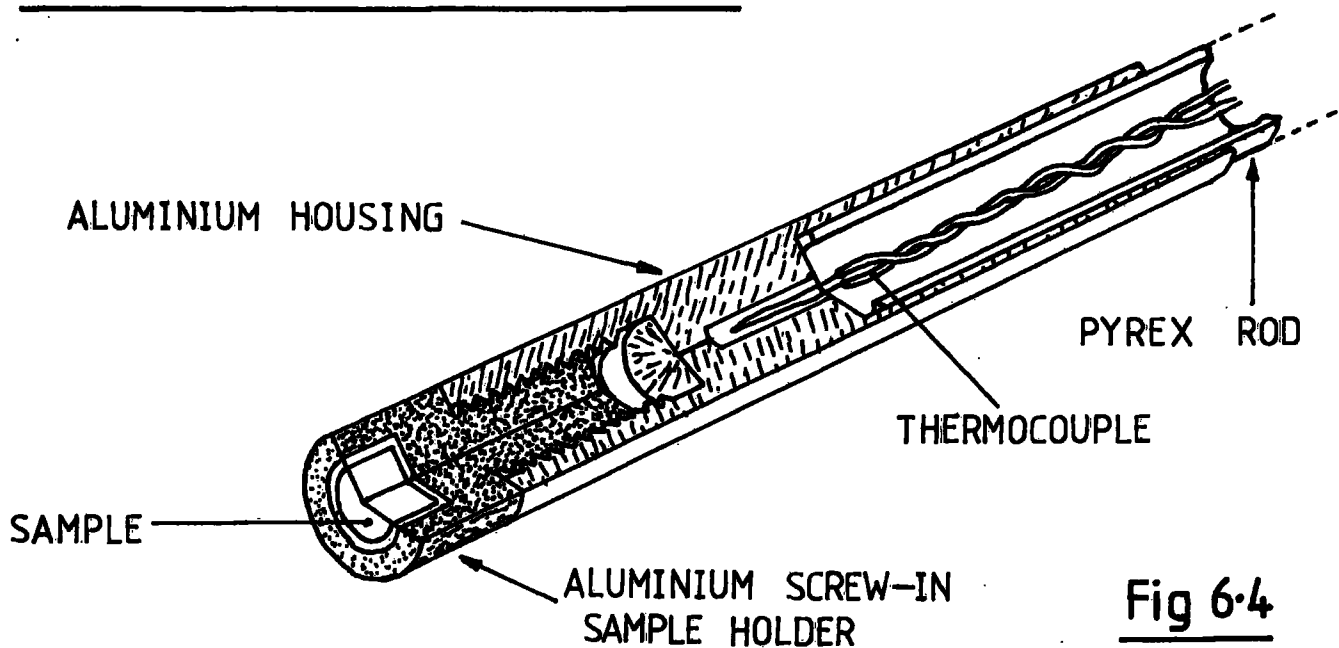
The elastic-after-effect of the leaf-springs was accounted for in the computer software (see section 6.6).

The lower movable disc, attached to the leaf-springs, was about 1 cm in thickness and made of nylon to produce a low moment of inertia giving a natural frequency of approximately 50 Hz. Such a frequency could be damped without introducing an appreciable limiting slew-rate to the dynamic

response of the magnetometer. In the event, damping was obviated by capacitative smoothing of the electrical output.

The sample support rod was made largely of 6 mm pyrex tubing having a length of about 30 cm with a metallic end-piece capable of accepting a screw-in sample holder on a 5 mm metric thread (fig 6.4).

THE SAMPLE SUPPORT ROD

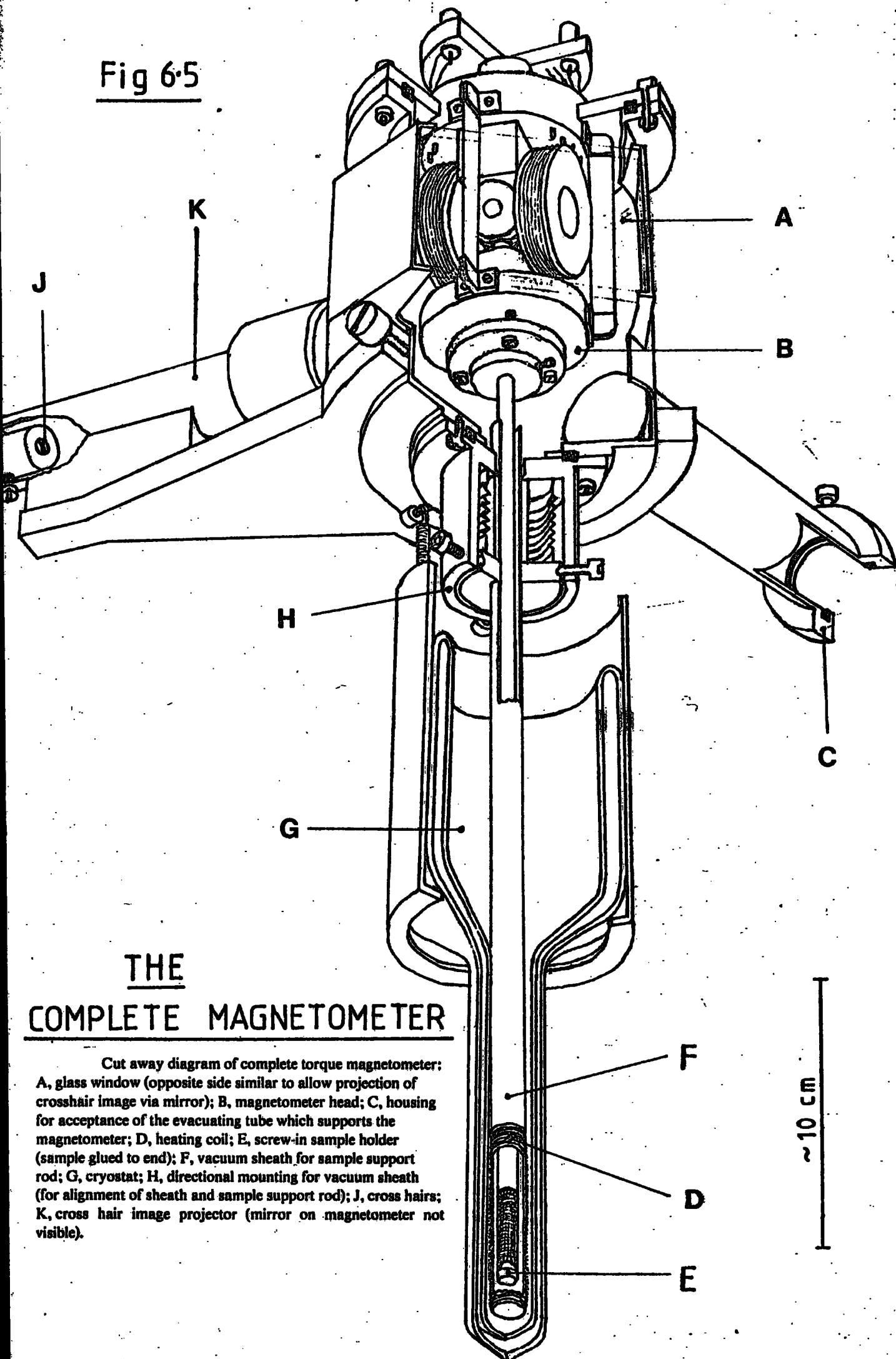


The 7 mm diameter, 3 cm long aluminium end-piece which was attached to the pyrex by a thermosetting cement, improved temperature measurements on the sample by thermally coupling the sensor in the rod to the metallic sample holder and sample. No adjustment to the sensor (a copper-constantan thermocouple read by a Schlumberger 4045 $1\mu\text{V}$ digital voltmeter) was necessary during sample change-over. The end of the sample support rod was found to produce parasitic torques during field rotation by reaction of the

induced eddy currents with the field. The size of the metal body was therefore kept to a minimum. The eddy-current torques, when comparable to sample torques, were counteracted electrically (see section 6.5 and figs 6.8 and 6.9). The support rod was attached to the magnetometer by an adjustable tufnol mount whereby the orientation of the rod and thereby the transverse position of the tip, could be manipulated through 3 brass screws symmetrically disposed around the base. This allowed the sample to be centered accurately on the rotation axis of the magnetometer movement; essential for accurate work since a non-central sample transferred torque resolved from the translational forces on the sample by field inhomogeneity and produced thereby an artificial signal.

The vacuum system surrounding the magnetometer (fig 6.5) prevented atmospheric condensation on the internal parts during low temperature work. It also reduced corrosion of the heated parts of the magnetometer during high temperature runs. The 30 cm long, 1 cm diameter stainless steel lower-sheath of the vacuum system was orientable to accommodate the sample support rod, the sealing action being performed by fine-gauge, ridged phosphor-bronze tubing. In the brass upper section of the vacuum system were two optically flat 8 cm x 6 cm windows of 6 mm float glass by which light could be reflected from the magnetometer mirror during calibration. The vacuum system physically supported the top of the magnetometer head on a stand by which the whole system was evacuated. Evacuation took place through a tubular 'O'-ring joint allowing a limited adjustment of the magnetometer position with respect to the field (see figure 6).

Fig 6.5



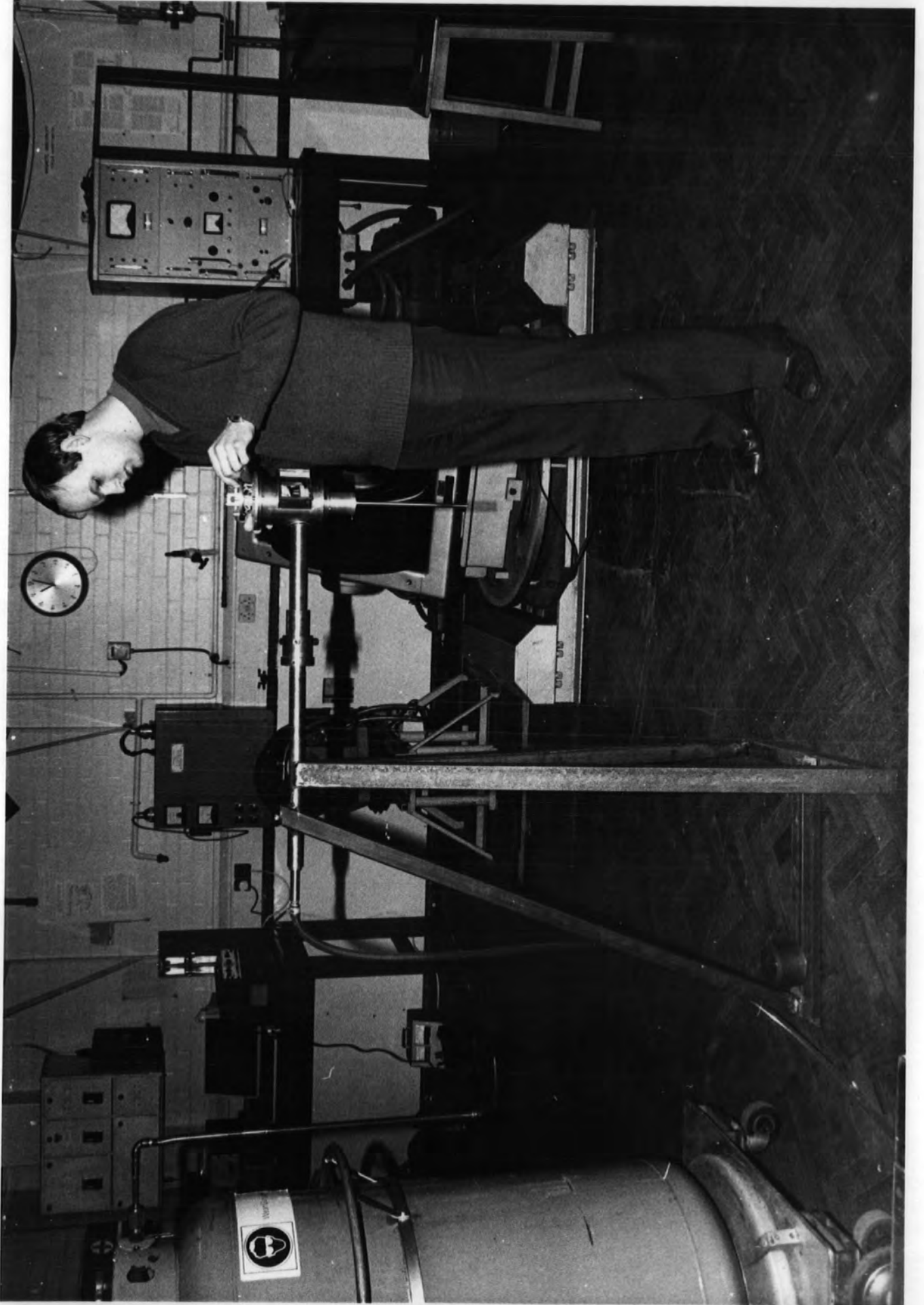
THE COMPLETE MAGNETOMETER

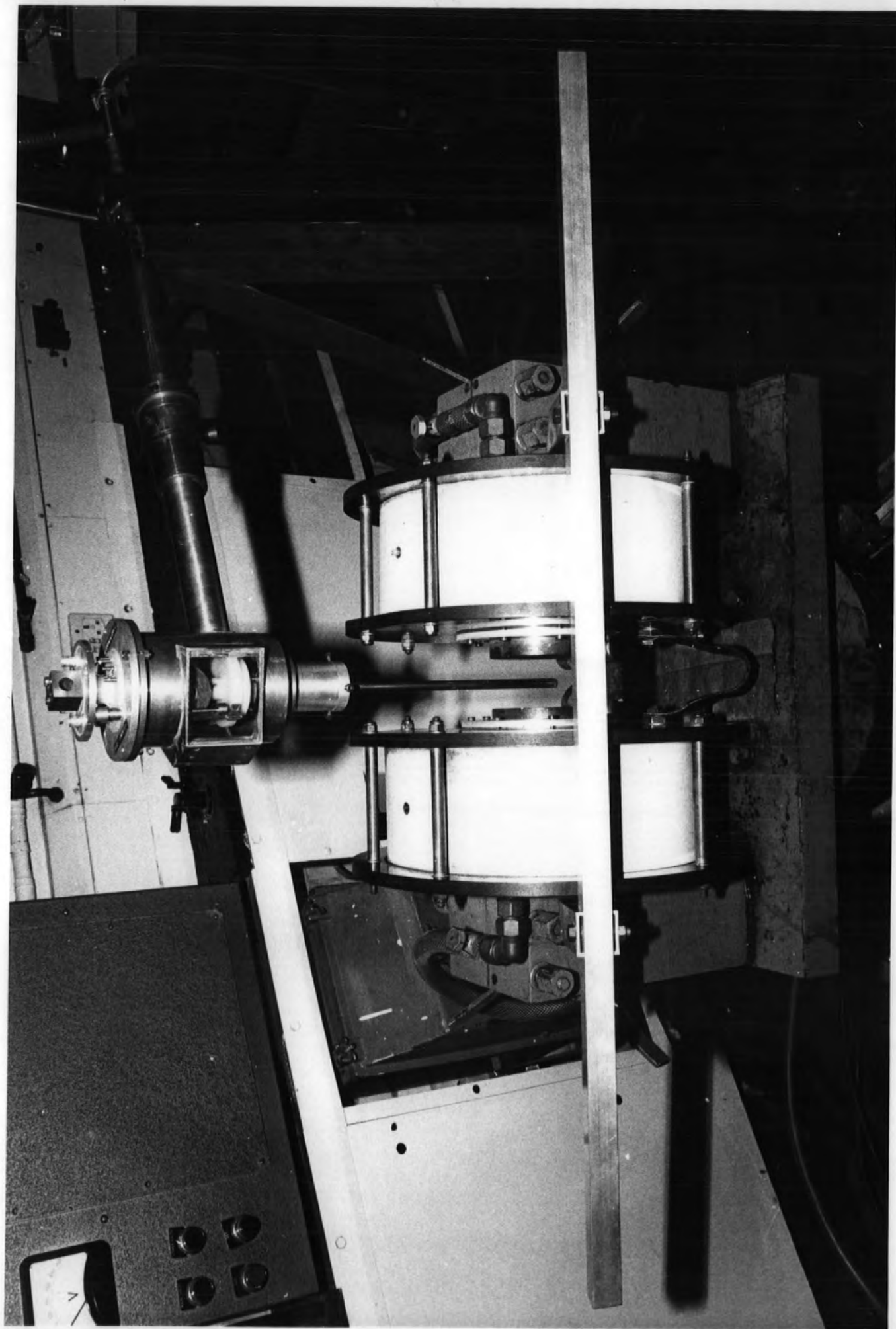
Cut away diagram of complete torque magnetometer:
 A, glass window (opposite side similar to allow projection of crosshair image via mirror); B, magnetometer head; C, housing for acceptance of the evacuating tube which supports the magnetometer; D, heating coil; E, screw-in sample holder (sample glued to end); F, vacuum sheath for sample support rod; G, cryostat; H, directional mounting for vacuum sheath (for alignment of sheath and sample support rod); J, cross hairs; K, cross hair image projector (mirror on magnetometer not visible).

~ 10 CM

Fig 6-6

THE MAGNETOMETER ON ITS STAND





A pyrex dewar around the lower sheath of the vacuum system was suitable for exposing the magnetometer to liquid nitrogen temperatures. To cool the sample to 77 K, about 10 torr of Helium was used as a transfer gas failing which about 85 K was possible. Intermediate cooling was obtained by rationing the nitrogen in the dewar. A maximum warm-up rate of about 3 K per minute was observed. A helium gas-flow cryostat normally used for X-ray diffractometry (Jones and Tanner, 1980) was available for the magnetometer and would allow the present 2 tesla magnet pole-piece configuration to be retained. The latter arrangement has not yet been used experimentally.

A coil around the lower sheath of the vacuum system allowed radiant heating of the sample. Temperatures of up to 650 K were obtained using a 20-turn nichrome coil in a matrix of thermosetting cement giving a power of about 50 watts at 20 V.

To reduce mechanical vibration to the magnetometer by the rotation of the magnet, both were separately attached to a common concrete base. The magnet and support stand are shown in figures 6.6 and 6.7. Further details of the magnet are given in the next section.

6.5. Electrical details of the magnetometer

The computer interface, microcomputer and software are dealt with in the next section.

The primary coils of the transducer, consisting together of 2500 turns of 34 swg copper wire (DC resistance about 1000 Ω) were fed with a 3 KHz AC signal. The pick-up coil,

consisting of 2500 turns of 40 swg copper wire, detected an induced signal when movement of the lower disc misaligned it from the null position. For a small displacement, the amplitude of this signal was proportional to the rotation of the lower disc and hence the torque on the sample. Depending on the sense of the rotation, the secondary voltage was either in phase or out of phase with the primary. Thus, if the signal was fed to a lock-in amplifier (fig 6.2) and a fraction of the primary voltage used as a reference, a DC output was produced proportional to the magnitude and sense of the torque. Use of the lock-in amplifier enabled effectively all unwanted electrical noise to be rejected. Rigidity of the apparatus was such that the shortest time-constant of the lock-in amplifier (10 ms on the Brookdeal type 401) gave sufficient damping to eliminate the modulating effect of the 50 Hz mechanical vibration. Hence torque curves could be obtained directly on the Phillips PM 8141 per recorder without fear of significant distortion due to delay in the response of the lock-in.

The transducer signal was increased by almost an order of magnitude by operating the primary coils in resonance using 0.01 μ f capacitor. Further attempts to sensitise the device using a ferrite core in the pick-up coil were successful but rejected on the grounds that the equipment became unacceptably subject to permeability changes in the region around the head; to the extent that movements of a human operator could be detected. The ferrite core was also unacceptable because its elongated shape tended to orientate in the stray magnetic field producing unwanted torque. In the final form, the transducer produced a signal of about 1.V pk-pk per radian

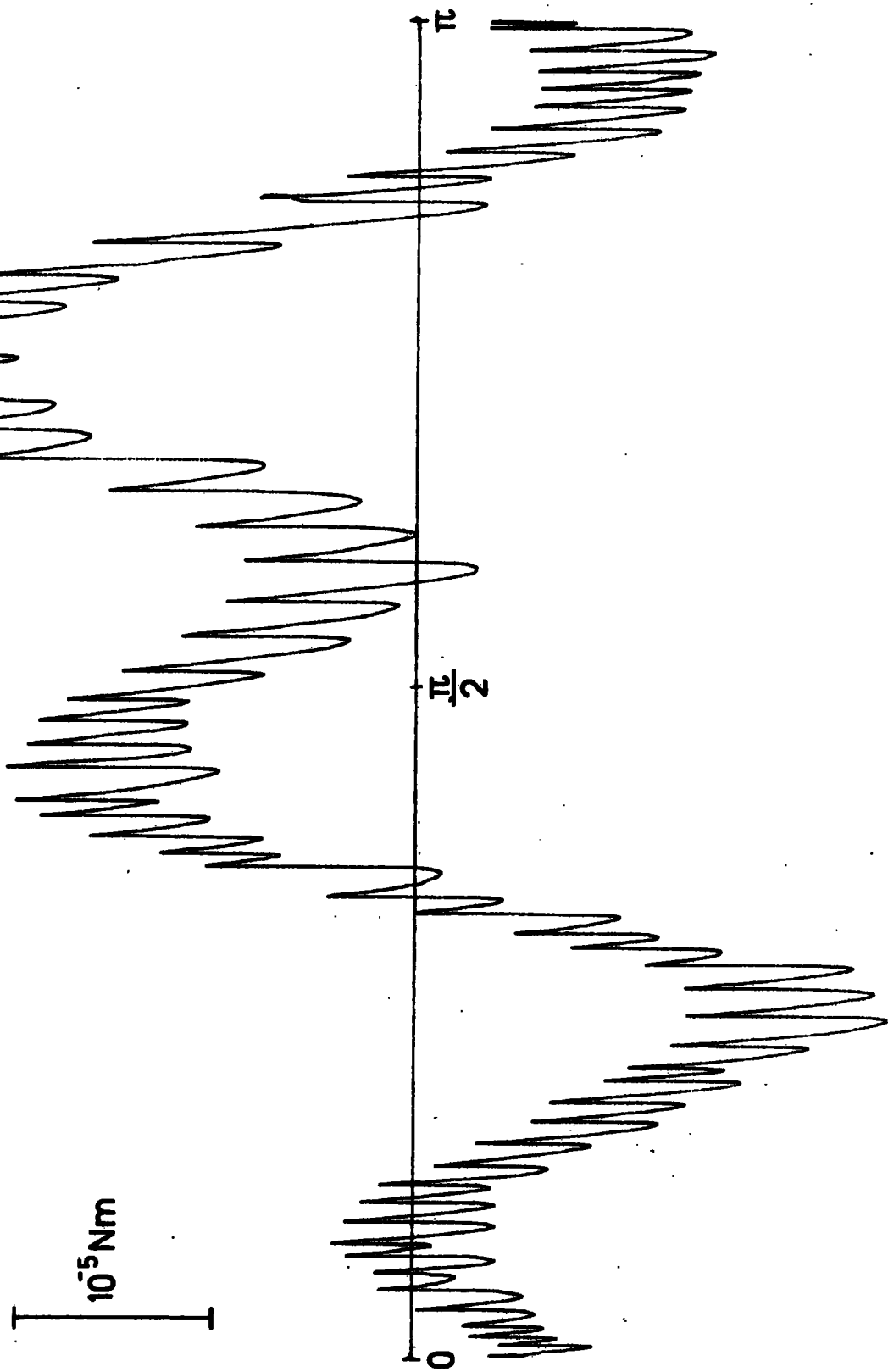
for a nominal oscillator output of 5 V pk-pk.

The potentiometer on the base of the magnet consisted of approximately 1 metre of nichrome wire having a resistance of about $2\ \Omega$ and linearity (gradient $d(\text{voltage})/dx$) constant to within about 2%. It was fed by a Farnell E 30/2 power supply stable to better than 0.1% with respect to time, load change or typical mains fluctuations.

For work at the lower end of the sensitivity range two supplementary items of electronics were necessary. The first was simply a variable amplitude phase shifter by which a proportion of the primary AC signal was added to back-off the relaxed-state pick-up coil output to generate a null signal, hence avoiding precise manipulation of the pick-up coil position. This phase-shifted signal was available from the feedback VPO 602 oscillator directly as an auxiliary output. The second circuit was required by the eddy-current torques mentioned earlier. These torques were dependent on the magnet angular velocity. Sporadic magnet rotation produced noise on the torque curves exemplified, at high sensitivity, by the curve shown in figure 6.8. The compensating circuit was a differentiator (fig. 6.10) which monitored the voltage signal arising from the potentiometer on the base of the magnet and returned a signal proportional to the time differential of any change in the potentiometer voltage. Empirical adjustment of both the proportionality constant and the time-constant of the differentiator capacitative output, yielded a signal capable of counteracting the spurious torque signal if injected in antiphase. The success of the technique is illustrated in the improvement of the former torque curve to that of figure 6.9, taken with similar sporadic magnet rotation.

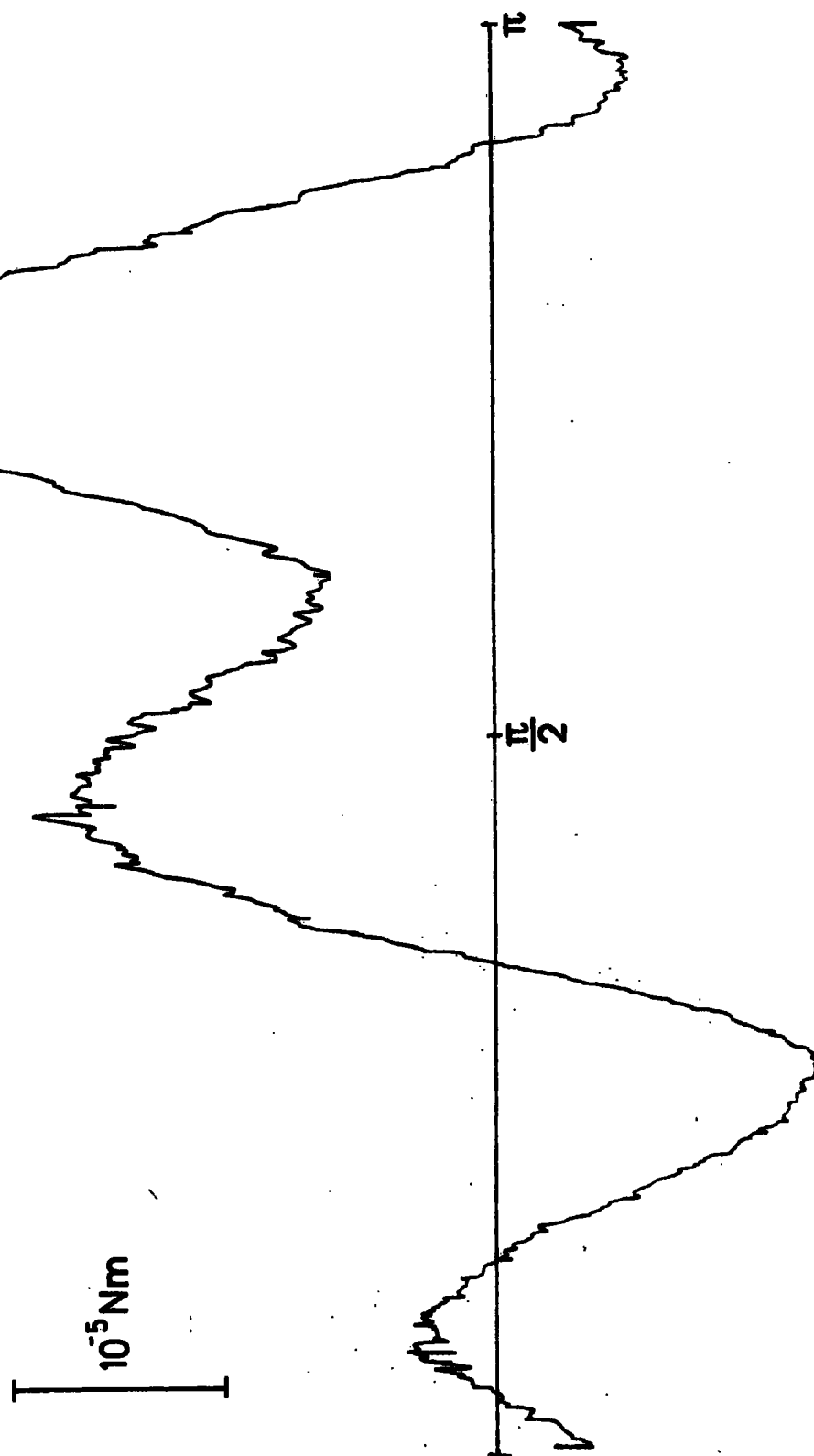
TORQUE CURVE FOR A 97 mg C-PLANE DISC OF COBALT SHOWING SPASMODIC INDUCED TORQUES FROM NON-UNIFORM FIELD ROTATION

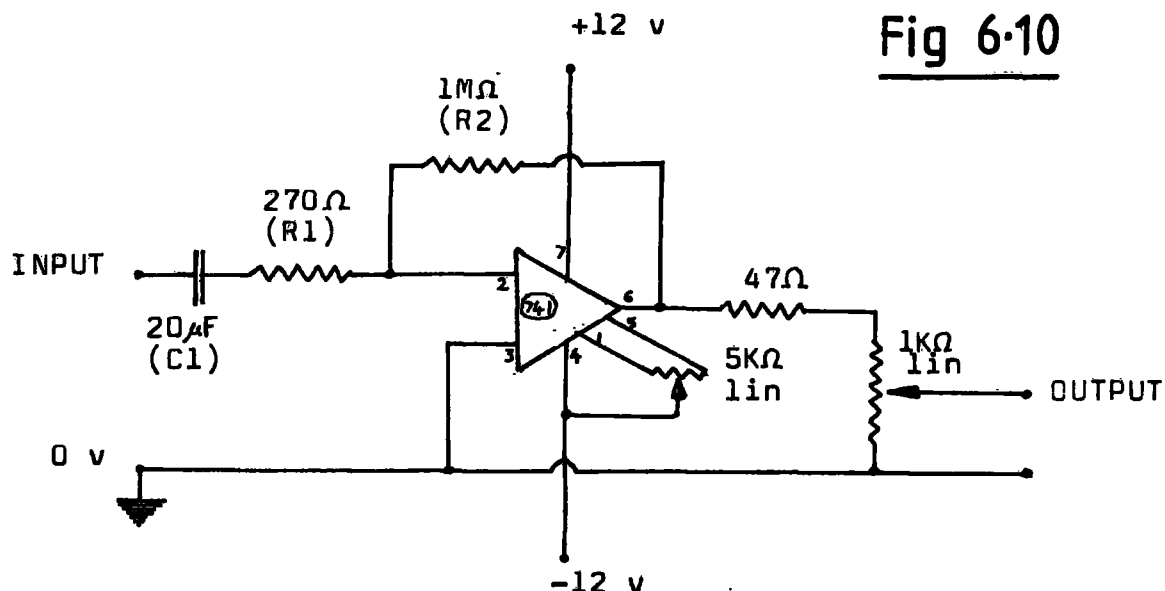
Fig 6.8



TORQUE CURVE AS FOR PRECEDING FIGURE WITH ELIMINATION
OF INDUCED TORQUES (SEE TEXT)

Fig 6.9





DIFFERENTIATOR CIRCUIT FOR TORQUE MAGNETOMETER

C1, R1 AND R2 ARE MATCHED TO SUIT THE PARTICULAR EQUIPMENT.

The electromagnet was constructed by Roe (1961) and was of conventional design. The coils were carried on pole-pieces and were water cooled using a closed circuit of de-ionised water flowing through a heat exchanger. The field obtainable with a pole-piece gap of 5.1 cm and a power dissipation of 40 KW was about 1.1 tesla. However, with added conical face pieces, 2 teslas could be obtained across a 2.2 cm gap. The magnet could be rotated through about 200° on a calibrated base accurate to a fraction of one degree.

6.6 Computer interface and software

6.6.1. Hardware

Recent advances in microprocessors have led to a number of very inexpensive microcomputers becoming available. The present magnetometer used a Commodore PET microcomputer which had up to 32 Kbytes of memory; and a BASIC compiler together with video display unit, tape deck, printer and keyboard. A number of interfaces were commercially available but a modular interface was adopted having the flexibility necessary for use elsewhere in the laboratory and potentially the option for stepper-motor control of the magnet position in a possible future development of the magnetometer. Two 12-bit analogue-to-digital converters were used in a Besselec Minicam system (Rodrigues and Siddons, 1979) which is commercially available from Bede Scientific Instruments, Coxhoe, Co. Durham. One ADC took a signal from the position potentiometer in the magnet base proportional to rotation angle. (With a 12-bit ADC, the resolution in angle was potentially a little better than 0.1°). The computer inspected this signal at a read rate of 30 Hz until the specified angular movement was reached and then the magnetometer output was read via the second ADC. This method of data collection had the advantage that the magnet could be rotated by hand and did not necessarily require expensive high power motors.

On-line torque magnetometry is not new and, in fact, it is mentioned four times in the literature (Abe and Chikazumi, 1976; Kanomata and Higuchi, 1976; Wilson et al., 1977; and Larsen and Livesay, 1979).

6.6.2. Software

As the Minicam interface incorporated an EPROM, the ADC outputs appeared to the operator as BASIC integer variables. One line of BASIC sufficed to read the ADC, for example;

```
30 A% = 3 : A = USR(5) : PRINT A
```

Line 30 set the address A% to that of the appropriate module (in this case 3) and USR (5) routine located a subroutine in the EPROM which returned the ADC output as variable A, subsequently printed on the video display unit. It thus proved very simple to write a BASIC program to collect the data.

In an early form of the magnetometer software, a torque data point was acquired after the position potentiometer voltage was recognised to be within one of a set of predetermined windows corresponding to angular intervals centred every 3°. The angular resolution was therefore dependent on the size of the voltage window. A small window would mean high resolution but unfortunately would increase the probability of the window being missed as the voltage from the position potentiometer was swept. The problem was solved by using large windows but including instructions within the software to read explicitly the position potentiometer voltage before and after recording the torque signal. The average position voltage was then linearly interpolated to yield an accurate angular position for the given torque. The resolution of the improved technique was as if the windows were of a voltage range corresponding to half of one bit of

the monitoring ADC and the reliability of acquisition at sweep rates of several degrees per second was about 99.95%. The earlier form of programing was used in the basal-plane anisotropy measurements of the Tb_xGd_{1-x} alloys (chapter 8). The more accurate work on cobalt (chapter 7) required the latter interpolation technique.

Certain corrections were written into the software to account for systematic distortion of the torque curve arising from the non-ideal behaviour of the magnetometer rather than intrinsic effects such as shear. Intrinsic corrections will be dealt with in those chapters reporting the analysis of the particular materials, on which these corrections depend.

A correction was made for the effects of a time-constant in the electronics monitoring the torque signal. The principal contributor was the capacitative smoothing on the ADC input with a constant of approximately 0.14 seconds. The effect of the exponential decay in the magnetometer response was to distort the torque curve, taken dynamically, in such a way as to effect the harmonic content and thereby the anisotropy derivation. The correction required that the precise times at which all data points were obtained were recorded using the internal clock of the microcomputer. These times allowed the distortion to be removed by enabling the computer to generate correct values for each data point from an inspection of the correction derived for the previous point and a knowledge of the last change in torque value and time. The recurrence relation by which the corrected torque curve was developed is given overleaf;

$$T_{AF} = \frac{t_c T_{AI} (1 - \text{Exp}(\frac{\Delta t}{-t_c})) - \Delta t (T_{BF} - T_{BI} \text{Exp}(\frac{\Delta t}{-t_c})) + T_{AI} \text{Exp}(\frac{\Delta t}{-t_c})}{t_c (1 - \text{Exp}(\frac{\Delta t}{-t_c}))} \dots(6.2)$$

where;

T_{AF} = actual (corrected) torque value

T_{BF}, T_{BI} = experimental torque value and previous value respectively

T_{AI} = previous corrected torque value

Δt = time elapsed between reading T_{BI} and T_{BF}

t_c = time-constant in torque output.

and where it is assumed that between the two data points

T_{BI} and T_{BF} torque varies linearly with respect to time. For

hand rotation of the magnet the linearity condition was approximated to over the small intervals between torque measurements.

Since the field rotation was paused briefly before the acquisition of the first data point, it was assumed that the time-constant correction for that point was zero ($T_{AI} = T_{BI}$).

The corrected torque curve was then generated recursively from the subsequent experimental torque values.

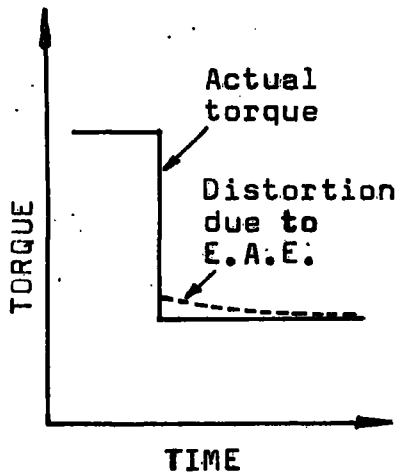
A correction was made for the distortion due to elastic-after-effect in the leaf-springs of the magnetometer head. It was found possible to describe the recovery of the position of the magnetometer after the instantaneous relaxation of an applied torque by a model in which the motion is resolved into two components:

1) An instantaneous movement of the magnetometer head to an angular deflection proportional to applied torque:

2) A movement proportional to an exponential decay but

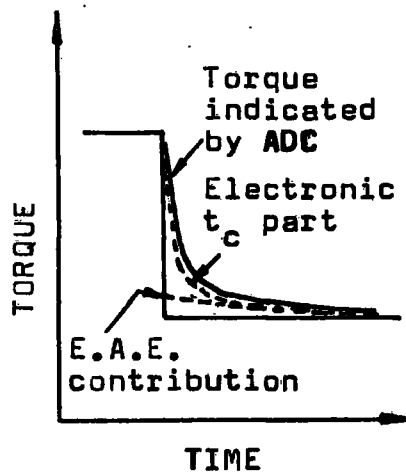
reduced in magnitude. Thus, for example, a torque step-function would be responded to mechanically as in figure 6.11.

Fig 6.11



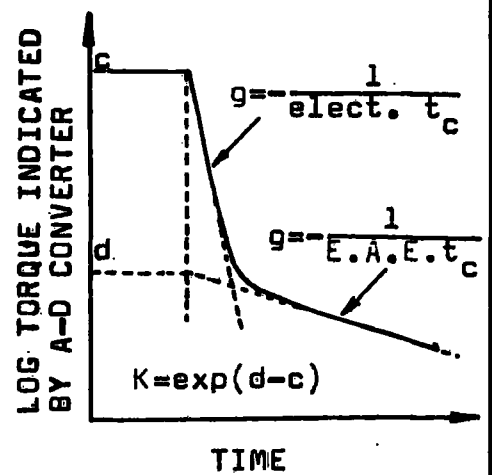
PLOT OF MODELLED RESPONSE OF TRANSDUCER IN THE ABSENCE OF ELECTRONIC SMOOTHING.

Fig 6.12



OBSERVED TORQUE INDICATED BY ADC; THE MODELLED RESPONSE PLUS ELECTRONIC TIME-CONSTANT.

Fig 6.13



LOG OF TORQUE AS SEEN BY COMPUTER SHOWING TWO REGIMES OF LINEAR DECLINE FROM WHICH THE TWO TIME-CONSTANTS AND K CAN BE CONSTRUCTED.

It must be emphasised that this model was appropriate because the displacement was measured in a way whereby the mechanical vibration, after a change in torque, could be ignored. Combining this model with the smoothing of a time-constant associated with the inspection of position, (see figure 6.12) that is the electronic time-constant, excellent agreement could be obtained between observed magnetometer output and that predicted for instantaneous relaxation. Two parameters were defined, the elastic-after-

effect time-constant and K , both represented in figure 6.11. A test program was written to sample the magnetometer output rapidly at regular intervals subsequent to a catastrophic relaxation of the torque and the results are portrayed graphically in figure 6.15 in section 6.8. Comparing this to the prediction of the model in figure 6.13, the gradients and intercepts defining the two time-constants and the value of K can be calculated. To account for the elastic-after-effect, time-constant corrections were generated for a complete torque curve using the elastic-after-effect time-constant but only a proportion of the full correction was applied to the data, namely K times the full correction, the retrospective scaling being done en bloc rather than point by point during the recursive calculation.

It was important to apply the electrical time-constant correction first and then later adjust for elastic-after-effect so as to take away the effects of the two in reverse of the order of occurrence in the equipment. The validity of the two corrections was manifest in the reproducibility of the harmonic content of particular torque curves whether obtained with a forward or backward traverse of the magnet.

It was found experimentally that the angular position indicated by the average of two voltage end-points, corresponding to an angular separation of 180° in the magnet position potentiometer, was about 2° from the expected position. Positional accuracy was improved by inferring angular position from a linear interpolation of voltages taken every 60° rather than at the extremes of a 180° interval. The effects of non-linearity in the position potentiometer were thus

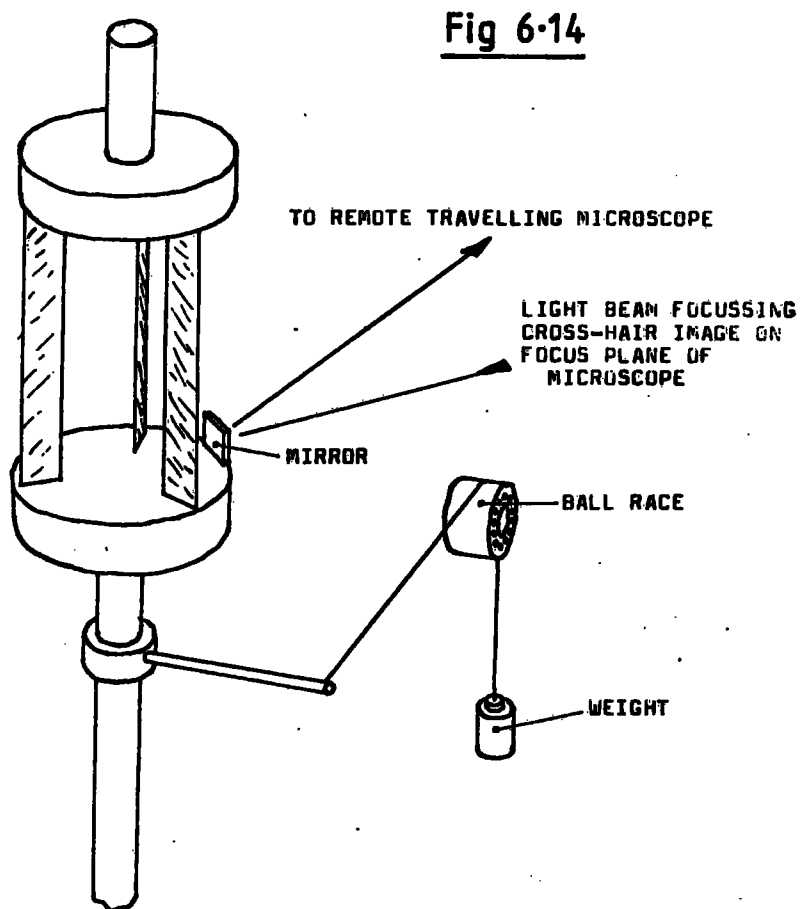
corrected to enable measurements to within about 0.2° using the voltage output.

The corrective measures described took about one minute to implement for a 60-point torque curve inputted in a similar time. A simple shear-correction and Fourier analysis of the curve using the trapezium rule modified for unequally spaced abscissa and yielding three coefficients took another minute. The speed of operation was such that in one day's running, during the Tb_xGd_{1-x} work, 86 torque curves were recorded and analysed.

A program which obtains five 90-point torque curves with all the corrective processes mentioned is given in Appendix D.

6.7 Calibration

In order to calibrate the torque magnetometer, the torsional constant of the magnetometer head was measured. This was done by deflecting the magnetometer with a known torque using a small beam fixed to the lower suspension acted upon by a weight (see fig 6.14). The weight was attached to the beam via a thread fed over a small, clean ball race in such a way that the weight was redirected normal to the vertical plane containing the beam and the vertical axis of the magnetometer. Sticking of the ball race was insignificant since the magnetometer deflection was reproducible for relaxation from each side of the equilibrium for several ball race angular positions. The rotation introduced in the magnetometer by the applied torque was determined by measuring the movement at a distance of 206 cm of a cross-wire image



CALIBRATION OF THE TORQUE MAGNETOMETER

A SIMPLE GRAVIMETRIC TECHNIQUE CAN PROVIDE VERY ACCURATE CALIBRATION OF TORQUE.

reflected from a 2.0 x 2.5 cm mirror mounted on the lower suspension using a remote travelling microscope accurate to 10 μm . In this way, the torsional constant was measured to better than 0.1%. Subsequently calibrations were carried out by cross-referencing the electrical output of the torque magnetometer with the torque indicated by an absolute measurement of the twist of the magnetometer head using the optical technique mentioned.

Conventional calibration methods, involving a search-coil carrying a known current in a known field, do not as easily obtain the accuracy of the gravimetric technique described here, either in the initial determination of the torsional constant of the magnetometer head or in the alternative calibration method of correlating the electrical output of the magnetometer head directly with a search-coil torque applied during each experimental run.

The technique of initially determining the torsional constant of the magnetometer head and subsequently determining electrical calibration from torques recovered from the head movement, was made possible by the fact that in the present magnetometer the torque is indicated accurately by the absolute movement of an elastic system which, having no electronic torsional feedback, has a consistent torsional constant. Magnetometers with torsional feedback involving electrical amplification stages, subject as they are to drift in gain, do not have fixed torsional constants from which meaningful torque values can be determined by absolute measurements of the magnetometer deflection, at least not to the accuracy desired of the present instrument. Here, however, the once-only application of a standard torque is sufficient for a lasting calibration of the head of the magnetometer.

During the measurement of torques which were too small to yield comparative optical measurements, the calibration was carried out by reducing the lock-in gain by an accurately known amount and introducing an arbitrary torque large enough to be measured accurately by the optical method.

The electrical signal could then be correlated to the optically measured torque and the final calibration obtained by multiplying by the factor change in the lock-in gain. The arbitrary torque was introduced by a cam incorporated in the magnetometer which could be made to bear appropriately on the lower suspension.

Due to the shape of the leaf-spring suspension, a change in the torsional constant of the head was produced by the weight of an attached sample. For the given geometry of the head, this effect was negligible, both for the mass of samples used and for the mass of the calibration beam, amounting to a proportional change of 10^{-5} per gram applied to the sample support rod.

6.8 Performance

The response of the combined magnetometer head and electronics to an instantaneous change in torque is illustrated in the graph of log torque (as read by the computer) VS time shown in figure 6.15. The parameters describing the response, as defined earlier, are derived in the figure and were found to be;

Elastic-after-effect time-constant : 0.87 sec

K : 0.082

Electronic time-constant : 0.14 sec

The graphical information was obtained by using the sampling program given in Appendix E set in operation just prior to relaxing the magnetometer head. The original

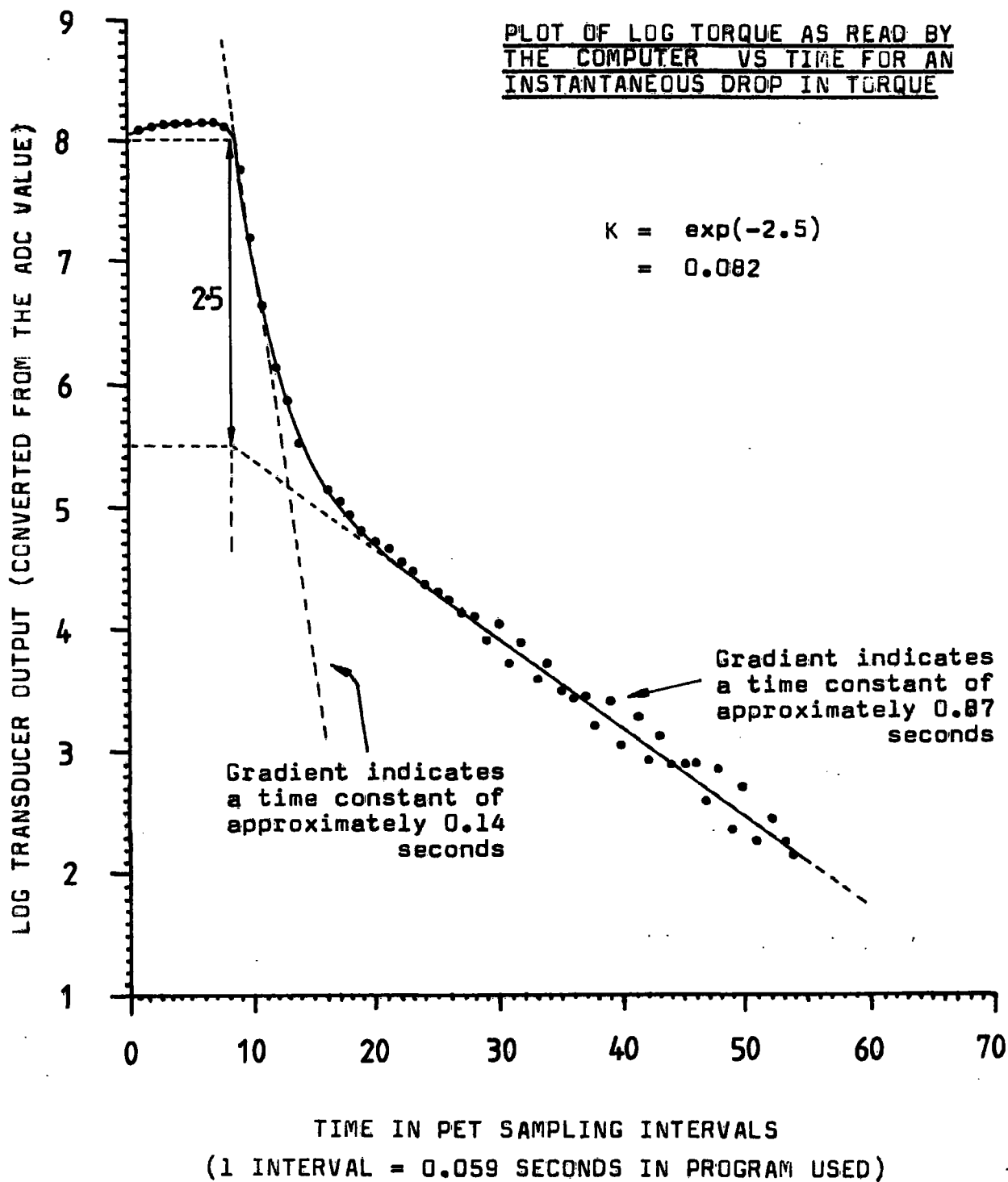


Fig 6-15

data is also given in the Appendix. The sampling time, limited by the execution rate of the ADCs was 0.059 seconds per measurement. Appropriate software counteracted the distortion of the torque curves arising from this non-ideal response (see section 6.6.2). Later software could therefore be written and annexed to the corrective routines by the operator as though no distortion had taken place.

The position potentiometer linearity was worse than 1% but accounted for in the software as mentioned earlier (section 6.6.2).

The linearity of the torque, as sampled by the computer, was excellent; $d(\text{torque read})/d(\text{torque applied})$ was constant to within 0.3% over a range of $\pm 10^{-2}$ Nm and required no software correction.

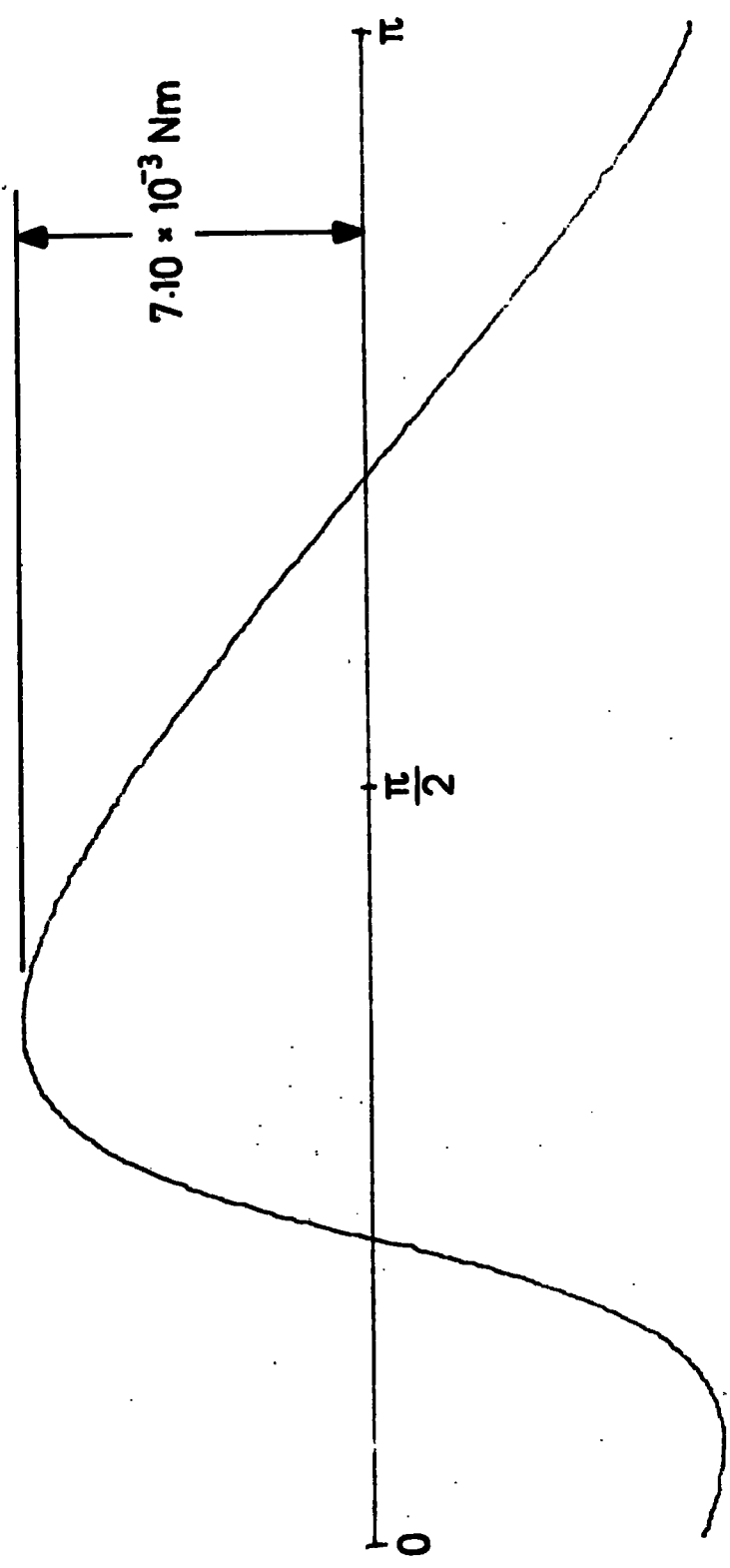
The maximum torque retainable by the magnetometer head without damage or fear of altering the properties of the leaf-springs was judged to be 0.2 Nm corresponding to a $1\frac{1}{2}^\circ$ movement of the lower suspension. Torques of about 1 Nm might be possible but operator nerves, if not accuracy, would suffer. An example of the quality of the torque curves produced on the X-Y plotter is given in figure 6.16.

The size of the lower vacuum sheath was such that samples no larger than 8 mm diameter could be measured. The longitudinal restriction was about 2 cm. However, if room temperature work was sufficient, the lower vacuum sheath could be removed leaving a 2.2 cm gap between the pole-pieces and therefore much greater room for the samples. The maximum field was about 2 teslas and the temperature range, with sheath, was 77-650 K.

TORQUE CURVE FOR A 97mg B-PLANE DISC OF COBALT

(293 K, 1.7 T)

Fig 6.16



Defining a lower limit for the torque range as that amplitude comparable to experimental noise for the average of five curves, the sensitivity limit of the present device was 10^{-6} Nm giving a dynamic range of $>10^5$; greater than any reported for a torque magnetometer having no interchangeable mechanical parts. The sensitivity of the mutual inductance technique for monitoring suspension position is manifest by the fact that at the highest sensitivity, movements of 10^{-7} radian could be measured; corresponding to a displacement of approximately 3\AA at the perimeter of a typical sample.

An analysis rate of about 3 seconds per data point was typical which included the execution of supplementary software suited to the particular crystal symmetry. A hard copy of either the explicit torque measurements or the anisotropy constants could be recorded after each run using the printer.

The capacity for data collection of a magnetometer with an on-line microcomputer is illustrated by the fact that, during the cobalt work (chapter 7), about 2×10^5 separate readings describing the state of the instrument were taken by the ADCs to establish the temperature dependence of the first four anisotropy constants.

CHAPTER SEVEN

THE MAGNETOCRYSTALLINE ANISOTROPY OF COBALT

7.1 Introduction

In the light of inconsistencies in the published results on the magnetocrystalline anisotropy of cobalt, the present work was undertaken. The dependence of the anisotropy constants on the sample quality and higher, normally disregarded harmonics in the shear corrected torque curves, was investigated. In determining the latter, the temperature profiles of K_3 and K_4 were found for the first time.

It was discovered that, in some cases, variation in existing results was due to an inadequate form of analysis in which the shear-correction of torque curves was incorrectly carried out. In others the variation was not easily rationalised.

The present work was aided by the magnetometer reported in chapter 6 having a high linearity and absolute accuracy with the convenience of on-line data processing.

An added incentive for the present work was that it could provide reliable data to test the theories of Szpunar and Lindgard (1979) who have attempted to model the temperature dependence of the anisotropy of cobalt/rare-earth alloys, and in particular cobalt, by considering the effects of lattice parameter changes with respect to temperature in a single-ion model. This model is given particular attention herein.

7.2 Previous work

Cobalt, having an HCP structure, has an anisotropy

energy expression which can be written as follows;

$$E_k = K_0 + K_1 \sin^2 \theta + K_2 \sin^4 \theta + K_3 \sin^6 \theta + K_4 \sin^6 \theta \cdot \cos 6\phi$$

as defined in chapter 2, equation 2.2. This equation is used (or a truncation of it) throughout the literature to parameterise the anisotropy; there are no reported instances of any of the other possible conventions being adopted in work on cobalt.

Attempts in the past to determine the magnetocrystalline anisotropy of cobalt have led to inconsistent results, the reported values of K_1 having a spread of about 20% at room temperature (Kaya, 1928; Honda and Masumoto, 1931; Gans and Czerlinski, 1932; Sucksmith and Thompson, 1954; Bozorth, 1954; Barnier et al., 1961; Kouvel and Hartelius, 1964; Chikazumi et al., 1965; Tajima and Chikazumi, 1967; Kadana, 1967; Sievert and Zehler, 1970; Rebouillat, 1972; Burd et al., 1977; Takahashi et al., 1978; Takahashi and Suzuki, 1979; Ono and Yamada, 1979; and Ono, 1981). This has arisen primarily because of the ill-conditioning of the anisotropy calculations from the data. In some cases, however, when torque magnetometry has been used (Bozorth, Tajima and Chikazumi, Sievert and Zehler, Chikazumi et al., Burd et al., Takahashi et al., Takahashi and Suzuki, Ono and Yamada, Ono) further errors have been introduced by failure to make adequate correction for the misalignment of the magnetisation with applied field, that is, several workers (Chikazumi et al., Takahashi et al., Takahashi and Suzuki) have Fourier analysed torque curves in their uncorrected form and sought to retrieve field-independent anisotropies using an extrapolation of the harmonics on a reciprocal field plot.

However no simple justification for such an extrapolation exists, rather it can be shown (Hofmann, 1964) that the Fourier coefficients of a torque curve sheared in proportion to its ordinate by $\sin^{-1}(T/(\sigma_s B_0^m))$, that is the shear-correction, do not tend to the unsheared values linearly with respect to $1/B$.

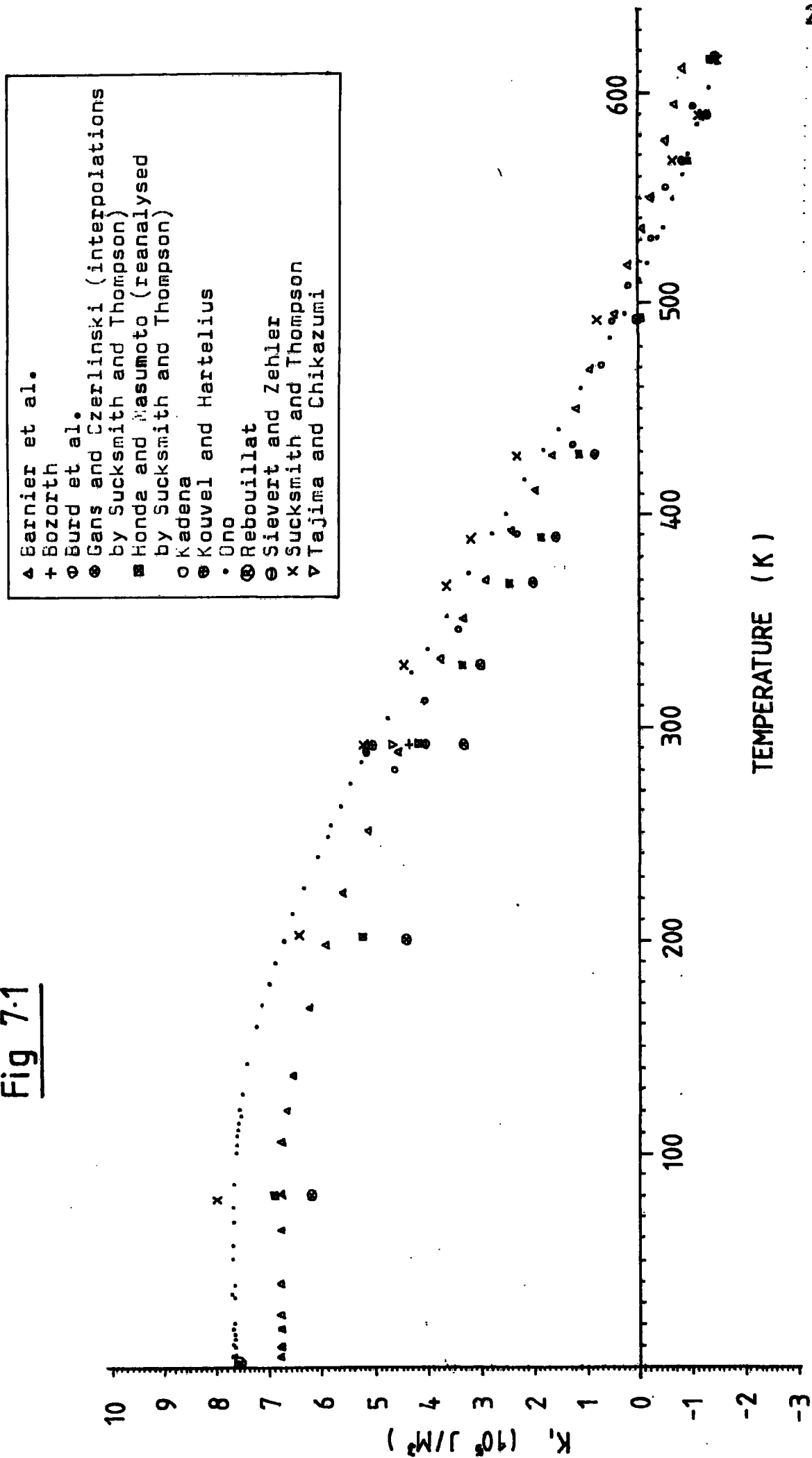
Callen and Callen (1960) as well as Aubert (1968) have shown that it is not only the free-energy of the crystal anisotropy which contributes to the form of the torque curve but a term arises due to "anisotropic magnetisation" (see chapter 2, section 2.6), which is dependent on the intensity of the applied field, and this results in a field dependence of the anisotropy constants. Thus a more fundamental anisotropy can be obtained by extrapolating to zero field, the field dependence of the anisotropy being regarded as a separate property. Direct extrapolation of the harmonics is therefore additionally questionable since it derives in principle the anisotropy constants at infinite field.

Of those workers who have made an adequate shear-correction or used other forms of magnetometry, there is still however disagreement. Sievert and Zehler, and Ono have shown experimentally that the anisotropy of cobalt has a truly field dependent term (not, at least in the latter case, the artefact of a wrong shear factor), yet the effect is too small to cause the given ambiguity in the anisotropy constants. Such a relative observation of the field dependence is possible irrespective of the absolute accuracy of the determination.

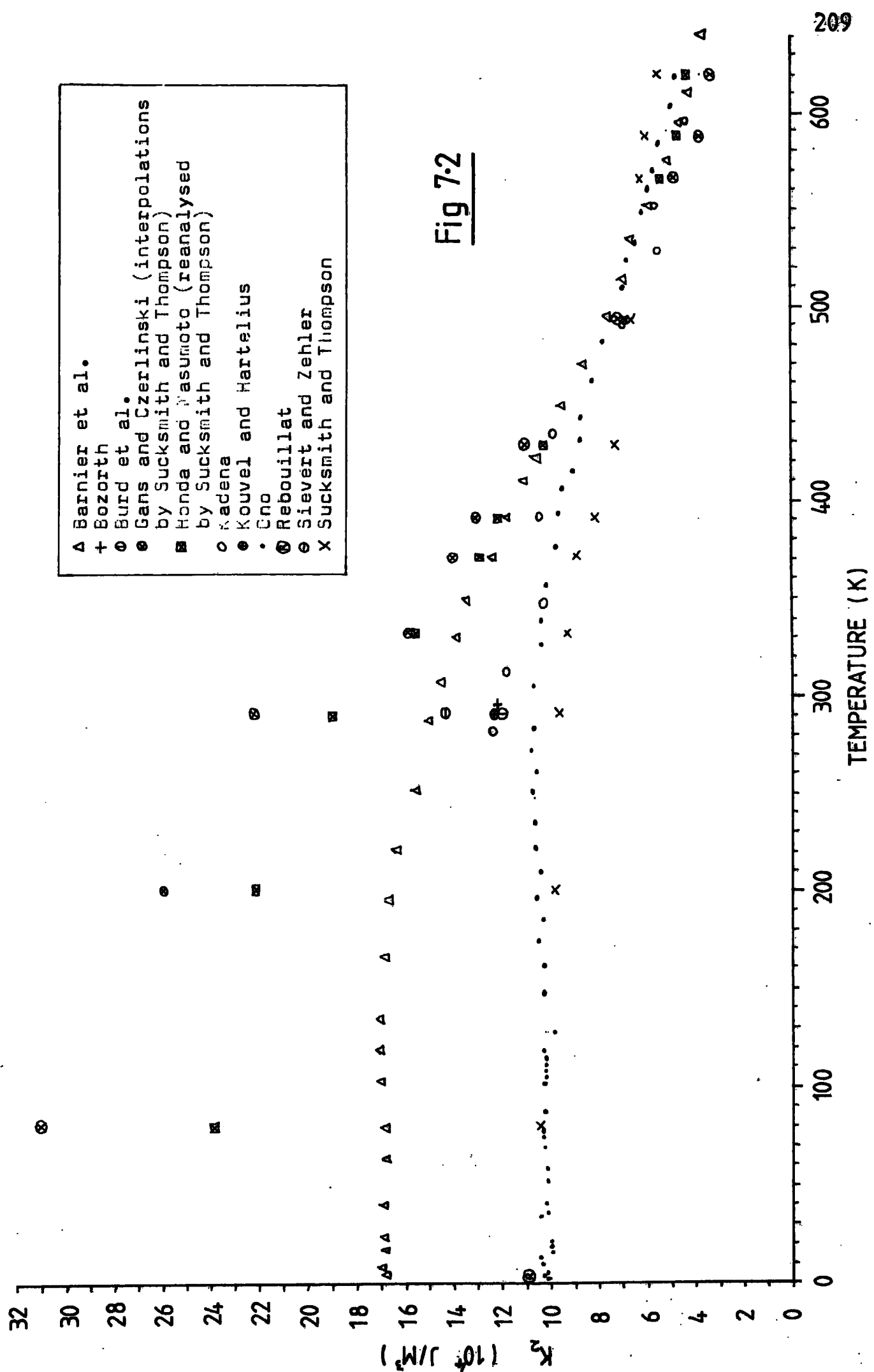
The data existing on cobalt is given in figures 7.1

PREVIOUS DATA FOR K, VS TEMPERATURE FOR COBALT

Fig 7.1



PREVIOUS DATA FOR K_2 VS TEMPERATURE FOR COBALT

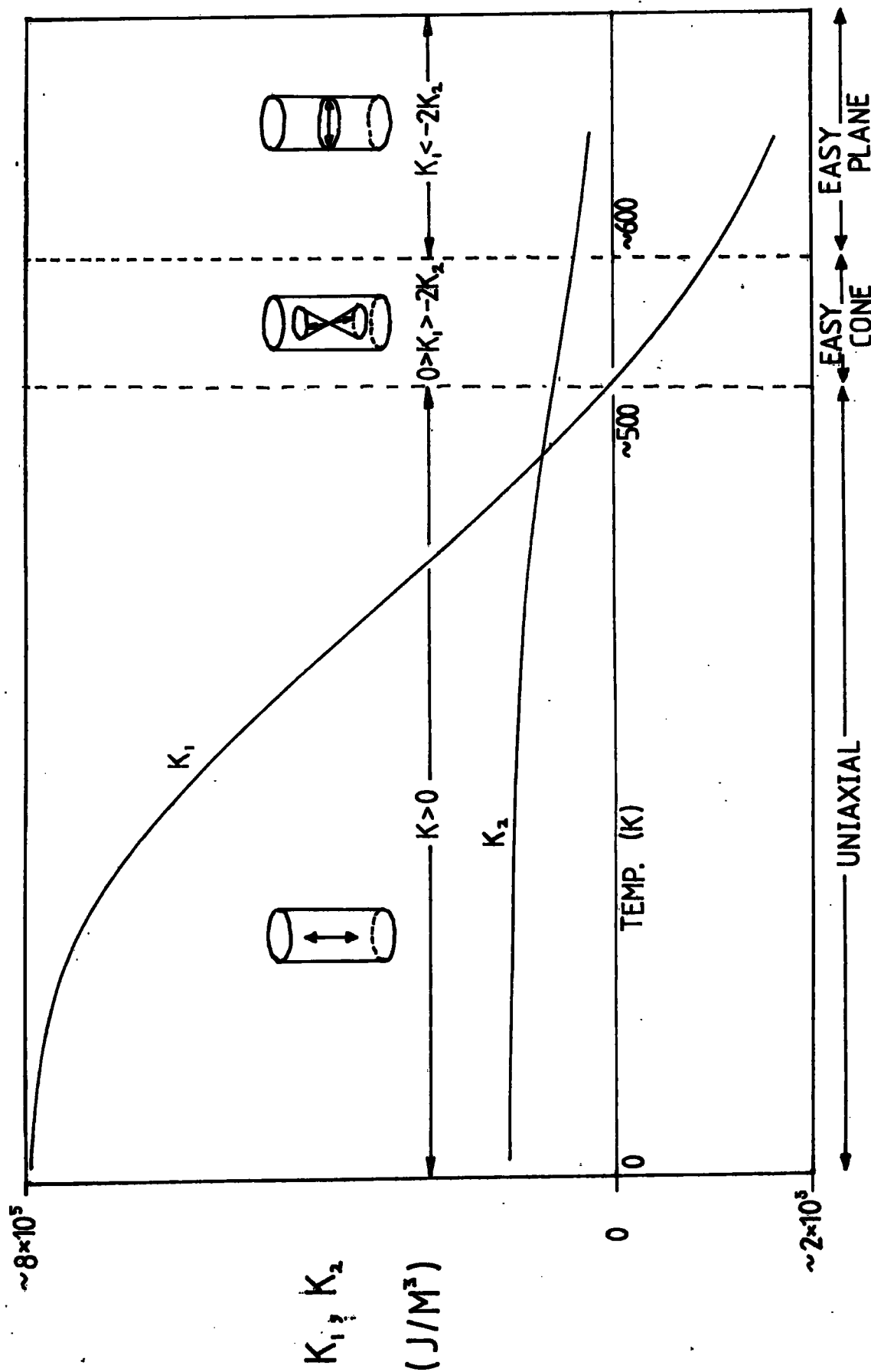


and 7.2 where results from inadequately corrected torque curves are rejected. Of this data the work of Ono stands out as being particularly accurate since his determinations of the true field dependence of the anisotropy, derived from shear-corrected torque curves, required relative measurements of the anisotropy to within a fraction of one percent. Significantly, however, the effects of the third uniaxial harmonic were not investigated.

Constants of higher order than K_1 and K_2 are not given by any source except for a discrete room temperature measurement of K_3 by Sievert and Zehler. It is felt that the value obtained by them is in error due to an inadequate shear-correction suggested by the difference between their lower order constants and those of Ono or, in retrospect, the present work. In any case the single K_3 value is much larger than obtained here for the corresponding temperature; they indicate a value of $-3.1 \times 10^4 \text{ J/m}^3$ compared to an average of about $-1.2 \times 10^4 \text{ J/m}^3$ for three samples in the current analysis.

As pointed out by Barnier et al. (1961,b), due to the inversion of K_1 at about 500 K and its continuation to a magnitude greater than K_2 , the easy-axis of cobalt undergoes a transition from the c-axis, through an easy cone symmetrically disposed around the c-axis, to an easy c-plane, as illustrated in figure 7.3. In fact a marginal six-fold energy dependence due to a finite K_4 is observed with respect to rotation of the magnetisation in the c-plane, so the easy cone is slightly deformed accordingly. The conical state covers about 80 K.

CHANGE IN EASY DIRECTION FOR COBALT WITH TEMPERATURE



SLIGHT SIX-FOLD SYMMETRY IN BASAL-PLANE

Fig 7.3

7.3 The samples

Four disc-shaped samples of cobalt were investigated. One c-plane disc and one b-plane disc were cut from the same float-zone crystal. b-plane discs were also cut from a Czochralski crystal and a Bridgman crystal. The masses, measured on an Oertling model 146 high precision balance, and approximate diameters are given in table 7.1. Sample purities were of the order of 99.99 % .

TABLE 7.1 DETAILS OF THE COBALT SAMPLES

SAMPLE No	ORIENTATION	MASS (mg)	DIAMETER (mm)	GROWTH METHOD
1	b-plane	97.67	3.8	Float-zone
2	b-plane	252.26	4.3	Bridgman
3	b-plane	120.27	4.9	Czochralski
4	c-plane	98	3.8	Float-zone:

The Czochralski crystal was grown by the author and Mr T. Brown, then of the Cavendish Laboratory, Cambridge, at Cambridge, on a Metals Research BCG 265 crystal puller. The float-zone crystal was supplied by Prof. Takahashi of Iwate University, Japan and the Bridgman crystal by Metals Research Ltd. The author's only involvement in the preparation of the sample discs was the spark erosion and planing of the Bridgman crystal transferred to the cutting machine on a goniometer from a Laue back-reflection X-ray camera by which it was oriented. Alignment of the disc with the nominal crystallographic plane was to an estimated precision of about 1°; an accuracy assumed for the remaining samples cut by experienced workers. All samples were circular to better

than 1%.

7.4 Experimental technique

The anisotropy measurements were carried out using the torque magnetometer of the previous chapter, its large dynamic range being particularly suited to the present measurements in which torque amplitudes varied from 10^{-2} Nm (~ 100 mg cobalt b-plane disc at 77 K) to 10^{-6} Nm (~ 100 mg c-plane disc at 400 K). The details of the magnetometer are given in chapter 6.

For the two float-zone samples (Nos. 1 and 4), measurements were made over the full temperature range of the magnetometer, that is 80 K - 610 K. These temperatures were obtained as described earlier. The remaining two cobalt samples were cooled to between 80 K and 300 K. Sample temperatures were measured to an estimated accuracy of 3 K accounting for, among other things, thermal lag during typical sweeps at about 100 K/hour.

All torque measurements were made at a single field strength, namely 1.618 ± 0.008 tesla, comparable to the field applied by Ono for much of his work and allowing reasonable comparison of the two data sets. The field was determined by using the magnetometer to measure the torque on a search-coil in a large uniform magnetic field and calibrating a Hall probe against the calculated field value. This was possible because of the high absolute accuracy of torsional measurements from the magnetometer. The probe was then applied to the central homogeneous region of the field of interest, which was too restricted for an accurate search-coil

measurement to be made directly. The main field was reproduced by duplicating the current through the magnet coils as read on a Schlumberger 4045 digital ammeter to a relative accuracy of about 0.1 %. The Hall probe used was a Hirst model FM 75. After making a shear-correction, anisotropies were derived from a Fourier analysis of the harmonic content of the torque curves. A field extrapolation was not carried out.

Samples were attached to the magnetometer using Høltz "Gun Gum" manufactured as an automobile exhaust sealant and ideal for the extremes of temperature encountered in the present investigation. Sample attachment is illustrated in figure 6.4. No clear assessment could be made of the anisotropies contributed by stresses associated with differential thermal contraction between sample, cement matrix and sample holder during heating or cooling, except that measurements for Araldite samples glued onto a plane surface, rather than recessed into a holder, showed no apparent difference. Inclination of the sample discs with respect to the field plane was estimated to be less than 3° giving a negligible cosinal error in the measured anisotropies.

The magnet pole pieces gave a central field homogeneity of better than 1% over a volume of about 1 cm^3 ; well in excess of the current sample volumes (0.01 cm^3).

Using the orientation adjustment of the sample-support-rod of the magnetometer, the tip of the rod was carefully centralised by minimising the indicated torques resolved from the sideways forces between a dummy polycrystalline

iron sample and a small bar-magnet. Careful replacement of the dummy with a cobalt sample ensured the concentricity of the latter with the magnetometer movement and similar immunity of the measured torques to pulling of the sample by field inhomogeneity. It was found empirically that parasitic torques due to field-pull could, for an unadjusted sample support rod, give torque signals with amplitudes of up to 2% of the room temperature uniaxial values and a greater proportional effect on the delicate harmonics to be extracted subsequently.

Non-linearity of the torque measurements as read by the computer was found to be no more than 0.3% (gradient range) corresponding to a maximum harmonic distortion to the second and third components of a torque curve of less than 0.15% and 0.1% of the first (principal) harmonic respectively with the likely distortion much less than this in practice. Harmonic distortion due to shape anisotropy (see results section) was found to be similarly very small given a 1% variation in the diameter of the sample and a tendency for this to be elliptical in form.

Software which performed the data acquisition and corrected for non-ideal magnetometer behaviour (see chapter 6, section 6.6) had already been written, and to this was annexed the analysis program specific to the present cobalt investigations. The full program is given in Appendix F and performed the shear-correction followed by a Fourier analysis. The analysis used a trapezium rule modified for data spaced unevenly along the abscissa resulting from the applied shear-correction and the method of data acquisition.

Least-squares curve-fitting was rejected on the grounds that it was slower by an order of magnitude than the Fourier method, which processed the five torque curves from one run of the program in about ten minutes to an adequate consistency in the determined values. The first three harmonics were determined as an average, after shear-correction, of the values obtained for each of the five curves from one run.

As a further means of rejecting noise in the torque curves, the phase of the higher harmonics with respect to the easy-axis was examined and only that component having a node at the easy-axis was used in the anisotropy derivation; higher harmonics which are out of phase with the easy-axis cannot be legitimate since they do not reflect the crystal symmetries. The relationships between the anisotropy constants and the Fourier coefficients (harmonics) are dealt with in chapter 4.

During each run of the magnetometer program the torque curve was calibrated from the movement of the magnetometer head, measured using a travelling microscope (see chapter 6, section 6.7), yielding a very accurate peak-peak torque value for the curve. The torque value was entered into the computer, thereafter to be equated automatically, at the end of data acquisition, to the range of the magnetometer output, allowing all the data to be converted to Nm. A request for the magnetisation value at the prevailing temperature, interpolated from the data of Myers and Sucksmith (1951), and requests for the sample volume and field strength were made to complete the information necessary for the computer to perform the shear-correction of the data and subsequently

the Fourier analysis.

The data acquisition was such that each experimental point was derived from four variables (two positional measurements taken before and after the torque input, the torque value itself and the time at which the torque value was taken), and each torque curve was measured at approximately every 2° along the $0 - 77$ interval. Since five curves were taken for each of about 100 program executions, the total number of points taken, each to a nominal 12-bit accuracy, was about 2×10^5 . An experiment such as this would have been impossible without on-line acquisition and processing of the data!

7.5 Results

Examples of the torque curves produced by the magnetometer on the X-Y recorder are given in figures 7.4 to 7.6 . Figure 7.4 shows that torque curve amplitudes saturate for cobalt in the 1.4 - 1.8 tesla field range even at liquid nitrogen temperatures for which the anisotropy is highest. It can be concluded, therefore, that the field of 1.618 tesla used throughout the present investigation was adequate for producing the single-domain state under all experimental conditions. Figure 7.5 and 7.6 show the uniaxial torque curves produced over two interesting temperature intervals covering the point of inversion of the first harmonic and the point of K_1 inversion respectively. The anisotropy data as computed on-line from the harmonics of the shear-corrected torque curves is given in figures 7.7 to 7.16 and tabulated in Appendix G. Comparison of the

TORQUE CURVES FOR A COBALT b-PLANE DISC

AT 90 K ILLUSTRATING AMPLITUDE SATURATION

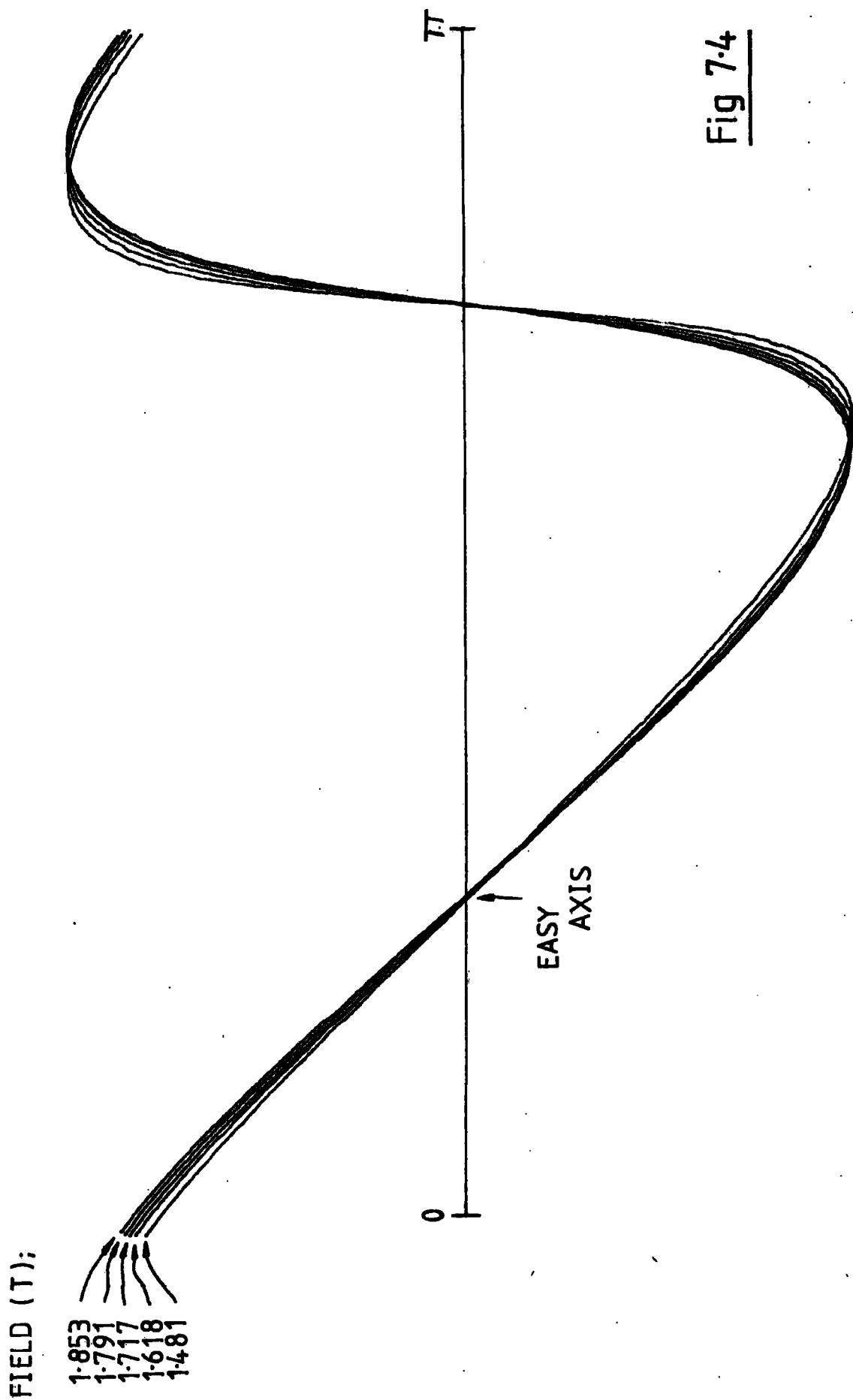


Fig 7.4

TORQUE CURVES FROM 0 TO π FOR A 97mg b-PLANE DISC OF COBALT
SHOWING INVERSION OF THE 2 θ HARMONIC AT ABOUT 543 K. (1.612 T)

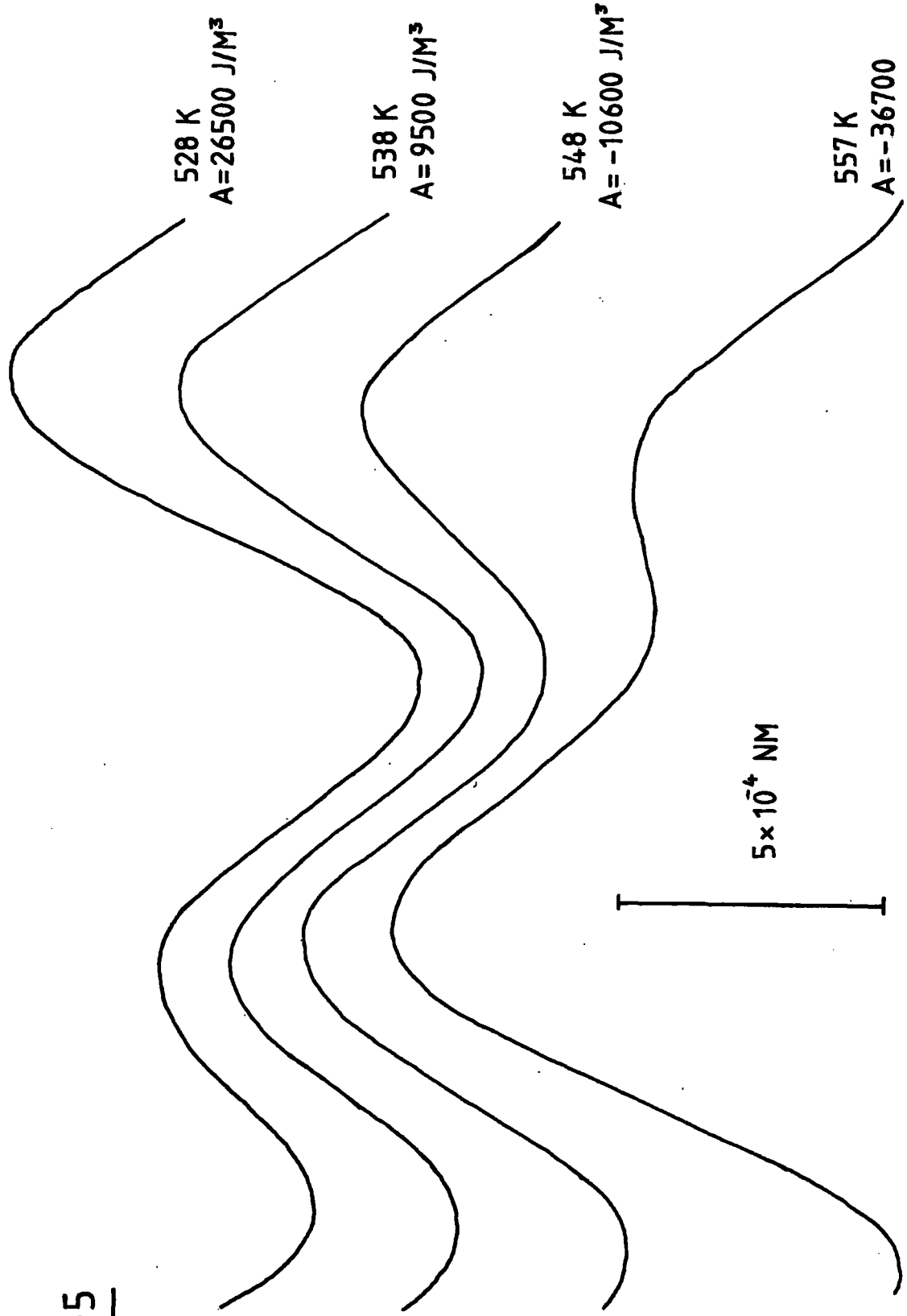


Fig 7.5

TORQUE CURVES FROM 0 TO π FOR A 97mg b-PLANE DISC OF COBALT
IN THE REGION OF K, INVERSION AT ABOUT 507 K (FIELD=1.612 T)

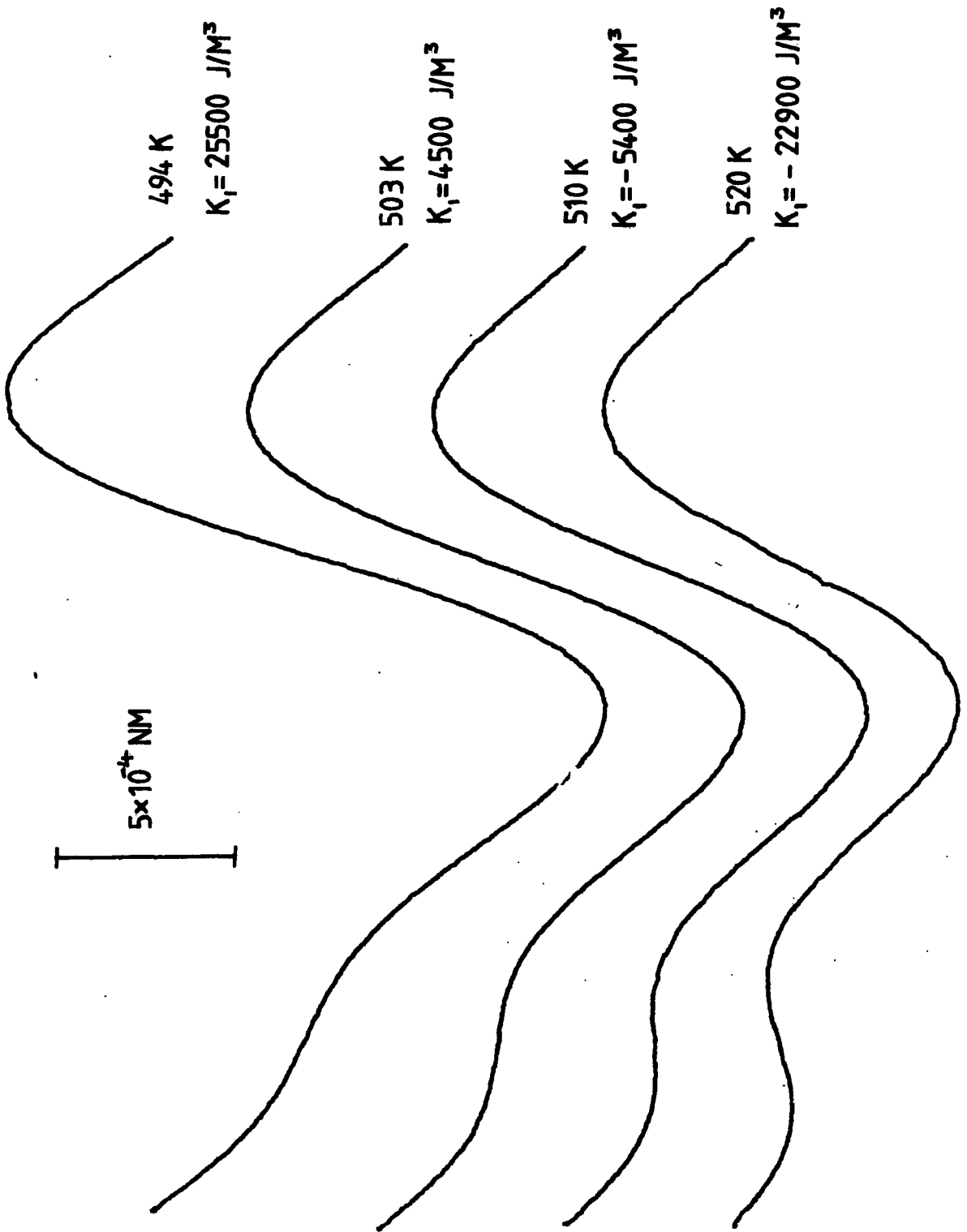
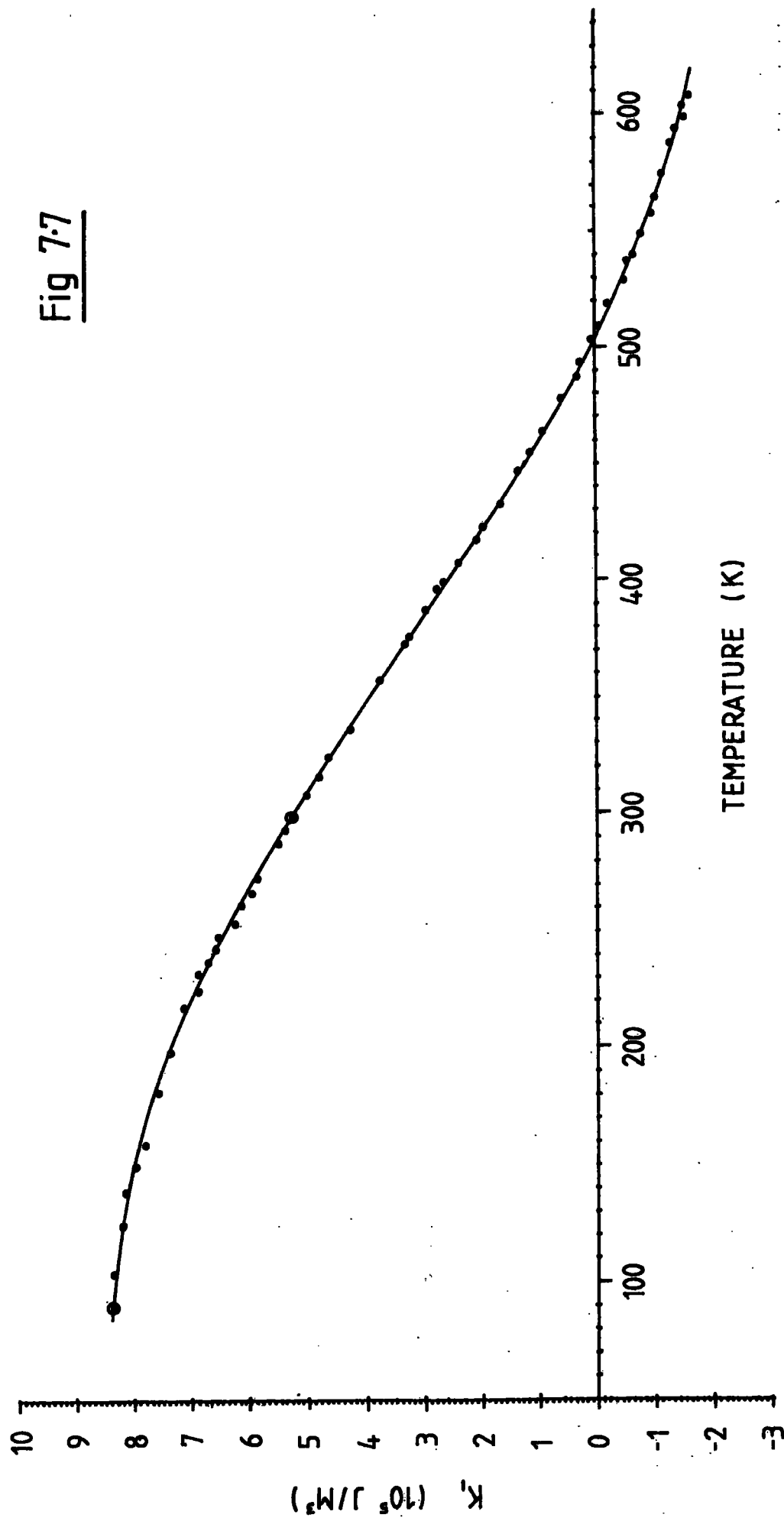


Fig 7.6

K_i VS TEMPERATURE FOR COBALT SAMPLE NÖ1

K, VS TEMPERATURE FOR COBALT SAMPLES Nö2 AND Nö3

Fig 7.8

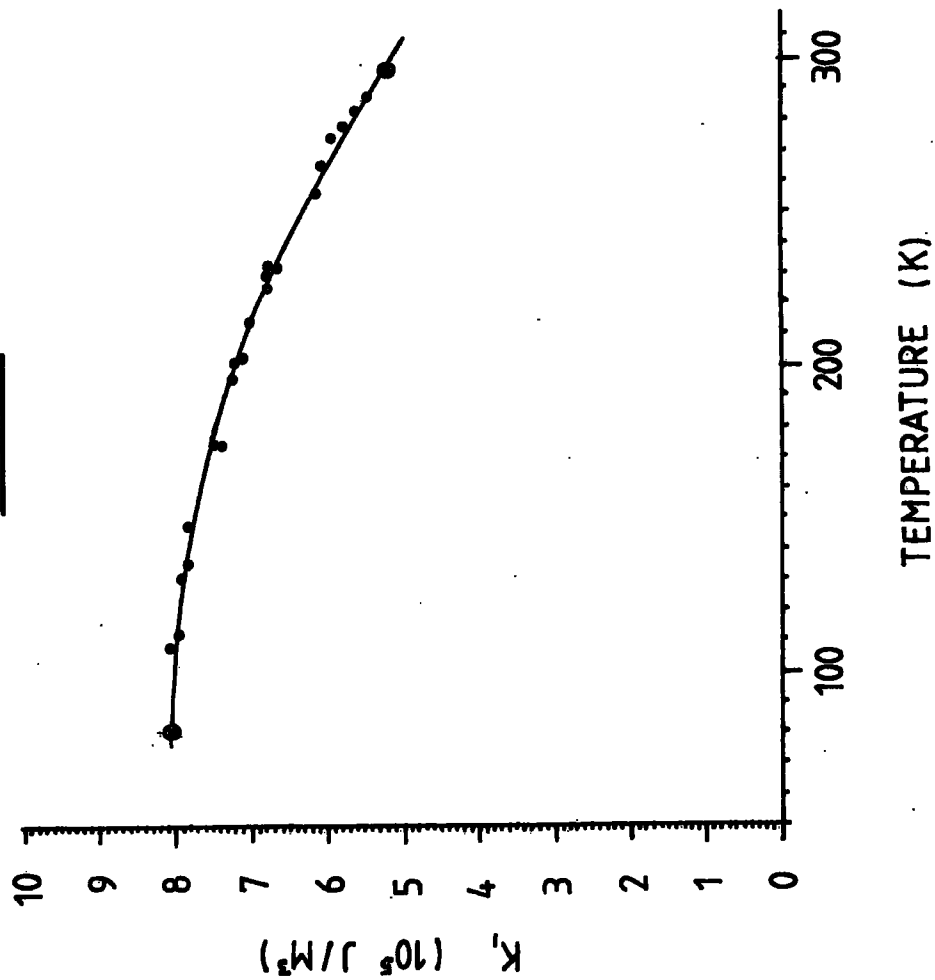
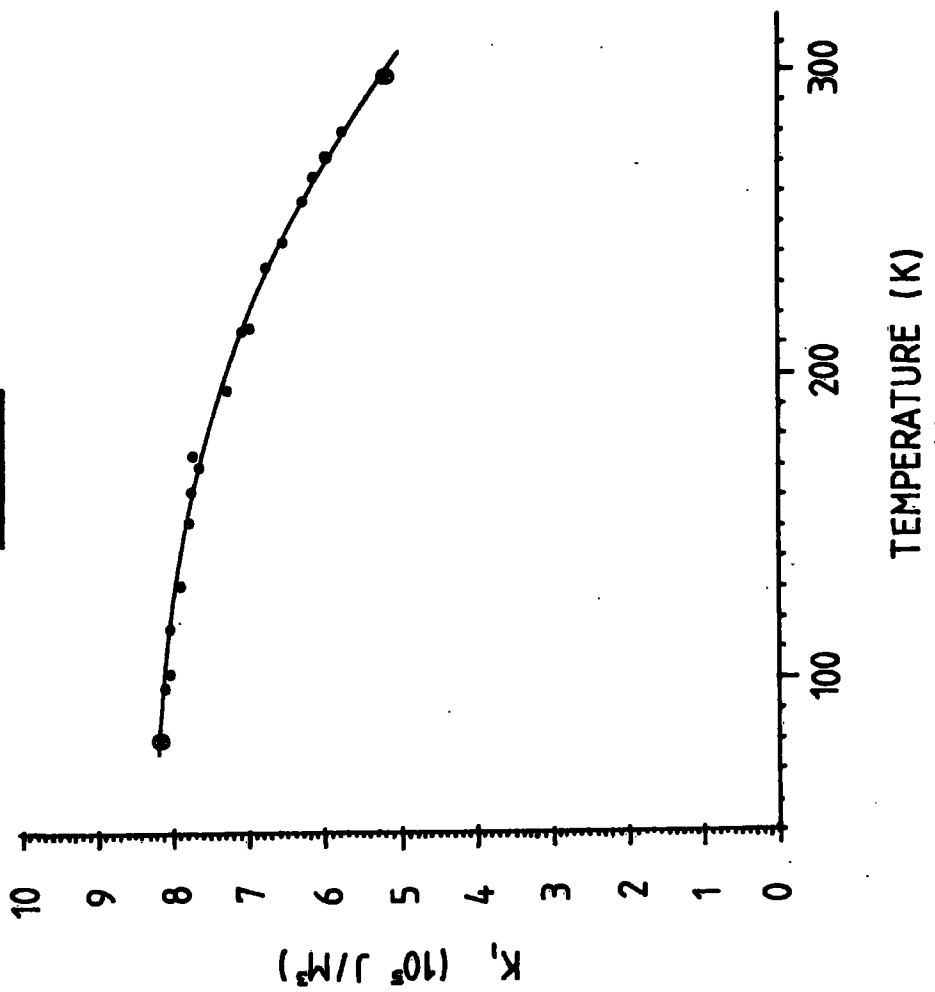
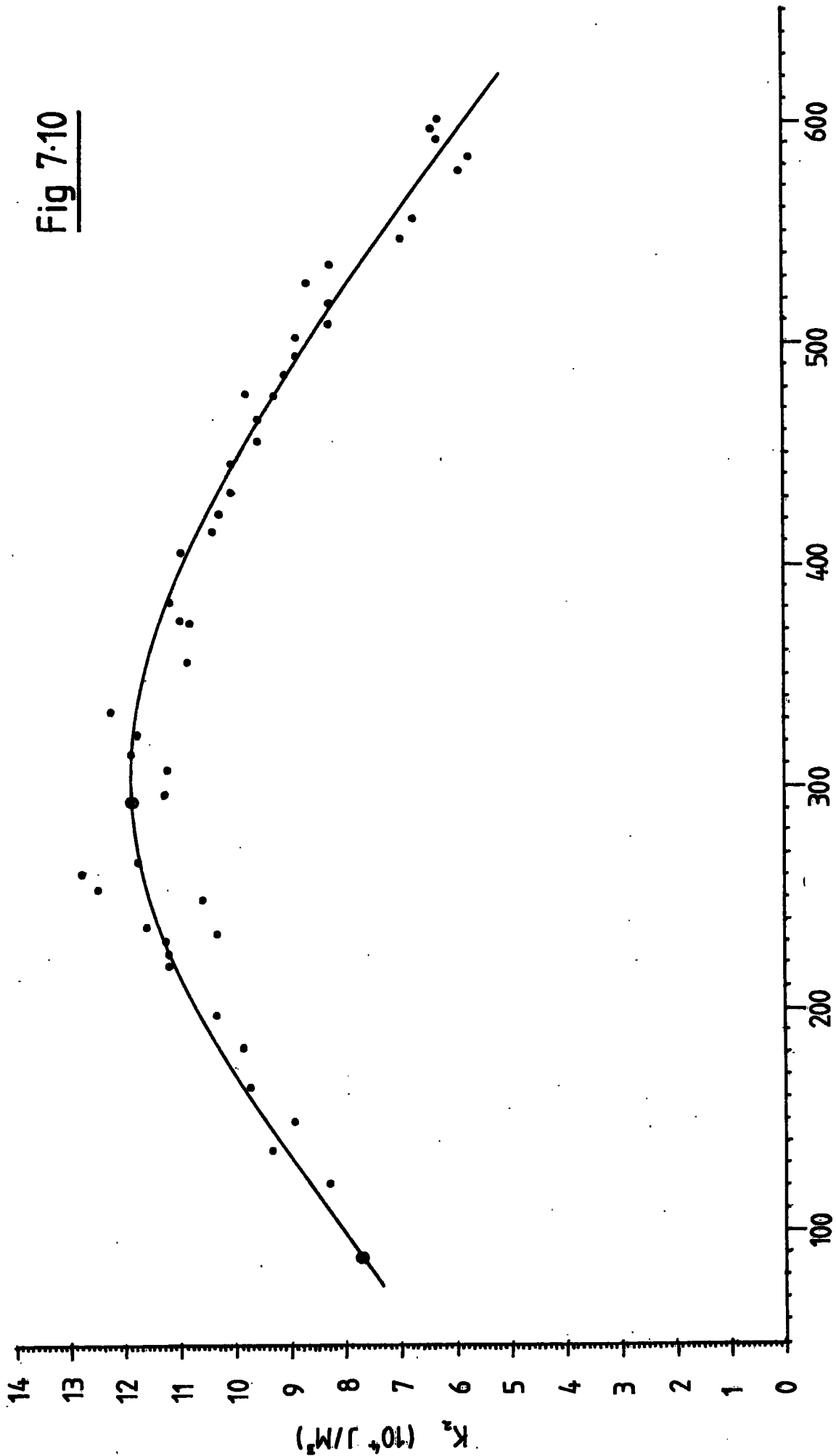


Fig 7.9



K₂ VS TEMPERATURE FOR COBALT SAMPLE NÖ1



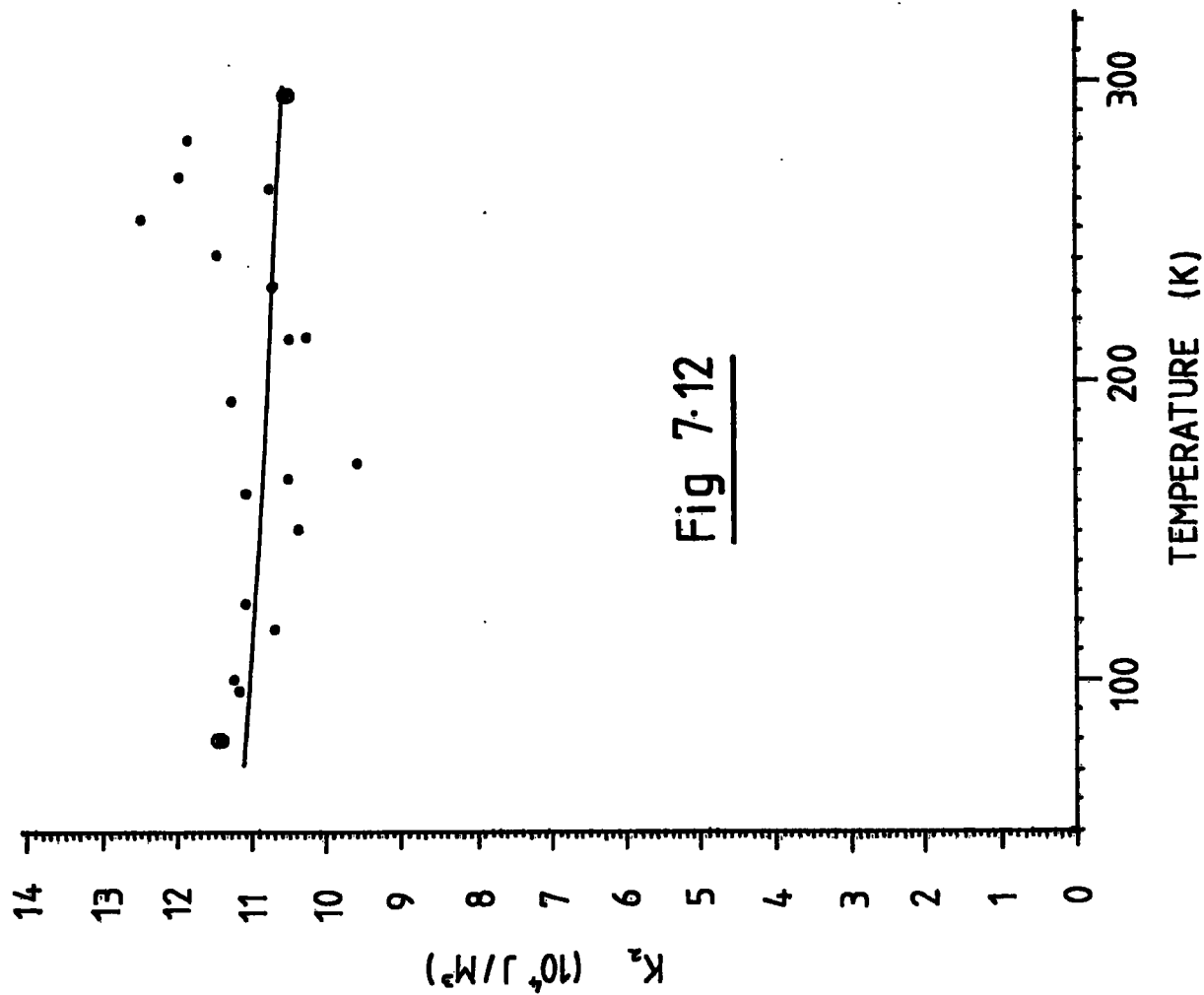


Fig 7.11

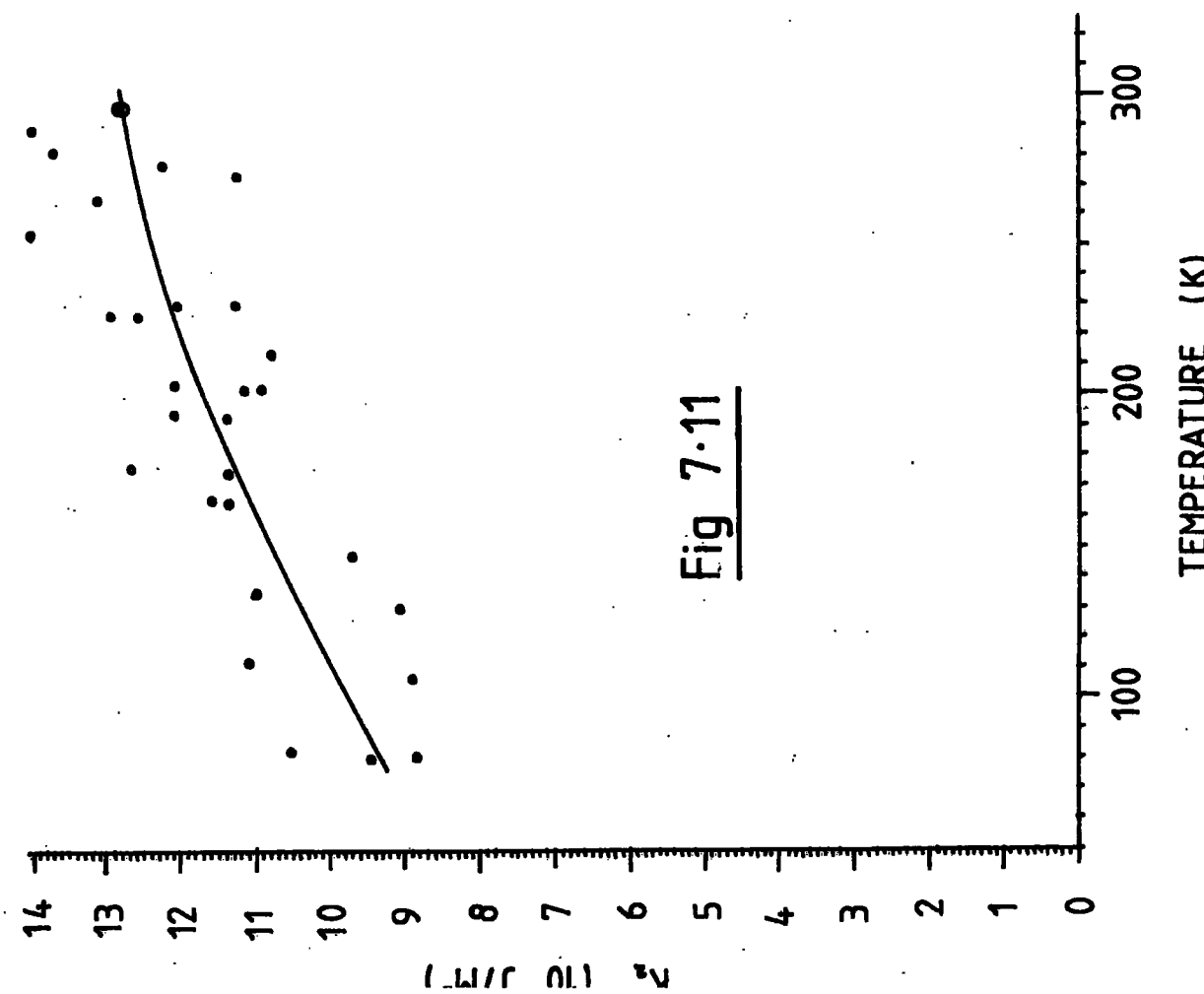
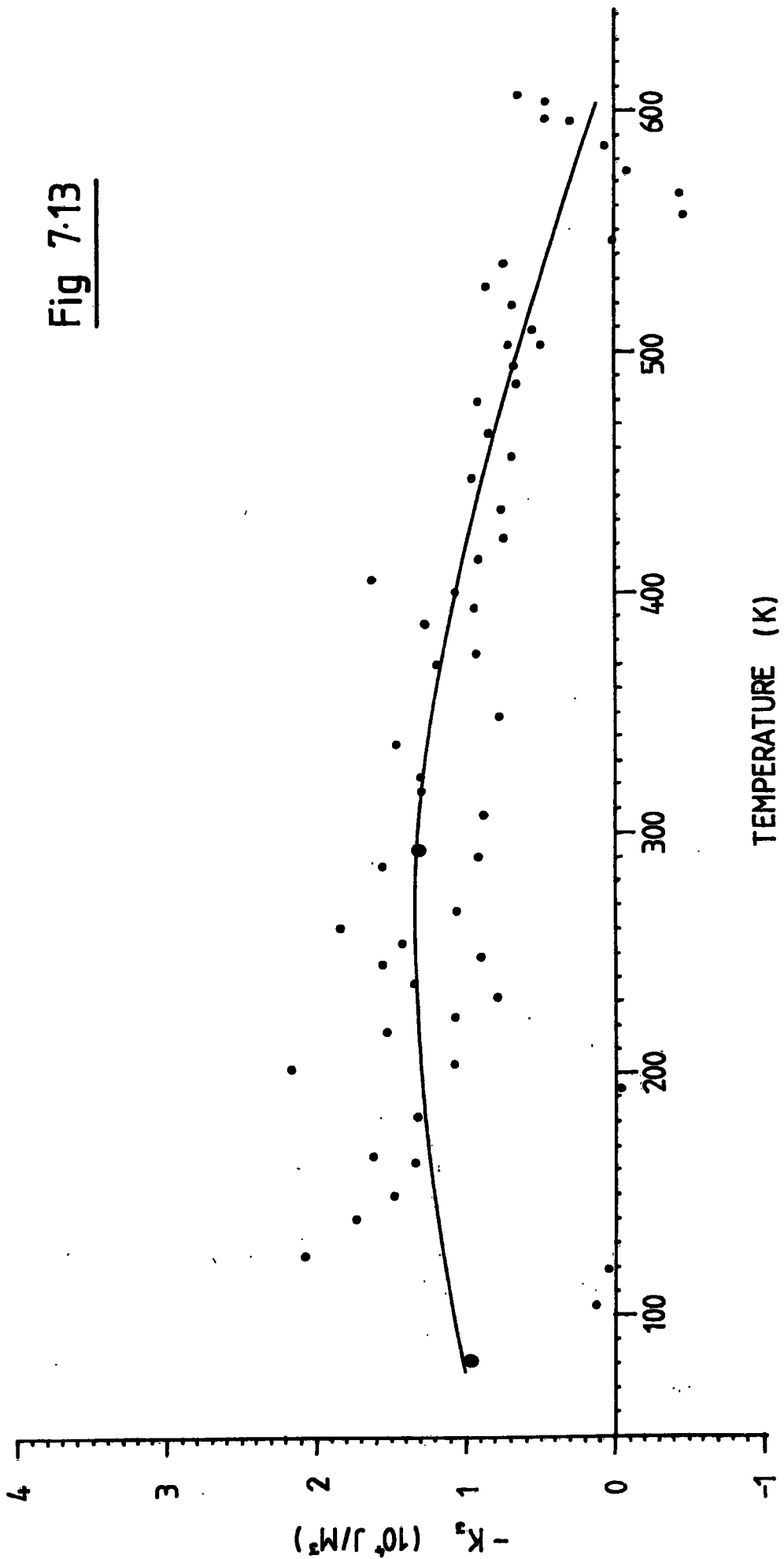


Fig 7.12

K₃ VS TEMPERATURE FOR COBALT SAMPLE Nö1



K₃ VS TEMPERATURE FOR COBALT SAMPLES Nö2 AND Nö3

Fig 7.14

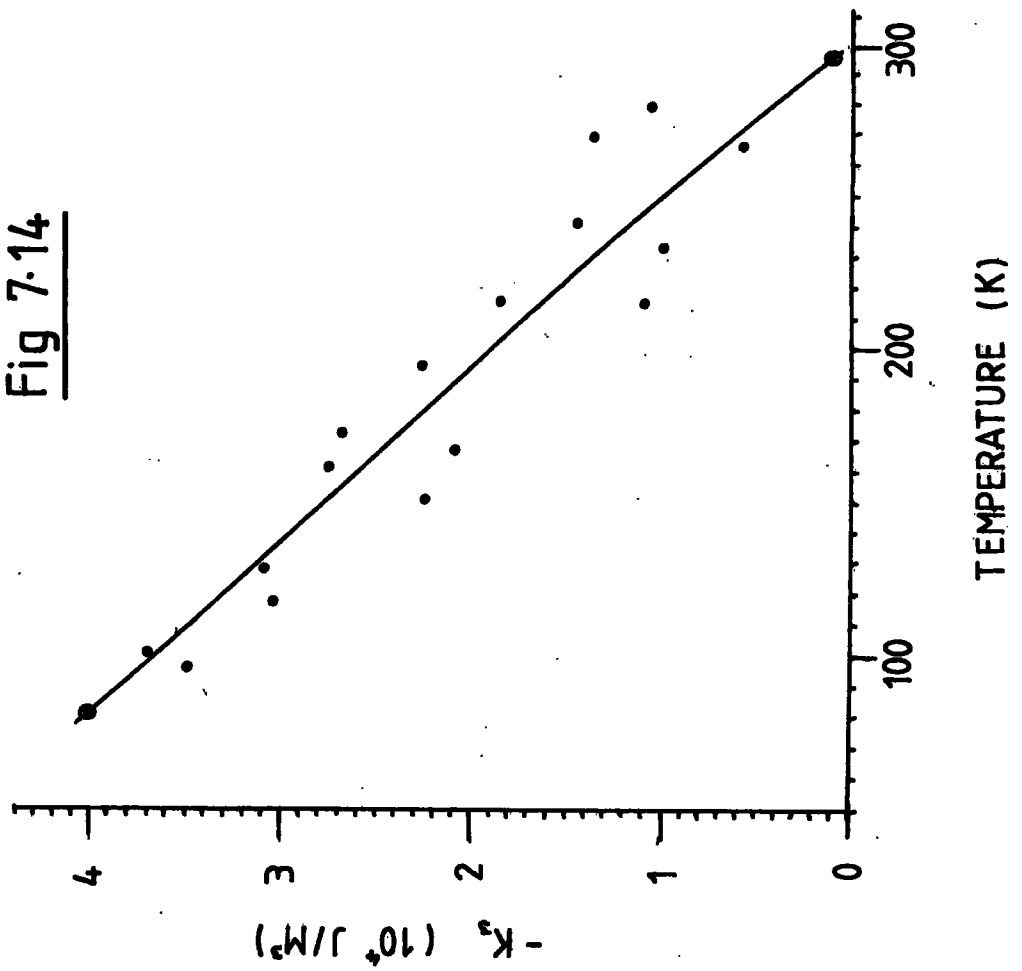
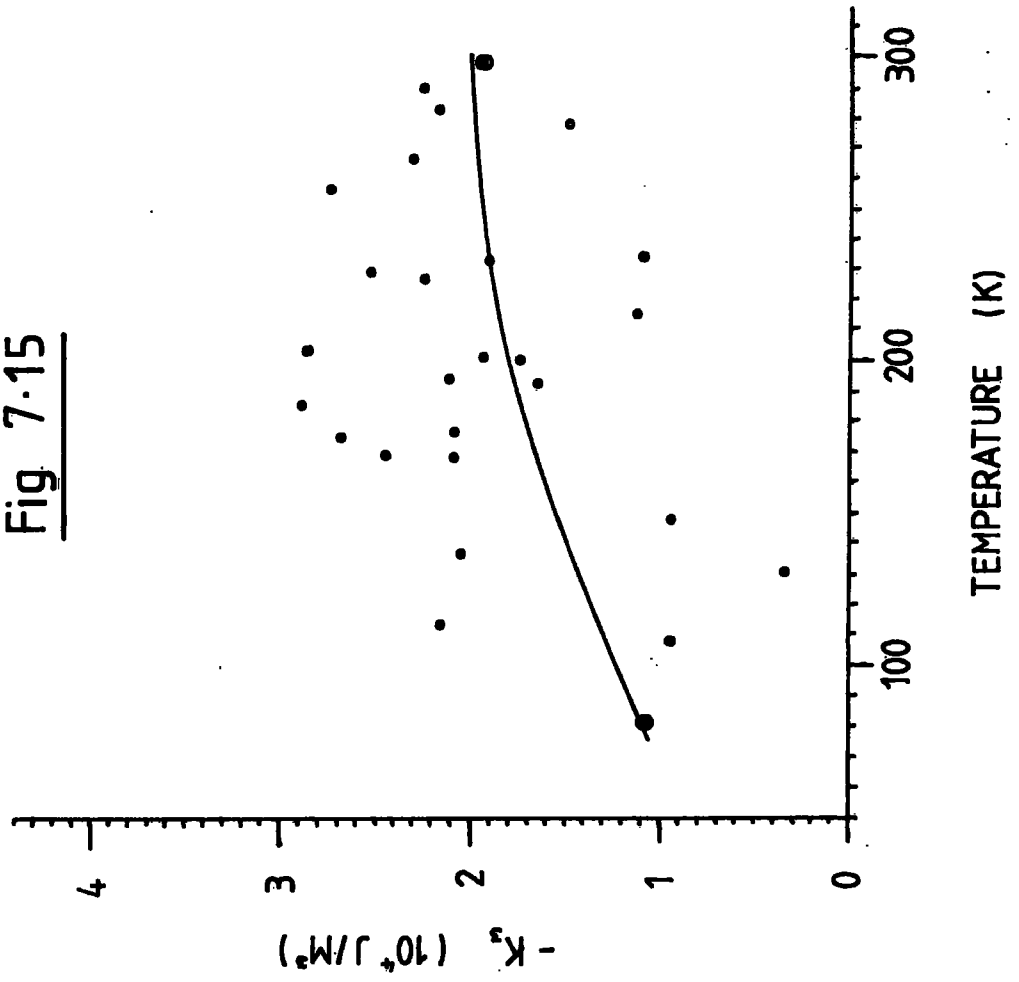
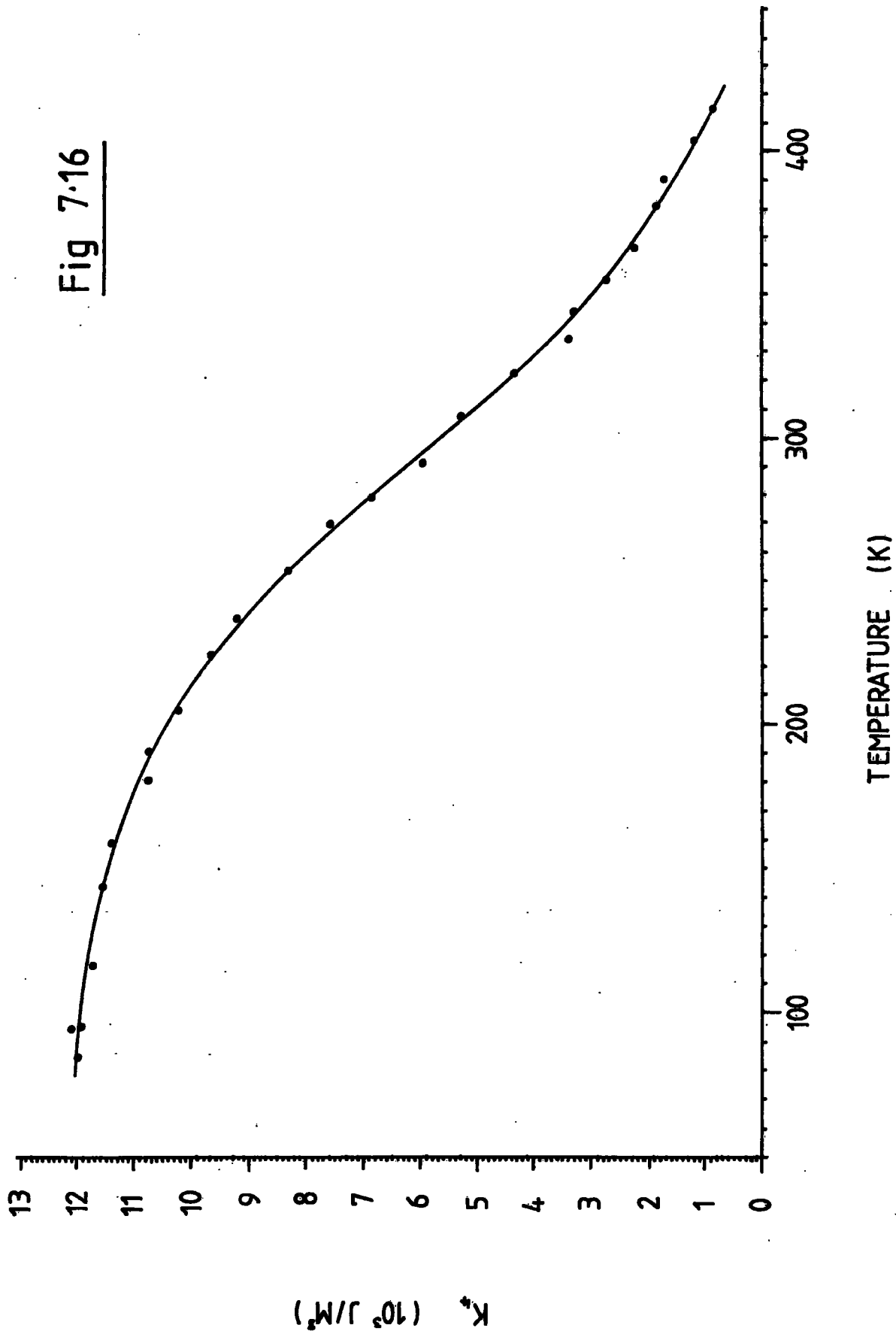


Fig 7.15



K₄ VS TEMPERATURE FOR COBALT SAMPLE Nö4

Fig 7.16

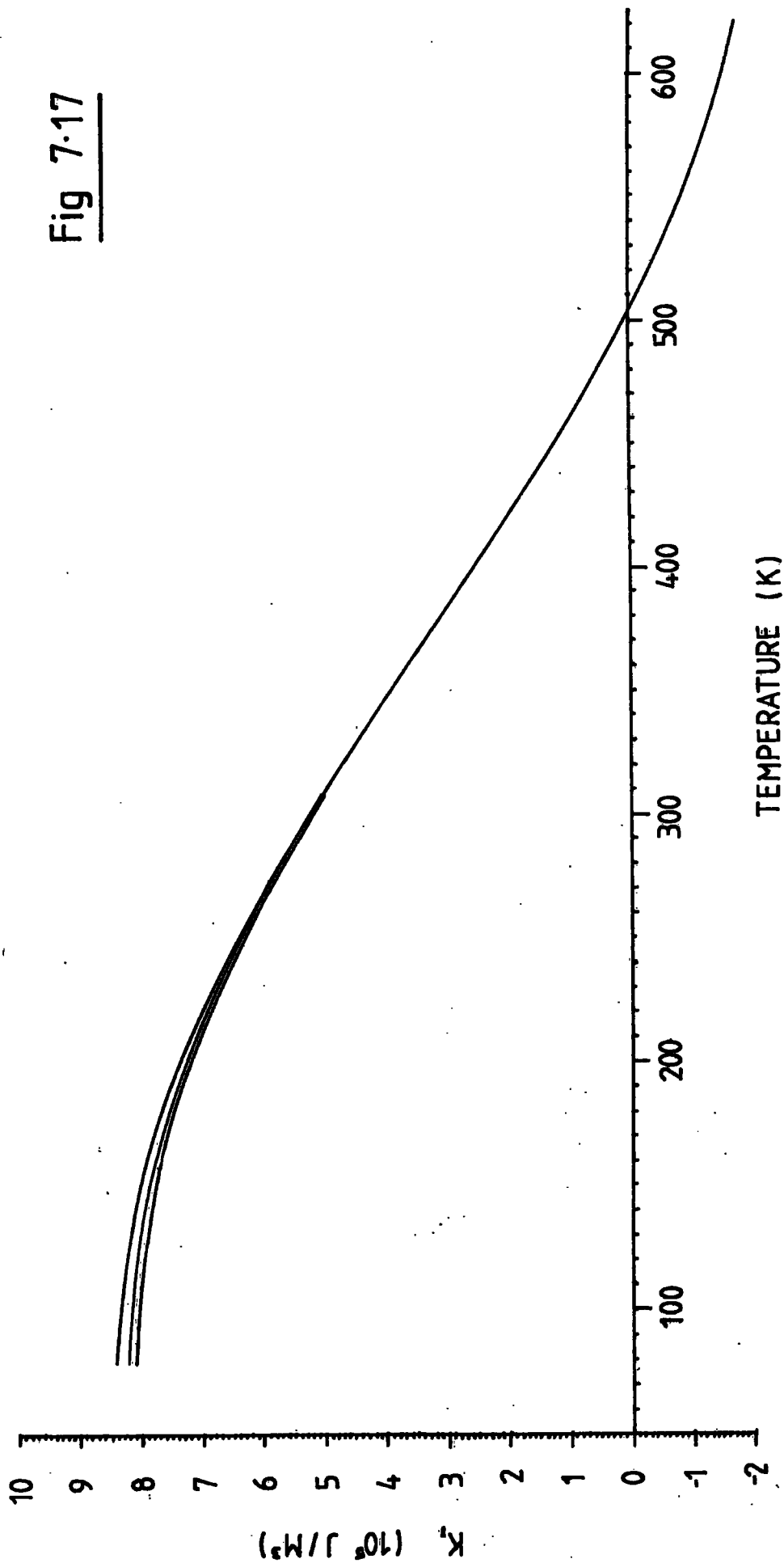


three K_1 plots is provided by figure 7.17 which reproduces simultaneously the three suggested fits. Figures 7.18 and 7.19 make a similar comparison for K_2 and K_3 .

As mentioned in chapter 4, section 4.2, there is no reliable method for correction of the anisotropy constants to a field-independent value. The quotation of the cobalt values at a given finite field is therefore necessary. However, Ono has shown that the field dependence of the anisotropy for cobalt is of the order of 1% in a 1 tesla field range above saturation for the K_1 constant. Therefore field extrapolations would be small irrespective of the likely means of achieving them.

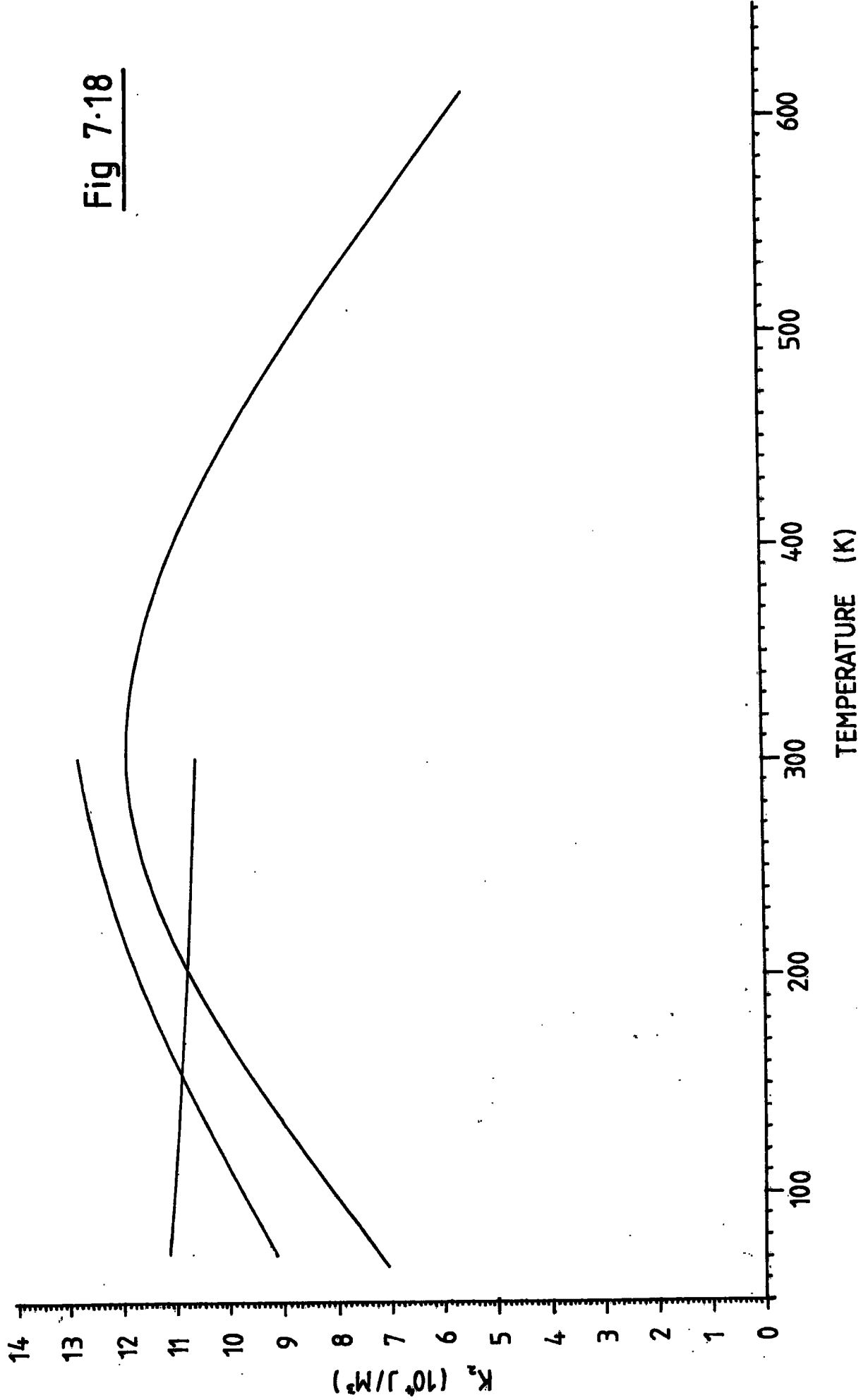
The inclusion of the third harmonic in the derivation of the anisotropies has had an adverse effect on the spread of the data. The third harmonic was in all cases small and typically about 0.5 % of the first harmonic. However in the anisotropy derivation it contributed disproportionately to the values of K_1 and K_2 , being weighted by a greater factor than the other harmonics. Consequently its error was multiplied and added to the values of the two first-order constants to increase their spread. The paradox of including the higher harmonics in the conventional, non-orthogonal expansion of the anisotropy energy used here, is that although mathematically, by definition, it ought to allow more accurate calculations of the constants, in practice, due to the spread in the harmonic values, results become more inaccurate since the constants are subject to the addition of errors from all contributing harmonics. Thus the spread for each constant diverges with respect to the number of harmonics used to

COMPARISON OF SUGGESTED K , FITS FOR THE THREE COBALT SAMPLES



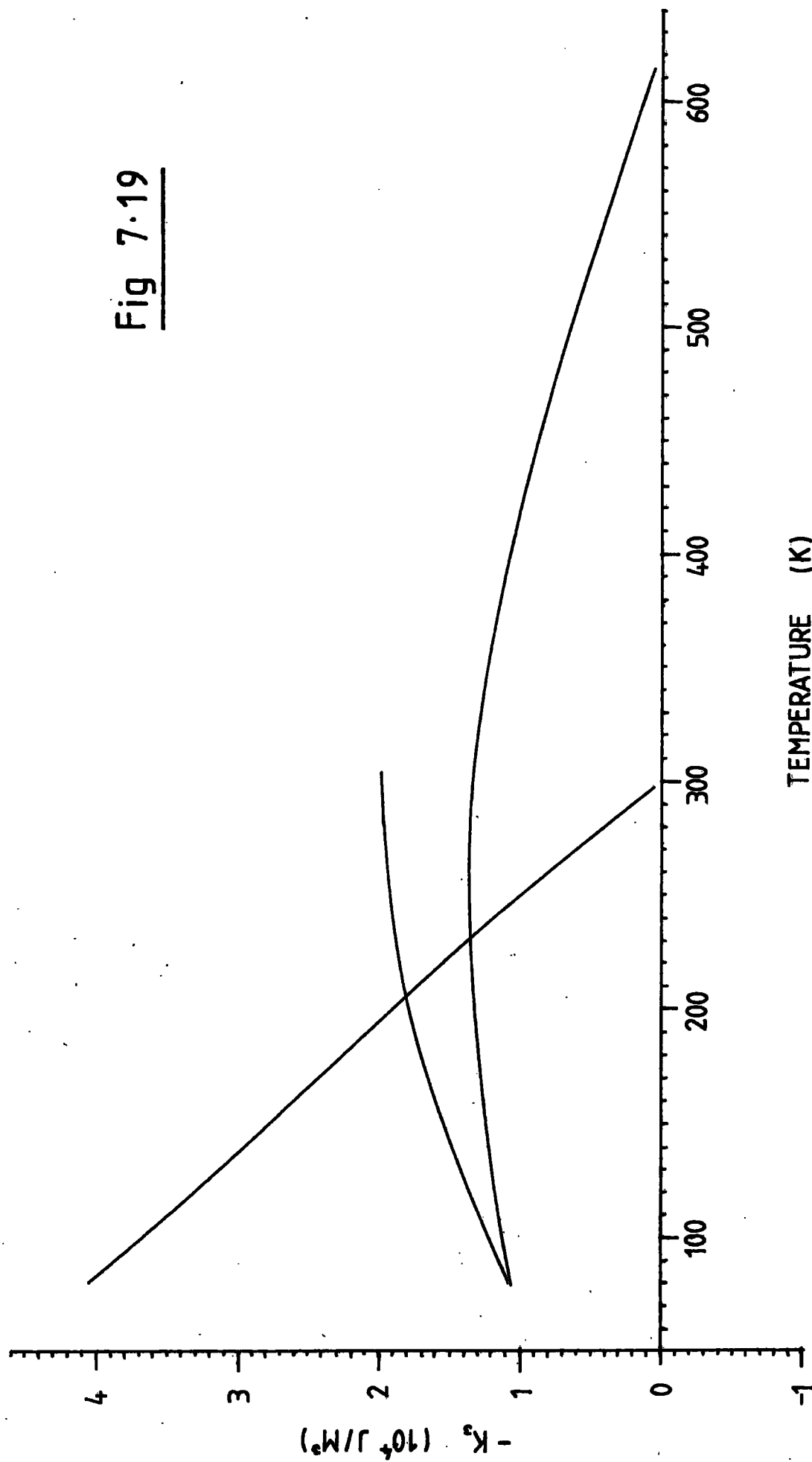
COMPARISON OF SUGGESTED K_2 FITS FOR THE THREE COBALT SAMPLES

Fig 7.18



COMPARISON OF SUGGESTED K_3 FITS FOR THE THREE COBALT SAMPLES

Fig 7.19



calculate it. It is therefore not necessarily expedient in practice to expand the energy to the highest possible order. An orthogonal functional expansion of the energy would be free from accumulating errors in the lower-order constants with respect to the number of harmonics included in the calculation deriving them. Arguably the (orthogonal) Fourier coefficients themselves are the most fundamental indicator of magnetocrystalline anisotropy and are, for this reason, given with the rest of the data in Appendix G.

The values of the constants show decreasing consistency with respect to order. Figure 7.17 and 7.18 illustrate the similarity between the principal anisotropy constants for the three samples; for K_1 they are within 3% of each other and 10% of the values given by Uno in all cases. Explicit comparison of these figures with existing data, including that of Uno, are given in figures 7.20 and 7.21.

The inconsistency of the present results demonstrates that sample variations, not necessarily intrinsic, have an effect on the anisotropy, even for carefully prepared specimens. Sample differences include:

- 1) The crystal quality;- related to initial purity, the particular growth technique and, in practice, subsequent handling.

- 2) The sample dimensions;- the circularity of the disc, the uniformity of thickness and the diameter/thickness ratio of the disc.

Distinguishing the effects of these is difficult. Furthermore it was discovered that an inconsistency in the anisotropy values for a given sample was evident, dependent on its short-

COMPARISON OF DATA FOR K, VS TEMPERATURE FOR COBALT; OLD AND NEW

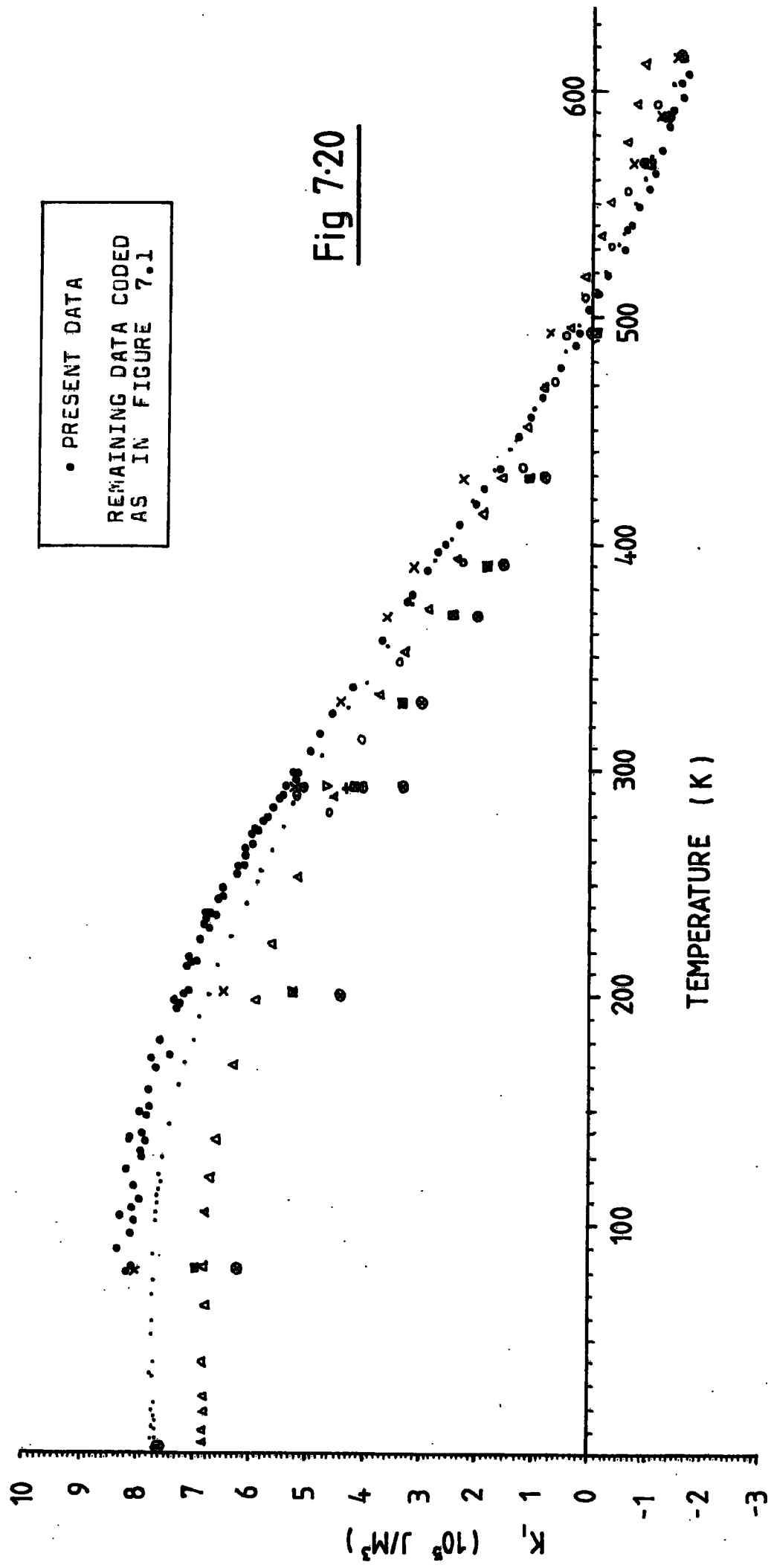
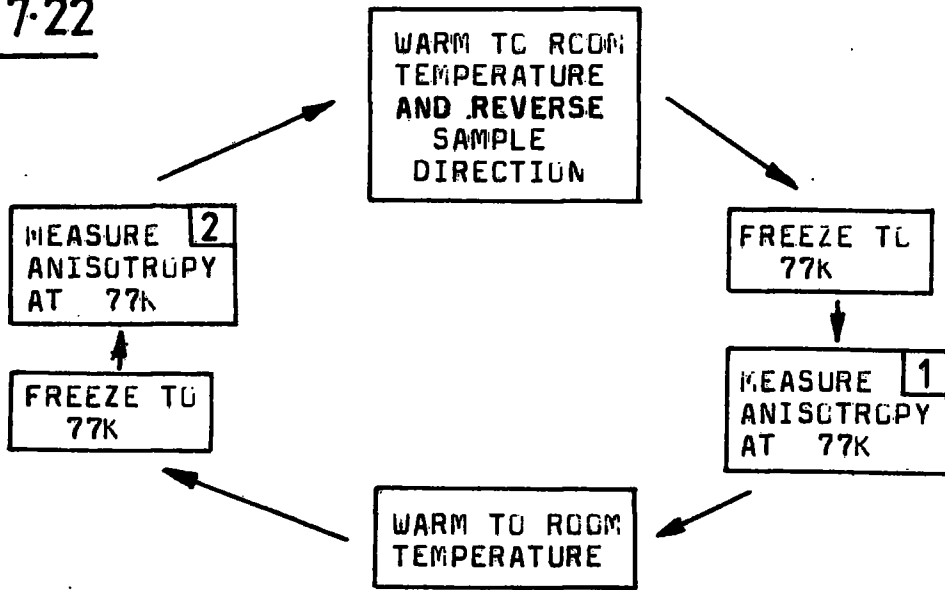
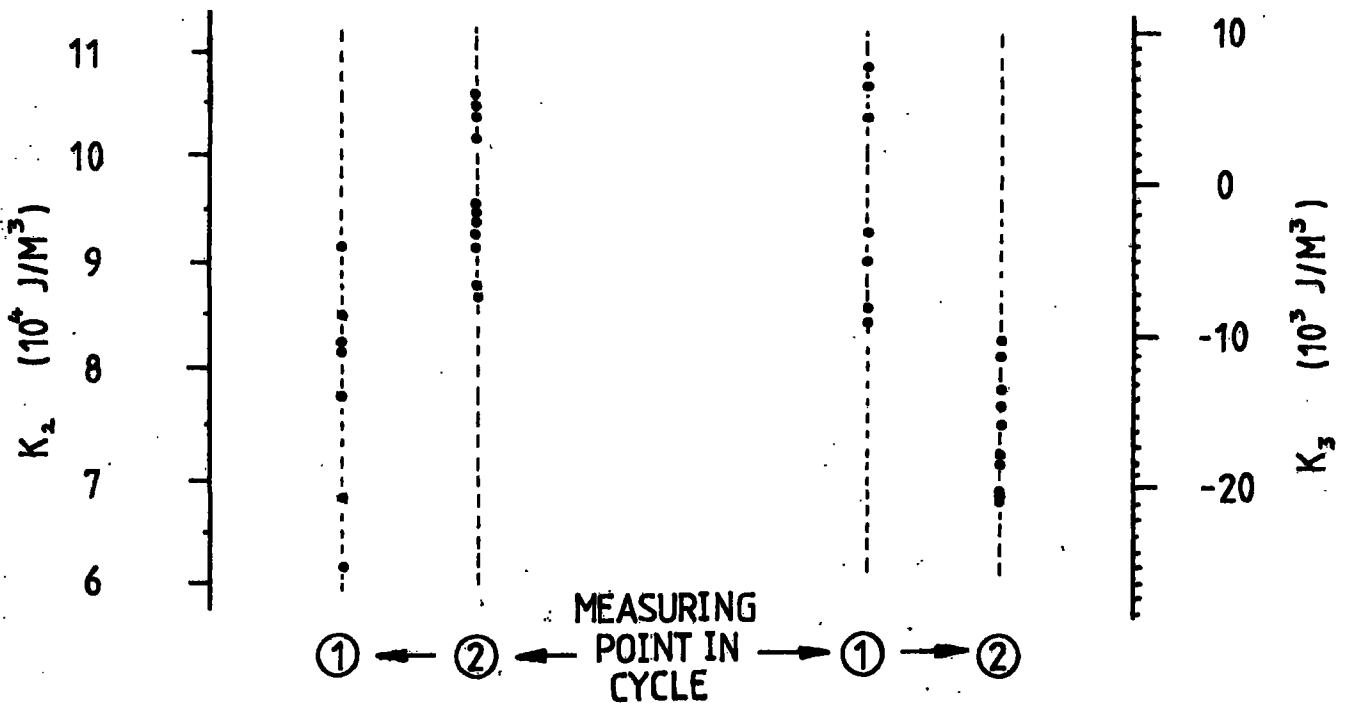


Fig 7-22



A REPRESENTATION OF ONE CYCLE OF EVENTS WHICH SHOWED THE "ANNEALING" OF THE MAGNETOCRYSTALLINE ANISOTROPY OF COBALT. (NOTE THAT THE MEASURING PROCESS INVOLVED ROTATING THE FIELD OVER A FIXED 180 INTERVAL SEVERAL TIMES)



K_2 AND K_3 DATA FOR COBALT SAMPLE No 3 AT 77K MEASURED AT DIFFERENT POINTS IN THE ABOVE CYCLE OF EVENTS

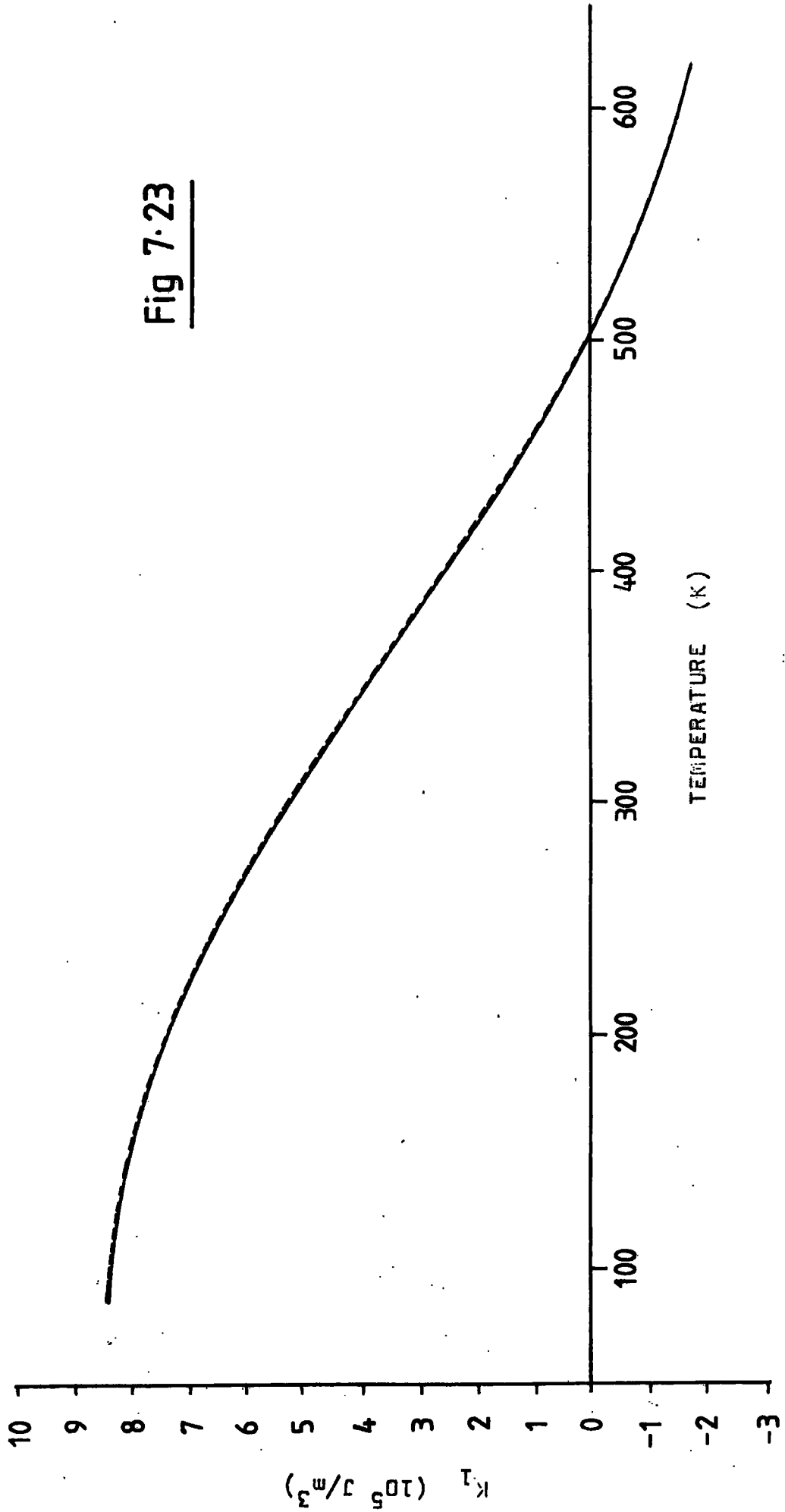
term history, that is, a form of annealing was found to occur.

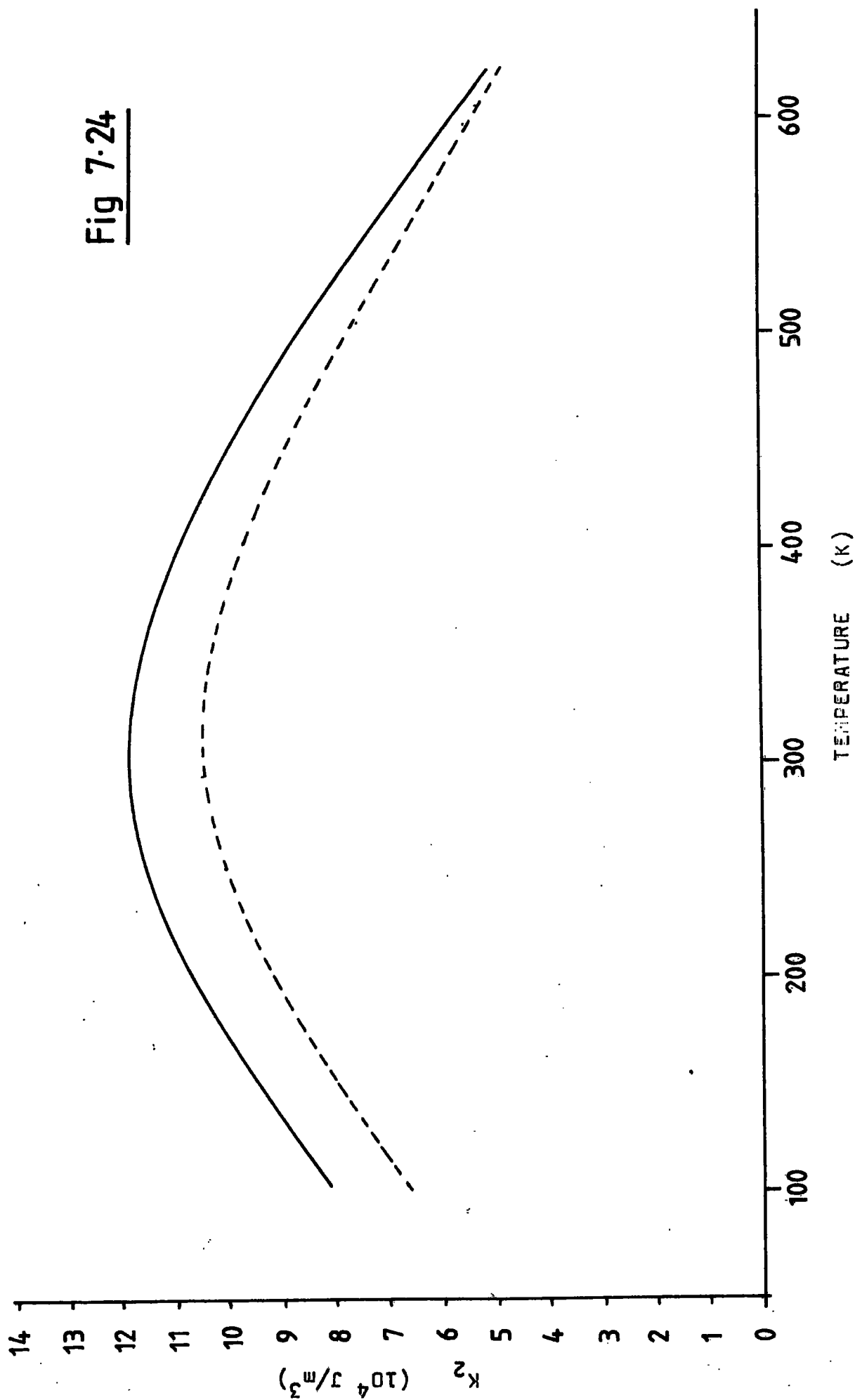
Defining loosely an annealing process as either forward and reverse movements of the field over the available 180° , or a cycling of the temperature up to about 300 K and back again, the progress of the anisotropy constants at 80 K, after a change in the sample orientation of 180° in the b-plane disc following complete annealing at its previous orientation, was as shown graphically in figure 7.22. K_2 and K_3 show the clearest change. The effect on K_3 was that a transition occurred which was greater than the magnitude of the completely annealed value averaged from opposite orientations. (Data reported for cobalt in this thesis is for the totally annealed case). Significantly, annealing was only observed at low temperatures, for which the anisotropy was approaching a value close to the threshold for multiple domain formation at the prevailing field by a phase-theory calculation. However, even if domains were present, perhaps at the edges of the disc (Kouvel and Graham, 1956, 1957), then the annealing mechanism is still obscure since it would correspond to a diminishing torsional hysteresis for which the exact progress of the domain pattern with respect to field orientation undergoes a transition. It is relevant to point out that if the annealing was due to the presence of domains, then their exclusion after field-cycling cannot be guaranteed, and consequently the low temperature results may be subject to a small error. It is also relevant to mention that this has neither been described nor accounted for in past determinations of the anisotropy constants.

Figures 7.23 to 7.24 show the precise effect of the

PLOT SHOWING THE EFFECT ON THE K_1 TEMPERATURE DEPENDENCE
FOR SAMPLE No 1 OF EXCLUDING THE THIRD HARMONIC FROM THE
ANISOTROPY DERIVATION
 (THE CHANGE IN K_1 IS LESS THAN 1% FOR ALL TEMPERATURES)

Fig 7.23





third harmonic on the calculation of the first two anisotropy constants and shows that the percentage change, especially in K_2 , can be significant, indicating the necessity of measuring the third harmonic for accurate determinations of the lower-order constants.

To quote the anisotropy constants as an energy per unit volume, the density of cobalt was required, energy per unit mass being unconventional. The value of 8.756 g/cm^3 was chosen and corrections for thermal expansion neglected (the volume changes less than 0.1% below room temperature (White, 1965) and probably less than 1% below 600K).

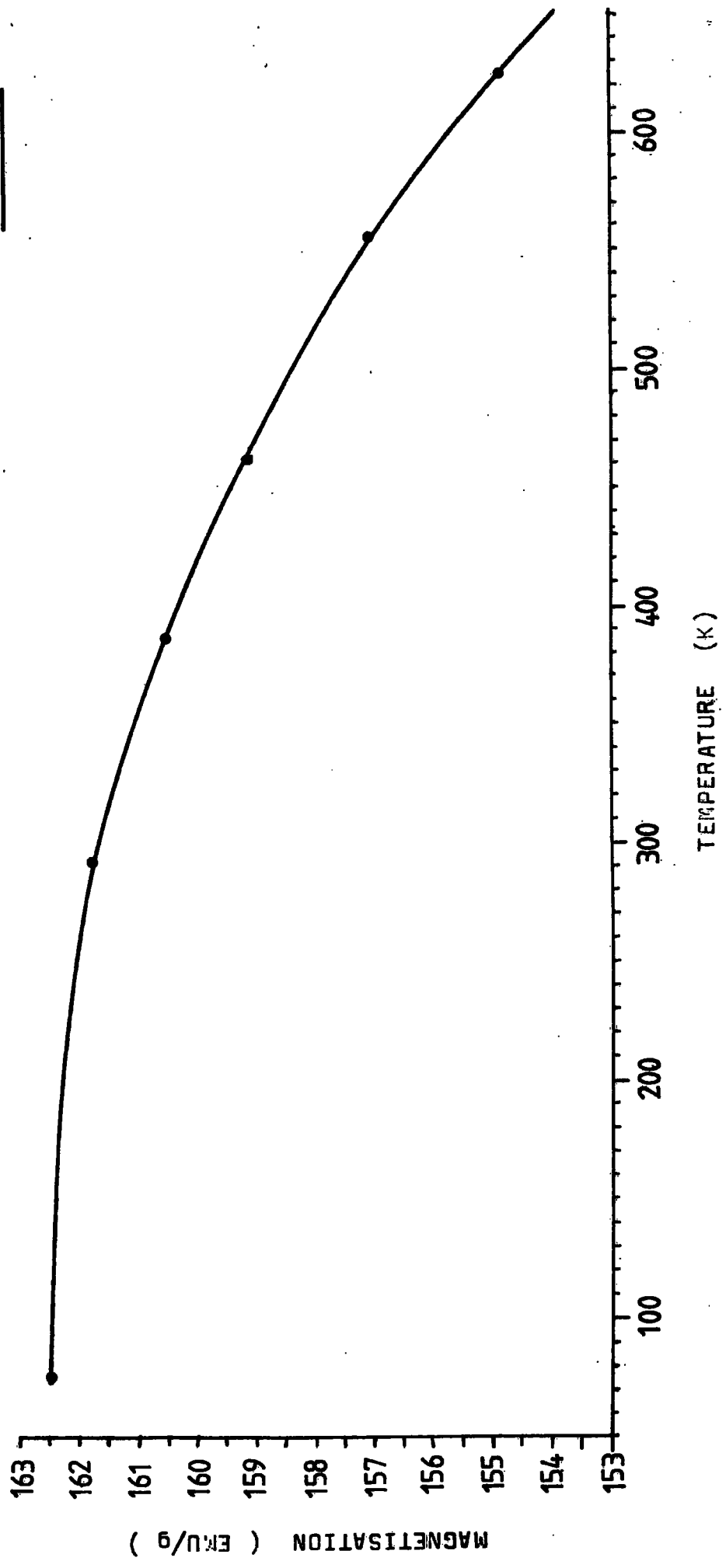
The magnetisation values used during the experiment, to allow on-line shear-correction, were derived from Myers and Sucksmith (1951); the only extensive data set reported numerically (c.f. Tyler, 1931, Barnier et al., 1961 a, and Rode and Hermann, 1964). These are shown in fig. 7.25.

The values of the anisotropy constants given in figures 7.7 to 7.16 include, by definition, the magnetostrictive energies associated with the motion of the magnetisation vector. Takahashi et al. (1978) calculated explicitly magnetostrictive contributions to the K_2 anisotropy constant for cobalt using the magnetostrictive constants reported by Masumoto et al. (1967) and Bozorth (1954) with the elastic constants of McSkimin (1955) and Tsukiji (1969). Details of the calculation are given in Appendix H; it yielded an anisotropic energy contribution of $3 \times 10^3 \text{ J/m}^3$ at room temperature and $1.7 \times 10^3 \text{ J/m}^3$ at 600 K. A similar calculation on K_1 was impossible for want of necessary data. However the proportional contribution to K_2 from magnetostriction

PLOT OF MAGNETISATION VS TEMPERATURE FOR COBALT

(FROM THE DATA OF MYERS AND SUCKSMITH)

Fig 7.25



is, on average, about one part in 10^2 , suggesting that conventional anisotropy plots for cobalt, derived from torque magnetometry or magnetisation curve measurements, reflect to reasonable accuracy the true magnetocrystalline anisotropy.

The critical nature of the shear-correction is illustrated in figures 7.26 to 7.28. These three figures indicate the effect on the calculated anisotropy constants of a 1% error in the shearing factor (the factor relating torque to an angular displacement) for a field value of about 1.8 tesla. The error would be cumulative, arising from uncertainties in the field value, the magnetisation value or the two quantities from which sample volumes were calculated, namely mass and density. Note that a shearing factor error of 1% produces a relative error of greater than 10% in K_3 for the majority of the temperature range covered. The anisotropy errors with respect to changes in the shear factor were computed, while the experiment was running, by applying differing shear-corrections to the original torque curves.

Chapter 4 discusses, among other things, certain non-intrinsic effects that introduce errors into the derived anisotropies. The two specific calculations made on the results of sample ellipticity and tilting of the sample disc, were in fact, tailored to suit the conditions of the present experiment. These calculations showed that errors in the anisotropy from the two effects were both small, amounting to about 10^3 J/m^3 in both cases and contributing primarily to the large K_1 constant rather than the higher-

PLOT OF K_1 VS TEMPERATURE FOR SAMPLE NO 1, SHOWING
 THE EFFECT OF A SYSTEMATIC ERROR OF -1% IN THE
 SHEAR-CORRECTION FACTOR (I.E. $1/(\sigma_{s0} V)$)

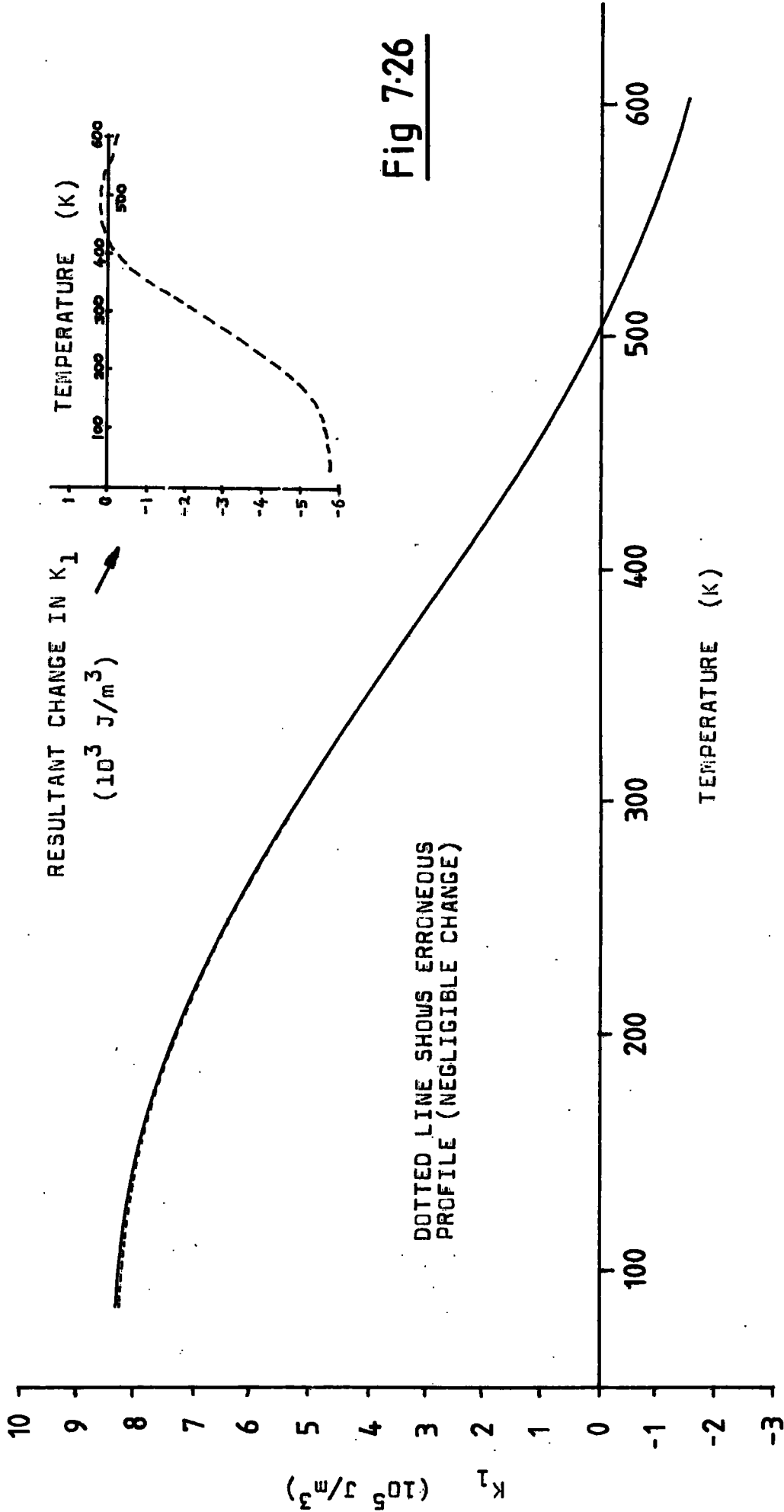


Fig 7-26

PLOT OF K_2 VS TEMPERATURE FOR SAMPLE No 1 SHOWING
THE EFFECT OF A SYSTEMATIC ERROR OF -1% IN THE
SHEAR-CORRECTION FACTOR (I.E. $1/(\alpha_{s0} V)$)

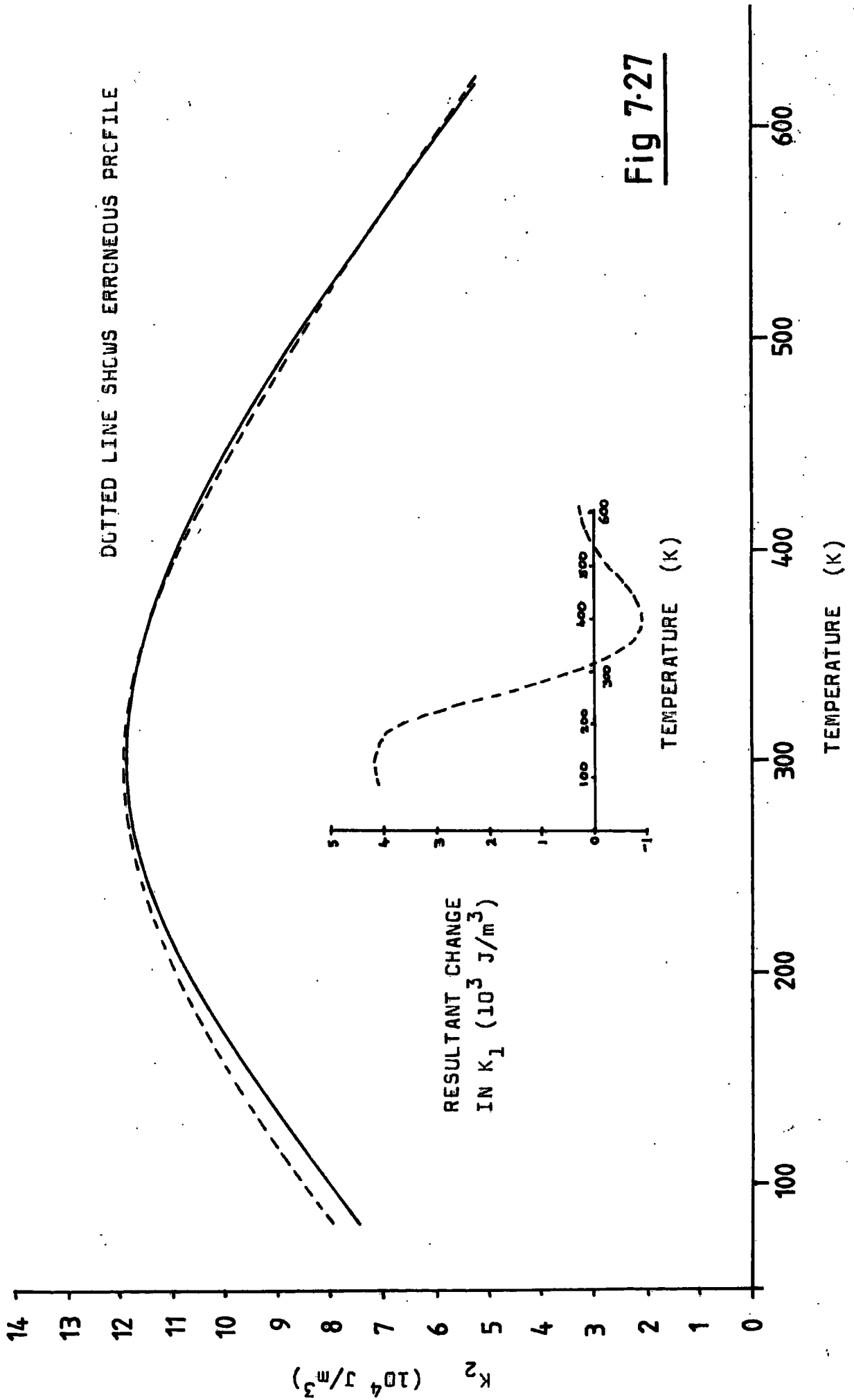
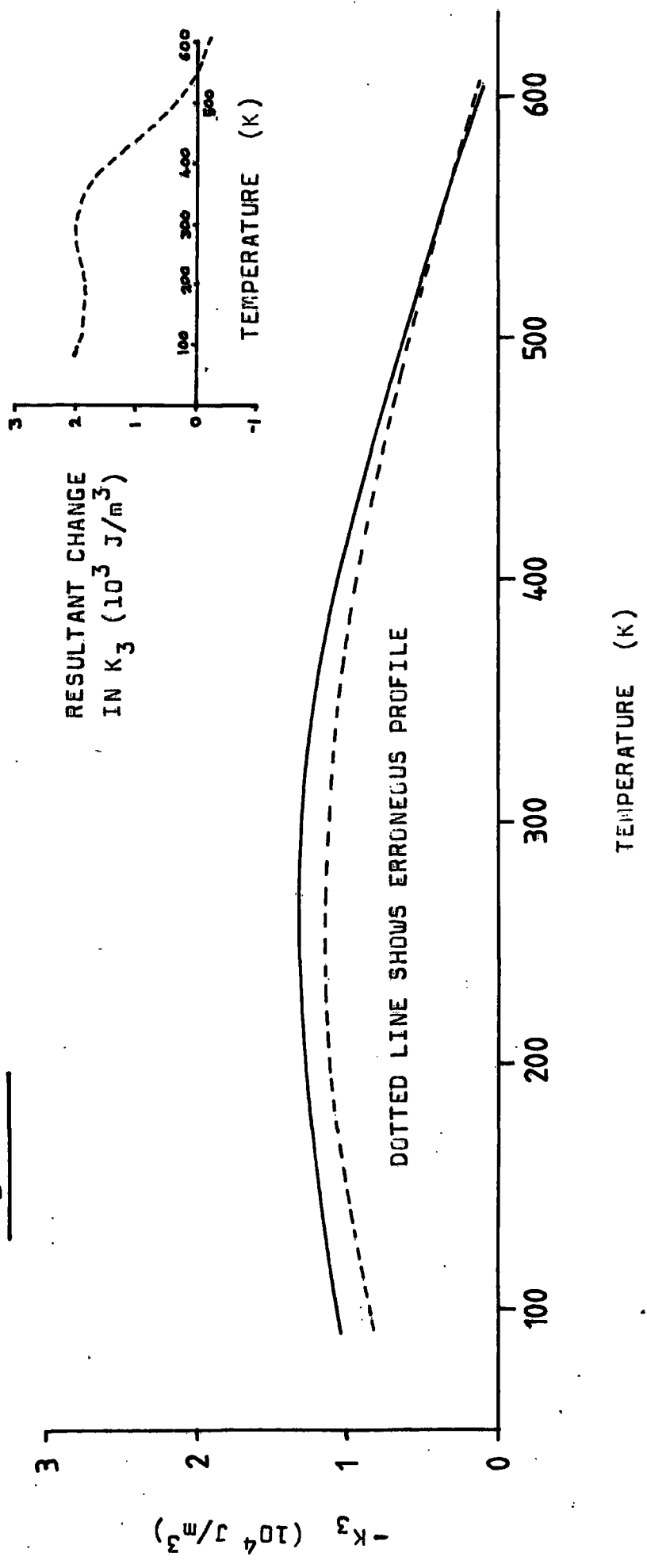


Fig 7-27

PLLOT OF K VS TEMPERATURE FOR SAMPLE No 1 SHOWING
THE EFFECT OF A SYSTEMATIC ERROR OF -1% IN THE
SHEAR-CORRECTION FACTOR (I.E. $1/(\sigma_{S0V})$)

Fig 7.28



DOTTED LINE SHOWS ERRONEOUS PROFILE

RESULTANT CHANGE
IN K_3 (10^3 J/m^3)

K_3 (10^4 J/m^3)

TEMPERATURE (K)

TEMPERATURE (K)

order constants for which such a contribution would be significant. The care taken in centralising the sample on the rotational axis of the magnetometer (see section on experimental technique) eliminated any significant error due to the third non-intrinsic effect mentioned in chapter 4, namely the torsional contribution from resolved forces created by field inhomogeneity on the sample magnetisation.

The overall error in the present anisotropy values for cobalt must, in the last analysis, be an estimate of the cumulative error produced by the equipment as a whole, (for example linearity problems in the magnetometer), the mathematical limitations (principally the truncation of the anisotropy expression fitted to the experimental torque curves), intrinsic sample effects that are subject to change (the annealing process) and non-intrinsic sample effects (for example anisotropy due to thermal stresses). Realistic current error estimates are $\pm 10^4 \text{ J/m}^3$ in K_1 , $\pm 10^4 \text{ J/m}^3$ for K_2 , $\pm 5 \times 10^3 \text{ J/m}^3$ for K_3 and $\pm 10^3 \text{ J/m}^3$ for K_4 .

Having taken into account most forms of experimental error, there remains evidence for an intrinsic sample dependence in the value of the magnetocrystalline anisotropy of cobalt. The origin of this variation may be the differing purity or crystal perfection of the specimens.

7.6 Theoretical modelling of the anisotropy

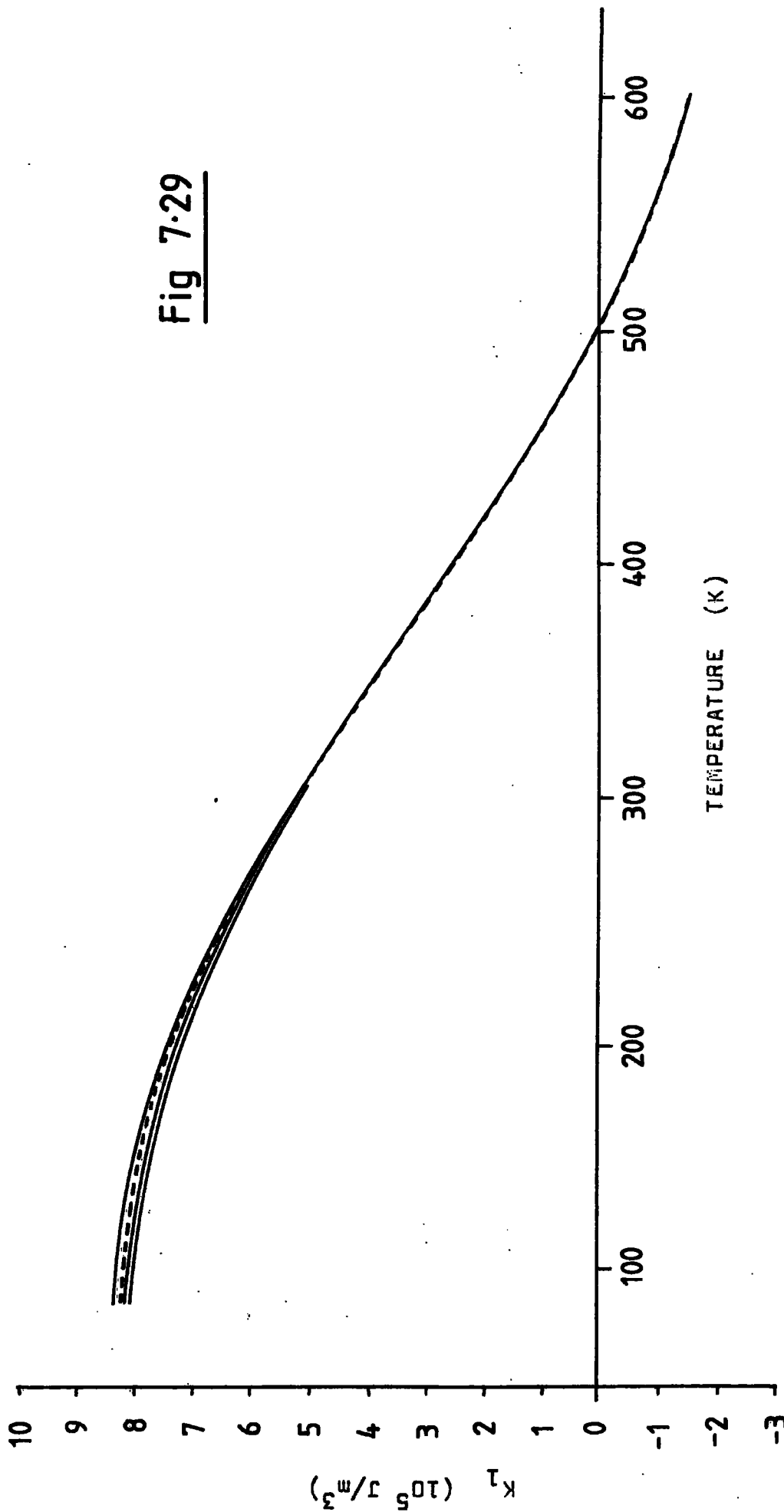
There have been many theoretical explanations made of the temperature variation of K_1 and K_2 for cobalt. These have involved either the single-ion model for the anisotropy (Zener, 1954; Carr, 1954, 1958; Szpunar and Lindgard, 1979)

a combination of single- and two-ion models (Yang, 1976), or the itinerant electron model (Mori et al., 1974; Ono and Yamada, 1979). Of these models, only that of Yang succeeds in fitting the data satisfactorily, but this is not necessarily significant since the model involves 4 adjustable parameters in the functional form to which the data is fitted; it may not be due to the resemblance of the model to physical reality.

All the above workers, with the exception of Zener and Yang, recognise the fact that, for an accurate prediction of the anisotropy, the change of the c/a lattice parameter ratio must be taken into account since it affects directly the crystalline electrostatic field upon which the anisotropy depends. Since the change in lattice parameter ratio with respect to temperature for cobalt is not known precisely, none of the models can be tested rigorously.

Figures 7.29 to 7.30 show plausible temperature dependences for the first two anisotropy constants of cobalt according to the simple single-ion model for c/a values devised to best generate the observed anisotropies. The postulated c/a values are compared to the available experimental data in figure 7.31. It can be seen that a totally self-consistent set of profiles for the temperature dependence of the anisotropies, as produced by the single-ion model, can fit the experimental data for K_1 and K_2 almost perfectly for a contrived c/a profile which fits the known profile to within the c/a experimental error. The details of these calculations are given in Appendix B with a paper by Szpunar awaiting publication. The c/a values

PLOT OF A POSSIBLE SINGLE-ION FIT (DOTTED LINE) TO THE
TEMPERATURE DEPENDENCE OF K_1 FOR COBALT; THE REQUIRED
 c/a TEMPERATURE DEPENDENCE IS GIVEN IN FIGURE 7.31.
 (THE THREE SOLID LINES REFER TO DATA FROM THE THREE SAMPLES)



PLOT OF A POSSIBLE SINGLE-ION FIT (DOTTED LINE) TO THE
TEMPERATURE DEPENDENCE OF K_2 FOR COBALT; THE REQUIRED
 c/a TEMPERATURE DEPENDENCE IS AS FOR THE K_1 FIT AND
GIVEN IN FIGURE 7.31.

(THE THREE SOLID LINES REFER TO DATA FROM THE THREE SAMPLES)

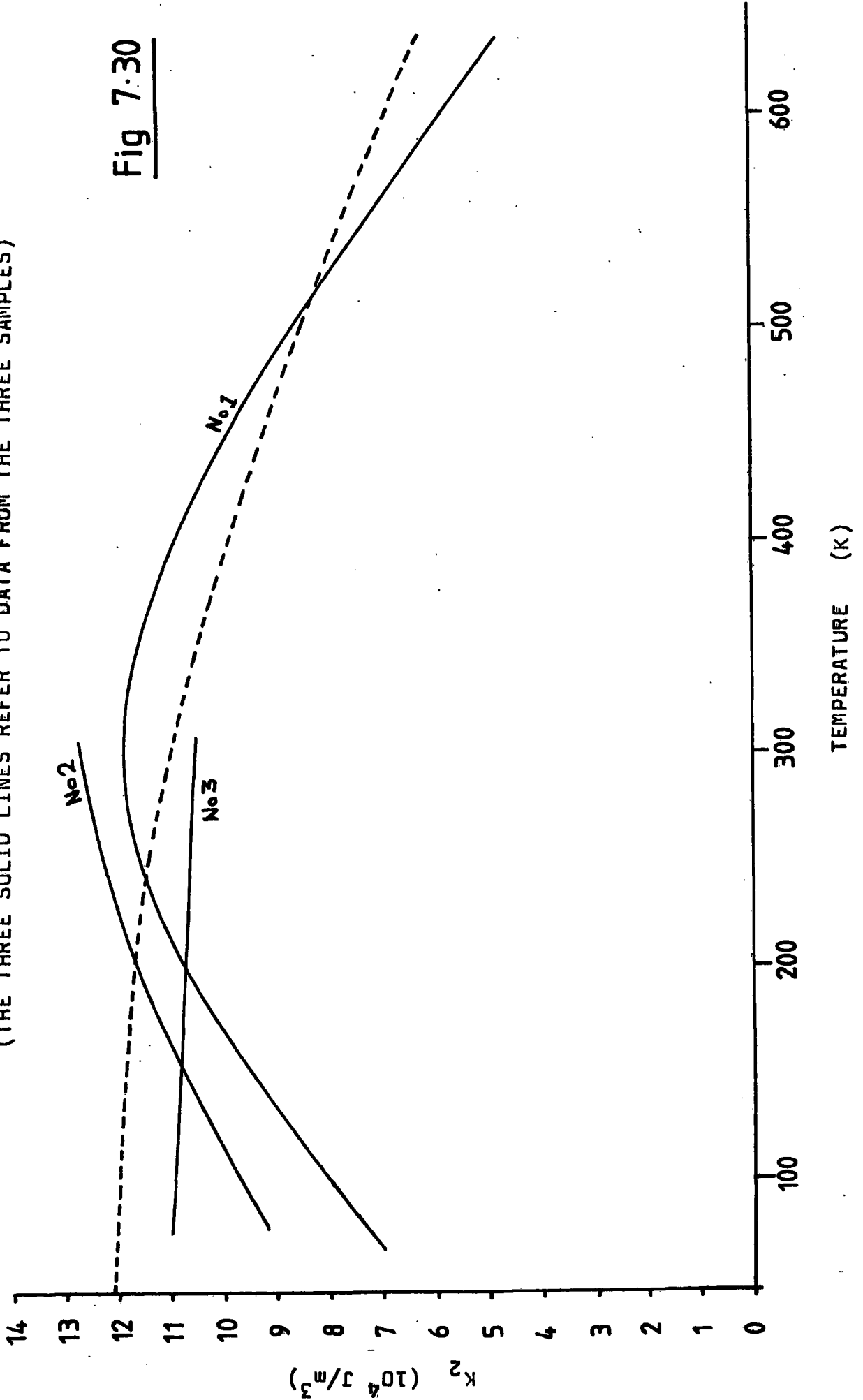
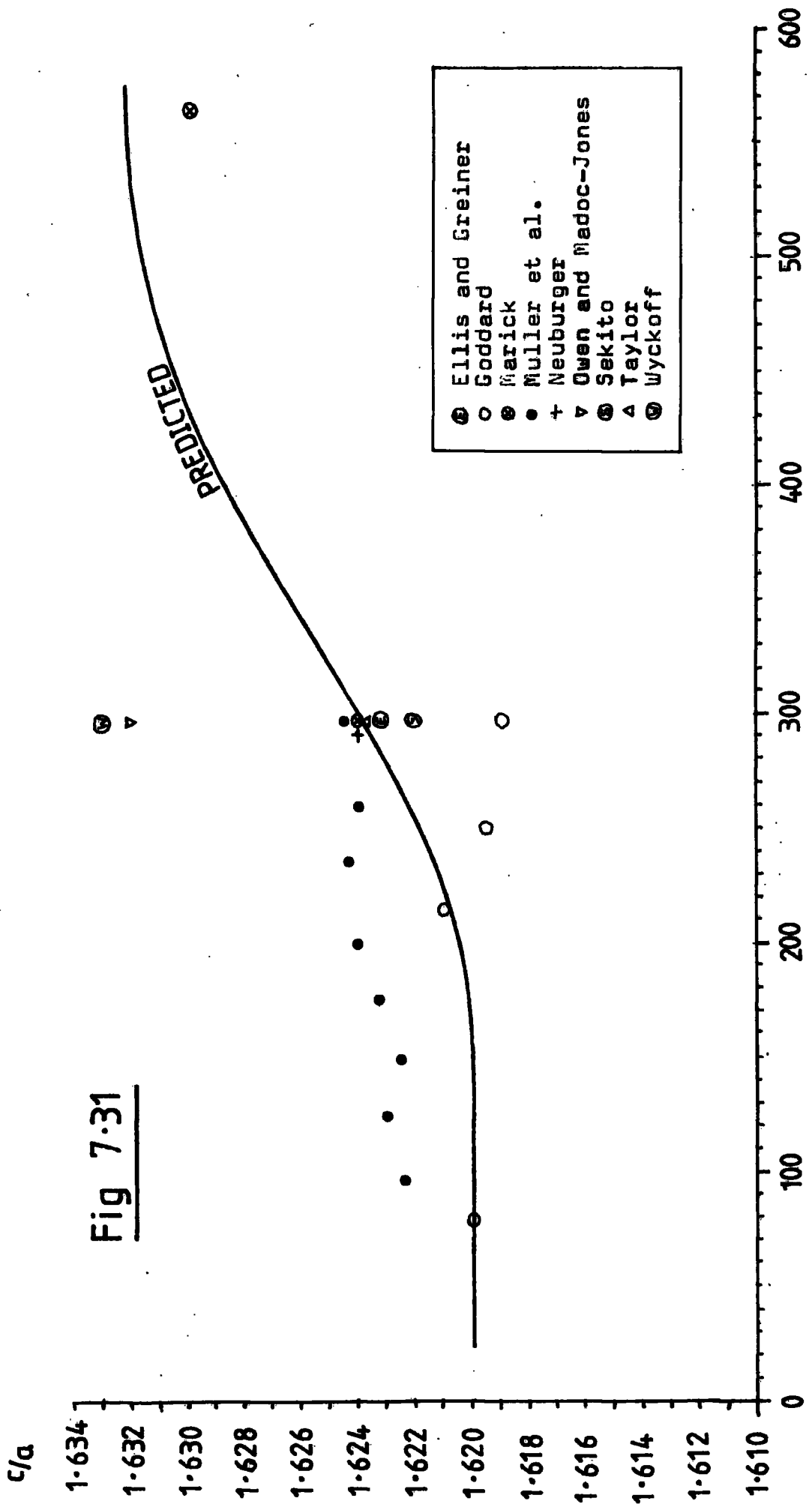


Fig 7.30

PLOT OF AVAILABLE c/a DATA WITH THE PREDICTED TEMPERATURE DEPENDENCE FROM A SINGLE-ION MODEL OF THE ANISOTROPY



TEMPERATURE (K)

for cobalt have been determined by Sekito (1927), Wyckoff (1931), Marick (1936), Neuburger (1936), Ellis and Greiner (1948), Taylor (1950), Owen and Madoc-Jones (1954), Müller et al., (1967) and Goddard (unpublished). Much of this work was carried out at room temperature only. All the available data is included in figure 7.31.

It must be emphasised that the single-ion model with lattice parameter effects has not been vindicated by the present work since the required c/a dependence on temperature is so uncertain. Furthermore, the values calculated by Szpunar for the first two anisotropy constants implicitly define, on the same model, values for the higher order constants, and these differ significantly from the measurements made herein. For instance, the values of K_3 and K_4 should, on the simple model, be proportional, which they are manifestly not according to figures 7.13 and 7.16. Even if, as for K_3 , there is a sample dependence in the values of the K_4 constant, which might obscure a more intrinsic proportionality, the ratio between the two as predicted by the model is such that the data could not be consistent with theory; the model gives $K_3 = -231 K_4$ whereas the experimental average ratio is about $K_3 = -2 K_4$.

7.7 Discussion

Crystal perfection is difficult to achieve in cobalt because of the structural phase transition that a crystal undergoes when cooling from melt temperatures. This occurs at 680 K for large single crystals but for polycrystalline materials with many grains, the FCC structure may be

retained, or partially retained, at room temperature (Owen and Madoc-Jones, 1954). Dislocations generated at the interface for the phase transition will be numerous. The somewhat belated analysis of the anisotropy of cobalt that has occurred in the literature has been the result of early difficulties in producing good crystals partly for this reason. Furthermore, any imperfections, once introduced, will have a significant effect on the local crystalline environment by the same mechanism that permits the FCC structure to be retained at room temperature in finely segregated polycrystals. It is therefore plausible that the anisotropy of cobalt crystals differs due to variations in the degree of disturbance to the crystal structure, and that such variations are responsible, in the present analysis, for the inconsistencies in the results. The fact that the crystals, from which samples No 1, No 2 and No 3 were taken, were all grown by differing techniques, is a good reason for expecting the necessary differences in sample perfection.

7.8 Conclusion

The present results for the magnetocrystalline anisotropy of cobalt indicate that there is an intrinsic sample dependence related to crystal perfection, the impurity variations between the present samples being too small to explain the differences. This is compatible with the history of inconsistent results for the anisotropy values reported in the literature.

The present analysis has yielded, for the first time,

the temperature profiles of the K_3 and K_4 anisotropy constants of cobalt. These have values which are typically about 1% of the large K_1 constant.

The inclusion of values for the third harmonic from the uniaxial torque curve in the derivation of the first two anisotropy constants has led, in the case of K_1 , to a negligible additional contribution to the computed value but, in the case of K_2 , to a contribution amounting to up to 10% of the original value.

Quantitative theories predicting the observed anisotropies of cobalt have not yet been proven. The two contending models (single-ion and itinerant electron), are both modified by the thermal change in the lattice parameter ratio and require an accurate knowledge of it. The attempt here to show the consistency of the predicted lattice parameter ratios, derived from the observed anisotropies using a single-ion model, with experimental values, has been indecisive; the available c/a data is too poor. The available models, which are not exclusive, cannot be validated without an accurate knowledge of the c/a temperature dependence.

CHAPTER EIGHTTHE MAGNETOCRYSTALLINE ANISOTROPY
OF TERBIUM/GADOLINIUM ALLOYS8.1 Introduction

The work described in this chapter is the continuation of a project at Durham on the properties of the terbium/gadolinium alloys and was carried out in collaboration with R.D.Hawkins (1982). The project was begun by A.A. Joraide (1980) who made magnetostriction measurements. During the present work on the anisotropy constants, Hawkins made measurements on a rotating sample magnetometer of his own construction and also performed, independently of the author, some torque magnetometry using a conventional ligament suspension feedback instrument (c.f. Pearsons magnetometer mentioned in chapter 4). The R.S.M. work was very limited and will not be mentioned here, but the latter yielded much of the K_4 data and thanks for this are again expressed.

The terbium/gadolinium alloys give a valuable insight into the anisotropy mechanism of terbium; a material which manifests an anomalously high energy density in this respect ($K_1 = 10^8 \text{ J/m}^3$ at 0K). This is because gadolinium, which in the pure crystal has only a very small anisotropy, acts as an almost ideal diluent for terbium since their crystalline fields are almost identical . Consequently gadolinium can be accommodated into the terbium lattice without, for instance, changing the single-ion contribution to the terbium anisotropy, since the crystalline environment for

each terbium ion remains essentially unchanged. Nor does the gadolinium contribute a significant masking anisotropy to that produced by the terbium. Thus, for a single-ion model, anisotropy would fall off linearly with respect to dilution, representing merely the proportional loss of the active material. However a two-ion model would predict a much faster decline in the anisotropy corresponding to a weakening of the fundamental mechanism due to separation of the terbium ions from each other.

The structure of all the terbium/gadolinium alloys is the same as that of cobalt, mentioned in the previous chapter, namely HCP, and the same anisotropy energy expression will be adopted;

$$E_k = K_0 + K_1 \sin^2 \theta + K_2 \sin^4 \theta + K_3 \sin^6 \theta + K_4 \sin^6 \theta \cdot \cos 6\phi$$

The choice of this convention is somewhat arbitrary since existing work has involved, in some cases, other conventions, particularly that of eqn. 2.5. In the present work only K_1 and K_4 were determined.

An important reason for repeating the investigation of the anisotropy constants for the terbium/gadolinium alloys is that errors could have arisen in previous results due to the presence of impurities in the alloys then available. This was suggested by the sharp dependence of the properties of gadolinium metal on the presence of non-magnetic inclusions in the crystal lattice as found by Smith et al. (1977), in particular the effect on the anisotropy. The availability of very high purity samples of terbium/gadolinium alloys from the Centre for Materials Science,

Birmingham, has encouraged, therefore, a fresh investigation of these alloys.

8.2 Existing work

8.2.1 On gadolinium

Measurements of the anisotropy constants of gadolinium are extensive and have been made by Corner et al. (1962), Graham (1962, 1963, 1967), Darby and Taylor (1964), Birss and Wallis (1964), Belov et al. (1968), Tajima (1971), Tohyama and Chikazumi (1973), Franse and Kihai (1977) and Smith (1978) using torque magnetometry, and Féron and Pauthenet (1969) and Féron et al. (1970 a,b) using magnetisation curves. Smith et al. showed that the presence of non-magnetic inclusions in gadolinium alters significantly the measured values of both the first anisotropy constant, K_1 , and the easy direction of magnetisation, and in subsequent work (Smith, 1978) made the most recent, most complete and most reliable results on particularly high purity samples. The temperature dependence of the first anisotropy constant, K_1 , was found by Smith (1978) to be associated with a combination of single- and two-ion mechanisms while K_2 seemed to suggest single-ion origin only. K_4 was found to follow the $2l^{\text{st}}$ power law with respect to magnetisation; consistent with the single-ion model. As already implied, the anisotropy of gadolinium is negligible compared to that of terbium ($K_1|_{OK} \approx -10^5 \text{ J/m}^3$).

8.2.2 On terbium

Terbium anisotropies have been given by Rhyne and Clark

VALUES OF THE ANISOTROPY COEFFICIENTS OF TERBIUM

Coeff.	Temp. (K)	Method	Value ($J m^{-3}$)	Author(s)	Date
κ_2^0	0	Torque	5.5×10^7	Rhyne & Clark	1967
"	80	"	4.6×10^7	"	"
"	4.2	Magnetisation	4.5×10^7	Rhyne et al.	1968
"	0	Torque (Paramagnetic Extrapol'n)	2.7×10^7	DuPlessis	1969
"	0	Magnetisation	$(5.65 \pm 1.10) \times 10^7$	Féron	"
"	80	"	3.5×10^7	"	"
"	0	Ferromagnetic Resonance	3.1×10^7	Wagner & Stanford	"
"	0	Magnetisation	3.5×10^7	Nikitin & Arutyunian	1979
κ_4^0	0	"	$(0.46 \pm 0.12) \times 10^7$	Féron	1969
"	80	"	0.25×10^7	"	"
κ_6^0	0	Magnetostriction	2.42×10^5	Rhyne & Clark	1967
"	80	"	0.69×10^5	"	"
"	0	Torque	2.44×10^5	Bly et al.	1968
"	80	"	1.0×10^5	"	"
"	0	"	2.9×10^5	DuPlessis	1969
"	0	Magnetisation	$(1.85 \pm 0.18) \times 10^5$	Féron	"
"	80	"	1.0×10^5	"	"
"	0	R.S.M.	2.96×10^5	Birss et al.	1977
"	80	"	0.9×10^5	"	"
"	4.2	Torque	3.5×10^5	Nikitin & Arutyunian	1979
"	78	"	0.92×10^5	"	"

TABLE 8.1

(1967), Bly et al. (1968), Rhyne et al. (1968), DuPlessis (1969), Féron (1969), Wagner and Stanford (1969), Féron et al. (1970 a,b), Shepherd (1976), Birss et al. (1977 a,b), Nikitin and Arutyunian (1979) and Corner (unpublished) using a variety of methods including torque magnetometry, analysis of magnetisation curves and magnetostriction coefficients, rotating sample magnetometry and ferromagnetic resonance. 0K and 80 K values are given in table 8.1. Additionally Birss et al. (1981), from anisotropic magnetisation in terbium, deduced K_4 values which declined from 7.5×10^4 to 0.4×10^4 J/m³ between 95 and 170 K. The work of Corner was done at Grenoble, France after the present results had been obtained. The temperature dependence of the first anisotropy constant, K_2^0 , has been measured by Rhyne and Clark, and Féron by torque magnetometry and the magnetisation curve method respectively and was found to fit the single-ion model quite well. The K_4^0 constant was found by Féron to fit the $I_{9/2}$ function strikingly well; again indicating the single-ion model. There is, however, a discrepancy between K_6^0 coefficients ($= K_4$) as reported by different authors. Féron, Rhyne and Clark and Bly et al. indicate that the K_6^0 coefficient follows the $I_{9/2} \cdot I_{5/2}$ functional dependence of the model of Rhyne and McGuire (1972), but Birss et al. (1977 a,b) describe a good single-ion dependence. The recent work of Corner has shown, in the case of K_2^0 , a fair single-ion dependence.

8.2.3 On terbium/gadolinium alloys

Of direct relevance to the present investigation is

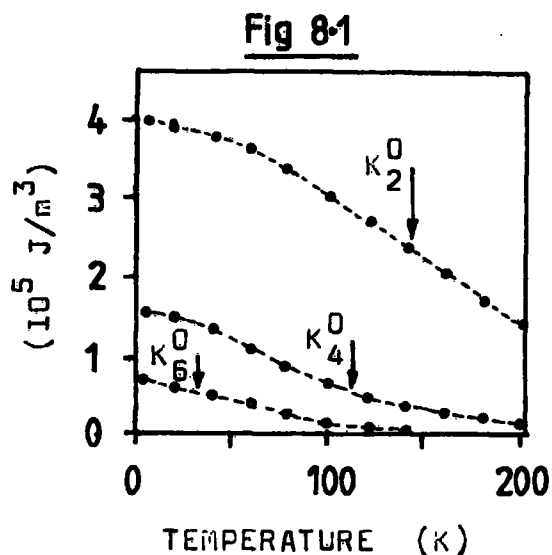
the work of Tajima and Chikazumi (1967 b) and Tajima (1971) who measured K_2^0 , K_4^0 and K_6^0 for one low terbium concentration alloy, the work also of Nikitin and Arutyunian (1979) and Corner (unpublished) in which K_2^0 and K_6^0 were measured for a number of alloy compositions, and the work of Bagguley et al. (1980 a,b) in determining K_1 and K_4 , again for a number of alloy compositions.

In order to draw comparisons between existing data, constants were **adjusted** to correspond to a single convention for the anisotropy expression, namely that of equation 2.2. The data of Tajima is given explicitly (fig 8.1) but no conversion was attempted since the anisotropies were too small in $Tb_{0.018}Gd_{0.982}$ for a useful comparison with the remaining data. Corner derived values of K_2^0 from magnetisation curves by assuming that K_4^0 and higher coefficients in the uniaxial anisotropy expression were zero, his K_2^0 values could therefore be scaled directly by 3/2 to yield K_1 (for the relationships between constants of the two relevant conventions see Appendix A). Nikitin and Arutyunian found that higher order coefficients were small and also neglected them, again enabling an easy conversion of K_2^0 to K_1 . Féron published K_2^0 and K_4^0 values (for pure terbium), so the K_1 derivation required the second term in equation A.12. The original uniaxial data of Féron is given explicitly in figures 8.2 and 8.3 and the derived values of K_1 appear in figure 8.4. The constants describing the basal-plane anisotropy acquire the same values in both conventions and can therefore be plotted interchangeably. All available data is portrayed in figures 8.1 to 8.7.

A single-ion model produces, given certain approximations, a linear dependence of the anisotropy on alloy composition.

Extrapolating the values of Tajima to 100% terbium, (regarding terbium as the active contributor to the anisotropy) gives a value which is within a factor of

two of that measured for pure terbium. Since the extrapolation is over two orders of magnitude in the concentration, this is good evidence for a single-ion anisotropy. For all measurements, the composition dependence of K_2^0 is such that extrapolations of the low terbium anisotropies underestimate the pure terbium value. The results of Corner on several alloy compositions suggest, by virtue of the temperature dependence of the



K_2^0 , K_4^0 AND K_6^0 VS TEMPERATURE FOR
 $Tb_{0.018}/Gd_{0.982}$ (AFTER TAJIMA)

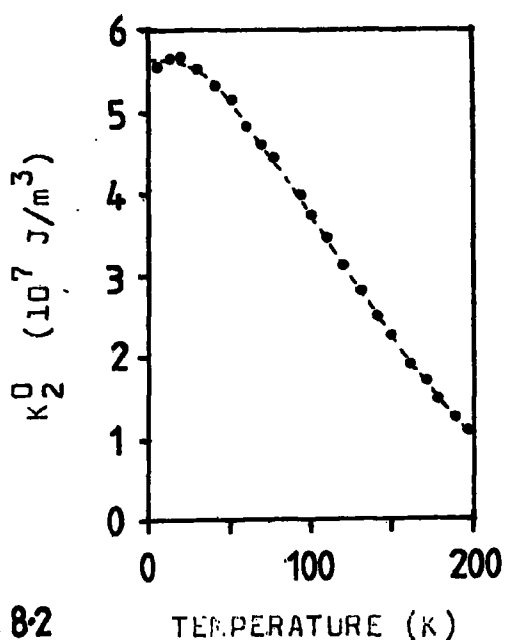


Fig 8-2

K_2^0 VS TEMPERATURE FOR
TERBIUM (AFTER FÉRON)

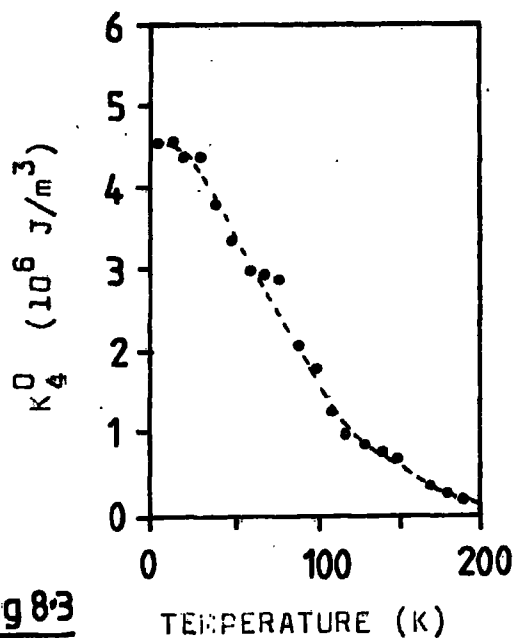
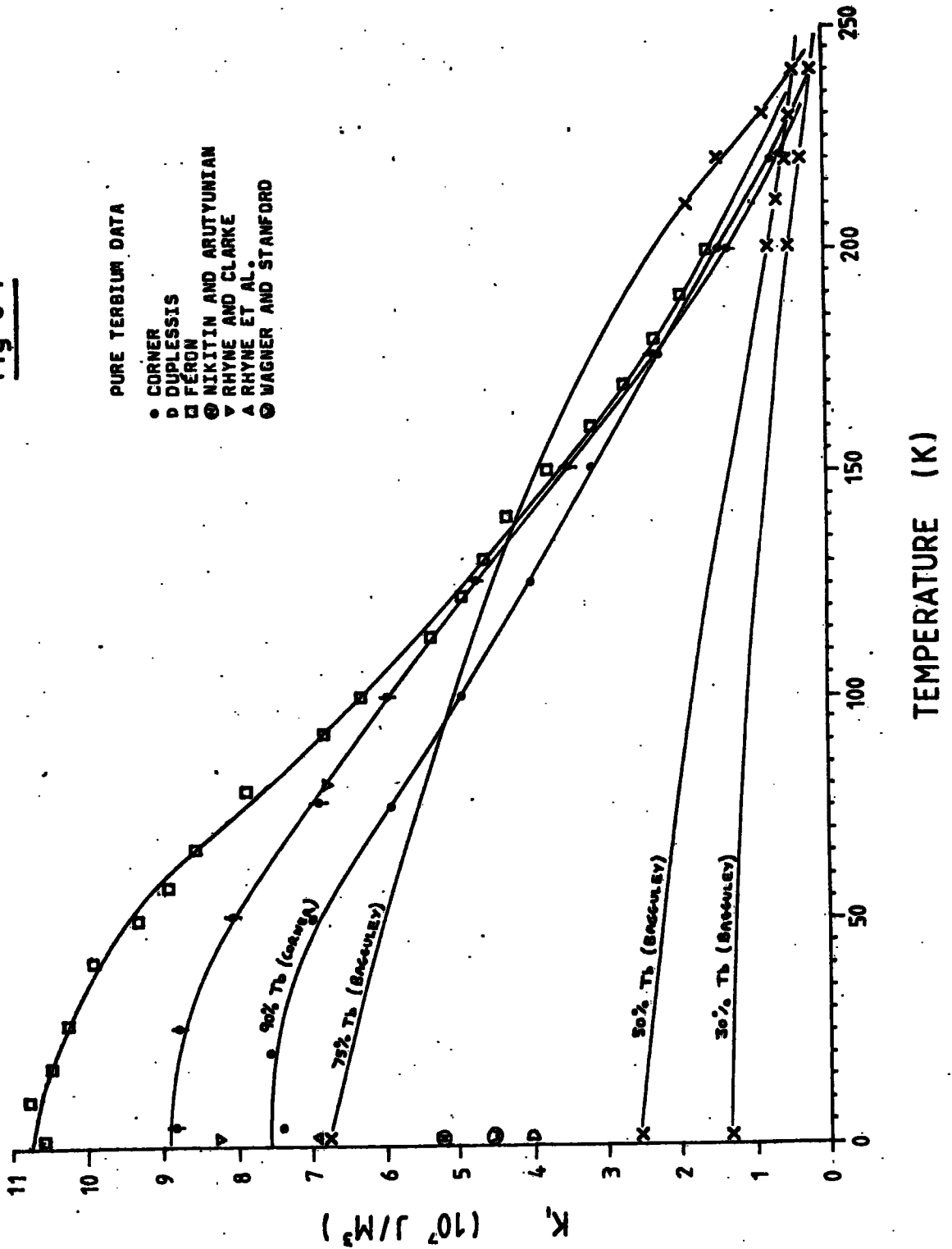


Fig 8-3

K_4^0 VS TEMPERATURE FOR
TERBIUM (AFTER FÉRON)

EXISTING DATA FOR K, VS TEMPERATURE FOR Tb_xGd_{1-x} ALLOYS

Fig 8.4



EXISTING DATA FOR K_4 VS TEMPERATURE FOR Tb_xGd_{1-x} ALLOYS

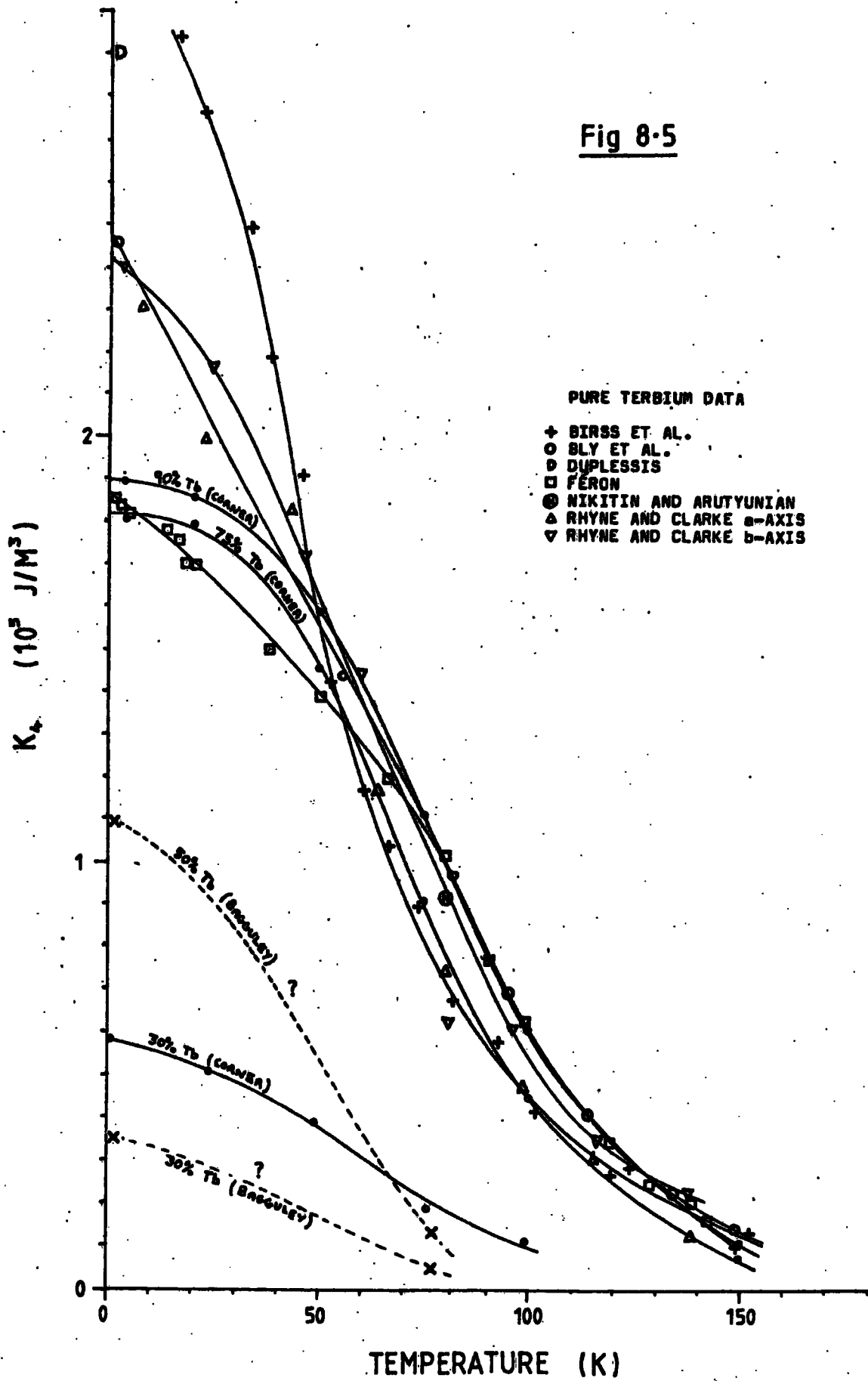
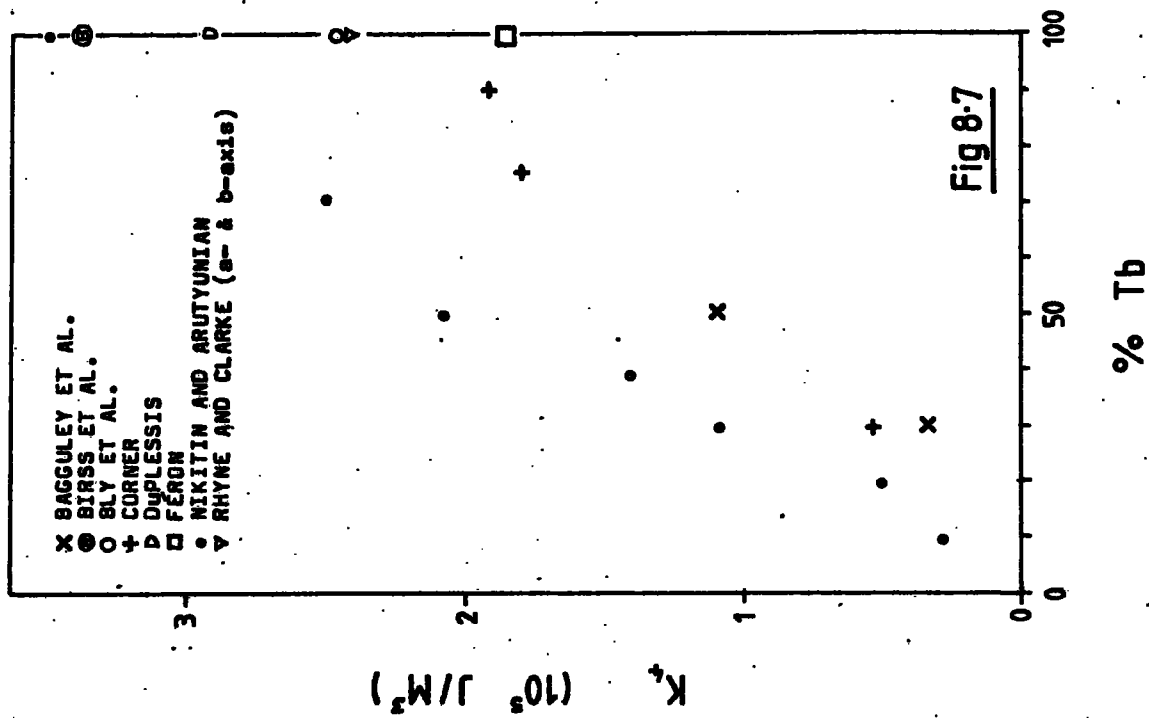
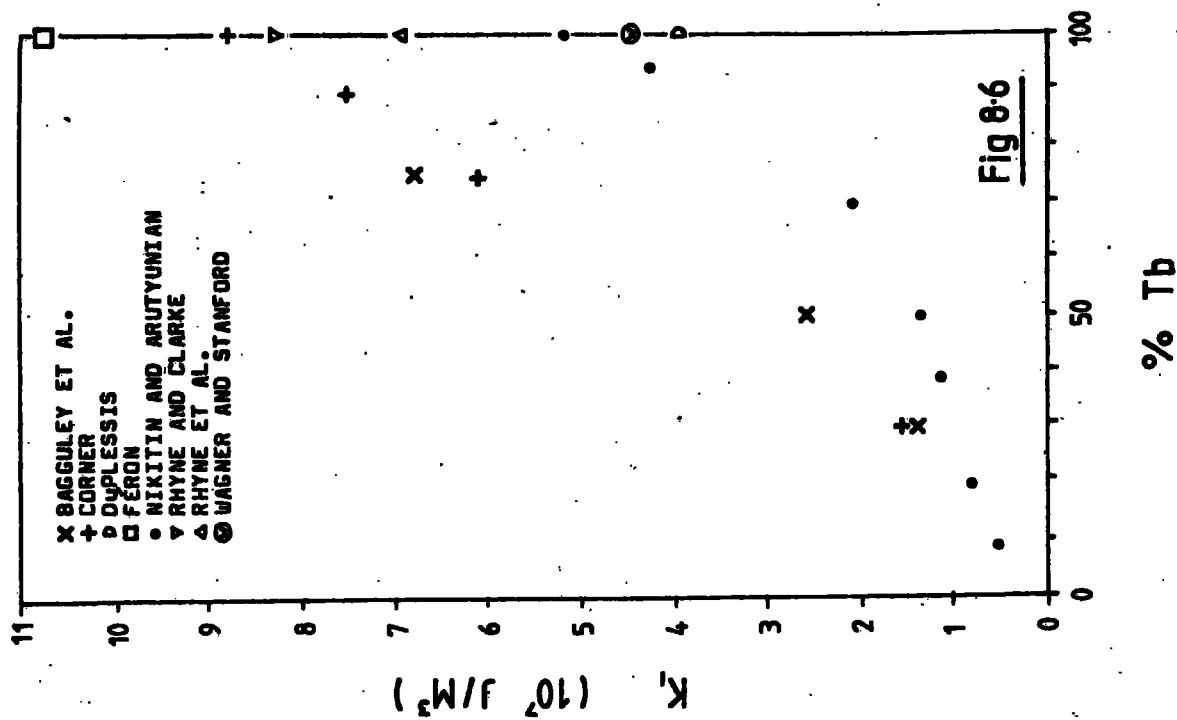


Fig 8-5

EXISTING DATA FOR K_1 AND K_2 VS COMPOSITION AT 0K FOR Tb-Gd ALLOYS



K_2^0 anisotropy constant, the single-ion model. However a simple fourth power law in the magnetisation gives a much better fit for the high terbium concentrations. The basal-plane (c-plane) data of Corner suggests very clearly the magnetoelastic model of Rhyne and McGuire for all compositions.

Tajima et al. used torque magnetometry to determine anisotropy constants. Nikitin and Arutyunian used magnetisation curve measurements to determine K_2^0 and torque magnetometry to measure K_6^0 . Bagguley et al. used a microwave absorption technique and Corner used magnetisation curve measurements throughout. Some of the differences in the results may be due to the difference in the techniques used, for instance the results of Bagguley et al. are, in some cases, at variance with the rest; but so is their method of determining the anisotropy. It may be that the resonance experiments of Bagguley et al., which measure the anisotropy during an oscillation of the local magnetisation vector in an effective field, due to the dynamic nature of the sensing technique, measure a fundamentally different anisotropy.

Existing measurements of the anisotropy of the terbium/gadolinium alloys show that there is no inversion of K_1 with respect to temperature as is observed in pure gadolinium, thus the easy-axis remains in the b-direction.

8.3 The samples

The constituents of the terbium/gadolinium alloys were purified by solid state electrotransport (see Verhoeven,

SAMPLE DETAILS

Sample No.	Atomic % Tb	Axis Jar to Disc Plane	Mass ± 0.1 mg	Diameter (mm)	Thickness (mm)	Density (1) (10^3 kg m ⁻³)	Density (2) (10^3 kg m ⁻³)	Demagnetising Factor, N
1	5	a	26.5	4.86	0.20	7.1	7.907	0.030
2	5	c	144.1	4.67	1.14	7.4	7.907	0.145
3	10	b	198.4	4.66	1.48	7.9	7.924	0.178
4	10	c	129.5	4.07	1.26	7.9	7.924	0.174
5	20	a	45.3	4.98	0.40	5.8	7.958	0.057
6	30	b	59.4	3.50	0.79	7.8	7.992	0.140
7	30	c	49.4	4.23	0.44	8.0	7.992	0.075
8	50	a	73.2	4.27	0.74	6.9	8.060	0.112
9	50	c	105.0	4.70	0.75	8.1	8.060	0.106
10	50	c	120.6	4.66	0.90	7.9	8.060	0.120
11	75	c	110.5	3.42	1.55	7.8	8.145	0.222
12	90	b	264.2	5.41	1.42	8.1	8.196	0.151
13	100	c	171.7	4.91	1.10	8.2	8.230	0.138

Details of the samples used. Density (1) is calculated using the measured values of mass, diameter and thickness. Density (2) is based on values given by Palmer et al. (1974). The demagnetising factors are obtained from the thickness-to-diameter ratio using the graph in Fig. 1 of Osborn (1945), and the corresponding error bars using the gradient of the graph. The single digits represent the error bar in the last decimal place.

TABLE 8.2

1966). In this method a large direct current is passed for about one week down a cylindrical sample heated to within about 200°C of its melting point. The large electric field effectively transports the impurities to one end of the bar. The process is carried out under extremely high vacuum or in a high purity inert gas (10^{-9} torr or equivalent). Charge sizes are determined by a compromise between the convenience of purifying a large amount of material in one run and the necessity of limiting diameter in order that the surface cooling per unit volume can adequately counteract the electrical joule heating. A typical sample diameter would be about 6 mm. Zone refining (page 55) was also carried out to purify the elements. The alloys were formed by recrystallisation annealing under argon. Final purities of about 99.9% were indicated by the ratio of the zero and room temperature resistances of samples taken from the same source. Purities were maintained by storing under argon where possible.

The samples were spark-cut into discs about 5 mm in diameter and about 1 mm thick with one of the three principal hexagonal axes normal to the disc plane. Sample masses were measured on an Oertling high precision balance, model 146, to better than 0.1%. Full details are given in table 8.2.

8.4 Experimental technique

The majority of the torque measurements on the terbium/gadolinium alloys were carried out on the instrument reported in chapter 6. The wide dynamic range and robust nature of this device made it uniquely appropriate for the

present measurements in which torques varying from 0.1 Nm (produced by the 260mg, 90% Tb, b-plane disc at 77 K) to 10^{-5} Nm (produced by the 130 mg, 10% Tb, c-plane disc at 260 K) could be accommodated without modification to the instrument. The fact that some of the c-plane work was done on a conventional ligament suspension feedback instrument was because the new magnetometer was incomplete at the time.

The particular ligament suspension magnetometer used here has been described by Corner et al. (1962) and in detail by Welford (1975) and Smith (1978). It is based on the design of Pearson described in chapter 4. The details of the construction are given in figures 8.8 to 8.11. Figure 8.8 is a simplified diagram of the electronics. The optoelectronic components consisted of two OCP 71 phototransistors sensing light reflected by a mirror on the suspension from a 150 W, 21.5 V bulb collimated by a 10 cm diameter, 30 cm focal length lens. The out-of-balance torque signal from the two amplifiers, each denoted A, was combined with the output of a position potentiometer on the base of the magnet to yield torque curves on a Phillips PM 8141 X-Y recorder. The magnetometer was interfaced to a Commodore PET microcomputer system identical to that described in chapter 6 allowing the automatic acquisition and processing of data. The software used was a simpler form to that developed for the new torque magnetometer and is given in Appendix I. Figure 8.9 is a self-explanatory diagram of the moving element of the magnetometer showing, among other things, the use of oil-damping vanes; a

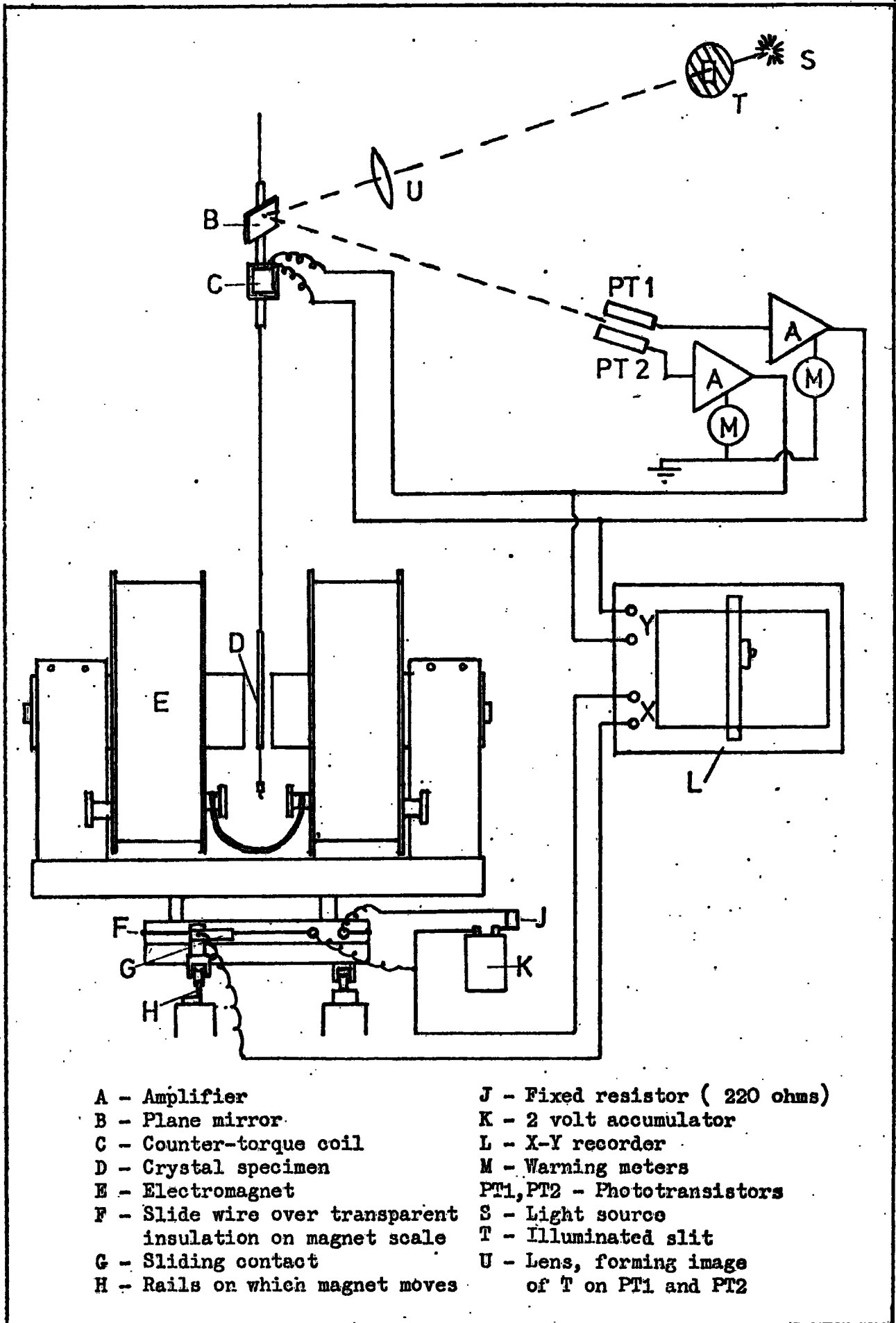


Fig 8-8 The Torque Magnetometer: Principles of Operation.

(after Welford)

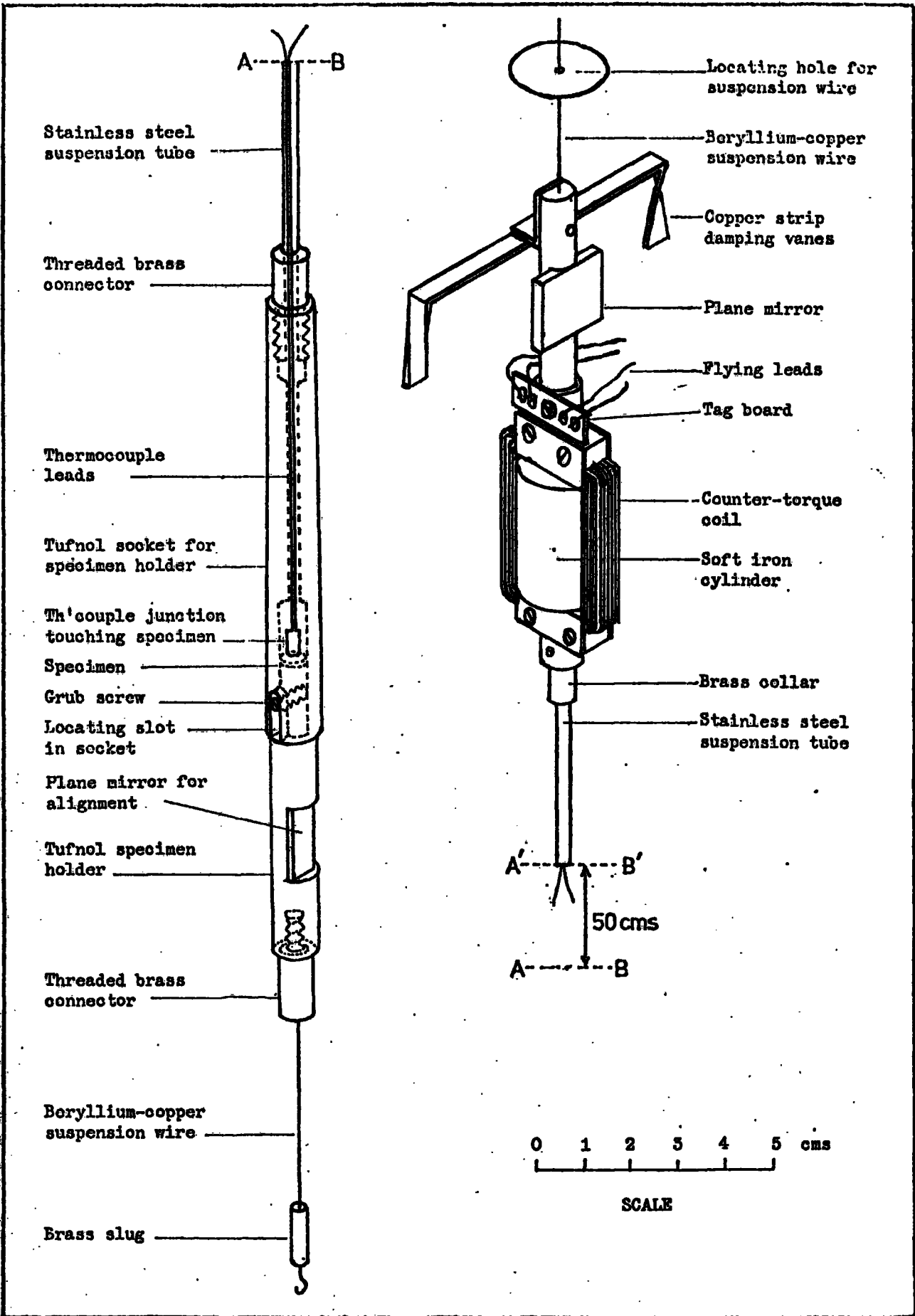


Fig 8-9 The Torque Magnetometer Movement.
(after Welford)

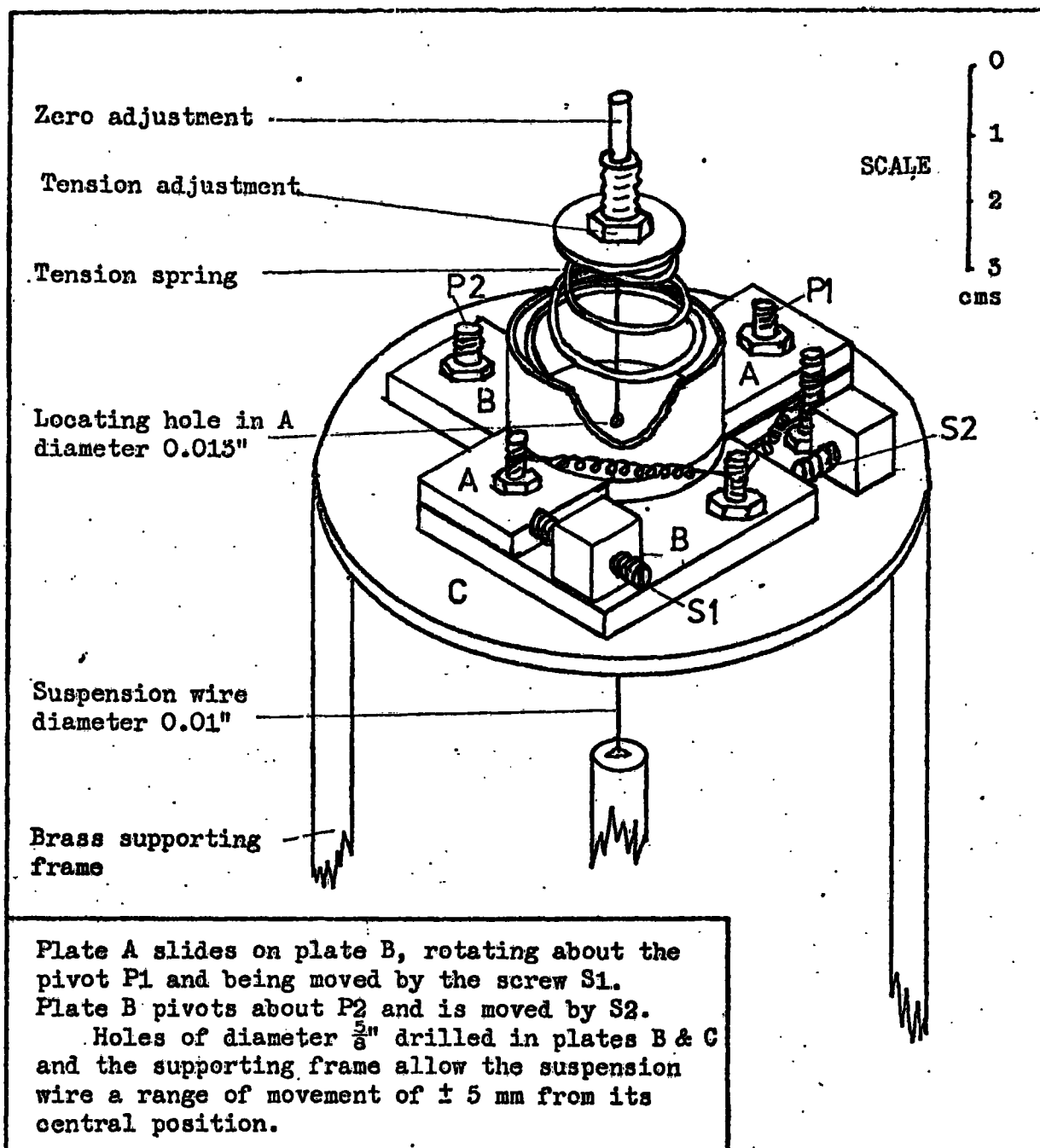


Fig 8-10 The Upper Suspension
(after Welford).

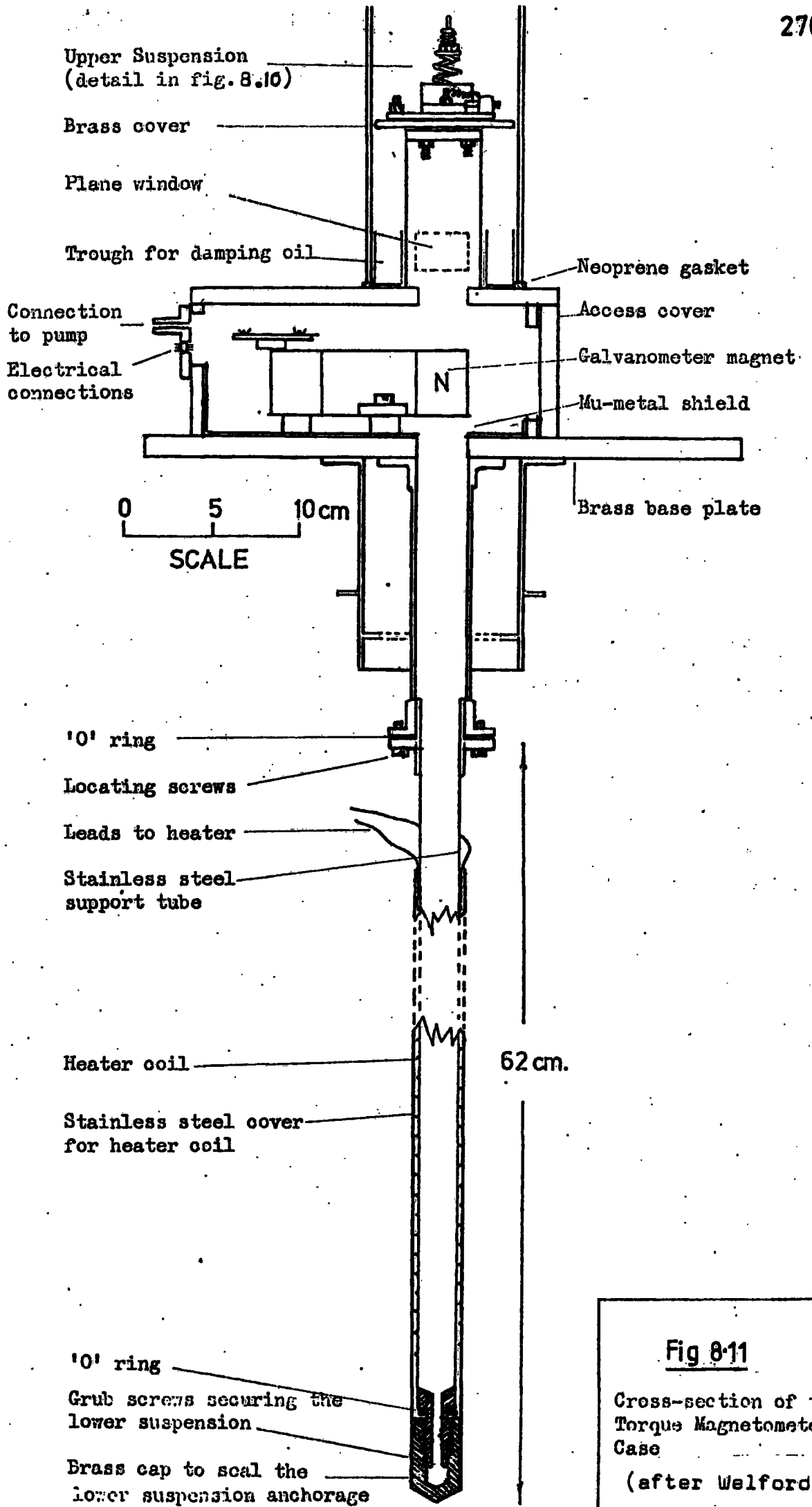


Fig 8-11
 Cross-section of the
 Torque Magnetometer
 Case
 (after Welford)

development of the original design of Pearson. The support for the upper suspension fibre is illustrated in figure 8.10 and a cross-section of the vacuum system is given in figure 8.11.

Calibration of the magnetometer was carried out using a 40 turn, 21.2 mm diameter search-coil of 42 SWG copper carrying current from a Farnell E30/2 power supply through a digital Avometer model DA 116. Field values were determined using a Hall probe and standard magnet. The calculated torques were found to indicate linearity in the magnetometer to within 1% for output signals of up to 0.1 V corresponding to the 10^{-3} Nm which covered all the K_4 determinations.

The ligament suspension magnetometer had a sample space suitable for discs of up to 6 mm diameter, which was adequate for the present work, and a temperature range of 77 K to 300 K. Temperature control was achieved by using a liquid nitrogen dewar to provide radiant cooling in competition with the conductive heating of an internal resistive coil. Infact a helium gas-flow cryostat was also available but in many cases the holding torque of the magnetometer was insufficient to constrain the high torques developed in the very low temperature regime, consequently the measurements were restricted to 77K and above. A copper-constantan thermocouple, fed to a Schlumberger 4045 digital voltmeter with $1\mu\text{V}$ resolution, measured sample temperatures with an estimated thermal lag of typically two or three degrees during temperature sweeps of the full range lasting about one hour. Field homogeneity in the conventional iron-

yoke electromagnet was better than 1% over a volume of 30 cm^3 about the field centre and up to 1.1 tesla was available for currents of 180 amps. (The magnet was that of Roe, 1961, mentioned in chapter 6, section 6.5.)

Attachment of the samples in the ligament suspension magnetometer was with Durofix. The attachment of the b- and a-plane discs to the new magnetometer required a much stronger glue due to the remarkable torques generated, especially by some of the high terbium samples (the force operating tangentially to the perimeter of a 5 mm terbium disc of 1 mm thickness in a high field is about 40 N and the force per unit area on the surface is therefore about $2.5 \times 10^6 \text{ N/m}^2$ or 340 Lbs/sq.in.). Samples fixed with Araldite were detached using chloroform as a solvent whereas Durofix required only acetone.

In the case of K_1 , the anisotropy data was obtained from torque curve gradients taken at the easy-axis. These were taken from the plots recorded on the Phillips PM 8141, rather than derived on-line, since for the very simple manual determinations of the curve inclination of this kind the inconvenience was minimal. The analysis method has been mentioned in chapter 4 and assumes that the contribution of higher constants in the uniaxial torque expression are negligible. The easy-axis method was necessary since saturation, that is achievement of the single domain state, was discontinuous in most of the samples at the available fields. The K_4 analysis was performed on-line and involved a straight forward Fourier analysis of the sixty data points, taken over the 180° rotation of the magnet, yielding the

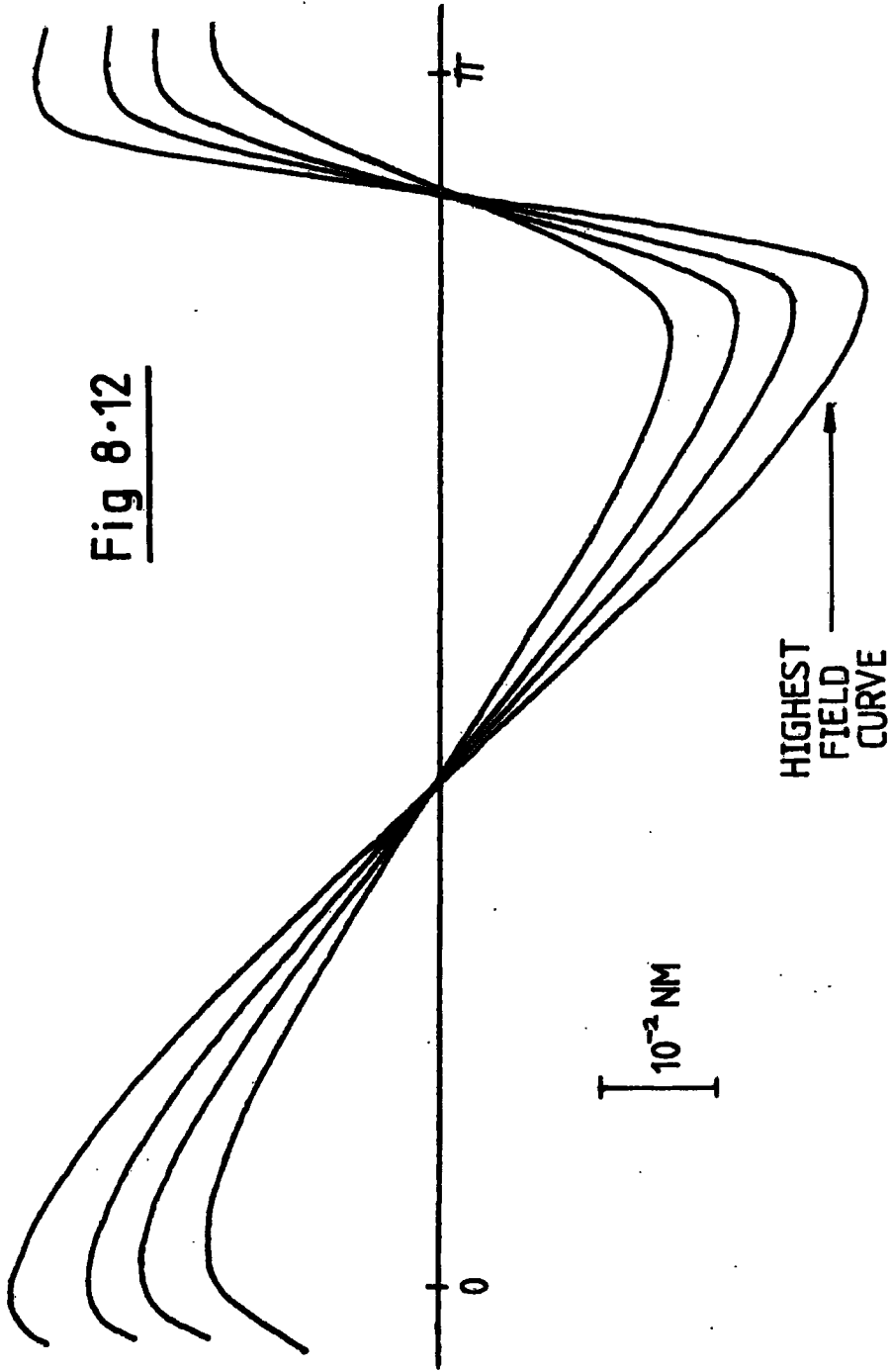
amplitude of the 6θ harmonic to which K_4 is simply related.

8.5 Results

Examples of the torque curves produced by the terbium/gadolinium alloys are given in figures 8.12 and 8.13. The 2θ and 6θ harmonics were the fundamental components of the uniaxial and basal-plane torque curves respectively.

K_1 measurements were made by deriving a corrected torque curve easy-axis gradient by applying a shear-correction to the small region of the torque curve for which this was legitimate; a region around the easy-axis of an angle dependent on the particular sample anisotropy and applied field strength and for which the single domain state occurs. The small section of corrected curve was then assumed to be part of a sinusoid produced by a material with finite K_1 constant only. The computed amplitude then yielded K_1 values which are portrayed in figure 8.14 and given explicitly in Appendix J with the field values used in each case. The derived anisotropies refer to finite field values (measured at about 1.8 tesla) and no field extrapolation has been attempted. Magnetisation values were assumed to be isotropic yet, as discussed in chapter 2, section 2.6, terbium alloys are materials for which this is not likely to be correct, at least for temperatures approaching the Curie point. Furthermore the errors introduced by assuming negligible higher-order constants will almost certainly be significant, yet for neither of the latter two effects is there quantitative information available to assess the erroneous contribution.

TYPICAL TORQUE CURVES PRODUCED BY HIGH UNIAXIAL ANISOTROPY IN THE DISC PLANE (73.2 mg α -PLANE DISC OF $Tb_{0.5}Gd_{0.5}$ AT 105 K IN FIELDS OF 1.16, 1.45, 1.70 AND 1.85 T)



TORQUE CURVES FOR A 171.7 mg c-PLANE DISC OF TERBIUM AT
81K IN FIELDS OF 1.16, 1.37, 1.58 AND 1.85 TESLA

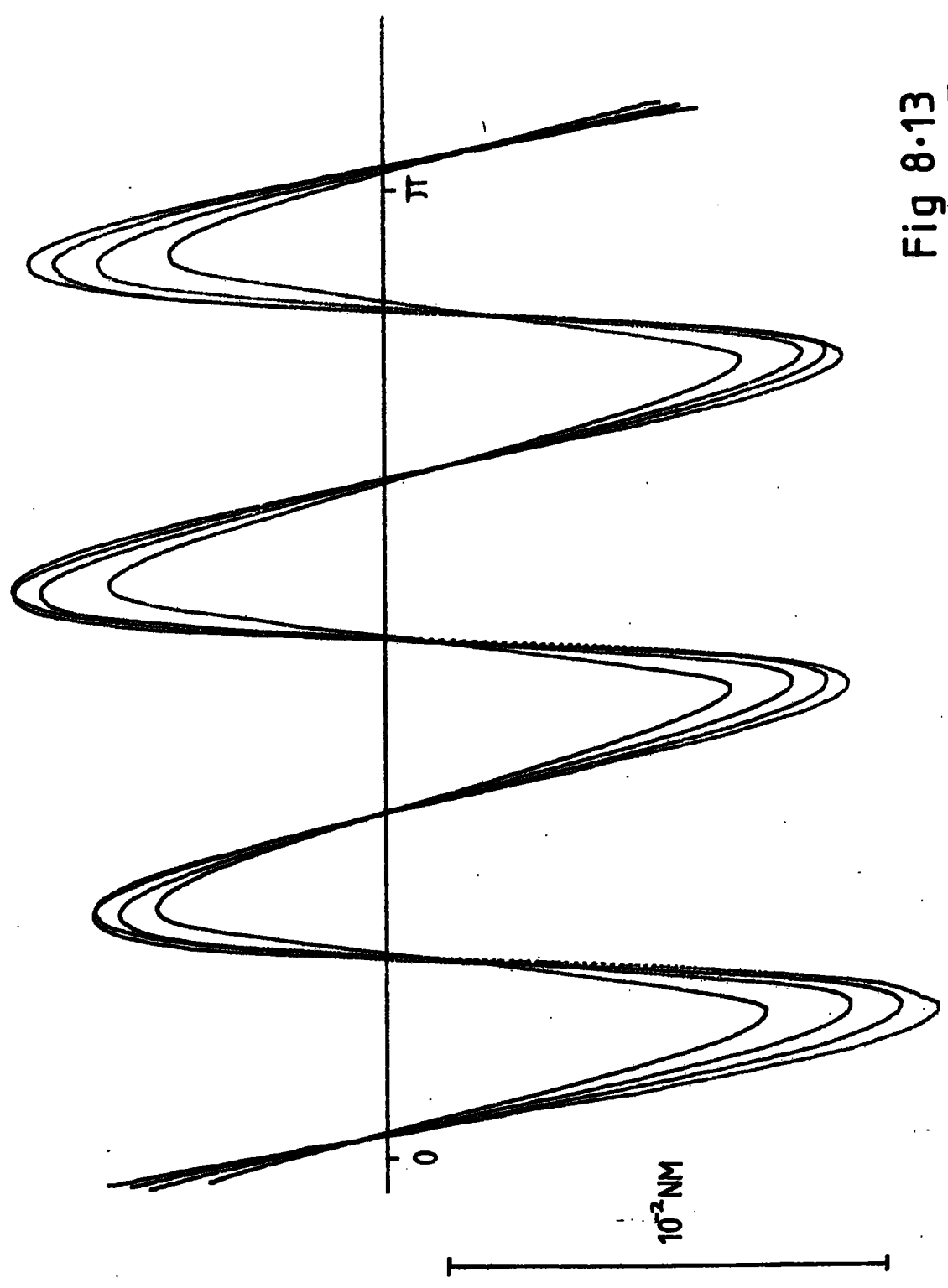
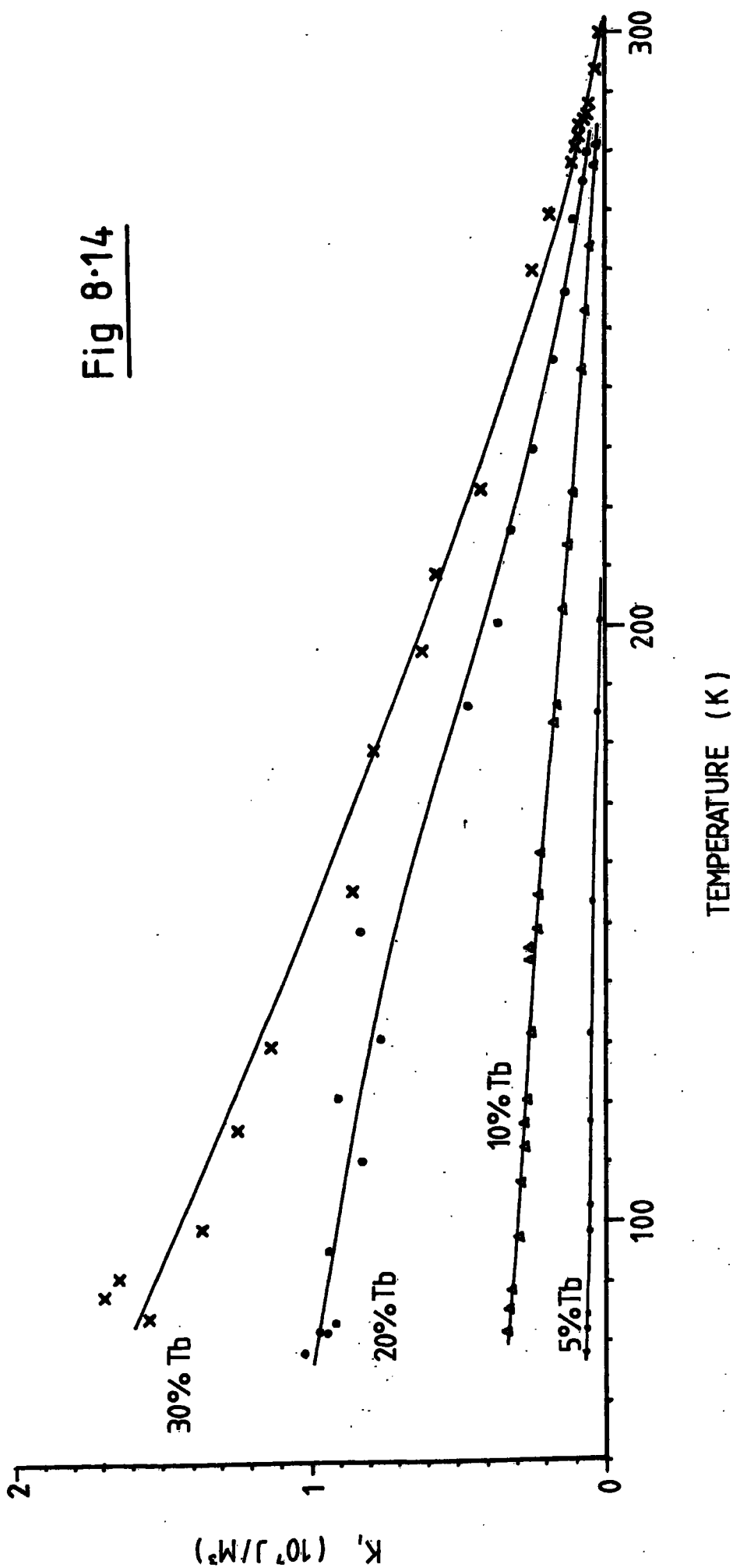


Fig 8.13

K_i VS TEMPERATURE FOR Tb_xGd_{1-x} ALLOYS

(PRESENT VALUES)



As mentioned earlier, K_4 data was derived from the amplitude of the 68 harmonic in the basal-plane determined by the computer which, in the absence of shear-correction and higher harmonics (this was assumed because the observed torque curves were apparently sinusoidal), was related very simply via the sample mass to the anisotropy constant at the prevailing field. A conventional extrapolation of the anisotropy constants at a given temperature to infinite field using a reciprocal-field plot yielded the data portrayed in figure 8.15 and recorded with the intermediate finite-field data in Appendix J.

The validity of an extrapolation of the kind applied here to K_4 is suspect, since there is no justification for assuming linearity in $1/B_0$. In fact it can be shown that for the higher terbium samples the applied fields could not have saturated the samples and that the increase in the measured anisotropies with respect to field was due rather to a canting of the magnetisation in different domain phases. The canting magnetisation was observed as an increasing torque amplitude due to an increasing resolution of the torque between local magnetisation vectors and the anisotropy field in the plane of the sample disc.

this latter mechanism would yield a fairly complex functional dependence between field and observed anisotropy. Thus even if intrinsically, in the single domain limit, anisotropy tended to a limit linearly with $1/B_0$, the extrapolation would be invalid for many samples due to the break down of the magnetisation into phases. However, of several arbitrary extrapolations attempted in powers of

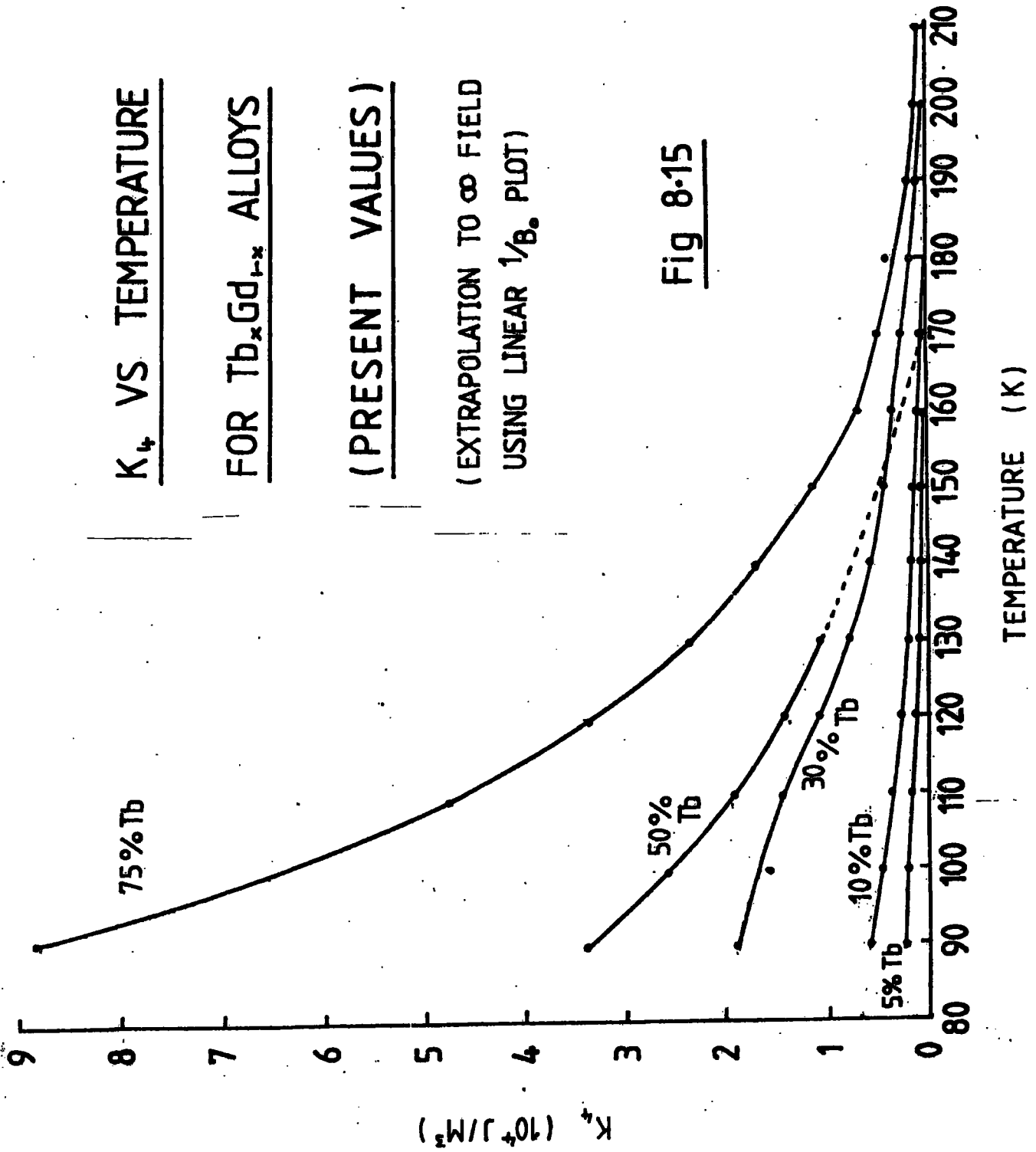
K_4 VS TEMPERATURE

FOR Tb_xGd_{1-x} ALLOYS

(PRESENT VALUES)

(EXTRAPOLATION TO ∞ FIELD
USING LINEAR $1/B_0$ PLOT)

Fig 8.15



$1/B_0$, linearity was best achieved with respect to K_4 by the simple $1/B_0$ relationship and this was consequently used.

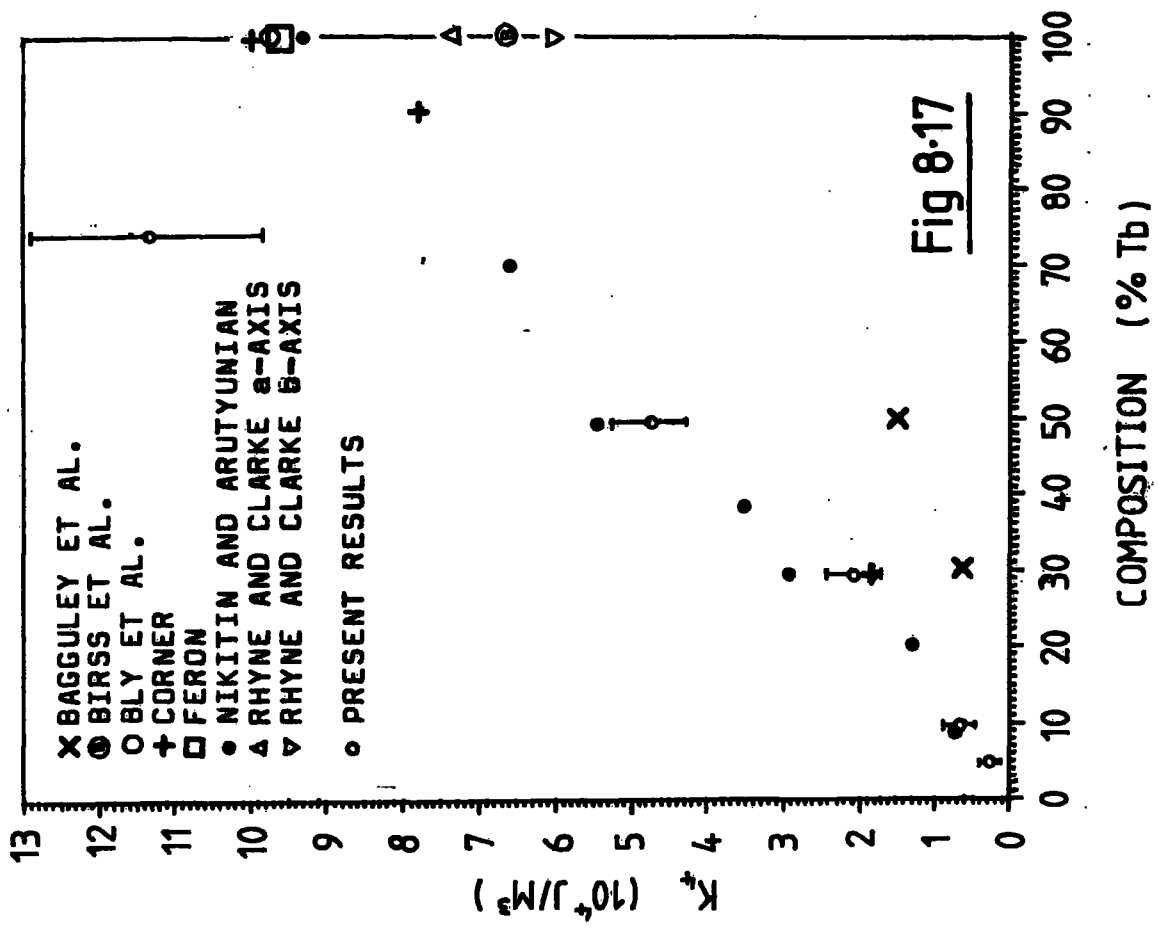
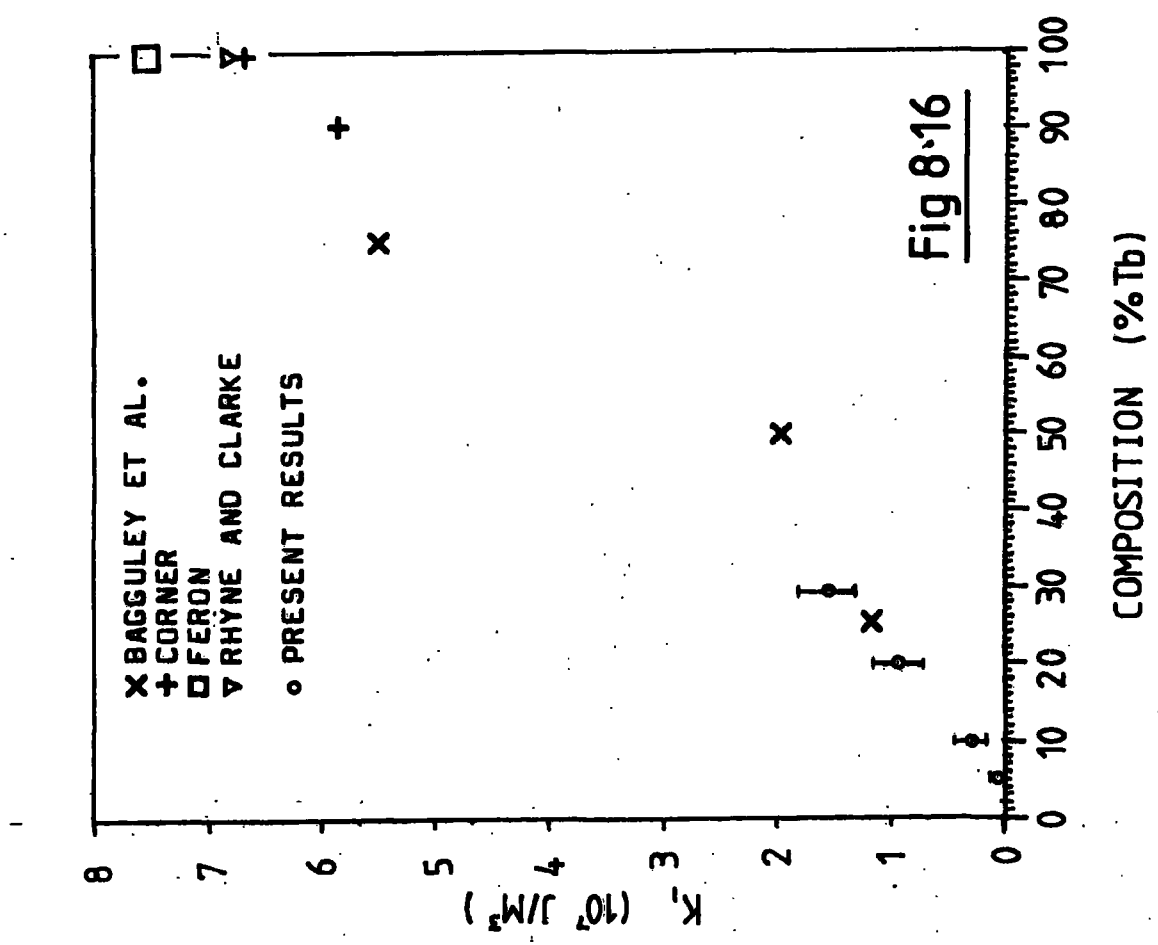
Plots of the composition dependence of both K_1 and K_4 at 80 K are given in 8.16 and 8.17. Extrapolations of the present data to 0 K by the best theoretical fit (anticipating the results of the next section) are given in figures 8.18 8.19. Comparisons with existing data are made in these figures. Figures 8.20 and 8.21 show direct comparisons of the present temperature profiles and those of others.

Such was the anisotropy of the high terbium concentrations that the K_1 analysis suffered from an ill-conditioning whereby the corrected easy-axis gradients approached parallelism with the torque axis. For this reason the 90% terbium plot is omitted since in some cases negative anisotropies were obtained (corrected curve gradients changed sign) and indeed the 50% terbium plot is rejected as inaccurate. Appendix J gives these results with the remaining data.

The corrections to the easy-axis gradient that were made in the derivation of K_1 required values of the magnetisation and two sources of the magnetisation with respect to temperature were available; the data of Bagguley et al. (1980 a,b) and the recent data of Corner. Both data sets agreed to within, typically, 1% and were consistent to that accuracy with interpolations derived by Joraide (1980) from data on pure gadolinium (Nigh et al., 1963) and pure terbium (Hegland et al., 1963). Magnetisation values of Bagguley et al. were arbitrarily adopted and interpolated where necessary for certain compositions. The values of the

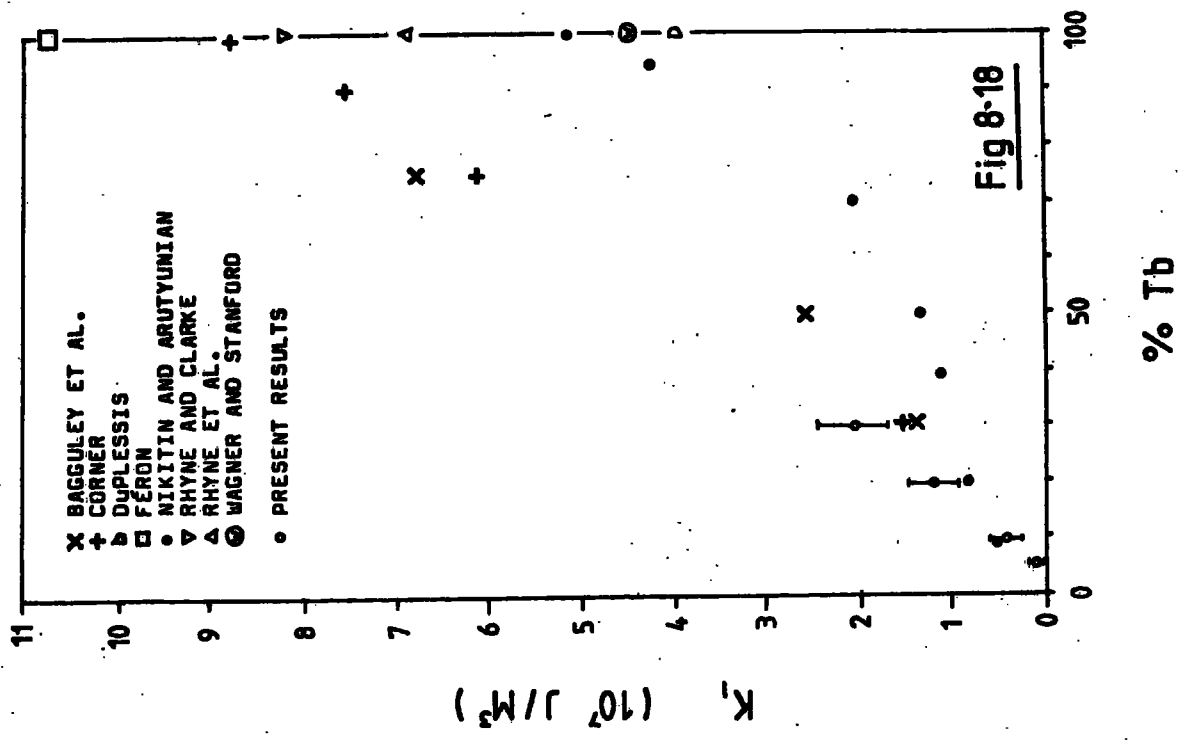
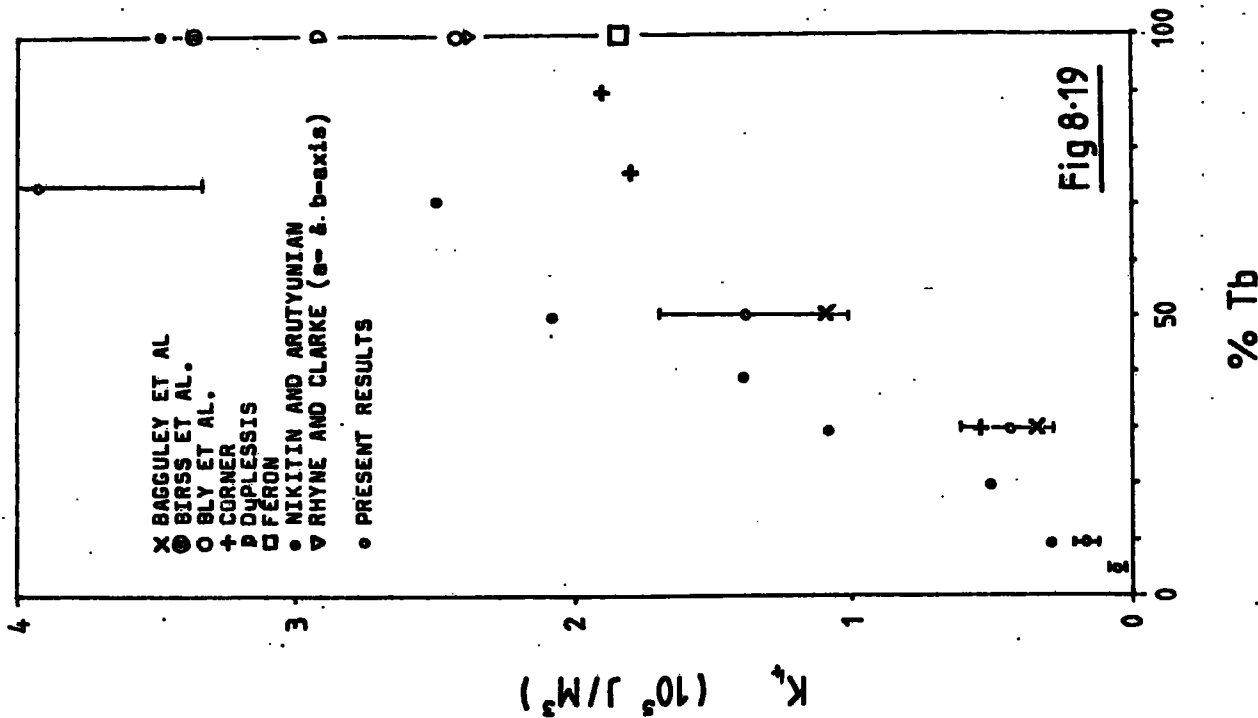
K₁ AND K₂ VS COMPOSITION FOR Tb_xGd_{1-x} ALLOYS AT 80 K;

COMPARISON OF PRESENT AND EXISTING DATA

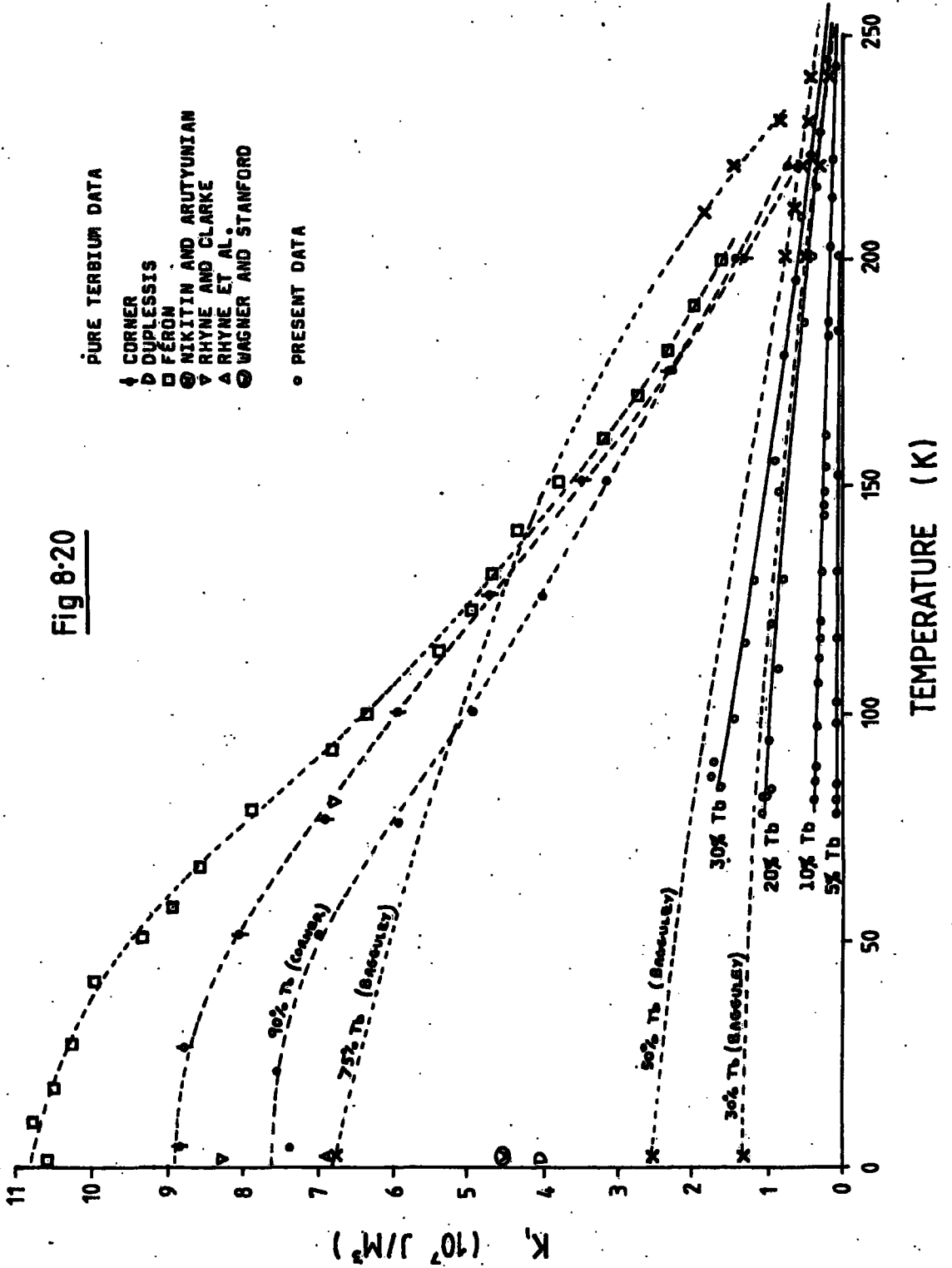


K_1 AND K_2 VS COMPOSITION AT 0 K FOR Tb_xGd_{1-x} ALLOYS: COMPARISON

OF PRESENT EXTRAPOLATIONS TO 0 K AND EXISTING DATA

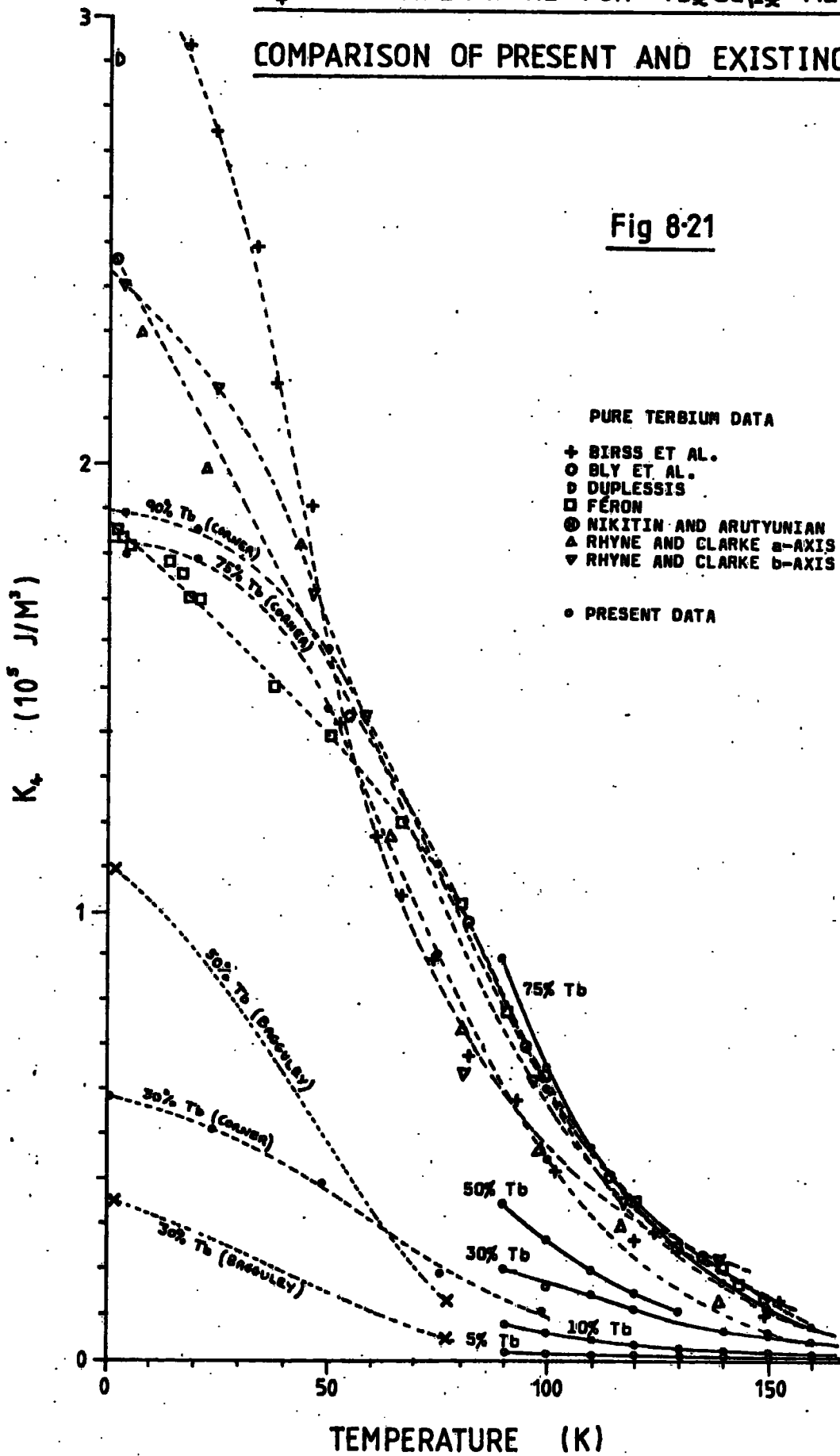


K₁ VS TEMPERATURE FOR Tb_xGd_{1-x} ALLOYS;
COMPARISON OF PRESENT AND EXISTING DATA



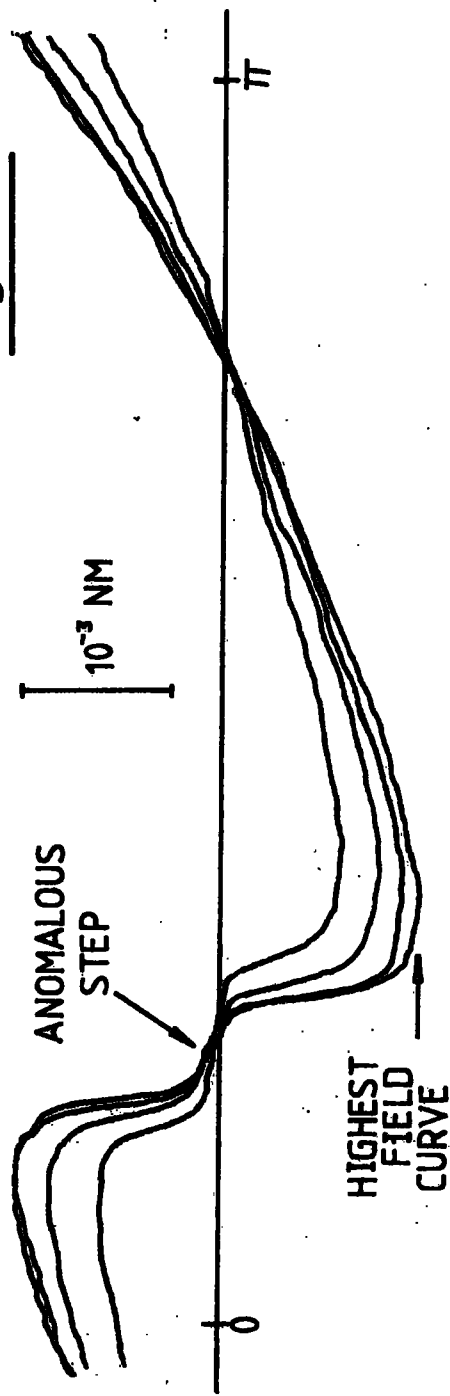
K_4 VS TEMPERATURE FOR Tb_xGd_{1-x} ALLOYS;
COMPARISON OF PRESENT AND EXISTING DATA

Fig 8-21



ANOMALOUS TORQUE CURVES PRODUCED BY A 26.5 mg
 α -PLANE DISC OF Tb_{0.05}Gd_{0.95} AT 181 K IN FIELDS OF
1.16, 1.45, 1.70 AND 1.85 TESLA

Fig 8.22



chosen magnetisations are tabulated in Appendix J along with the easy-axis torque gradients from which, after correction, the K_1 values were derived.

The errors that have arisen in the present measurements of the anisotropy of the terbium/gadolinium alloys, arising ultimately from the small fields available from the conventional electromagnet of the current apparatus, have prevented, in the last analysis, a clear assessment of whether there is a change in the anisotropy with respect to sample purity. It is yet unproved that there is a purity dependence of the magnitude observed in gadolinium by Smith et al. (for example 20% change in K_1 for a 1% oxygen addition) in the terbium/gadolinium alloys.

One particular observation made during the present investigation was that for a certain temperature and alloy composition anomalous torque curves are produced. This was mentioned by Tajima who offered no explanation and it has not been reported since. The anomaly is shown in figure 8.22 and represents a reduction in the observed torque in an interval around the hard-axis.

8.6 Theoretical modelling of the anisotropy

The theoretical temperature dependences of the anisotropy constants for several models have been discussed in chapter 2. On the basis of these, least squares fits for the predicted functional forms were made to the experimental results reported here. The fits are;

- 1) A simple power law in the reduced magnetisation $m(T)$;

$$K_1(T) \text{ or } K_4(T) = a(m(T))^b \quad \dots(8.1)$$

2) A single-ion fit due to Callen and Callen featuring the reduced hyperbolic Bessel function (of order appropriate to the constant being described) of the inverse Langevin function of the reduced magnetisation (see Appendix K);

$$K_1(T) = cI_{5/2}(\mathcal{L}^{-1}(m(T))) \quad \dots(8.2)$$

$$K_4(T) = cI_{13/2}(\mathcal{L}^{-1}(m(T))) \quad \dots(8.3)$$

Note that the model of Callen and Callen defines the temperature dependences of the K_n^n constants and that in equation 8.1 the functional form is valid only if the higher order constants in the anisotropy energy expression are assumed to be zero since here the constants are defined in a different expression, where constants only correlate by a simple scaling factor if the subsequent ones are zero. However this assumption has already been made in order to derive experimental values for both K_1 and K_4 .

3) An ad-hoc two ion model with a square dependence on reduced magnetisation;

$$K_1(T) \text{ or } K_4(T) = d(m(T))^2 \quad \dots(8.4)$$

4) A combination of the single- and two-ion models;

$$K_1(T) = eI_{5/2}(\mathcal{L}^{-1}(m(T))) + f(m(T))^2 \quad \dots(8.5)$$

$$K_4(T) = eI_{13/2}(\mathcal{L}^{-1}(m(T))) + f(m(T))^2 \quad \dots(8.6)$$

5) A special K_4 fit due to Rhyne and McGuire from a model which considers magnetoelastic interactions between ions;

$$K_4 = gI_{9/2}(\mathcal{L}^{-1}(m(T))) \cdot I_{5/2}(\mathcal{L}^{-1}(m(T))) \quad \dots(8.7)$$

K₁ AND K₄ TEMPERATURE DEPENDENCE FOR Tb_xGd_{1-x} ALLOYS

Adjustable Parameter	K ₁				K ₄				
	5% Tb	10% Tb	20% Tb	30% Tb	5% Tb	10% Tb	30% Tb	50% Tb	75% Tb
a	0.890	3.88	12.19	20.9	0.55	1.75	4.81	13.76	30.02
b	4.90	2.95	3.00	3.3	12.82	15.10	10.61	16.03	15.97
$\Sigma(\delta^2)$	0.041	0.265	5.72	14.78	0.0019	0.005	0.12	0.097	0.36
c	0.72	3.87	12.04	19.76	0.99	2.67	12.31	19.82	45.60
$\Sigma(\delta^2)$	0.094	0.399	7.70	13.75	0.008	0.018	1.10	0.37	0.67
d	0.636	3.34	10.54	16.93	0.18	0.38	1.30	2.48	4.27
$\Sigma(\delta^2)$	0.158	1.475	17.70	38.05	0.037	0.37	4.05	16.87	57.47
e	2.24	5.01	13.19	24.00	0.77	2.41	9.52	18.92	43.10
f	-1.36	-1.00	-1.02	-3.67	0.051	0.054	0.44	0.17	0.37
(e + f)	0.88	4.01	12.17	20.33	0.82	2.46	9.96	19.09	43.47
$\Sigma(\delta^2)$	0.042	0.331	7.34	11.18	0.004	0.012	0.59	0.31	0.10
g	-	-	-	-	0.55	1.43	6.14	10.19	22.25
$\Sigma(\delta^2)$	-	-	-	-	0.0022	0.016	0.21	0.98	16.66

The "best-fit" adjustable parameters for the theoretical temperature dependences of the anisotropy constants K₁ and K₄. With the exception of the dimensionless parameter b, values are in 10⁶ J m⁻³ for K₁ and 10⁴ J m⁻³ for K₄. a, c, d, (e+f) and g correspond to the zero-temperature anisotropy constants. The least-squares error is shown.

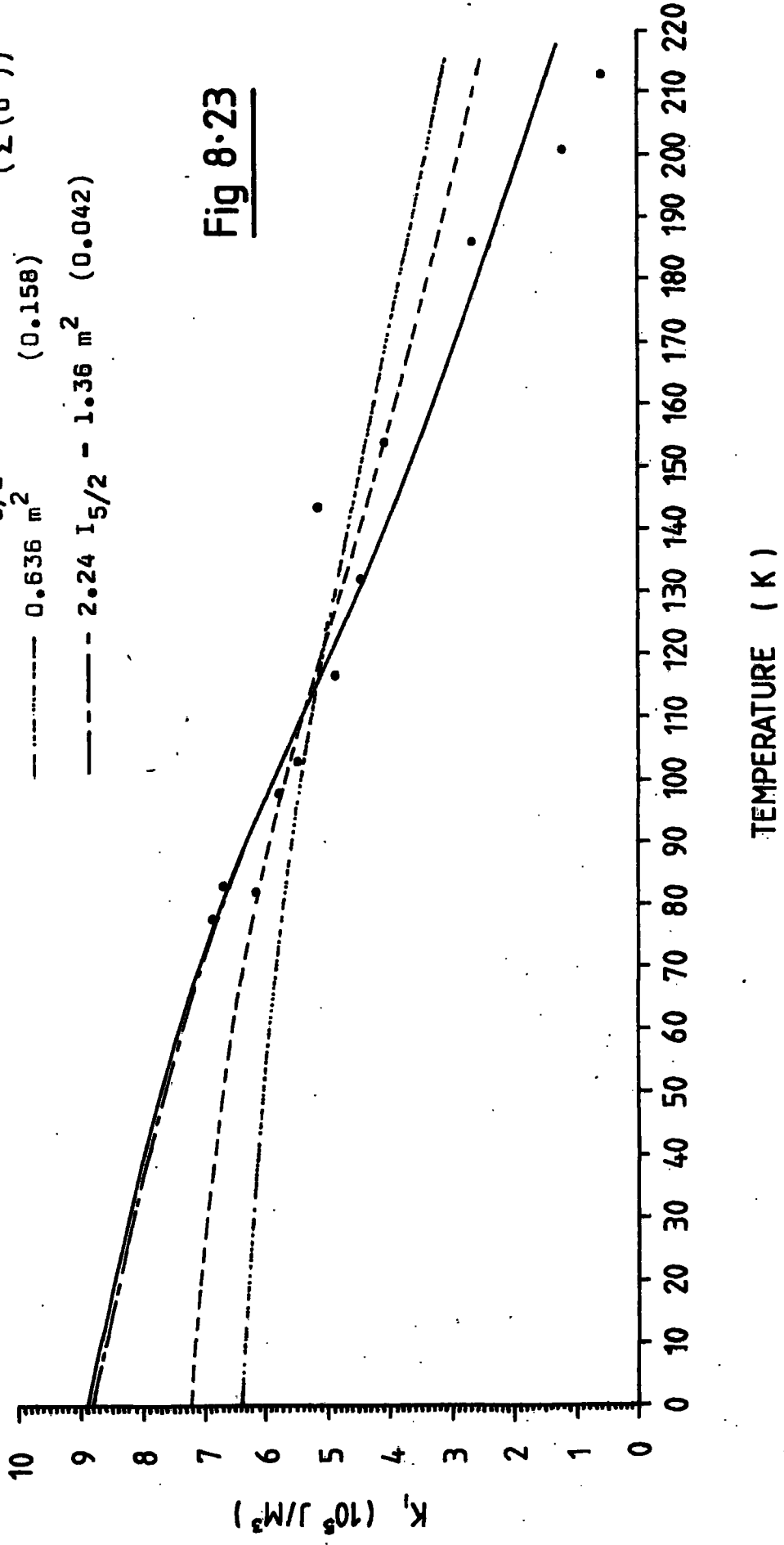
TABLE 8.3

All the experimental data is given in figures 8.23 to 8.31 showing the behaviour of each of the two constants for various alloy compositions. With these are given the best functional temperature fits using each model by adjusting the available parameters by a least squares criterion. These parameters, featured in equations 8.1 to 8.7, are given on each figure and corporately in table 8.3 and refer to the best available curve for each model. Appendix J gives three computer programs (in BASIC) which were written to assist in the analysis. The particular values for a , c , d , g and the sum $e+f$ are the anisotropy constants extrapolated to zero temperature. Table 8.3 and figures 8.23 to 8.31 also indicate the sum of the squares of the residuals in each attempted theoretical fit which, for a given temperature profile belonging to one alloy composition and anisotropy constant, indicate the relative merits of each functional form. The fits giving the smallest error-sum are used to give the 0 K values of the anisotropy plotted in figures 8.18 and 8.19. In all cases the reduced magnetisation was derived using the data of Bagguley et al., applied earlier in the K_1 calculations, and given in Appendix J. Theoretical models with two adjustable parameters will, ipso facto, yield better fits than those with one ; care should be taken in drawing comparisons between one- and two-parameter theories.

As a qualitative comment on the theoretical temperature dependences of equations 8.1 to 8.7, it is evident that in all cases except two (K_1 , 30% Tb and K_4 , 75% Tb) the simple power law gives the best fit, and for the exceptions when it

THEORETICAL FITS FOR K_1 VS TEMPERATURE FOR $Tb_{0.05}Gd_{0.95}$ ALLOY

- $0.890 m^{4.90}$ (0.041)
 - - - $0.72 I^{5/2}$ (0.094)
 - · - · $0.636 m^2$ (0.158)
 - - - $2.24 I^{5/2} - 1.36 m^2$ (0.042)
- ($\Sigma(\delta^2)$)



TEMPERATURE (K)

THEORETICAL FITS FOR K_1 VS TEMPERATURE FOR $Tb_{0.1}Gd_{0.9}$ ALLOY

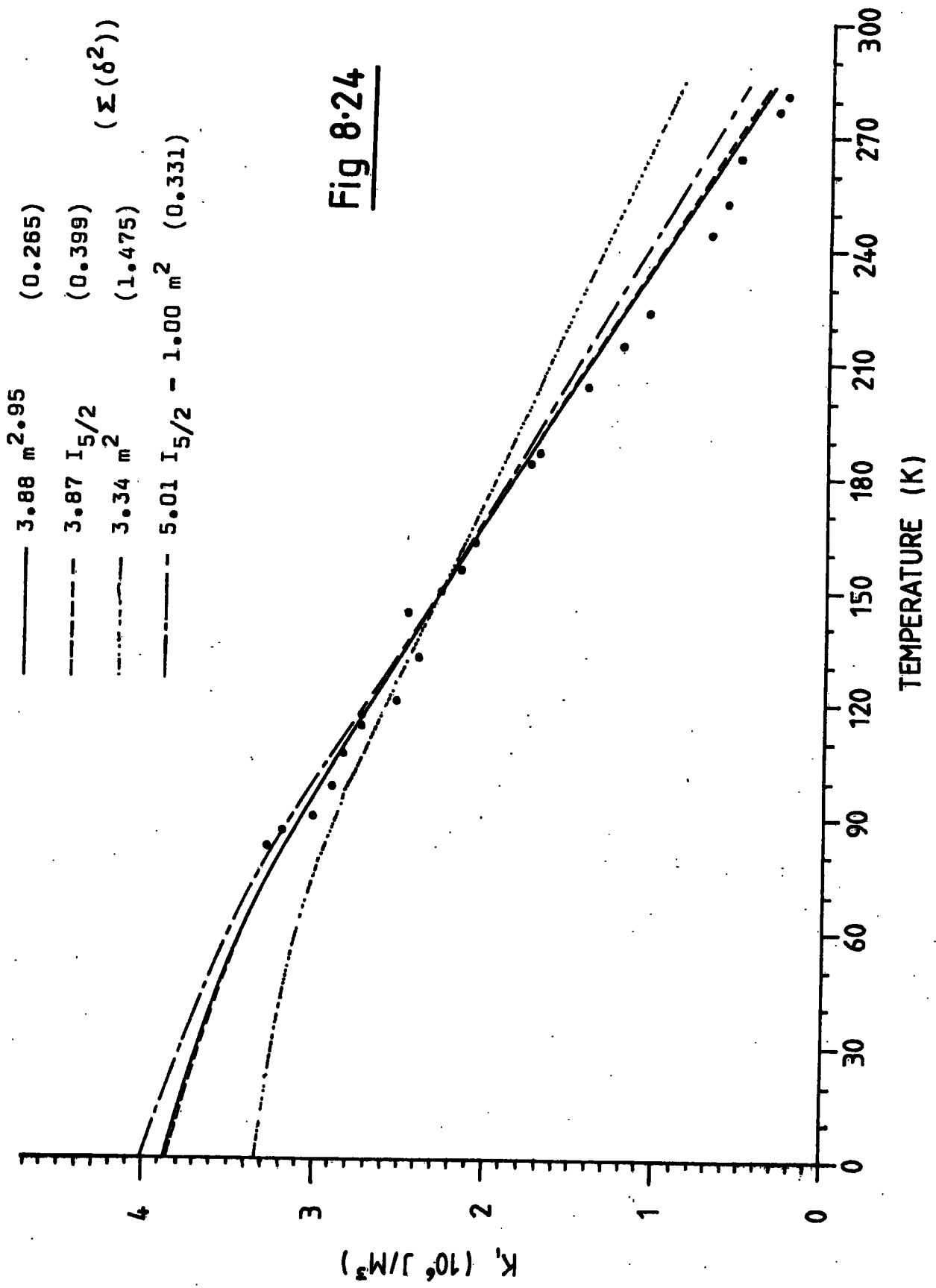


Fig 8.24

THEORETICAL FITS FOR K_1 VS TEMPERATURE FOR $Tb_{0.2}Gd_{0.8}$ ALLOY

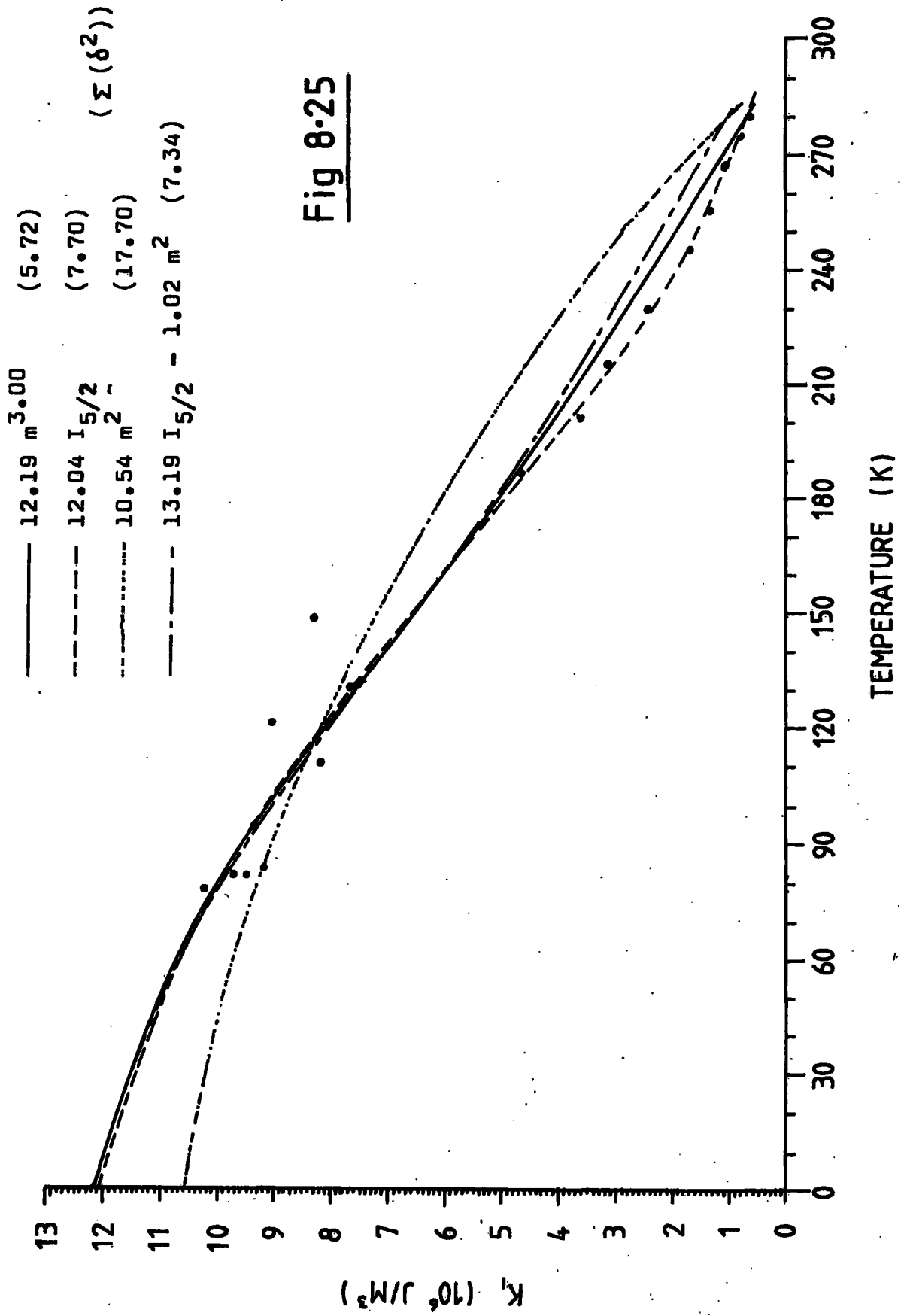


Fig 8.25

THEORETICAL FITS FOR K_i VS TEMPERATURE FOR $Tb_{0.3}Gd_{0.7}$ ALLOY

- 20.9 $m^{3.3}$ (14.78)
 - 19.76 $I_{5/2}$ (13.75)
 - 16.93 m^2 (38.05)
 - - - - 24.0 $I_{5/2} - 3.67 m^2$ (11.18)
- ($\Sigma(\delta^2)$)

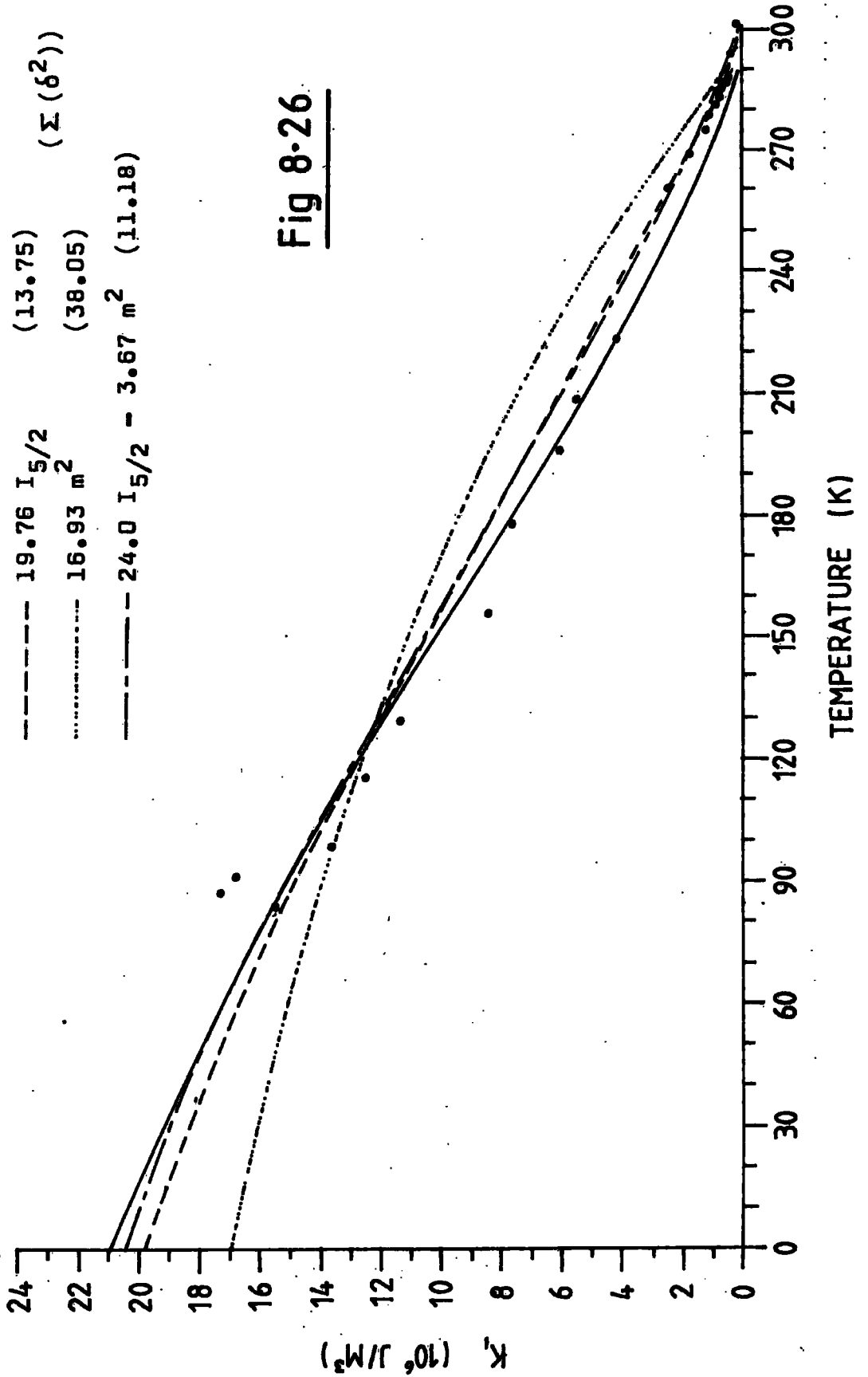
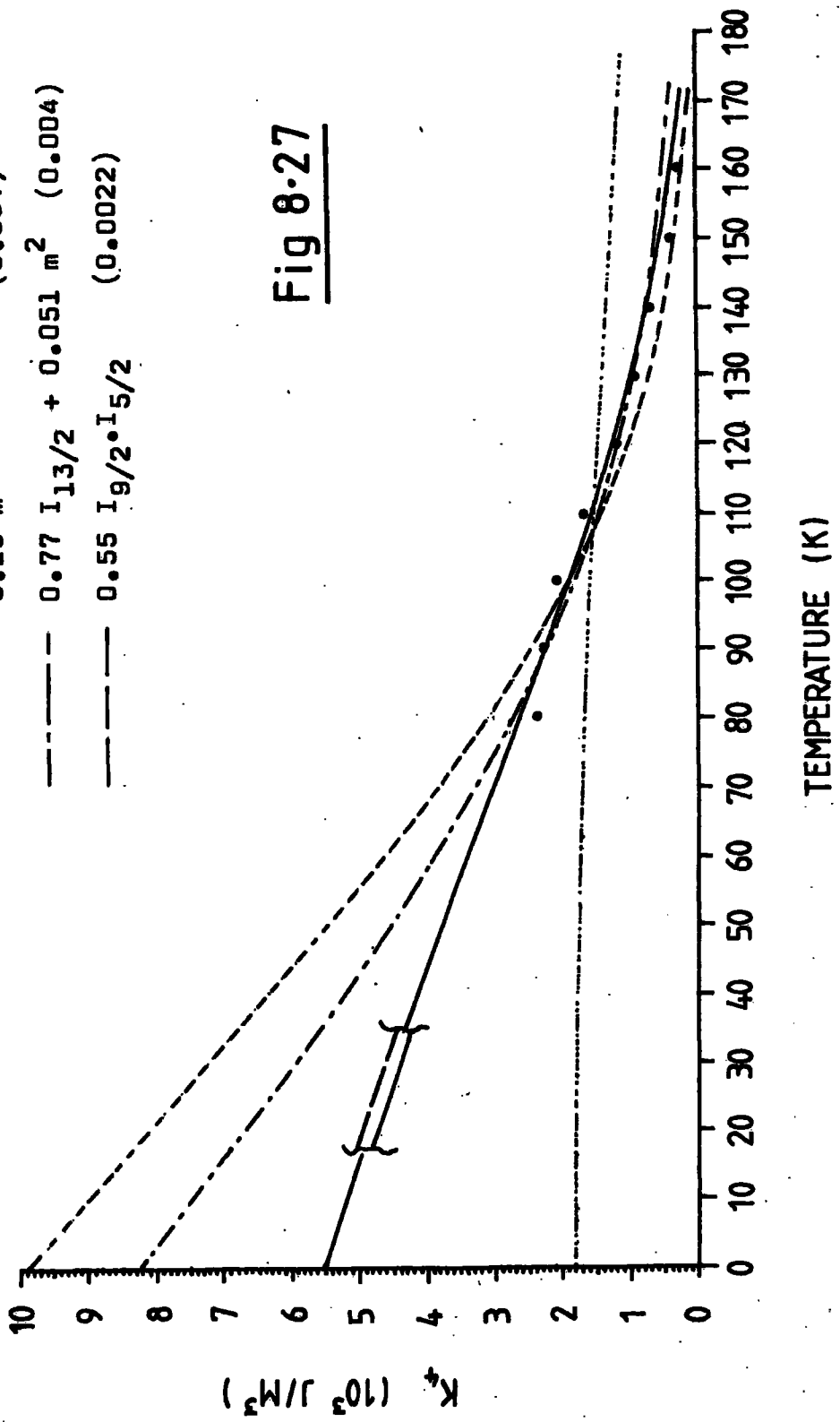


Fig 8-26

THEORETICAL FITS FOR K_4 VS TEMPERATURE FOR $Tb_{0.05}Gd_{0.95}$ ALLOY

- 0.55 $m^{12.82}$ (0.0019)
 - - - 0.99 $I_{13/2}$ (0.008)
 - · · 0.18 m^2 (0.037)
 - · - 0.77 $I_{13/2} + 0.051 m^2$ (0.004)
 - - - 0.55 $I_{9/2} \cdot I_{5/2}$ (0.0022)
- ($\Sigma(\delta^2)$)



TEMPERATURE (K)

THEORETICAL FITS FOR K_4 VS TEMPERATURE FOR $Tb_{0.1}Gd_{0.9}$ ALLOY

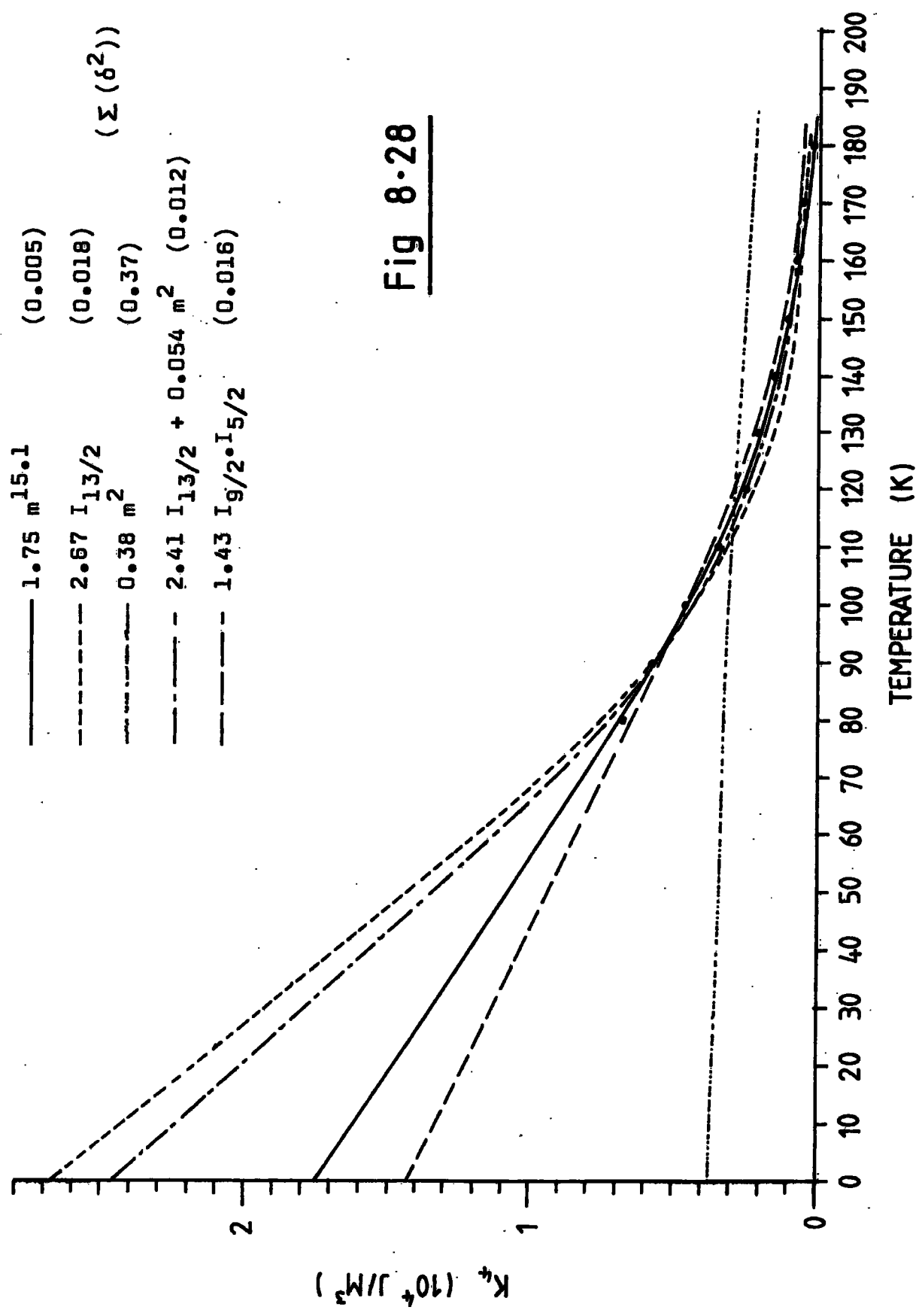


Fig 8-28

TEMPERATURE (K)

K_4 (10^4 J/M^3)

THEORETICAL FITS FOR K_4 VS TEMPERATURE FOR $Tb_{0.3}Gd_{0.7}$ ALLOY

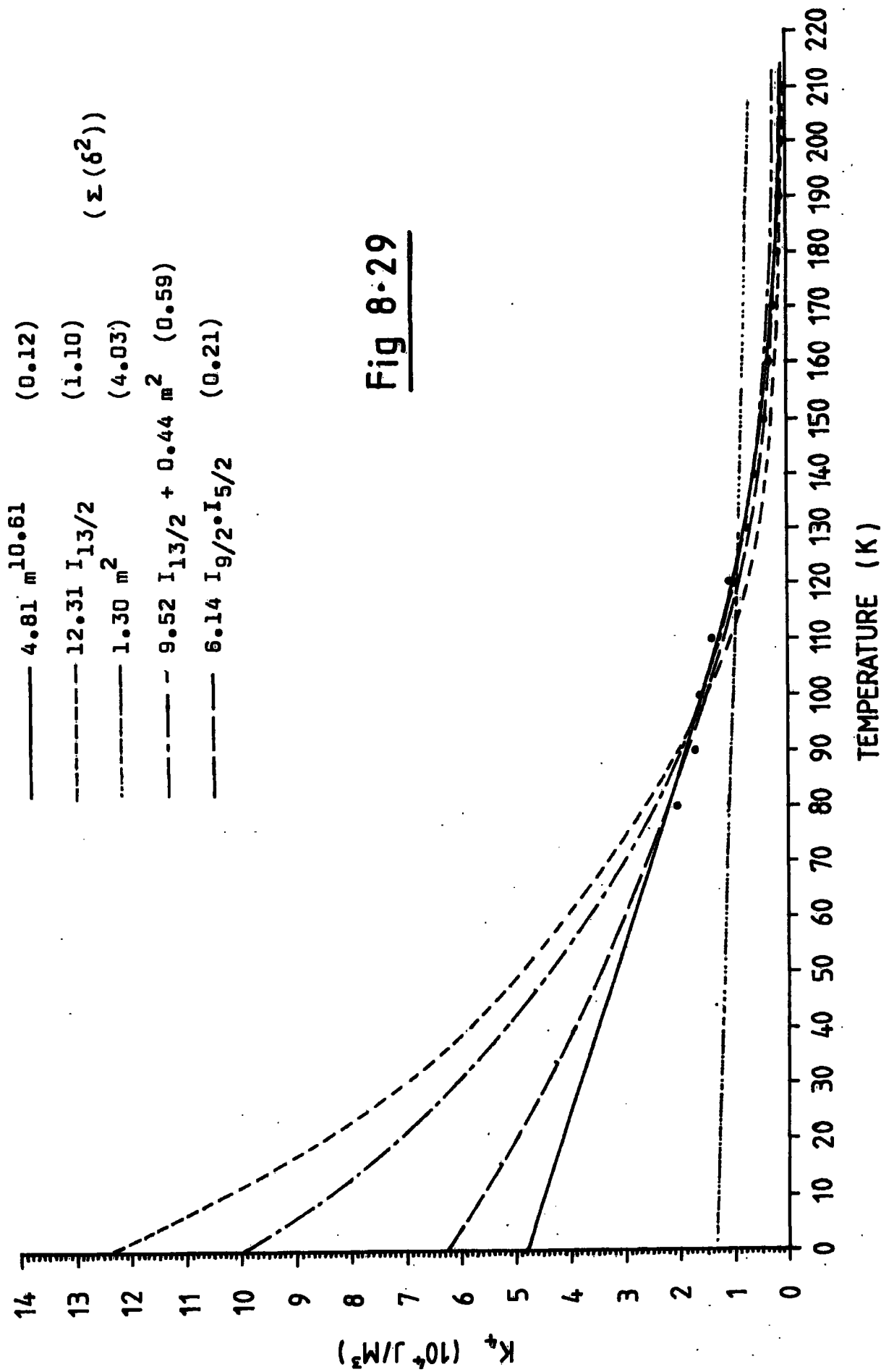
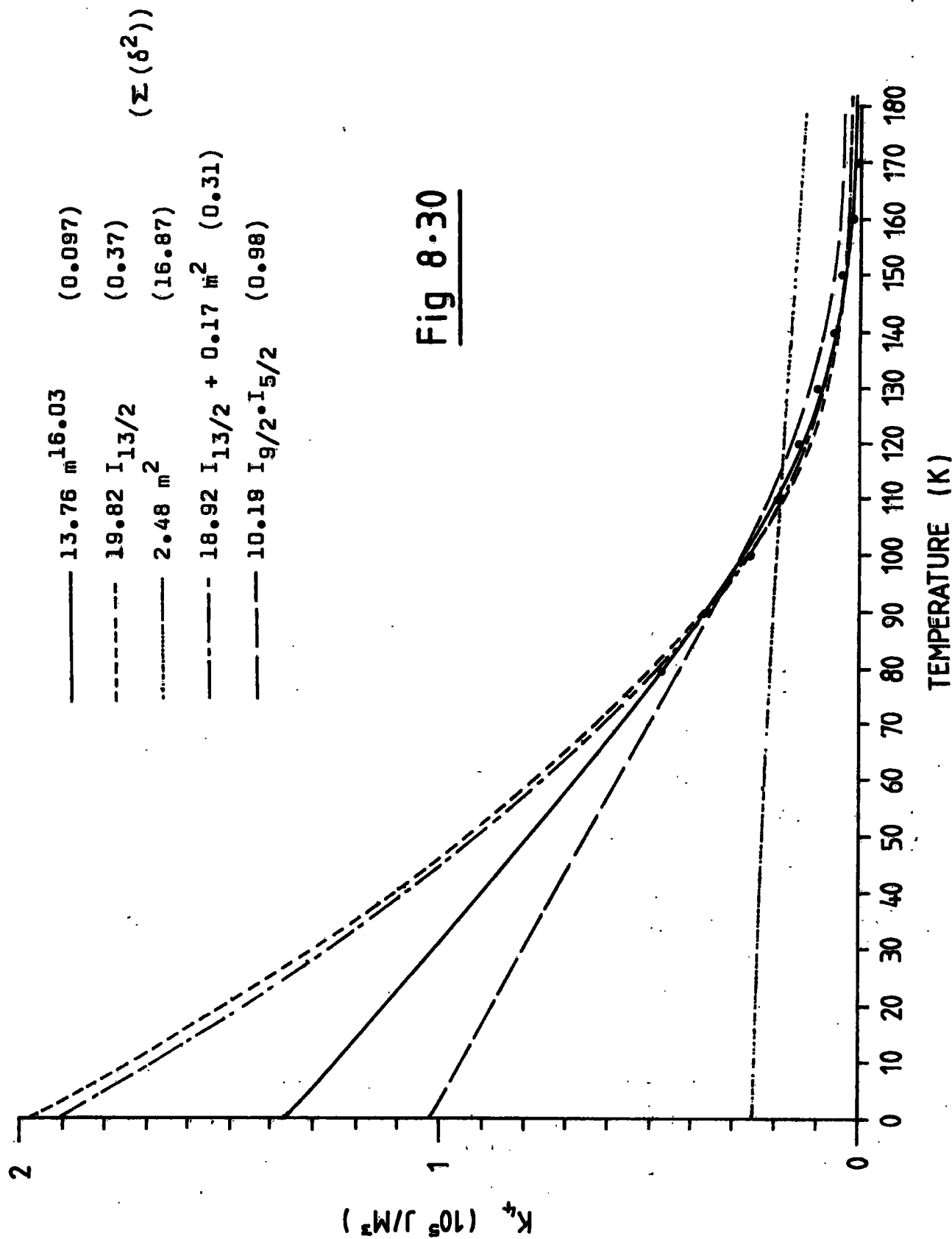


Fig 8·29

THEORETICAL FITS FOR K_4 VS TEMPERATURE FOR $Tb_{0.9}Gd_{0.1}$ ALLOY



THEORETICAL FITS FOR K_4 VS TEMPERATURE FOR $Tb_{0.75}Gd_{0.25}$ ALLOY

- 30.02 $m^{15.97}$ (0.36)
 - - - - 45.6 $I_{13/2}$ (0.67)
 - · - · 4.27 m^2 (57.47)
 - · - · - 43.1 $I_{13/2} + 0.37m^2$ (0.1)
 - 22.25 $I_{9/2} \cdot I_{5/2}$ (16.66)
- ($\Sigma(\delta^2)$)

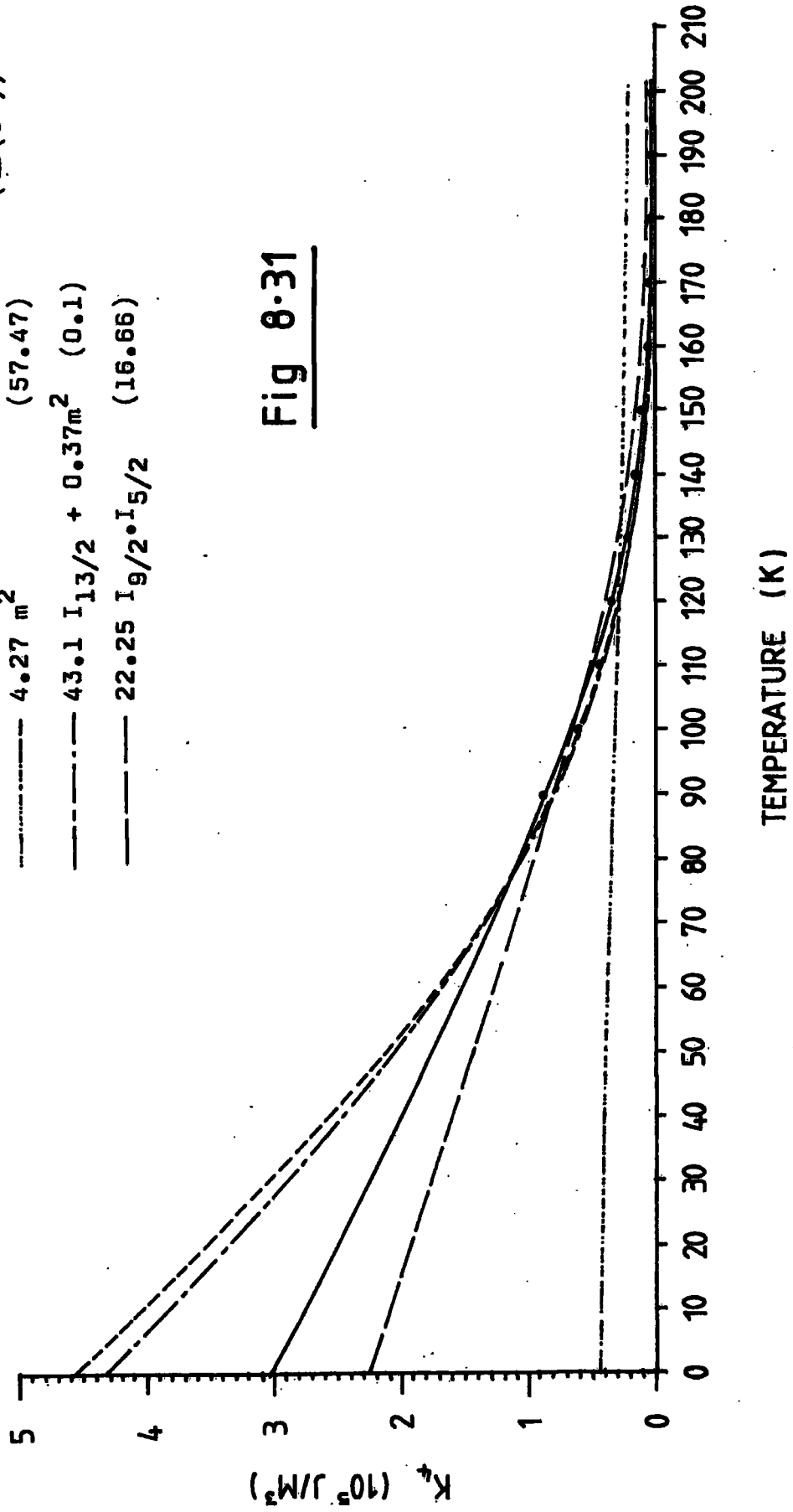


Fig 8.31

does not, it compares favourably with the best alternative. Apart from the 5% Tb values, the K_1 power dependence is very close to the value of 3 predicted by the $L(L+1)/2$ law. The K_4 power law fluctuates between indices of 10 and 16 with no obvious trend with respect to alloy composition. These values are noticeably at variance with the predicted 21st power dependence of the $L(L+1)/2$ law. At the opposite extreme to the power law, the ad-hoc two-ion model is manifestly inconsistent with the data, giving the worst fit in all cases.

Of real significance is the comparison between the single-ion model, parameterised by the constant c , and the simple power law. For all compositions, K_1 shows a good single-ion dependence, indeed 30% Tb shows greater consistency with this model than the power law. The inclusion of a two-ion component in the single-ion model has little effect on the fitting. However the K_4 values do not indicate the single-ion law as clearly; the power law is noticeably superior. Furthermore the inclusion of two-ion effects is more beneficial than in the previous case though the magnitude of the corrective two-ion component is still small ($f/e < 5\%$ always).

The magnetoelastic model for K_4 shows good agreement with some of the data but such inaccuracy at higher terbium concentrations that it casts doubt on the significance of the low terbium fits.

The mechanism responsible for the magnetocrystalline anisotropy of terbium would seem to be of single-ion origin and, in particular, predicted well by the theory of Callen

and Callen. This judgement is, however, a simplification, as revealed by the differing success of the single-ion model for different anisotropy constants.

Confirming the conclusion about the single-ion model are the composition dependences of the two constants. K_1 demonstrates linearity at 80 K within experimental error (figs. 8.16 and 8.17). Extrapolations to 0 K are less valid in drawing a conclusion in this respect since a model must be assumed in making such an extrapolation. However the linearity in K_1 still survives the extrapolation to 0 K for any plausible fit. The K_4 values at both 80 K and extrapolated to 0 K are linear with respect to composition, within experimental error, if the 75% Tb values are rejected. This rejection is justifiable since these values would, of all the measurements made on the alloys, be subject to errors due to sample saturation problems in the original experiment, and in any case are values which differ most markedly from those of other workers.

Most of the theoretical fits mentioned herein have not been attempted before on the anisotropy data of terbium/gadolinium alloys. However Bagguley et al. demonstrate some consistency of the $L(L+1)/2$ power law with their data, particularly that the K_4 temperature dependence follows the necessary 21st power dependence on the reduced magnetisation. The temperature dependence of the pure terbium anisotropy constants have been modelled in detail by Rhyne and Clark (1967), Féron (1970 a,b) and Birss et al. (1977 a,b). These are consistent with what has been found presently for the alloys in that the Callen and Callen single-ion model

fits the anisotropy well for K_2^0 and K_4^0 (c.f. K_1 for the alloys) but the K_6^0 (c.f. K_4 for the alloys) seems to fit less well if a consensus of the basal-plane results is to be believed. If the basal-plane measurements made most recently are more reliable, then it can be said that the single-ion model, without exception, successfully describes the temperature dependence of the anisotropy of terbium, which is in agreement with the broad conclusion reached here on the alloys.

8.7 Discussion

A linear decline in the anisotropy with respect to the dilution of the terbium in the terbium/gadolinium alloys has been cited as evidence for the single-ion model of the anisotropy. This assumes that the dilution of terbium ions in a gadolinium host is a means of separating them from each other in an unchanged crystal field and that the proportional loss in the anisotropy correlates merely to the loss of active material, each ion having the same anisotropy irrespective of its proximity to another. By this reasoning non-linearity would indicate some two-ion contribution to the anisotropy.

The reasoning behind the foregoing argument is, however, questionable, in particular the assumption that the crystal field is unchanged with respect to alloy composition. In practice a c/a ratio alteration will occur in the HCP structure with respect to alloy composition assisted by the changing magnetostriction of the alloy. Tajima (1971) has discussed the effects of this on the crystal field and

concluded that a non-linearity of perhaps 20% could be introduced in the anisotropy composition dependence in the terbium/gadolinium alloys, even if the single-ion model were valid. Such deviations are observed in the consensus of existing data for K_1 , for which Tajima's comments are valid, and are of the sense predicted, in that extrapolations of low terbium anisotropies to 100% terbium undervalue the more reliable explicit measurements of the pure terbium anisotropy. Thus the evidence of existing experimental data is that the Callen and Callen single-ion anisotropy model describes the K_1 values well, and in particular the single-ion result for the composition dependence of K_1 is obeyed convincingly after account is made of the c/a variation.

The success of the present investigation has been limited by the low fields available experimentally, which have resulted in excessive extrapolations of the K_4 data with respect to field and a calculation of K_1 in which, to first order, K_2 was neglected. Comparison between present K_1 values and those reported elsewhere on less pure materials are, however, good, and suggest minimal dependence on impurity concentrations of the kind observed in gadolinium. The unpublished work of Corner on samples of equal purity to those used here, also from the Centre for Materials Science, Birmingham, gives K_1 values which are consistent with those reported elsewhere, confirming that a negligible purity dependence in the anisotropy is observed in these alloys over the purity range of materials investigated in the past.

8.8 Conclusion

The magnetocrystalline anisotropy constants of several terbium/gadolinium alloys have been measured. These are consistent, with the exception of the K_4 values at high terbium concentrations, with existing data, and suggest both in the temperature profiles and composition dependences that the anomalously high anisotropy of terbium is of single-ion origin. This is indicated most clearly by the K_1 measurements.

In the small area of disagreement between the current results and those of others, the errors seem likely to be the consequence of the low fields provided by the conventional electromagnet used in the present investigation.

There is no evidence that the improved purity of the materials used in the present work over those used by others has affected the anisotropy values for the alloys.

APPENDIX A : RELATION BETWEEN THE
ANISOTROPY CONSTANTS AND COEFFICIENTS

Theoretical models for the magnetocrystalline anisotropy commonly employ an expression for the energy which involves spherical harmonics;

$$E_K/V = \sum_{L=0}^{\infty} \sum_{m=-L}^{+L} (K_L^m)' Y_L^m(\theta, \phi) \quad \dots(A.1)$$

where the $Y_L^m(\theta, \phi)$ are the spherical harmonics;

$$Y_L^m(\theta, \phi) = (-1)^m \sqrt{\frac{(2L+1)(L-m)!}{4(L+m)!}} P_L^m(\cos\theta) \cdot \text{Exp}(i|m|\phi) \quad \dots(A.2)$$

and $P_L^m(x)$ are associated Legendre polynomials;

$$P_L^m(x) = (-1)^m \frac{(2L-2m)!}{2^L m! (L-m)! (L-2m)!} x^{L-2m} \quad \dots(A.3)$$

and $(K_L^m)'$ are the anisotropy constants, often called coefficients to distinguish them from the phenomenological parameters of equation 2.2. The spherical harmonic expression is often simplified to an expression involving only the Legendre polynomials; the hexagonal simplification has already been given in chapter 2 (eqn. 2.5) where;

$$P_L(x) = \sum_{m=-L}^{+L} P_L^m(x) \quad \dots(A.4)$$

The relationship between the anisotropy constants of equation 2.2 and the coefficients of equation 2.5 can be derived easily from the appropriate expansions for the terms in the two energy expressions. The derivation is as follows:

The first three Legendre polynomials occurring in equation 2.5 can be expanded explicitly;

$$P_2(\cos\theta) = 1/4 (1+3\cos 2\theta) \quad \dots(A.5)$$

$$P_4(\cos\theta) = 1/64 (9+20\cos 2\theta+35\cos 4\theta) \quad \dots(A.6)$$

$$P_6(\cos\theta) = 1/512 (50+105\cos 2\theta+126\cos 4\theta+231\cos 6\theta) \quad \dots(A.7)$$

These can then be converted to expressions involving powers of the sines using the relations;

$$\cos 2\theta = 1-2\sin^2\theta \quad \dots(A.8)$$

$$\cos 4\theta = 1-8\sin^2\theta+8\sin^4\theta \quad \dots(A.9)$$

$$\cos 6\theta = 1-18\sin^2\theta+48\sin^4\theta-32\sin^6\theta \quad \dots(A.10)$$

giving;

$$P_2(\cos\theta) = 1-3/2 \sin^2\theta$$

$$P_4(\cos\theta) = 1-5\sin^2\theta+35/8 \sin^4\theta$$

$$P_6(\cos\theta) = 1-21/2 \sin^2\theta+189/8 \sin^4\theta-231/16 \sin^6\theta \quad \dots(A.11)$$

The desired relations are then obtained by comparing coefficients in the above expressions with those of equation 2.2, giving;

$$K_1 = -3/2 K_2^0 - 5K_4^0 - 21/2 K_6^0 - \dots \quad \dots(A.12)$$

$$K_2 = 35/8 K_4^0 + 189/8 K_6^0 + \dots \quad \dots(A.13)$$

$$K_3 = -231/16 K_6^0 - \dots \quad \dots(A.14)$$

$$K_4 = K_6^0 + \dots \quad \dots(A.15)$$

and correspondingly;

$$K_2^0 = -2/3 K_1 - 16/21 K_2 - 176/231 K_3 - \dots \quad \dots(A.16)$$

$$K_4^0 = 8/32 K_2 + 144/385 K_3 + \dots \quad \dots(A.17)$$

$$K_6^0 = -16/231 K_3 - \dots \quad \dots(A.18)$$

$$K_6^6 = K_4 + \dots \quad \dots(A.19)$$

APPENDIX B : SINGLE-ION CALCULATIONS
OF THE COBALT ANISOTROPY AFTER SZPUNAR

This appendix is the precis of a paper written by Dr. B. Szpunar which is awaiting publication.

The Temperature Dependence of the Anisotropy Constants of
Cobalt

In the proposed model the single-ion model is assumed to be dominant in cobalt.

A similar model was proposed previously by Szpunar and Lindgard (1979) as an explanation for the high anisotropy of the YCo_5 compounds. It has been found that the crystal field parameters depend on the lattice parameters to an extent which accounts for the fact that the anisotropy of YCo_5 is about ten times that of cobalt. The quasispin model was used for the description of the exchange interaction (Liu, 1976). It is however unclear what numbers to take for the spin and orbital moment for cobalt; the magnetisation temperature dependence is close to the Brillouin function suggesting $J = \frac{1}{2}$. In the ground state the total spin quantum number of seven d-electrons in the cobalt (2+) ion is 4.5. In the crystal the orbital moment is almost quenched and the total magnetic moment on the atom is 1.7 μ_B . Liu assumed for the quasispin of cobalt the value equals one.

Lindgard and Danielsen (1975) have given the relationships between anisotropy constants (for equation 2.2 of this thesis) and the crystal field parameters, B_L^m ;

$$K_1 = -3/2 B_2^0 (\langle O_2^0 \rangle - \langle O_2^2 \rangle) - 5B_4^0 (\langle O_4^0 \rangle - 3\langle O_4^2 \rangle) - 21/2 B_6^0 (\langle O_6^0 \rangle - 5\langle O_6^2 \rangle) \dots (B.1)$$

$$K_2 = 35/8 B_4^0 (\langle O_4^0 \rangle - 4\langle O_4^2 \rangle + \langle O_4^4 \rangle) + 63/8 B_6^0 (3\langle O_6^0 \rangle - 20\langle O_6^2 \rangle + 5\langle O_6^4 \rangle) \dots (B.2)$$

$$K_3 = -231/16 B_6^0 (\langle O_6^0 \rangle - 15/2 \langle O_6^2 \rangle + 3\langle O_6^4 \rangle - 1/2 \langle O_6^6 \rangle) \dots (B.3)$$

$$K_4 = 1/16 B_6^0 (\langle O_6^0 \rangle - 15/2 \langle O_6^2 \rangle + 3\langle O_6^4 \rangle - 1/2 \langle O_6^6 \rangle) \dots (B.4)$$

where $\langle O_L^m \rangle$ is the temperature average of the Stevens operators O_L^m . For total angular momentum quantum number equal to one, only O_2^2 and O_2^0 are non-zero and K_2 , K_3 and K_4 are also therefore zero. If any information is desired on the higher anisotropy constants, the highest total angular momentum quantum number must be assumed. This means that many more projections on the quantisation axis are allowed; in the limit obtaining the classical situation where thermal fluctuations may change the spin directions arbitrarily. In this work the assumption is made that J for cobalt is equal to the ground state value.

An effective factor for obtaining the macroscopic moment correctly can be introduced. For the classical limit the temperature dependence of the Stevens operators is;

$$\langle O_L^m \rangle = c(m(T))^{L(L+1)/2} \dots (B.5)$$

where $m(T)$ is the reduced magnetisation. From the experimental curves of magnetisation as a function of temperature, and the above equations, the temperature

dependence of the anisotropy constants could be predicted. From the preceding formulae, one simple relationship is;

$$K_3/K_4 = -231/16 B_6^0 / 1/16 B_6^6 = -231 B_6^0 / B_6^6 \quad \dots(B.6)$$

The relationship between the temperature and the anisotropy constants for cobalt can be explained from the equations given by Dixon (1972) for the dependence of the crystal field parameters on the c/a lattice parameter ratio;

$$B_2^0 = (1.633 - c/a) \quad \dots(B.7)$$

$$B_4^0 = (0.1127 - (0.752(1.633 - c/a))) \quad \dots(B.8)$$

$$B_6^0 = (0.260 - (0.369(1.633 - c/a))) \quad \dots(B.9)$$

$$B_6^6 = -(2.52 - (0.815(1.633 - c/a))) \quad \dots(B.10)$$

Even very small changes in the lattice parameter ratio of cobalt have a big influence on the anisotropy constants. A simple substitution of equations B.7 to B.10 into the earlier expressions for the anisotropy constants allowed, given a temperature dependence of the Stevens operators in the form of equation B.5, relationships to be established between c/a ratios and the anisotropy constants. Using these relationships, given the temperature dependence of the c/a ratio, the temperature profiles of the anisotropy constants could be calculated in detail. However a more accurate knowledge of the c/a ratio of cobalt is needed before this can be meaningful. Calculations of the c/a dependence from given anisotropy values show reasonable consistency with available experimental data for c/a values. This is in a calculation which begins with two self-consistent

temperature profiles, for the first two anisotropy constants, that fit the experimental temperature plots for K_1 and K_2 to the best possible accuracy. (These profiles are given in figures 7.29 and 7.30 and the deduced c/a dependence is given in figure 7.31 of this thesis.) The derived values of the K_3 and K_4 constants in this scheme are not however consistent with the measured values of K_3 and K_4 , in particular the predicted ratio between K_3 and K_4 of equation 8.6 is not obeyed.

In conclusion, the calculations for K_1 and K_2 for cobalt which have been made here for a single-ion model, taking into account the changing c/a ratio with respect to temperature, are in agreement with experimental data given the uncertainty in present c/a measurements. However the temperature dependence of the higher constants cannot be explained, but these, it must be noticed, are very small anyway.

APPENDIX C : TORQUE CURVES FOR
MATERIALS WITH UNIAXIAL CRYSTAL
ANISOTROPY - UNSATURATED CASE

As an example of the phase theory treatment of torques generated by an unsaturated ferromagnetic crystal having magnetocrystalline anisotropy, the simplest possible case will be discussed here.

A demagnetising factor can be attributed to an ellipsoid representing the ratio of the magnetisation to the "demagnetising field" experienced internally by the sample due, in the simple model, to free magnetic poles on the surface of the sample. Taking such a specimen, with a uniaxial easy-axis along the direction of cylindrical symmetry, and an anisotropy energy described by a single constant, K_1 , the total energy of the specimen in a magnetic field is given by;

$$E_{\text{tot}}/V = PK_1 \sin^2 \alpha + (1-P)K_1 \sin^2 \beta \quad \dots(\text{C.1})$$

$$- (PB_0 \sigma_s \cos(\delta - \alpha) - (1-P)B_0 \sigma_s \cos(\delta + \beta)) / \mu_0$$

$$+ (1/(2\mu_0)) D \sigma_s^2 ((P \sin \alpha + (1-P) \sin \beta)^2 + (P \cos \alpha - (1-P) \cos \beta)^2)$$

where P is the volume fraction of one of the two possible domain phases, α and β are the angles of the magnetisation characteristic of each phase with respect to the nearest

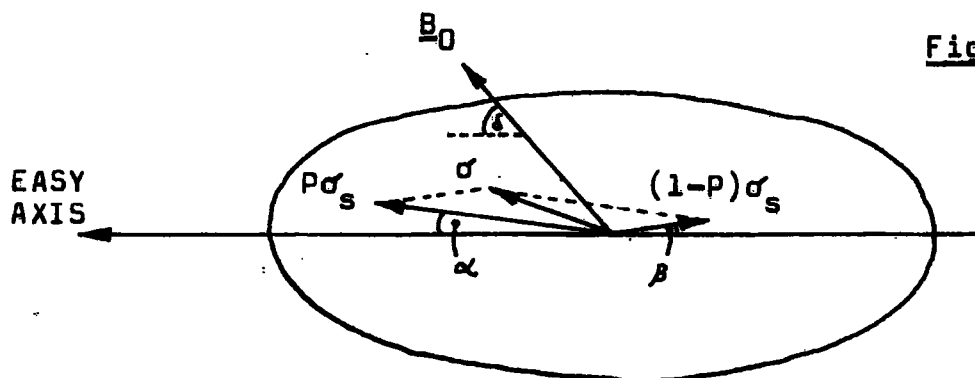


Fig. C.1

easy-axis, D is the demagnetising factor for the ellipsoid and δ is the angle of the applied field to an easy direction in the specimen. The terms are illustrated in figure C.1.

The first line of equation C.1 represents the magneto-crystalline energy produced by the canting of the two domain phases away from the easy-axis, the second line of the equation is simply the Zeeman energy of the net magnetisation (σ), that is the vectorial average of the two phases, with the applied field, and the third line is the magnetostatic self energy of the net magnetisation. Terms which account for the energy of the domain walls are always rejected since phase theory does not describe the details of the domain structure.

The values of α , β and P which give the energetically most stable state can be obtained by solving the three simultaneous equations that result from setting each of the three partial differentials $\frac{\delta E}{\delta P}$, $\frac{\delta E}{\delta \alpha}$ and $\frac{\delta E}{\delta \beta}$ to zero. The three simultaneous equations are, after simplification;

$$2K_1 \sin \alpha \cos \alpha - \frac{B_0 \sigma_s}{\mu_0} \sin(\delta - \alpha) + \frac{D \sigma_s^2}{\mu_0} (1 - P) \sin(\alpha + \beta) = 0 \quad \dots (C.2)$$

$$2K_1 \sin \beta \cos \beta - \frac{B_0 \sigma_s}{\mu_0} \sin(\delta + \beta) + \frac{D \sigma_s^2}{\mu_0} (1 - P) \sin(\alpha + \beta) = 0 \quad \dots (C.3)$$

$$K_1 (\sin^2 \alpha - \sin^2 \beta) - \frac{B_0 \sigma_s}{\mu_0} (\cos(\delta - \alpha) + \cos(\delta + \beta)) + \frac{D \sigma_s^2}{\mu_0} (2P - 1) (1 + \cos(\alpha + \beta)) = 0 \quad \dots (C.4)$$

These solve to give;

$$\alpha = \beta = \sin^{-1} \left(\frac{B_0 \sigma_s \sin \delta}{2K_1 \mu_0 + D \sigma_s^2} \right) \quad \dots (C.5)$$

and;

$$P = 1/2 + \frac{B_0 \cos \delta}{2D\sigma_s \cos \alpha} \quad \dots(C.6)$$

The torque on the unsaturated sample can be expressed readily in terms of the parameters already described; it is simply the sum of the torques produced by each domain phase separately in the applied field;

$$T = B_0 \sigma_s (P \sin(\delta - \alpha) - (1 - P) \sin(\delta + \beta)) \quad \dots(C.7)$$

which simplifies to;

$$T = B_0 \sigma_s ((2P - 1) \cos \alpha \sin \delta - \sin \alpha \cos \delta) \quad \dots(C.8)$$

given the equality of α and β . Invoking the explicit expression for α given in equation C.5 completes the reduction to yield, for conditions where $P < 1$, that is in the unsaturated case;

$$T = \frac{B_0^2}{2D} \sin 2\delta \left(1 - \frac{D\sigma_s^2}{2K_1 \mu_0 + D\sigma_s^2} \right) \quad \dots(C.9)$$

Note that equation C.9 refers to the case where only the K_1 anisotropy constant is finite and, incidentally, that the shape anisotropy of the ellipsoid is included as an additional quantity in this anisotropy.

APPENDIX D : A DATA ACQUISITION
PROGRAM FOR THE NEW MAGNETOMETER

The following program, written in BASIC, obtains five 90-point torque curves for a 0 to π interval and carries out all the corrective processes mentioned in chapter 6, section 6.6.2. The angular data is stored in the dimensioned variables MU(I,D) where I runs from 1 to 90 and D runs from 2 to 6. The torque data is stored in the variables BA(I,D). The program prints out all corrected data along with an index number for a data point pair and a time at which each data point pair was taken.

```

4010 REM:INITIALISING INTERFACE
4020 POKE1,0:POKE2,148:AX=1:NX=1:TX=1
4030 REM:TAKING SAMPLE CHARACTERISTICS
4040 PRINT"TORQUE MAGNETOMETER PROGRAMME"
4050 PRINT"SWITCH PRINTER ON"
4060 INPUT"VOLUME OF SAMPLE IN CC",V
4070 INPUT"MASS OF SAMPLE IN GRAMS",MA
4080 INPUT"PRECISE ANGLE OF EASY AXIS (DEGREES)",EA
4090 EA=EA*PI/180
4100 REM:DIMENSIONING NECESSARY VARIABLES
4110 DIMBA(91,5):DIMTI(90,5):DIMH(5)
4120 DIMAS(90,5):DIMMP(90,5):DIMC(8)
4130 DIMA(8,5):DIMB(8,5):DIMMQ(90,5)
4140 DIMT(90):DIMD(8):DIMEE(5)
4150 DIMMU(91,5):DIMFF(5):DIMR(8,5)
4160 DIMF(13):DIMG(6):DIMBB(6)
4170 REM:CALIBRATING POSITION POTENTIOMETER
4180 FORN=1TO4
4190 PRINT"MAGNET TO"(N-1)*60"DEGREES THEN PRESS RETURN",
4200 GETA$:IFA$=""GOTO4200
4210 PRINT"OK"
4220 AX=7
4230 FORI=1TO20
4240 H(N)=H(N)+USR(5):NEXTI
4250 H(N)=H(N)/20
4260 PRINT"TO D NUMBER 7 READS "H(N)
4270 NEXTN
4280 REM:TORQUE CURVE AQUISITION
4290 E=(H(4)-H(1))/200
4300 FORD=2TO6
4310 PRINT"
4320 PRINT"SET CURRENT TO NEXT VALUE IF NECESSARY"
4330 PRINT"SET MAGNET TO START"

```



```

4900 FORK=2T089
4910 IFBA<K,D>>CCTHEN4930
4920 CC=BA<K,D>:EE<D>=(BA<K-1,D>+BA<K,D>+BA<K+1,D>)/3
4930 NEXTK
4940 REM:AMPLITUDE AND DISTORTION DETERMINATION
4950 FORK=2T090:TT=TT+BA<K,D>*(MU<K+1,D>-MU<K-1,D>)/(2*pi)
4960 NEXTK
4970 TT=TT+BA<1,D>*(MU<2,D>-MU<90,D>+pi)/(2*pi)
4980 G<D+1>=(DD<D>-EE<D>)/2
4990 FF<D>=TT-(DD<D>+EE<D>)/2
5000 REM:TORQUE OFFSET CORRECTION
5010 FORK=1T090
5020 BA<K,D>=BA<K,D>-TT
5030 NEXTK
5040 REM:DATA PRINT OUT
5045 GOTO5130
5050 OPEN1,4
5060 PRINT#1,"":PRINT#1,"DATA FOR CURVE"D"
5070 FORI=1T090
5080 PRINT#1,"<I",I,"MU="MU<I,D>","BA="BA<I,D>";
5090 PRINT#1,"TI="TI<I,D>"">"
5100 NEXTI
5120 CLOSE1
5130 NEXTD

```

Note that in this particular program, A% = 7 is the address for the position potentiometer analog-to-digital module, and that A% = 6 is the address for the magnetometer analog-to-digital module. These address numbers are explained in section 6.6.2.

APPENDIX E : THE SAMPLING PROGRAM
FOR MEASURING THE ELASTIC-AFTER-
EFFECT AND TIME-CONSTANT OF THE
NEW MAGNETOMETER

The following program allows a sequence of readings of the magnetometer output to be taken at regular intervals of 0.059 seconds, corresponding to the cycle time for the program on the particular microcomputer used (a Commodore PET). Readings are converted to logarithms and printed out in the form illustrated in table E.1. The data provided by the program when set in action just prior to an instantaneous relaxation of the magnetometer head allowed the time-constant and elastic after-effect to be determined (see chapter 6, section 6.6.2).

```

1 OPEN1,4:CMD1,LIST
10 POKE1,0:POKE2,148:AX=1:TX=1:NX=1
20 DIMA(200):AX=3
22 PRINT"PRESS RETURN FOR TRANSDUCER OUTPUT          PREVIEW TO STOP"
23 A=TI
24 IF(TI-A)<200GOTO24
25 PRINTUSR(5)
26 GETB$:IFB$=""GOTO25
30 INPUT"RELAXED OUTPUT",R
40 PRINT"PRESS RETURN TO TRIGGER READING SEQUENCE"
42 GETK$:IFK$=""GOTO42
43 PRINT"OK"
45 C=TI
50 FORI=1TO200
60 A(I)=LOG(ABS(USR(5))+.1-R)
70 NEXTI
75 B=TI
80 OPEN1,4
83 PRINT#1,"TRANSDUCER RELAXATION DATA"
85 FORI=1TO200
90 PRINT#1,""A(I),
100 NEXTI
105 PRINT#1,"" :PRINT#1,"TIME SPREAD="B-C
110 CLOSE1

```

The information of table E.1 is the actual data plotted in figure 6.15 from which results for the magnetometer head were derived.

TABLE E.1

TRANSDUCER RELAXATION DATA

8.09073936	8.1029194	8.09897714	8.10443153	8.11135802	8.1250687	8.1306774
8.13684812	8.09928094	7.75280776	7.18394659	6.64131271	6.20677752	5.8467
2775	5.48935087	5.35233195	5.11259002	5.01794187	4.89858579	4.76302827
70138905	4.60616969	4.52287495	4.45550941	4.30541553	4.29182837	4.17592455
4.09600984	4.07923093	3.852273	4.00914972	3.66612247	3.852273	3.55820113
3.64021428	3.46885603	3.40452518	3.43720782	3.13983262	3.37873817	3.0087
1982	3.26193532	2.89591194	3.09557761	2.89591194	2.83907846	2.89591194
57261223	2.83907846	2.31253542	2.6461748	2.20827441	2.40694511	2.20827441
2.09186406	2.31253542	2.09186406	2.31253542	2.09186406	2.09186406	1.96009
478	1.96009478	1.96009478	1.62924054	1.96009478	1.41098697	1.9
6009478	1.13140211	1.80828877	1.13140211	1.41098697	1.62924054	1.13140211
1.62924054	1.13140211	1.80828877	1.13140211	1.62924054	.741937346	1.41098
697	.741937346	.741937346	.741937346	.741937346	1.41098697	.741937346
1098697	.741937346	1.13140211	.741937346	1.13140211	1.13140211	.741937346
1.13140211	.741937346	1.13140211	.741937346	.741937346	.741937346	.741937
346	1.13140211	.741937346	1.13140211	.0953101813	1.13140211	.741937346
41937346	.741937346	.741937346	.741937346	.741937346	1.13140211	.741937346
1.13140211	.741937346	.741937346	1.13140211	.741937346	.741937346	.74193
7346	.741937346	.741937346	.741937346	.741937346	.0953101813	.741937346
0953101813	.0953101813	.741937346	.0953101813	.741937346	.0953101813	.7419
37346	.741937346	.741937346	.0953101813	.0953101813	.0953101813	.0953101813
.0953101813	.0953101813	.0953101813	.741937346	.0953101813	.741937346	.0
953101813	.0953101813	.0953101813	-2.30258508	.0953101813	-2.30258508	.09531
01813	-2.30258508	.0953101813	.0953101813	.0953101813	.0953101813	-2.3025850
8	.0953101813	.0953101813	.0953101813	.0953101813	.0953101813	.0953101813
.0953101813	.0953101813	.0953101813	.0953101813	.0953101813	.0953101813	.0953101813
0953101813	.0953101813	.0953101813	.741937346	.741937346	.0953101813	.0953
101813	.0953101813	.0953101813	.0953101813	.741937346	.0953101813	.0953101
813	.0953101813	.0953101813	.0953101813	.0953101813	.0953101813	.095310181
3	.0953101813	.0953101813	.0953101813	.0953101813	.0953101813	.095310181
0953101813	.0953101813	.0953101813	.0953101813	-2.30258508	-2.30258508	.
TIME SPREAD=	726					

APPENDIX F : THE PROGRAM USED
IN THE COBALT EXPERIMENT

The following program was annexed to the acquisition program of Appendix D and performed the Fourier analysis of the corrected data obtained by it. The program takes about 15 minutes to run on a Commodore PET, produces values for the first three anisotropy constants (uniaxial materials) and prints these out on an attached printer. The program also shows the shear corrected torque curve on the video display of the computer.

```

5140 REM:SHEAR CORRECTION
5150 BB<1>=1.618;BB<2>=1.618;BB<3>=1.618;BB<4>=1.618;BB<5>=1.618
5160 FORJ=1T05
5170 PP=TM*1000/(MA*MS*BB<J>*G<5>)
5180 FORN=1T090
5190 LL=PP*BA<N,J>
5200 AS<N,J>=MU<N,J>+ATN(LL/(ABS<1-LL↑2>↑.5))
5210 NEXTN:NEXTJ
5220 REM:FOURIER ANALYSIS
5230 FORN=1T05:FORI=1T08
5240 A<I,N>=0;B<I,N>=0
5250 A<I,N>=(AS<1,N>-AS<89,N>+π)*BA<90,N>*COS<2*I*AS<90,N>)
5260 B<I,N>=(AS<1,N>-AS<89,N>+π)*BA<90,N>*SIN<2*I*AS<90,N>)
5270 A<I,N>=A<I,N>+(AS<2,N>-AS<90,N>+π)*BA<1,N>*COS<2*I*AS<1,N>)
5280 B<I,N>=B<I,N>+(AS<2,N>-AS<90,N>+π)*BA<1,N>*SIN<2*I*AS<1,N>)
5290 FORJ=2T089
5300 A<I,N>=A<I,N>+(AS<J+1,N>-AS<J-1,N>)*BA<J,N>*COS<2*I*AS<J,N>)
5310 B<I,N>=B<I,N>+(AS<J+1,N>-AS<J-1,N>)*BA<J,N>*SIN<2*I*AS<J,N>)
5320 NEXTJ
5330 A<I,N>=A<I,N>/π;B<I,N>=B<I,N>/π
5340 NEXTI
5350 NEXTN
5360 REM:FINDING IN-PHASE AND OUT-OF-PHASE HARMONICS
5370 FORN=1T08
5380 D<N>=0
5390 C<N>=0
5400 FORJ=1T05
5410 R<N,J>=A<N,J>*SIN<EA*2*N>-B<N,J>*COS<EA*2*N>
5420 D<N>=D<N>+R<N,J>/5
5430 C<N>=C<N>+(A<N,J>*(COS<EA*2*N>)+B<N,J>*(SIN<EA*2*N>))/5
5440 NEXTJ:NEXTN
5450 REM:ERROR ANALYSIS
5460 LS=0
5470 SL=1
5480 IFABS<D<2>>>ABS<D<1>>THENSL=2

```



```

6090 IFINT(8*T(J+40))=5THENPRINT"-";GOTO6120
6100 IFINT(8*T(J+40))=6THENPRINT"-";GOTO6120
6110 IFINT(8*T(J+40))=7THENPRINT"-";GOTO6120
6120 FORI=0TOT(J)
6130 PRINT" ";
6140 NEXTI
6150 NEXTJ
6160 GETK#:IFK#=""GOTO6160
6170 REM:ALTERNATIVE FOURIER ANALYSIS
6180 FORN=1TO5;FORI=1TO8
6190 A(I,N)=0;B(I,N)=0
6200 A(I,N)=BA(90,N)*(SIN(2*I*(AS(1,N)+PI))-SIN(2*I*AS(89,N)))
6210 B(I,N)=BA(90,N)*(COS(2*I*(AS(1,N)+PI))-COS(2*I*AS(89,N)))
6220 A(I,N)=A(I,N)+BA(1,N)*(SIN(2*I*(AS(2,N)+PI))-SIN(2*I*AS(90,N)))
6230 B(I,N)=B(I,N)+BA(1,N)*(COS(2*I*(AS(2,N)+PI))-COS(2*I*AS(90,N)))
6240 FORJ=2TO89
6250 A(I,N)=A(I,N)+BA(J,N)*(SIN(2*I*AS(J+1,N))-SIN(2*I*AS(J-1,N)))
6260 B(I,N)=B(I,N)+BA(J,N)*(COS(2*I*AS(J+1,N))-COS(2*I*AS(J-1,N)))
6270 NEXTJ
6280 A(I,N)=A(I,N)/(I*PI*2);B(I,N)=-B(I,N)/(I*PI*2)
6290 NEXTI
6300 NEXTN
6310 GOTO5360

```

APPENDIX G : THE COBALT DATA

The following tables are a compilation of the cobalt anisotropy data derived in the present work. The Fourier coefficients of the torque curves are also given; expressed as an energy per unit volume. Interpolated values for the magnetisation are given (from the data of Myers and Sucksmith, 1951) and the number N refers to the number of experimental runs of the magnetometer, in which on each occasion five separate torque curves were taken, which were carried out to derive the given anisotropies. Magnetisation values are not given with the basal-plane data since, for these, no shear correction was required and σ_s values were therefore irrelevant.

ANISOTROPY DATA FOR COBALT SAMPLE Nö 4

TEMP (K)	N	D (J/M ³)	K ₄ (J/M ³)
85.5	1	2010	12050
94	1	2040	12210
94.5	1	2020	12090
117	1	1970	11810
145	1	1960	11740
160	1	1930	11560
183	1	1810	10870
192	1	1800	10810
206	1	1730	10360
225	1	1620	9700
239	1	1540	9220
255.5	1	1390	8340
271	1	1260	7580
290.5	1	1130	6803
293	6	995	5970
309	1	887	5320
324	1	725	4350
337	1	578	3470
346	1	568	3410
356	1	459	2750
369	1	368	2210
381	1	313	1880
393	1	287	1720
405	1	188	1130
417	1	138	830

TABLE G.1

TABLE G-2

TEMP (K)	N	σ_s (EMU/G)	A (J/M ³)	B (J/M ³)	C (J/M ³)	K ₁ (J/M ³)	K ₂ (J/M ³)	K ₃ (J/M ³)
90	6	162.50	904100	-31700	-1900	835000	78500	-10000
103	1	162.46	894300	-29200	-300	835000	60800	-1600
119	1	162.41	888100	-30900	-100	826000	62600	-500
125	1	162.39	893500	-35200	-4000	811000	102700	-21500
139	1	162.34	890700	-34000	-3200	813000	93700	-17100
150	1	162.31	870300	-33400	-2800	795000	89500	-15100
165	1	162.26	862300	-36100	-3000	781000	96400	-16100
166	1	162.26	867500	-39000	-2500	782000	98200	-13500
182	1	162.21	843300	-39500	-2500	757000	98700	-13200
192	1	162.15	835900	-41500	+20	753000	82800	+100
204	1	162.13	825100	-45400	-4100	722000	123600	-21900
205	1	162.13	823700	-44300	-2000	729000	104900	-10900
219	1	162.09	806500	-44400	-2900	709000	111900	-15400
224	1	162.07	783300	-48200	-2000	691000	112000	-10400
233	1	162.04	781000	-45800	-1500	685000	103500	-8000
239	1	162.02	769600	-47400	-2600	667000	115500	-13800
244	1	162.01	760300	-47200	-3000	657000	118200	-15900
249	2	161.99	751700	-45800	-1700	655000	105100	-9000
255	1	161.97	729900	-52000	-2600	618000	125100	-14100
262	1	161.95	721200	-50400	-3500	610000	128500	-18500
268	1	161.93	699200	-50600	-2000	592000	117200	-10700
289	1	161.86	657000	-52600	-2900	543000	128800	-15700
293	10	161.83	643600	-49100	-2480	538000	118000	-13200
297	1	161.80	633000	-48900	-1700	530000	111600	-9200
309	1	161.63	605500	-49200	-1700	502000	111800	-8900
318	1	161.51	582500	-49100	-2400	477000	117600	-12900
325	1	161.42	559400	-48500	-2500	455000	116800	-13200
337	1	161.26	527700	-49700	-2800	420000	121700	-14900
358	1	160.98	471900	-48300	-1400	371000	108100	-7700
372	1	160.79	426400	-45400	-2200	329000	108600	-11900
373	1	160.75	425800	-47800	-1700	325000	109500	-9300
386	1	160.60	397500	-46700	-2400	297000	112300	-12600
393	1	160.46	375700	-47100	-1800	276000	108800	-9700
400	1	160.33	354600	-46900	-2000	255000	109300	-10400
406	1	160.21	329500	-42700	-3000	231000	109700	-16200
419	1	159.96	299900	-45500	-1700	204000	104100	-8800
423	1	159.88	288100	-45500	-1400	193000	101900	-7300
434	1	159.66	251600	-44600	-1400	158000	100800	-7700
448	1	159.39	222600	-43700	-1800	130000	101400	-9400
458	1	159.20	196100	-42700	-1300	107000	98500	-6800
468	1	158.99	172500	-41800	-1500	84300	95800	-8100
474	1	158.75	148600	-42200	-1700	59100	98000	-9100
488	1	158.56	121300	-40400	-1200	36900	90400	-6400
494	1	158.43	108100	-39500	-1200	28500	88700	-6500
503	2	158.23	88200	-40100	-1100	4500	89400	-6100
510	1	158.08	71900	-37200	-1000	-5400	82400	-5400
520	1	157.86	54100	-36700	-1200	-22900	83000	-6400
528	1	157.69	26500	-37100	-1600	-52400	87000	-9600
538	1	157.47	9500	-36300	-1200	-66800	82400	-6500
548	1	157.25	-10600	-34900	0	-80300	69700	0
557	1	157.03	-36700	-37500	+900	-109000	67900	+4700
566	1	156.74	-45400	-30600	+900	-104000	54300	+4600
576	1	156.41	-60400	-30100	+150	-120000	58900	+800
586	1	156.07	-77600	-28600	-100	-135000	57800	-400
593	1	155.84	-94800	-29300	-500	-135000	62900	-2900
597	1	155.71	-103800	-28300	-800	-163000	63400	-4300
604	1	155.48	-107100	-27700	-900	-165000	62200	-4600
607	1	155.38	-118200	-28100	-1200	-178000	65800	-6400

ANISOTROPY DATA FOR COBALT SAMPLES Nö2 AND Nö3

TEMP (K)	N	σ_s (EMU/G)	A (J/M ³)	B (J/M ³)	C (J/M ³)	K ₁ (J/M ³)	K ₂ (J/M ³)	K ₃ (J/M ³)
108	2	162.44	887000	-37600	-1800	806000	89600	-9600
112	1	162.43	879000	-39100	-4000	789000	110500	-21500
130	1	162.37	882000	-42700	-600	794000	90400	-3400
135	1	162.35	870000	-39800	-3800	779000	110000	-20300
147	1	162.31	868000	-41900	-1700	779000	97500	-9100
166	2	162.26	856000	-40800	-4300	762000	116000	-22700
174	1	162.24	843000	-49300	-2000	738000	114000	-10500
176	1	162.23	844000	-40300	-5800	746000	127000	-31000
192	1	162.15	826000	-45000	-3100	727000	115000	-16500
194	1	162.15	829000	-44600	-4000	728000	121000	-21200
201	2	162.14	819000	-41200	-3500	727000	110000	-18400
204	1	162.13	812000	-39200	-5400	717000	121000	-28700
213	1	162.11	800000	-45900	-2100	702000	109000	-11100
227	1	162.06	776000	-46700	-4100	670000	127000	-22100
228	1	162.05	780000	-45400	-4700	675000	129000	-25200
232	1	162.04	773000	-48200	-2000	671000	112000	-10600
233	1	162.04	768000	-46600	-3500	664000	122000	-18900
236	1	161.97	732000	-49700	-5100	617000	140000	-27300
265	1	161.94	715000	-48500	-4300	605000	131000	-22900
272	1	161.92	696000	-53200	-900	587000	114000	-5000
277	1	161.90	683000	-50600	-2700	574000	123000	-14600
282	1	161.89	673000	-52500	-4000	556000	137000	-21400
289	1	161.86	662000	-53200	-4200	543000	140000	-22400
297	6	161.80	629000	-49500	-3700	519000	128000	-19600
← SAMPLE Nö 2 ↑								
↓ SAMPLE Nö 3 →								
91	3	162.54	886000	-26900	-7500	810000	114000	-40200
96	1	162.49	882000	-29900	-6600	802000	113000	-35100
106	1	162.47	879000	-29800	-7000	801000	113000	-37200
117	1	162.41	877000	-30700	-5700	799000	107000	-30400
129	1	162.38	870000	-32500	-5700	788000	111000	-30600
131	1	162.31	860000	-34900	-4200	778000	103000	-22200
162	1	162.28	836000	-35000	-5200	770000	112000	-27700
168	1	162.26	846000	-37200	-3900	760000	106000	-21000
172	1	162.24	843000	-28300	-5000	772000	96100	-26400
193	1	162.15	821000	-39500	-4300	729000	113000	-22700
215	1	162.10	794000	-43700	-2000	701000	104000	-10800
217	1	162.09	791000	-44300	-3400	692000	116000	-18200
234	1	162.04	763000	-46200	-1900	665000	107000	-10000
233	1	162.01	750000	-46900	-2700	648000	115000	-14300
236	1	161.97	722000	-44900	-4400	619000	125000	-23400
264	1	161.95	709000	-50000	-1100	606000	108000	-5600
270	1	161.93	697000	-50400	-2500	589000	121000	-13300
280	1	161.89	679000	-51300	-2000	570000	119000	-10700
297	6	161.80	615000	-52500	-100	510000	106000	-500

TABLE G.3

APPENDIX H : THE MAGNETOSTRICTIVE
CONTRIBUTION TO THE MEASUREMENTS
OF THE ANISOTROPY OF COBALT

The following derivation is given by Takahashi et al. (1978).

The magnetoelastic contribution to the magneto-crystalline anisotropy constants for the HCP structure is given by Birss (1966) and by Brooks and Goodings (1968) for K_1 and K_2 ;

$$\Delta K_1 = -R_0((C_{11}+C_{12})(\lambda_A+\lambda_B)+2\lambda_C C_{13})-(R_0+R_1)(C_{13}(\lambda_A+\lambda_B)+C_{33}\lambda_C) - 1/2 (-\lambda_A-\lambda_C+4\lambda_D)^2 C_{44} \dots(H.1)$$

$$\Delta K_2 = -1/2 C_{11}(\lambda_A^2+\lambda_B^2)-C_{12}\lambda_A\lambda_B-C_{13}\lambda_C(\lambda_A+\lambda_B) - 1/2 C_{33}\lambda_C^2+1/2 C_{44}(-\lambda_A-\lambda_C+4\lambda_D)^2 \dots(H.2)$$

where λ_A , λ_B , λ_C and λ_D are the magnetostriction constants (an alternative convention to those of chapter 2, section 2.5). The C_{ij} are the elastic stiffness constants and R_0 and $R_0 + R_1$ are the anomalous thermal expansions perpendicular and parallel to the c-axis respectively. The expansion data is not, at the present time, available for cobalt.

The magnetoelastic effects in K_2 can, by inspection of equation H.2, be derived without a knowledge of the thermal expansion data. Using $\lambda_A = -45 \times 10^{-6}$, $\lambda_B = -95 \times 10^{-6}$, $\lambda_C = 110 \times 10^{-6}$ and $\lambda_D = -100 \times 10^{-6}$ from Bezorth (1954), and using $C_{11} = 3.07 \times 10^{11}$ N/m², $C_{12} = 1.65 \times 10^{11}$ N/m², $C_{13} = 1.03 \times 10^{11}$ N/m², $C_{33} = 3.58 \times 10^{11}$ N/m² and $C_{44} = 0.76 \times 10^{11}$ N/m² at 300 K from McSkimmin (1955), a contribution to K_2 of

$3 \times 10^3 \text{ J/m}^3$ can be demonstrated at room temperature. At 600 K the value is found to be $\approx 1.7 \times 10^3 \text{ J/m}^3$ using $\lambda_A = -14 \times 10^{-6}$, $\lambda_B = -65.3 \times 10^{-6}$, $\lambda_C = 86 \times 10^{-6}$ and $\lambda_D = -58.2 \times 10^{-6}$ from Tsukiji (1969) and $C_{11} = 2.4 \times 10^{11} \text{ N/m}^2$, $C_{12} = 2.4 \times 10^{11} \text{ N/m}^2$, $C_{13} = 1.33 \times 10^{11} \text{ N/m}^2$, $C_{33} = 2.5 \times 10^{11} \text{ N/m}^2$ and $C_{44} = 0.45 \times 10^{11} \text{ N/m}^2$ from Masumoto et al. (1967). Thus the contribution to K_2 by magnetoelastic effects was, at room temperature, smaller by a factor of 100 than the measured values of K_2 and, at 600 K, smaller by a factor of 10.

APPENDIX I : THE MAGNETOMETER
PROGRAM USED DURING THE WORK
ON TERBIUM/GADOLINIUM ALLOYS

The following program was used in the analysis of the terbium/gadolinium alloys. It is a longer program than that used in the cobalt analysis but less sophisticated in both the method of data collection and in the processing of the obtained torque curves (see chapter 6, section 6.6.2). The program does, however, allow a choice of crystal symmetries to be studied. One torque curve only is taken during each run. Execution, for a 60-point analysis takes about two minutes. The analysis of K_4 only was carried out using this program since the K_1 values were derived from a torque gradient method (from the X-Y recorder plots) due to the failure of the available fields to saturate the high terbium samples over the full angular range of the field.

```

0 REM:MAGNETOMETER PROGRAMME
10 POKE1,0:POKE2,148:AX=1:NX=1:TX=1:REM INITIALISATION FOR INTERFACE
15 REM:AA IS ANGLE A/D ADDRESS NO.,TA IS MAGNETOMETER ADDRESS NO.
16 AA=6:TA=1
20 CO=0:TT=TI:REM ZERO TIMER,ZERO COUNTER
30 REM:INPUT DATA FOR EXPERIMENT
40 GOSUB1000
50 REM:READINGS TAKEN FROM MAGNETOMETER
60 GOSUB 2000
70 REM:TORQUE READINGS MULTIPLIED BY MAGNETOMETER TORQUE FACTOR
80 REM ANGLES CONVERTED TO RADIANS; SHEARING CORRECTION APPLIED
90 GOSUB 3000
100 REM:FOURIER ANALYSIS ROUTINE
110 GOSUB4000
120 REM:DISPLAY FOURIER COEFFS. & OTHER IMPORTANT DATA
130 GOSUB5000
140 REM:CONVERT FOURIER COEFFS. TO SINE COEFFS. AND PHASE ANGLES
150 GOSUB6000
160 REM:RELATE SINE COEFFS. TO ANISOTROPY CONSTANTS
170 GOSUB7000
500 PRINT"ANOTHER RUN ? (Y OR N)"
502 GETZ$:IFZ$=""THEN502
503 IFZ$="N"THEN970

```

```

505 CO=10
510 INPUT"WHAT IS NEW FIELD STRENGTH ";B0:PRINT
520 GOTO50
970 PRINT:PRINT" PROGRAMME ENDS.":PRINT" TIME TAKEN WAS ";
980 PRINTINT((TI-TT)/60);" SECONDS.":PRINT:PRINT:PRINT
990 END
1000 PRINT"TORQUE MAGNETOMETER PROGRAMME"
1001 PRINT"BEFORE ANY FURTHER ACTION, ENSURE THAT ALL UNITS HAVE BEEN";
1002 PRINT" SWITCHED ON FOR AT LEAST 5 MINUTES, TO ENSURE THAT THERMAL "
1005 PRINT" STABILITY IS ATTAINED"
1010 PRINT"REDUCE MAG. FIELD TO ZERO SO THAT MAGNETOMETER OFFSET MAY";
1011 PRINT" BE MEASURED.":PRINT
1012 PRINT"WHEN READY PRESS RETURN.":PRINT
1013 GETA$:IFA$=""THEN1013
1014 A%=TA:FORI=1TO100:T0=T0+USR(5):NEXTI
1015 T0=INT(T0/100)
1016 INPUT"WHAT IS SAMPLE SYMMETRY (HEX. OR CUBIC) ";S$:PRINT:IFS$<"H"GOTO1025
1017 PRINT"WHAT IS ORIENTATION OF SAMPLE WRT BASAL":PRINT
1018 INPUT"PLANE (PAR. OR PERP.) ";O$:PRINT
1019 IFO$>"PAX."THENINPUT"WHAT IS VALUE OF PHI ";TH:PRINT
1020 GOTO1030
1025 INPUT"SAMPLE ORIENTATION (IE. 100,110,ETC.) ";CO$:PRINT
1030 K=1:REM:K IS MAGNETOMETER CALIBRATION FACTOR
1035 PRINT"MAG. FIELD MAY BE SWITCHED BACK ON NOW.":PRINT
1040 INPUT"FIELD STRENGTH (TESLA) =";B0:PRINT""
1055 PRINT"MAGNET MUST BE ROTATED FROM LOW ANGLE TO HIGH ANGLE.":PRINT
1060 PRINT"ROTATE MAGNET TO STARTING POSITION":PRINT""
1070 INPUT"WHAT IS STARTING ANGLE ";P:A%=AA:A=USR(5):PRINT
1080 PRINT"ROTATE TO FINAL POSITION - >180DEG.ROUND"
1090 INPUT"WHAT IS FINAL ANGLE ";Q:A%=AA:B=USR(5):PRINT
1092 IFB=ATHENPRINT"YOU HAVE NOT ROTATED THE MAGNET":GOTO1055
1100 REM:NEXT FINDS EQNS.FOR CONVERSION OF A/D OUTPUT TO ANGLE (RAD.).
1110 M=(A-B)*180/((P-Q)*PI):C=A-P*M*PI/180
1120 DEF FNA(V)=M*V+C :DEF FNB(W)=(W-C)/M
1130 RETURN
2000 REM:DATA COLLECTION SUBROUTINE
2070 ZZ=0
2080 IFCO=10THEN2095
2090 INPUT"NUMBER OF READINGS TO BE TAKEN ";NO:DIM AT(NO,2):DIM ER(NO):PRINT
2092 DIM ET(NO)
2095 E=(B-A)/(10*NO)
2100 FORI=0TONO:J=PI*I/NO+P*PI/180:AT(I,1)=FNA(J):NEXTI
2110 PRINT"RESET MAGNET TO START POSITION.":PRINT
2120 PRINT"WHEN READY TO TAKE READINGS PRESS RETURN":PRINT
2130 PRINT"THEN ROTATE MAGNET SLOWLY.":PRINT
2135 GETY$:IFY$=""GOTO2135
2136 A%=AA:R=0:FORI=1TO20:R=R+USR(5):NEXT
2137 R=R/20:IFR>AT(0,1)THENPRINT"YOU HAVE NOT RESET THE MAGNET":GOTO2110
2138 PRINT"OK"
2140 FORI=0TONO
2150 A%=AA:R=USR(5)
2160 IFR<AT(I,1)GOTO2150
2170 IFR>(AT(I,1)+E)GOTO2210
2180 A%=TA:AT(I,2)=USR(5):PRINT I:NEXTI
2185 IFZZ>0GOTO2250
2190 PRINT"ALL READINGS HAVE BEEN TAKEN.":PRINT
2200 GOTO2500
2210 ER(ZZ)=I:ZZ=ZZ+1:NEXTI
2250 FORJ=0TOZZ:ET(J)=ER(J):NEXTJ
2260 XX=ZZ:ZZ=0

```

```

2310 PRINT"SEVERAL OF THE DATA POINTS HAVE BEEN MISSED.":PRINT
2315 PRINT"POINTS MISSED ARE :-":FORI=0TOXX-1:PRINTET(I);:NEXTI:PRINT
2320 PRINT"RESET MAGNET TO START POSITION.":PRINT
2330 PRINT"WHEN READY TO RETAKE THESE READINGS PRESS RETURN. ":PRINT
2340 GETA$: IFA$=""THEN2340
2345 PRINT"OK"
2350 FORI=0TOXX-1
2360 AX=AA:R=USR(5)
2370 IFR<AT(ET(I),1)GOTO2360
2380 IFR>(AT(ET(I),1)+E)GOTO2400
2390 AX=TA:AT(ET(I),2)=USR(5):PRINT ET(I):NEXTI
2395 IFZZ>0GOTO2250
2396 GOTO2410
2400 ER(ZZ)=ET(I):ZZ=ZZ+1:NEXTI
2405 IFZZ>0GOTO2250
2410 PRINT"ALL READINGS HAVE BEEN TAKEN.":PRINT
2500 RETURN
3000 REM:DATA CORRECTION SUBROUTINE
3100 FORI=0TONO
3110 AT(I,2)=(AT(I,2)-T0)*K
3120 AT(I,1)=FNB(AT(I,1))
3130 NEXTI
3140 RETURN
4000 REM:FOURIER ANALYSIS ROUTINE
4090 IFCO=10THEN4120
4100 INPUT"ENTER HIGHEST FOURIER COEFF.WANTED ":F:PRINT
4110 DIM A(F):DIM B(F):DIMC(F):DIMD(F)
4120 FORI=0TOFSTEP2
4130 A(I)=(AT(1,1)-AT(0,1))*AT(0,2)*COS(I*AT(0,1))
4140 B(I)=(AT(1,1)-AT(0,1))*AT(0,2)*SIN(I*AT(0,1))
4150 A(I)=A(I)+(AT(NO,1)-AT((NO-1),1))*AT(NO,2)*COS(I*AT(NO,1))
4160 B(I)=B(I)+(AT(NO,1)-AT((NO-1),1))*AT(NO,2)*SIN(I*AT(NO,1))
4170 FORJ=2TO(NO-1)
4180 A(I)=A(I)+(AT((J+1),1)-AT((J-1),1))*AT(J,2)*COS(I*AT(J,1))
4190 B(I)=B(I)+(AT((J+1),1)-AT((J-1),1))*AT(J,2)*SIN(I*AT(J,1))
4200 NEXTJ
4210 A(I)=A(I)/PI:B(I)=B(I)/PI
4220 NEXTI
4230 RETURN
5000 REM:FOURIER COEFFICIENTS DISPLAY
5100 PRINT"J FIELD STRENGTH ",B0:PRINT
5105 PRINT"MAGNETISATION =":MS:PRINT
5110 PRINT" NUMBER OF READINGS ",NO:PRINT
5130 PRINT" FOURIER COEFFICIENTS ARE :-":PRINT
5140 FORI=2TOFSTEP2
5145 A(I)=INT(1E4*A(I))/1E4
5146 B(I)=INT(1E4*B(I))/1E4
5150 PRINT" _ A(";I;")=";A(I),"B(";I;")=";B(I)
5160 NEXTI
5180 RETURN
6000 REM:CONVERSION TO SINE COEFFICINETS AND PHASE ANGLES
6100 PRINT"MIN FORM C(I)SIN(I*X+D) WE HAVE":PRINT
6110 FORI=0TOFSTEP2
6120 C(I)=INT(1E4*((A(I)*A(I)+B(I)*B(I))↑0.5))/1E4
6125 TN=A(I)/(B(I)+1E-30)
6130 D(I)=ATN(TN)
6131 IFTN<0ANDB(I)>0THEND(I)=D(I)+PI

```

```

6132 IFTN>0ANDB(I)<0THEND(I)=D(I)-π
6135 D(I)=INT(1E4*D(I))/1E4
6140 PRINT"C("I")="C(I), "D("I")="D(I)
6150 NEXTI
6170 RETURN
7000 REM: CALCULATION OF ANISOTROPY CONSTANTS
7004 IFCO=10THEN7010
7005 DIMS(F)
7010 FORI=0TOFSTEP2
7020 S(I)=C(I)
7030 IFABS(D(I)-D(2))>2.6ANDABS(D(I)-D(2))<3.8THENS(I)=-S(I)
7040 NEXTI
7090 IFS$<"H"THEN7500
7100 IFO$>"PAX"THEN7300
7200 K4=S(6)/-6
7210 PRINT"K4 ="K4
7220 GOTO7910
7300 K1=-S(2)+2*S(4)-3*S(6)
7310 K2=2*S(4)-8*S(6)
7320 K3=16*S(6)/3
7330 PRINT"K1 ="K1:PRINT:PRINT"K2 ="K2:PRINT:PRINT"K3+"PH"*K4 ="K3
7340 GOTO7710
7500 IFCO$<"100"THEN7600
7510 K1=-2*S(4)
7520 PRINT"K1 ="K1:PRINT
7530 GOTO7710
7600 IFCO$<"110"THEN7700
7610 K1=-1.6*(S(4)-4*S(2))
7620 K2=25.6*(S(4)-1.5*S(2))
7630 PRINT"K1 ="K1:PRINT:PRINT"K2 ="K2:PRINT
7640 GOTO7710
7700 PRINT"SYMMETRY OF AN UNKNOWN TYPE.":PRINT
7710 PRINT"IF YOU WISH TO SEE THE FOURIER COEFFS.ⓧ AGAIN PRESS F . OTHERWISE
RESS";
7720 PRINT" RETURN.":PRINT
7730 OETA$: IFA$=""THEN7730
7740 IFA$="F"THENGOSUB6000:RETURN
7910 RETURN
10000 STOP
READY.

```

APPENDIX J : DATA FOR THE TERBIUM/
GADOLINIUM ALLOYS WITH PROGRAMS FOR
THE TEMPERATURE DEPENDENCE ANALYSIS

Table J.1 gives the easy-axis gradients for samples of the given specification for a range of temperatures. These apply to the uniaxial torque curves (that is, with the 2 θ harmonic fundamental). From these values were calculated the K_1 data given in table J.2 along with magnetisation values derived from Bagguley et al. (1980 a,b). Table J.2 also gives the reduced magnetisations, the inverse Langevin function of the reduced magnetisations and the reduced hyperbolic Bessel function of the inverse Langevin function of the reduced magnetisations. Table J.3 is the interpolated K_4 data as actually measured at the given fields; it is not subject to the uncertainties that surround the extrapolated data (table J.4) for which an arbitrary functional field dependence was assumed.

Programs J.1, J.2 and J.3 helped in the fitting of the theoretical temperature dependences to the anisotropy data (chapter 8, section 8.6). The first program simply derives the inverse Langevin function of a stated reduced magnetisation. Reduced hyperbolic Bessel functions (see Appendix K) were found from a set of tables (see, for example, Joraide, 1980). The second program accomplishes the least-squares fit of all the functional forms cited in section 8.6 from data of the type provided by table J.2. The third program simply reconstructs the theoretical fits from the parameters produced by the previous program, at selected temperatures.

DATA FOR TERBIUM/
GADOLINIUM ALLOYS

INTERPOLATED K_4 DATA FOR Tb_xGd_{1-x} ALLOYS

%Tb	B(T)	T=80K	90K	100K	110K	120K	130K	140K	150K	160K	170K	180K	190K	200K	210K	220K	230K	240K	250K
5	0.41	0.80	0.72	0.64	0.54	0.36	0.23	0.15	0.09	0.04	--	--	--	--	--	--	--	--	--
	0.50	1.13	1.06	0.90	0.67	0.41	0.25	0.18	0.14	--	--	--	--	--	--	--	--	--	--
	0.63	1.40	1.28	1.13	0.88	0.58	0.43	0.29	0.20	0.14	0.13	0.12	0.12	--	--	--	--	--	--
	0.83	1.60	1.49	1.36	1.17	0.80	0.59	0.41	0.27	0.17	0.10	--	--	--	--	--	--	--	--
10	1.20	5.87	4.65	3.61	2.85	2.14	1.57	1.20	0.90	0.66	0.49	0.37	0.28	0.19	--	--	--	--	--
	1.38	6.03	4.81	3.71	2.85	2.20	1.66	1.26	0.94	0.68	0.50	0.34	0.23	0.17	--	--	--	--	--
	1.72	6.21	4.97	3.96	2.97	2.16	1.61	1.24	0.90	0.63	0.46	0.30	0.17	0.06	--	--	--	--	--
	1.86	6.16	5.06	3.89	3.06	2.33	1.79	1.32	0.97	0.69	0.49	0.26	0.16	0.00	--	--	--	--	--
30	0.42	1.10	1.10	1.05	0.89	0.71	0.55	0.41	0.31	0.22	0.15	0.10	0.07	0.05	0.04	0.03	0.02	0.01	0.01
	0.50	1.28	1.20	1.08	0.91	0.74	0.57	0.43	0.32	0.24	0.16	0.12	0.09	0.06	0.05	0.04	0.04	--	--
	0.63	1.42	1.35	1.26	1.07	0.83	0.59	0.45	0.34	0.25	0.18	0.12	0.08	0.05	0.03	0.02	0.01	0.01	0.00
	0.83	1.59	1.40	1.35	1.15	0.90	0.68	0.51	0.37	0.27	0.19	0.12	0.07	0.04	0.02	--	--	--	--
50	1.20	3.09	2.55	2.08	1.64	1.22	0.88	0.65	0.48	0.33	0.21	0.15	0.08	0.06	--	--	--	--	--
	1.32	3.16	2.66	2.12	1.64	1.24	0.92	0.64	0.44	0.30	0.21	0.13	0.08	0.04	--	--	--	--	--
	1.49	3.17	2.69	2.19	1.70	1.26	0.90	0.64	0.47	0.30	0.17	0.12	0.06	0.01	--	--	--	--	--
	1.86	3.72	2.97	2.28	1.76	1.31	0.93	--	--	--	--	--	--	--	--	--	--	--	--
75	1.20	--	3.98	3.39	2.88	2.32	1.74	1.24	0.85	0.56	0.36	0.21	0.09	0.05	--	--	--	--	--
	1.27	--	4.53	3.80	3.09	2.33	1.72	1.22	0.87	0.60	0.39	0.21	0.14	0.05	0.03	--	--	--	--
	1.38	--	5.11	4.17	3.25	2.43	1.88	1.28	0.90	0.62	0.44	0.26	0.14	0.04	--	--	--	--	--
	1.49	--	5.22	4.15	3.25	2.43	1.77	1.26	0.90	0.62	0.41	0.27	0.16	0.07	0.04	--	--	--	--
100	1.86	--	5.68	4.42	3.51	2.61	1.92	1.40	0.96	0.60	0.40	0.26	0.13	0.06	--	--	--	--	--
	1.20	5.30	--	--	--	--	--	--	--	--	--	--	--	--	--	--	--	--	--
	1.38	6.55	--	--	--	--	--	--	--	--	--	--	--	--	--	--	--	--	--
	1.59	7.00	--	--	--	--	--	--	--	--	--	--	--	--	--	--	--	--	--
1.86	7.43	--	--	--	--	--	--	--	--	--	--	--	--	--	--	--	--	--	

The anisotropy constant K_4 ($\times 10^3$ J m⁻³ for 5%, 10%; $\times 10^4$ J m⁻³ for other compositions) measured at various fields and temperatures for six different alloy compositions of gadolinium-terbium.

TABLE J.3

EXTRAPOLATED K_4 DATA FOR Tb_xGd_{1-x} ALLOYS

TABLE J-4

$\%Tb/T(K)$	80	90	100	110	120	130	140
5	0.24	0.23	0.21	0.17	0.12	0.09	0.07
10	0.68	0.58	0.46	0.34	0.25	0.20	0.15
30	2.08	1.74	1.68	1.43	1.10	0.78	0.60
50	4.74	3.67	2.65	1.99	1.47	1.00	0.60
75	--	8.77	6.23	4.58	3.13	2.24	1.68
100	11.36	--	--	--	--	--	--

$\%Tb/T(K)$	150	160	170	180	190	200	210
5	0.04	0.03	--	--	--	--	--
10	0.10	0.07	0.05	0.01	--	--	--
30	0.43	0.32	0.23	0.14	0.07	0.03	0.03
50	0.42	0.17	0.01	--	--	--	--
75	1.15	0.67	0.47	0.38	0.20	0.09	--

The values of the anisotropy constant K_4 ($\times 10^4 \text{ J m}^{-3}$) extrapolated to infinite field using a reciprocal-field plot.

PROGRAM J.1

```

10 PRINT"INVERSE LANGEVIN FUNCTION PROGRAM"
20 INPUT"M(T):";M
30 X=.5
40 A=EXP(X)+EXP(-X)
50 B=EXP(X)-EXP(-X)
60 C=A-B+2*(1+1/(X+2))/A
70 D=B-B+2*(1/X+M)/A
80 E=X
90 X=INT(1000*(X+D/C)+.5)/1000
100 PRINTX
110 IFX=E THEN 20
120 GOTO40

```

PROGRAM J.2

```

10 PRINT"LEAST SQUARES FIT"
20 INPUT"NO OF DATA POINTS:";N
30 DIMK(N),L(N),M(N),I(N)
40 FORL=1TON
50 INPUT"M(T),I(5/2),K1: ";M(L),I(L),K(L)
51 NEXT L
56 INPUT"ANALYSIS NUMBER";TT
62 PRINT"MANUAL (M) OR AUTOMATIC (A) ITERATION ROUTINE ?"
64 GET A$;IF A$=""THEN64
66 IF A$="M" THEN 2000
68 IF A$<"A"THEN 64
70 M1=0;M2=0;CO=0;DO=0;EO=0;N1=0;N2=0;I=1
75 M1=M1+I
80 GOSUB1000
90 SR=SQ
100 M1=M1+I
110 GOSUB1000
120 IF SQ<SRAND CO=0THEN SR=SQ;CO=10;M1=M1+I;GOTO110
130 IF CO=0THEN CO=20;M1=M1-2*I;GOTO110
140 IF SQ<SR AND CO=10THEN SR=SQ;M1=M1+I;GOTO110
150 IF CO=10THENC0=30;M1=M1-I;M2=M2+I;GOTO110
160 IF SQ<SRAND CO=20THEN SR=SQ;M1=M1-I;GOTO110
170 IF CO=20THENC0=30;M1=M1+I;M2=M2+I;GOTO110
180 IF SQ<SR AND CO=30THEN SR=SQ;M2=M2+I;GOTO110
190 IF CO=30THEN CO=40;M2=M2-I;GOTO110
192 IF SQ<SR AND CO=40THEN SR=SQ;M2=M2-I;GOTO110
194 IF SQ>SR AND CO=40 THEN M2=M2+I;GOTO210
210 CO=0
220 IF DO=0 ANDEO=0THEN SS=SR;N1=M1;N2=M2;DO=10;GOTO100

```

```

230 IFDO=10 ANDSR<SS THEN SS=SR:N1=M1:N2=M2:GOTO100
270 IFEO=0 THEN M1=N1+I:M2=N2-I:EO=10:DO=0:GOTO110
280 IF EO=10 AND SR<SS THEN SS=SR:N1=M1:N2=M2:M1=N1+I:M2=N2-I:GOTO110
290 IFEO=10 THEN EO=20:M1=N1-2*I:M2=N2+2*I:GOTO110
300 IF EO=20 AND SR<SS THEN SS=SR:N1=M1:N2=M2:M1=N1-I:M2=N2+I:GOTO110
310 IFEO=20 THEN 320
320 IFI=.001 THEN M1=N1:M2=N2:GOTO340
330 I=I/10:M1=N1:M2=N2:GOTO75
340 PRINT"FINAL RESULT:":GOSUB1000
350 GOTO2000
1000 IFTT=1 THEN GOSUB3000
1001 IFTT=2 THEN GOSUB4000
1002 IFTT=3 THEN GOSUB5000
1003 IFTT=4 THEN GOSUB6000
1004 IFTT=5 THEN GOSUB7000
1005 IFTT=6 THEN GOSUB8000
1050 PRINT"M1:"M1," M2:"M2,"SQ:"SQ
1050 PRINT""
1060 RETURN
2000 INPUT "GUESS M1,M2: ";M1,M2
2001 IFTT=1 THEN GOSUB3000
2002 IFTT=2 THEN GOSUB4000
2003 IFTT=3 THEN GOSUB5000
2004 IFTT=4 THEN GOSUB6000
2005 IFTT=5 THEN GOSUB7000
2006 IFTT=6 THEN GOSUB8000
2060 PRINT SQ
2065 PRINT"NEW ANALYSIS? (Y OR N)"
2066 GETA$:IFA$="" THEN 2066
2067 IFA$="Y" THEN 56
2068 IFA$="N" THEN 2070
2069 IFA$<>"Y" THEN 2066
2070 GOTO2000
3000 SQ=0
3010 FOR P=1 TO N
3020 L(P)=M1*M(P)^M2
3030 SQ=SQ+(L(P)-K(P))^2
3040 NEXT P
3050 RETURN
4000 SQ=0
4010 FOR P=1 TO N
4020 L(P)=M1*I(P)
4030 SQ=SQ+(L(P)-K(P))^2
4040 NEXT P
4050 RETURN
5000 SQ=0
5010 FOR P=1 TO N
5020 L(P)=M1*M(P)^2
5030 SQ=SQ+(L(P)-K(P))^2
5040 NEXT P
5050 RETURN
6000 SQ=0
6010 FOR P=1 TO N
6020 L(P)=M1*I(P)+M2*M(P)^2
6030 SQ=SQ+(L(P)-K(P))^2
6040 NEXT P
6050 RETURN

```

PROGRAM J.3

```
10 DIMT(8);DIMM(8);DIMI(8);DIMJ(8);DIMK(8)
20 INPUT"%TB";TB
30 PRINT"K1 ANALYSIS ?(Y OR N)"
40 GET A$;IFA$=""GOTO40
50 IF A$="N"THEN B$="K4";GOTO120
60 B$="K1"
70 FORN=1TO8
80 INPUT"TEMPERATURE";T(N)
90 INPUT"REDUCED MAGNETISATION";M(N)
100 INPUT"I(5/2)";I(N)
110 NEXTN;GOTO190
120 FORN=1TO8
130 INPUT"TEMP";T(N)
140 INPUT"REDUCED MAGNETISATION";M(N)
150 INPUT"I(5/2)";K(N)
160 INPUT"I(9/2)";J(N)
170 INPUT"I(13/2)";I(N)
180 NEXTN
190 INPUT"A";A
200 INPUT"B";B
210 INPUT"C";C
220 INPUT"D";D
230 INPUT"E";E
240 INPUT"F";F
250 INPUT"G";G
260 OPEN1,4
270 FORN=1TO6;PRINT#1,"";NEXTN
280 PRINT#1,B$,"TB%="TB
290 FORN=1TO8
300 PRINT#1,T(N),A*M(N)+B,C*I(N),D*M(N)+E,I(N)+F*M(N)+G,
310 IFB$="K4"THEN PRINT#1,G*J(N)*K(N);GOTO330
320 PRINT#1,""
330 NEXTN
340 CLOSE1
350 GOTO20
```

APPENDIX K : HYPERBOLIC BESSEL FUNCTIONS

The temperature dependence of the anisotropy constants for the terbium/gadolinium alloys has been given in terms of the reduced hyperbolic Bessel functions. These are derived from Bessel's modified differential equation;

$$x^2 \ddot{y} + x \dot{y} - (x^2 + n^2)y = 0 \quad (n \geq 0) \quad \dots(K.1)$$

which has solutions of the form;

$$I_n(x) = i^{-n} J_n(ix) = \text{Exp}(-in\pi/2) J_n(ix) \quad \dots(K.2)$$

where $J_n(x)$ are ordinary Bessel functions of the first kind. The $I_n(x)$ are termed hyperbolic Bessel functions, and can be expressed in terms of the series;

$$I_n(x) = \sum_{k=0}^{\infty} \frac{(x/2)^{n+2k}}{k! \Gamma(n+k+1)} \quad \dots(K.3)$$

The reduced hyperbolic Bessel functions are defined as;

$$\hat{I}_n(x) = \frac{I_n(x)}{I_{1/2}(x)} \quad \dots(K.4)$$

and thus;

$$\hat{I}_{3/2}(x) = \text{Coth}x - 1/x \quad \dots(K.5)$$

is the familiar Langevin function, $\mathcal{L}(x)$. Using the recurrence relation;

$$\hat{I}_{n+1}(x) = \hat{I}_{n-1}(x) - \frac{2n}{x} \hat{I}_n(x) \quad \dots(K.6)$$

together with equations K.2 and K.3, the following analytic expressions can be derived:

$$\hat{I}_{5/2}(x) = 1 + 3/x^2 - (3/x)\text{Coth}x \quad \dots(K.7)$$

$$\hat{I}_{9/2}(x) = 1 + 45/x^2 + 105/x^4 - (105/x^3 + 10/x)\text{Coth}x \quad \dots(\text{K.8})$$

$$\hat{I}_{13/2}(x) = 1 + 210/x^2 + 4725/x^4 + 10395/x^6 - (21/x + 1260/x^3 + 10395/x^5)\text{Coth}x \quad \dots(\text{K.9})$$

Values for the reduced hyperbolic Bessel functions have been tabulated (see, for example, Joraide, 1980).

REFERENCES

- ABE, K. AND CHIKAZUMI, S. "Computer Controlled Torque Magnetometer for Automatic Determination of Crystal Orientation" Jap. J. Appl. Phys. 15, 619 (1976).
- ABRAHAM, A. AND BLEANEY, B. "Electron Paramagnetic Resonance of Transition Ions" Clarendon Press, Oxford (1970).
- AKULOV, N. "On the Quantum Theory of the Temperature Dependence of the Magnetisation Curve" Z. Phys. 100, 197 (1936).
- ALBERTS, H.L. AND ALBERTS, L. J. De Physique. Supplement to vol 32, C1 - 110 (1971).
- ALDENKAMP, A.A., MARKS, C.P. AND ZIJLSTRA, H. "Frictionless Recording Torque Magnetometer" Rev. Sci. Inst. 31, 544 (1960).
- American Institute of Physics Handbook. McGraw-Hill Book Company, New York (1957), p. 4-54.
- AMIGHIAN, J. "Magnetocrystalline Anisotropy of Nickel-Vanadium Alloys" Ph.D. Thesis, Durham University.(1975).
- APILAT, V. Ya., OLEINIK, G.M. AND EIDEL'MAN, L.G. "Meter for Growth Rate of Single Crystals from the Melt" Prikl. Tekh. Eksp. 3, 216 (1966).
- ASTI, G. AND BOLZONI, F. "Theory of First Order Magnetisation Processes: Uniaxial Anisotropy" J. Mag. Mag. Mat. 20, 29 (1980).
- AUBERT, G. Ph.D. Thesis, Grenoble (1966).
- AUBERT, G. "Magnetic Anisotropy of Ferro- and Ferrimagnets" J. Mag. Mag. Mat. 19, 396 (1980).
- AUBERT, G. "Torque Measurements of the Anisotropy Energy and Magnetisation of Nickel" J. Appl. Phys. 39, 504 (1968).
- AUBERT, G. AND FRAZAU, L. "Measurements of the Anisotropic Magnetisation of Nickel" Phys. Letts. 31A, 54 (1970).

AUTENSHLYUS, N.I., BETIN, Yu.P., DOBROVENSKI, V.V., ZBARSKII, A.Ya., KOTIK, U.I. AND SHENDEROVICH, I.L. "A Device for Controlling the Diameter of Crystals Grown from the Melt" Instr. Exp. Tech. 18, 612 (1975).

BACHMANN, K.J., KIRSCH, H.J. AND VETTER, K.J. "Programmed Czochralski Growth of Metals" J. Cryst. Growth 7, 290 (1970).

BAGGULEY, D.M.S., PARTINGTON, J.P., ROBERTSON, J.A. AND WOODS, R.C. "Magnetisation, AC Susceptibility and Microwave Absorption in Tb and $Tb_{0.3}Gd_{0.7}$ " J. Mag. Mat. 20, 56 (1980 a).

BAGGULEY, D.M.S., PARTINGTON, J.P., ROBERTSON, J.A. AND WOODS, R.C. "Magnetisation and Microwave Absorption in Tb/Gd Alloys" J. Phys. F 10, 967 (1980 b).

BANERJEE, S.K. AND STACEY, F.D. "Methods in Paleomagnetism" ed. D.W. Collinson, K.M. Creer and S.K. Runcorn pp. 470-6.

BARDSLEY, W., HURLE, D.T.J., JOYCE, G.C. AND WILSON, G.C. "The Weighing Method of Automatic Czochralski Growth. II: Control Equipment" J. Cryst. Growth 40, 21 (1977).

BARDSLEY, W., GREEN, G.W., HOLLIDAY, C.H. AND HURLE, D.T.J. "Automatic Control of Czochralski Crystal Growth" J. Cryst. Growth 16, 277 (1972).

BARDSLEY, W., GREEN, G.W. AND HURLE, D.T.J. "The Meniscus in Czochralski Growth" J. Cryst. Growth 23, 341 (1974).

BARNIER, Y., PAUTHENET, R. AND RIMET, G. "Temperature Variation of the Anisotropy Constants and Spontaneous Magnetisation of Cobalt in the Hexagonal Phase" C. R. Acad. Sci. 252, 2839 (1961).

BARNIER, Y., PAUTHENET, R. AND RIMET, G. "Study of the Change in the Easy Direction of Magnetisation in Cobalt" C. R. Acad. Sci. 253, 400 (1961).

BARRON, R. AND HOFFMAN, R.W. "Saturation Magnetisation and Perpendicular Anisotropy of Nickel Films" J. Appl. Phys. 41, 1623 (1970).

BATES, C.A. AND SZYMCZAK, H. "The Phonon-induced Temperature Dependences of the Magnetocrystalline Anisotropy Constants" J. Mag. Mag. Mat. 16, 563 (1980).

BELOGUROV, Yu.P., KOSTENKO, V.I., NECHMIR, V.M. AND RADKEVICH, A.V. "A Multi-range Recording Level Gauge" Prib. I. Syst. Uprav. 8, 48 (1970).

BELOV, K.P., LEVITIN, R.Z. AND PONOMARJOV, B.K. "Anisotropy of Magnetisation and Magnetostriction in Single Crystals of Tb, Dy, Er and Gd in Pulsed Fields up to 150 KOe" J. Appl. Phys. 39, 3285 (1968).

BIRSS, R.R. "Symmetry and Magnetism" 2nd Edition, North Holland p. 193.(1966).

BIRSS, R.R. AND HEGARTY, B.C. "The Magnetisation Process in Nickel Single Crystals: I" Brit. J. Appl. Phys. 17, 1241 (1966).

BIRSS, R.R. AND HEGARTY, B.C. "A Torque Magnetometer for use at High Pressures" J. Sci. Instrum. 44, 621 (1967).

BIRSS, R.R. AND KEELER, G.J. "The Advantages of Using Spherical Harmonics to Analyse Data on Magnetocrystalline Anisotropy and Other Non-linear Anisotropic Properties" Phys. Stat. Sol. B 64, 357 (1974).

BIRSS, R.R., KEELER, G.J. AND LEO, P.D. "Temperature Dependence of the Anisotropic Magnetisation of Terbium" J. Mag. Mag. Mat. 25, 1 (1981).

BIRSS, R.R., KEELER, G.J. AND SHEPHERD, C.H. "A Magnetometer Suitable for Measurements of Magnetocrystalline Anisotropy in a Superconducting Solenoid from 4K to 300K" J. Phys. E 9, 963 (1976).

BIRSS, R.R., KEELER, G.J. AND SHEPHERD, C.H. "Measurements of the Basal Plane Anisotropy Energy of Terbium at Low Temperatures" Physica 86 B, 47 (1977 a).

BIRSS, R.R., KEELER, G.J. AND SHEPHERD, C.H. "Temperature Dependence of the Magnetocrystalline Anisotropy Energy of Terbium in the Basal-Plane" J. Phys. F 7, 1669 (1977 b).

BIRSS, R.R. AND MARTIN, D.J. "The Magnetisation Process in Hexagonal Ferromagnetic and Ferrimagnetic Single Crystals" J. Phys. C 8, 189 (1975).

- BIRSS, R.R. AND SHEPHERD, C.H. "A Capacitance Torquemeter Suitable for Use in a Split-pair Magnet from 4 to 300K" J. Phys. E 11, 935 (1978).
- BIRSS, R.R. AND WALLIS, P.M. "A New Torque Meter or Torque Magnetometer" J. Sci. Instrum. 40, 551 (1963).
- BIRSS, R.R. AND WALLIS, P.M. "A Torque Magnetometer for a Wide Range of Temperatures" J. Sci. Instrum. 42, 322 (1965).
- BIRSS, R.R. AND WALLIS, P.M. "The Temperature Variation of Magnetocrystalline Anisotropy for Nickel and Gadolinium" Proc. Int. Conf. on Magnetism, Nottingham, pp. 744-747 (1964).
- BIRSS, R.R. AND WALLIS, P.M. "Temperature Dependence of Magnetocrystalline Anisotropy" J. Appl. Phys 39, 1347 (1968).
- BLUMBERG, H. "Levitation Correction for the Weighing Method of Automatic Crystal Growth" Krist. und Tech. 15, K23-4 (1980).
- BLY, P.H., CORNER, W.D., TAYLOR, K.N.R. AND DARBY, M.I. "Magnetic Anisotropy of Rare-Earth Metals" J. Appl. Phys. 39, 1336 (1968).
- BOYD, E.L. "Magnetic Anisotropy in Single Crystal Thin Films" I.B.M. J. Res. Dev. 4, 116 (1960).
- BOZORTH, R.M. "Ferromagnetism" Van Nostrand (1951).
- BOZORTH, R.M. "Magnetostriction and Anisotropy of Single Crystals of Hexagonal Cobalt" Phys. Rev. 96, 311 (1954).
- BRANSKY, J., HIRSCH, A.A. AND BRANSKY, I. "Use of a Commercial Electric Microbalance for Highly Sensitive Magnetic Torque Measurements" J. Sci. Instrum. 1, 790 (1968).
- BRENNER, R. "Remarks on Zener's Classical Theory of the Temperature Dependence of Magnetic Anisotropy Energy" Phys. Rev. 107, 1539 (1957).
- BROOKS, M.S.S. "Spin-Wave Theory of Magnetocrystalline Anisotropy in Terbium and Dysprosium" J. Phys. C 2, 1016 (1969).
- BROOKS, M.S.S. AND ENGAMI, T. "Theory of Highly Anisotropic Ferromagnets: I: Magnetic Anisotropy and Magnetostriction" J. Phys. C 6, 513 (1973 a).

- BROOKS, M.S.S. AND ENGAMI, T. "Theory of Highly Anisotropic Ferromagnets: II: Renormalisation of the Magnon Energies in the Heavy Rare-Earths" J. Phys. C 6, 3719 (1973 b).
- BROOKS, M.S.S. AND ENGAMI, T. "Theory of Highly Anisotropic Ferromagnets: III: Relationship between Microscopic and Macroscopic Anisotropy and Magnetostriction in HCP Ferromagnets" J. Phys. C 7, 979 (1974).
- BROOKS, M.S.S. AND GOODINGS, D.A. "Spin-Wave Theory of the Magnetocrystalline Anisotropy in Gadolinium Metal" J. Phys. C 1, 1279 (1968).
- BRUKHATOV, N.L. AND KIRENSKI, L.V. "Anisotropy of the Magnetic Energy in Single Crystals of Nickel as a Function of Temperature" Phys. Zeits. d. Sowjetunion 12.5, 602 (1937).
- BURD, J., HUQ, M. AND LEE, E.W. "The Determination of Magnetic Anisotropy Constants from Torque Curves" J. Mag. Mat. 5, 135 (1977).
- BYRNES, W.S. AND CRAWFORD, R.G. "Improved Torque Magnetometer" J. Appl. Phys. 29, 493 (1958).
- CALLEN, E.R. AND CALLEN, H.B. "Anisotropic Magnetisation" J. Phys. Chem. Solids 16, 310 (1960).
- CALLEN, E.R. AND CALLEN, H.B. "Magnetostriction, Forced Magnetostriction and Anomalous Thermal Expansion in Ferromagnets" Phys. Rev. 139, A455 (1965).
- CALLEN, H.B. AND CALLEN, E.R. "The Present Status of the Temperature Dependence of Magnetocrystalline Anisotropy, and the $L(L+1)/2$ Power Law" J. Phys. Chem. Solids 27, 1271 (1966).
- CALLEN, H.B. AND SHTRIKMAN, S. "A Probability Density Common to Molecular Field and Collective Excitation Theories of Ferromagnetism" Solid State Commun. 3, 5 (1965).
- CARR, W.J. "Theory of Ferromagnetic Anisotropy" Phys. Rev. 108, 1158 (1957).
- CARR, W.J. "Temperature Dependence of Ferromagnetic Anisotropy" J. Appl. Phys. 29, 436 (1958 a).

- CARR, W.J. "Temperature Dependence of Ferromagnetic Anisotropy" Phys. Rev. 109, 1971 (1958 b).
- CHARAP, S.H. "Anisotropy of the Intrinsic Domain Magnetisation of a Ferromagnet" Phys. Rev. 119, 1538 (1960).
- CHARAP, S.H. "Concerning the Theory of Anisotropic Magnetisation" J. Phys. Chem 20, 315 (1961).
- CHIKAZUMI, S. "Physics of Magnetism" Wiley, New York (1964).
- CHIKAZUMI, S., WAKIYAMA, T. AND YOSIDA, K. "Uniaxial Magnetic Anisotropy of Iron-Group Transition Metals and Alloys" Proc. Int. Conf. on Magnetism, Nottingham, pp. 756-759 (1964).
- CONDON, J.H. AND MARCUS, J.A. "Fermi Surface of Calcium by the de Haas-van Alphen Effect" Phys. Rev. 134, A446 (1964).
- COOPER, B.R. "Spin Waves and Magnetic Resonance in Rare-Earth Metals: Thermal, Applied-field and Magnetoelastic Effects" Phys. Rev. 169, 281 (1968).
- COOPER, B.R. "Magnetic Properties of Rare-Earth Metals" Solid State Physics 21, 393 (1968).
- COQBLIN, B. "The Electronic Structure of Rare-Earth Metals and Alloys: the Magnetic Heavy Rare-Earths" Academic Press, (1977).
- CORNER, W.D., ROE, W.C. AND TAYLOR, K.N.R. "The Magnetocrystalline Anisotropy of Gadolinium" Proc. Phys. Soc. 80, 927 (1962).
- CORNER, W.D. AND TANNER, B.K. "The Easy Direction of Magnetisation in Gadolinium" J. Phys. C 9, 627 (1976).
- CROFT, G.T., DONAHOE, F.J. AND LOVE, W.F. "Automatic Recording Torsional Magnetic Susceptibility Balance" Rev. Sci. Instrum. 26, 360 (1955).
- CRANGLE, J. "The Magnetic Properties of Solids" Edward Arnold, London (1977).
- CZOCHRALSKI, J. Z. Physik. Chem. 92, 219 (1918).
- DARBY, M.I. AND ISAAC, E.D. "Magnetocrystalline Anisotropy of Ferro- and Ferrimagnets" IEEE Trans. Magnetics MAG-10, 259 (1974).

- DARBY, M.I. AND TAYLOR, K.N.R. "Basal Plane Magnetocrystalline Anisotropy in Single Crystal Gadolinium" Proc. Int. Conf. on Magnetism, Nottingham, pp. 742-743 (1964).
- DeBOER, Von.H., HAARS, H., MICHAELIS, W. AND SCHLIMME, E. "Quadrant Electrometer for Measurement of Small Torsional Moments" *Feinwerk. und Messtech.* 88, 237 (1980).
- DEY, S.K. "An Electrostatic Torque Meter for Magnetic Film Measurements" *Jap. J. Appl. Phys.* 11, 1628 (1972).
- DIGGES, T.G., HOPKINS, R.H. AND SEIDENSTICKER, R.G. "The Basis of Automatic Diameter Control Utilising "Bright Ring" Meniscus Reflections" *J. Cryst. Growth* 29, 326 (1975).
- DIXON, J.M. "Lattice Sums and Ionic Enhancement Potentials in Metallic Hosts" *Phys. Letts.* 40A, 117 (1972).
- DOMNEY, K.E. "Computer Controlled Growth of Single Crystal Ingots" *Solid State Tech.* Oct. 1971, 41.
- DORING, W. "The Directional Dependence of Crystal Energy" *Ann. Physik, Series 7*, 1, 102 (1958).
- DROKIN, A.I. AND SLOBODOSKOI, L.I. "Concerning the Temperature Dependence of the Magnetic Anisotropy Constants of Ferromagnets and Ferrites" *Sov. Phys. JETP* 24, 682 (1967).
- DuPLESSIS, P.De.V. "Magnetic Anisotropy of Some Heavy Rare-Earth Metals" *Physica* 41, 379 (1969).
- EGAMI, T. "The Effect of Zero-Point Energy on the Magnetocrystalline Anisotropy of the Rare Earth Metals" *J. Phys. C* 5, L85 (1972).
- ELLIOT, J.F., LEGVOLD, S. AND SPEDDING, F.H. "Some Magnetic Properties of Gadolinium Metal" *Phys. Rev.* 91, 28 (1953).
- ESCUDIER, P. "Anisotropic Magnetisation: An Important Parameter in the Study of Magnetocrystalline Anisotropy" *Ann. Phys.* 9, 125 (1975).
- ELLIS, W.C. AND GREINER, E.S. "Metals Handbook" Cleveland Ohio: American Society for Metals, p. 1137 (1948).
- FÉRON, J.-L. "On the Magnetocrystalline Anisotropy of Terbium, Dysprosium and Holmium" *C. R. Acad. Sci., Ser. B.* 269, 611 (1969).

- FÉRON, J.-L., HUG, G. AND PAUTHENET, R. "Magnetocrystalline Properties of Single-Crystal Rare-Earths of the Second Series", "Les Elements de Terres Rares", Vol. II, C.N.R.S., pp. 19-30 (1970 a).
- FÉRON, J.-L., HUG, G. AND PAUTHENET, R. "Magnetic Properties of Several Rare-Earth Single Crystals" Z. Angew. Phys. 30, 61 (1970 b).
- FÉRON, J.-L. AND PAUTHENET, R. "Contribution to the Study of the Magnetic Properties of a Single Crystal of Gadolinium" C. R. Acad. Sci., Series B. 269, 549 (1969).
- FLETCHER, F.J., DeSA, A., O'REILLY, W. AND BANERJEE, S.K. "A Digital Vacuum Torque Magnetometer for the Temperature Range 300-1000K" J. Sci. Instrum. 2, 311 (1969).
- FRANSE, J.J.M. AND GERSDORF, R. "Magnetic Anisotropy of Gadolinium Metal at 4K under Pressure" Phys. Rev. Letts. 45, 51 (1980).
- FRANSE, J.J.M. AND MIHAI, V. "The Easy Direction of Magnetisation in Gadolinium as a Function of Pressure and Temperature" Physica 86B, 49 (1977).
- FULINSKI, W. AND GROTOWSKI, W. "Automatic Torque Meter" Pol. Tech. Rev. 4, 26 (1976).
- FUKUDA, T., WASHIZUKA, S., KOKOBUN, Y., USHIZAWA, J. AND WATANABE, M. "Growth of Large Diameter GaP Single Crystals by a Computer Controlled LEC Technique" Proc. of Ninth Int. Symp. on Gallium Arsenide and Related Compounds. p.43-46. I.O.P. Bristol (1982).
- GANS, R. AND CZERLINSKI, E. Schr. Konigsb. Gelehrt. Ges. Naturw. Kl. 9, 1 (1932).
- GARABEDIAN, F.G., KESTIGIAN, M., COHEN, M.L. AND Von THUNA, P.C. "Automatic Crystal Diameter Control System" Amer. Ceramic Soc. Bull. 55, 726 (1976).
- GARTNER, K.J., RITTINGHAUS, K.F. AND SEEGER, A. "An Electronic Device Including a TV System for Controlling the Crystal Diameter During Czochralski Growth" J. Cryst. Growth 13, 619 (1972).

- GENGNAGEL, H., DRESSEL, H., BAUMERT, W. AND SAUERTEIG, H. "A Recording Anisotropy Meter for High and Low Temperatures and its Applications" *Exp. Tech. der Physik* 11, 301 (1963).
- GERBER, R. AND VILIM, F. "An Automatic Compensated Torque Balance for the Measurement of Magnetic Anisotropy in the Broad Temperature Range from the Helium Temperature Upwards" *J. Phys. E* 1, 389 (1968).
- GORILETSKY, V.I., NEMENOV, V.A., PROTSENKO, V.G., RADKEVICH, A.V. AND EIDELMAN, L.G. "Automated Pulling of Large Alkali Halide Single Crystals" *J. Cryst. Growth* 52, 509 (1981).
- GRADMANN, U., KUMMERLE, W. AND THAM, R. "High Sensitivity Torsion Magnetometers for Oligatomic Films" *Appl. Phys.* 10, 219 (1976).
- GRAHAM, C.D. "Magnetocrystalline Anisotropy of Gadolinium" *J. Phys. Soc. Japan* 17, 1310 (1962).
- GRAHAM, C.D. "Some Magnetic Properties of Gd Single Crystals" *J. Appl. Phys.* 34, 1341 (1963).
- GRAHAM, C.D. "Basal-Plane Anisotropy of Gadolinium" *J. Appl. Phys.* 38, 1375 (1967).
- GRAHAM, C.D. AND LOMMEL, J.M. "Effect of Pressure During Evaporation on the Magnetic Properties of Nickel Films" *J. Phys. Soc. Japan* 17, Supp. B1. 571 (1962).
- GRIESSEN, R. "A Capacitance Torquemeter for de Haas-van Alphen measurements" *Cryogenics*, June 1973, 375.
- GROSS, U. AND KERSTEN, R. "Automatic Crystal Pulling with Optical Diameter Control Using a Laser Beam" *J. Cryst. Growth* 15, 85 (1972).
- HAKNER, R. *Phys. Rev.* 181, 1723 (1969).
- HARRISON, F.W. "Some Aspects in the Design of a Torque Magnetometer" *J. Sci. Instrum.* 33, 5 (1956).
- HAUSMANN, K. "The Validity of the Tenth Power Law of the Magnetic Crystal Energy" *Phys. Stat. Sol.* 38, 809 (1970).
- HAWKINS, R.D. "The Magnetocrystalline Anisotropy of Gadolinium/Terbium Alloys" Ph.D. Thesis. Durham University (1982).

- HEGLAND, D.E., LEGVOLD, S. AND SPEDDING, F.H. "Magnetisation and Electrical Resistivity of Terbium Single Crystals" *Phys. Rev.* 131, 158 (1963).
- HEISENBERG, W. "On the Theory of Ferromagnetism" *Z. Physik* 49, 619 (1928).
- HODGMAN, C.D. "Handbook of Chemistry and Physics" 38th Edn. Cleveland, Ohio: Chemical Rubber. (1957).
- HOFMANN, Von.U. "On the Extrapolation of Torque Curves to Infinite Field" *Exper. Tech. Phys.* 12, 417 (1964).
- HUMPHREY, F.B. AND JOHNSTON, A.R. "Sensitive Automatic Torque Balance for Thin Magnetic Films" *Rev. Sci. Instrum.* 34, 348 (1963).
- HURLE, D.T.J. "Control of Diameter in Czochralski and Related Crystal Growth Techniques" *J. Cryst. Growth* 42, 473 (1977).
- INGERSON, W.E. AND BECK, F.J. "Magnetic Anisotropy in Sheet Steel" *Rev. Sci. Instrum.* 9, 31 (1938).
- JAHN, L. AND MULLER, H.G. "The Coercivity of Hard Ferrite Single Crystals" *Phys. Stat. Sol.* 35, 723 (1969).
- JAYARAMAN, V. AND DUTTA-ROY, S.K. "A Torque Magnetometer for Thin Ferromagnetic Films" *Indian J. Pure and Appl. Phys.* 14, 762 (1976).
- JONES, D.W., FARRANT, S.P., FORT, D. AND JORDAN, R.G. "Mostly Metals, Sometimes Elements, Occasionally Crystals" *Inst. Phys. Conf. Ser. No. 37*, Chapter 2, pp. 11-22 (1978).
- JONES, F.J. AND TANNER, B.K. "A Double-Axis X-ray Diffractometer for Magnetostriction Measurements" *J. Phys. E* 13, 1183 (1980).
- JORAIDE, A.A. "Magnetostriction of Gadolinium/Terbium Alloys" Ph.D. Thesis, University of Durham (1980).
- JOZSEF, P. "Automatic Crystal Diameter Control" Report KFKI-79-32. Hungarian Acad. Sci. Budapest. (June 1979).
- KADENA, Y. "Temperature Dependence of Magnetocrystalline Anisotropy of Cobalt" *J. Sci. Hiroshima Univ., Ser AII*, 31, 21 (1967).

- KANOMATA, A. AND HIGUCHI, T. "On-Line Real-Time System Using a Microcomputer for Analysis of Magnetic Torque Curves" Trans. Inst. Electron. and Commun. Eng. Japan Sect. E. E59, 41 (1976).
- KANTOR, K., OZSGYANI, L., PIPO, M. AND RONAKY, J. "Measurement of the Relative Deflection of two Torsion Balances in the 10^{-9} Rad. Sensitivity Range" Acta Physica Acad. Sci. Hungaricae 32, 177 (1972).
- KASUYA, T. "A Theory of Metallic Ferro- and Antiferromagnetism on Zener's Model" Prog. Theor. Phys. (kyoto) 16, 45 (1956).
- KAYA, S. Tohoku Sci. Rep. 17, 1157 (1928).
- KAZAKOV, A.A. AND ROZHKINA, V.A. "Calculation of the High Temperature Dependence of Single-Ion Anisotropy Constants" Sov. Phys. Solid State 14, 1666 (1973).
- KEFFER, F. "Temperature Dependence of Ferromagnetic Anisotropy in Cubic Crystals" Phys. Rev. 100, 1692 (1955).
- KHAN, W.I. AND MELVILLE, D. "A Method of Determining the Third Order Anisotropy Constant K_3 for Uniaxial Ferromagnets: Application to $\text{Nd}_{0.37}\text{Sm}_{0.63}\text{Co}_5$ " J. Mag. Mag. Mat. 23, 117 (1981).
- KIM, K.M., KRAN, A. AND PAZ, O. "Technique for Monitoring Diameter Variation in Czochralski Growth" I.B.M. Tech. Disclosure Bull. 25, 298 (1982).
- KING, A.P., ROBINSIN, G., CUNDALL, J.A. AND HIGHT, M.J. "An Electrostatic Automatic Torque Magnetometer for Measuring the Properties of Magnetic Thin Films" J. Sci. Instrum. 41, 766 (1964).
- KITTEL, C. "Introduction to Solid State Physics 5th Edn." Wiley, New York (1976).
- KOBAYASHI, N. "Hydrodynamics in Czochralski Growth: Computer Analysis and Experiments" J. Cryst. Growth 52, 425 (1981).
- KOUVEL, J.S. AND GRAHAM, C.D. "On the Determination of Magnetocrystalline Anisotropy Constants from Torque Measurements" Proc. Conf. Mag. Mat., Boston, pp. 85-100 (1956).

- KOUVEL, J.S. AND GRAHAM, C.D. "On the Determination of Magnetocrystalline Anisotropy Constants from Torque Measurements" J. Appl. Phys. 28, 340 (1957).
- KOUVEL, J.S. AND HARTELIUS, C.C. "Effect of Hydrostatic Pressure on the Magnetocrystalline Anisotropy of Cobalt" J. Phys. Chem. Solids 25, 1357 (1964).
- KUNTSEVICH, S.P. AND PALEKHIN, V.P. "Strain-Gauge Anisometer for Measurement of the Energy Constants of Magnetic Crystallographic Anisotropy" Instr. and Exper. Tech. 16, 259 (1973).
- KYLE, T.R. AND ZYDZIK, G. "Automated Crystal Puller" Mat. Res. Bull. 8, 443 (1973).
- LANDAU, L. AND LIFSHITZ, E. "Theory of the Dispersion of Magnetic Permeability in Ferromagnetic Bodies" Phys. Zeits. d. Sowjetunion 82, 153 (1935).
- LARSEN, J.W. AND LIVESAY, B.R. "Automatic Torque Magnetometer for Vacuum-to-High-Pressure Hydrogen Environments" Rev. Sci. Instrum. 10, 1285 (1979).
- LAUDISE, R.A. "The Growth of Single Crystals" Prentice Hall, Electrical Engineering Series (1970).
- LAWTON, H. AND STEWART, K.H. "Magnetisation Curves for Ferromagnetic Single Crystals" Proc. Roy. Soc. A193, 72 (1948).
- LEVINSON, J. US Patent No 2908004 Oct 6th 1959.
- LEVITIN, R.Z., PEREKALINA, T.M., SHLYAKHINA, L.P., CHISTYAKOV, O.D. AND YAKOVENKO, V.L. "Nature of Magnetic Anisotropy of Dysprosium. Paramagnetic Susceptibility of Dysprosium-Gadolinium Alloys" Soviet Physics JETP 36, 742 (1973).
- LINDGARD, Per.A. "Theory of Rare-Earth Alloys" Phys. Rev. B 16, 2168 (1977).
- LINDGARD, Per.A. AND DANIELSEN, O.. "Theory of Magnetic Properties of Heavy Rare-Earth Metals: Temperature Dependence of Magnetisation, Anisotropy and Resonance" Phys. Rev. B 11, (1975).
- LIU, S.H. "Quasispin Model of Itinerant Magnetism" Phys. Rev. B 13, 3962 (1976).

- LORENZINI, R.E., NEFF, F.S. AND BLAIR, D.J. "An Overview of Silicon Crystal Growing Processes" Solid State Tech. Feb. 1974, 33.
- MARICK, L. "Variation of the Resistance and Structure of Cobalt with Temperature and a Discussion of its Photoelectric Effect" Phys. Rev. 49, 831 (1936).
- MASUMOTO, H., SAITO, H. AND KIKUCHI, M. Sci. Rep. RITU A19, 172 (1967).
- MAXIM, Gh. "A Sensitive Torque Magnetometer for the Measurement of Small Magnetic Anisotropies" J. Sci. Instrum. 2, 319 (1969).
- MASON, W.P. "Derivation of Magnetostriction and Anisotropic Energies for Hexagonal, Tetragonal and Orthorhombic Crystals" Phys. Rev. 96, 302 (1954).
- MATEIKA, D., FLISIKOWSKI, P., KOHLER, H. AND KILIAN, R. "Automatic Crystal Pulling Equipment for Czochralski Growth" J. Cryst. Growth 41, 262 (1977).
- McKEEHAN, L.W. Phys. Rev. 43, 1025 (1933).
- McKEEHAN, L.W. Phys. Rev. 52, 18 (1937).
- McMASTERS, O.D., HOLLAND, G.E. AND GSCHNEIDER, K.A. "Single Crystal Growth by the Horizontal Levitation Zone Melting Method" J. Cryst. Growth 43, 577 (1978).
- McEWAN, K.A. "Magnetic and Transport Properties of the Rare-Earths", Chapter 6 of "Handbook on the Physics and Chemistry of Rare-Earths", ed. Gschneider, K.A., Jr. and Eyring, L. North Holland (1978).
- McSKIMMIN, H.J. "Measurement of the Elastic Constants of Single Crystal Cobalt" J. Appl. Phys. 26, 406 (1955).
- METZ, E.P.A., MILLER, R.C. AND MAZELSKI, R. "A Technique for Pulling Single Crystals of Volatile Materials" J. Appl. Phys. 33, 2016 (1961).
- MIKAHEYEV, P.A., GOGOLEV, V.A., YEL'KIN, A.Ye. AND ZABELINA, I.A. "A Method of Measuring Torsion Angles" Optical Tech. 39, 447 (1972).
- MILLER, D.S. "A Recording Torque Magnetometer" Rev. Sci. Instrum. 21, 605 (1950).

- MITSEK, A.I. "Polymorphism and Magnetic Anisotropy in Cobalt and its Alloys" Zh. Tekh. Fiz. (USSR) 50, 2269 (1980).
- MORI, N., FUKUDA, Y. AND UKAI, T. "The Magnetocrystalline Anisotropy of Cobalt and its Alloys" J. Phys. Soc. Japan 37, 1263 (1974).
- MORRISH, A.H. "The Physical Principles of Magnetism" Wiley, New York (1965).
- MÜLLER, S., DUNNER, P. AND PRANGHE, N.S. Z. Angew. Phys. 22, 403 (1967).
- MYERS, H.P. AND SUCKSMITH, W. "The Spontaneous Magnetisation of Cobalt" Proc. Roy. Soc. A 207, 427 (1951).
- NÉEL, M.L. "The Laws of Magnetisation and of the Subdivision into Elementary Domains of a Single Crystal of Iron" J. de Phys. et le Rad. Ser. 7. 5, 241 (1944).
- NÉEL, L., PAUTHENET, R., RIMET, G. AND GIRON, V.S. "On the Laws of Magnetisation of Ferromagnetic Single Crystals and Polycrystals. Application to Uniaxial Compounds" J. Appl. Phys. Supplement to Vol. 31, 27S (1960).
- NEILSEN, M., BJERRUM MOLLER, H. AND MACKINTOSH, A.R. "Magnon Interactions in Terbium" J. Appl. Phys. 41, 1174 (1970).
- NEUBURGER, M.C. Z. Kristallogr. 93, 1 (1936).
- NEUGEBAUER, C.A. "Saturation Magnetisation of Nickel Films of Thickness Less Than 100\AA " Phys. Rev. 116, 1441 (1959).
- NIGH, H.E., LEGVOLD, S. AND SPEDDING, F.H. "Magnetisation and Electrical Resistivity of Gadolinium Single Crystals" Phys. Rev. 132, 1092 (1963).
- NIKITIN, S.A. AND ARUTYUNIAN, N.P. "Magnetic Anisotropy of Alloys of Terbium with Yttrium and Gadolinium" Sov. Phys. JETP 50, 962 (1979).
- NIKITIN, S.A., SHELUOKO, N.A., POSYADO, V.P. AND CHUPRIKOV, G.E. "Magnetic, Magnetoelastic and Electric Properties of Single Crystal Terbium-Gadolinium Alloys" Sov. Phys. JETP 46, 530 (1977).
- OFTE, D. "The Viscosities of Liquid Uranium, Gold and Lead" J. Nucl. Mat. 22, 28 (1967).

- O'KANE, D.F., KWAP, T.W., GULITZ, L. AND BEDNOWITZ, A.L. "Infra-Red TV System of Computer Controlled Czochralski Crystal Growth" J. Cryst. Growth 13, 624 (1972).
- OKKERSE, B. "A Method of Growing Dislocation-Free Germanium Crystals" Phillips Tech. Rev. 21, 340 (1959).
- ONO, F. "Magnetic Field Dependence of the Magnetocrystalline Anisotropy Energy in HCP Co" J. Phys. Soc. Japan 50, 2564 (1981).
- ONO, F. AND YAMADA, O. "Temperature Dependence of the Uniaxial Magnetocrystalline Anisotropy Energy of Co" J. Phys. Soc. Japan 46, 462 (1979).
- OSBORNE, J.A. "Demagnetising Factors of the General Ellipsoid" Phys. Rev. 67, 351 (1945).
- OWEN, E.A. AND MADOC-JONES, D. "Effect of Grain Size on the Crystal Structure of Cobalt" Proc. Phys. Soc. B67, 456 (1954).
- PAIGE, D.M. AND TANNER, B.K. "A Robust Inexpensive Torque Magnetometer with On-Line Data Analysis" J. Phys. E 15, 128 (1982).
- PATZNER, E.J., DESSAUER, R.G. AND POPONIAK, M.R. "Automatic Diameter Control of Czochralski Crystals" SCP and Solid State Tech. Oct.1967, 25.
- PALMER, S.B., LEE, E.W. AND ISLAM, M.N. "The Elastic Constants Gd, Tb and Eb" Proc. Roy. Soc. A 338, 341 (1974).
- PEARSON, R.F. "The Magnetocrystalline Anisotropy of Gallium and Aluminium Substituted Magnetite" J. de Phys. et le Rad. 20, 409 (1959).
- PEARSON, R.F. "Magnetic Anisotropy", Chapter 3 of "Experimental Magnetism", Vol. 1, ed. Kalvius, G.M. and Tebble, R.S., Wiley (1979).
- PENOYER, R.F. "Automatic Torque Balance for Magnetic Anisotropy Measurements" Rev. Sci. Instrum. 30, 711 (1959).
- PHILLIPS, J.H. AND SHEPHERD, R.G. "The Analysis of Torque Measurements Made with a Torque Magnetometer on Ferromagnetic Single-Crystal Specimens with Low Magnetocrystalline Anisotropy" J. Phys. D 3, 721 (1970).
- PEARSUN, R.F. Mullard Res. Lab. Rep. No 2159 (1956).

- PIKIN, S.A. "Temperature Dependence of the Anisotropy Energy in a Ferromagnet" Sov. Phys. Solid State 10, 1368 (1968).
- POLIVANOV, K.M. AND KALUGIN, Ye.I. "Torque Curves in the Presence of Uniaxial Ferromagnetic Anisotropy" Sov. Phys. Phys. Met. Metall. 26, 31 (1968).
- PRUETT, H.D. AND LIEN, S.Y. "X-Ray Imaging Technique for Observing Liquid Encapsulation Czochralski Crystal Growth" J. Electrochem. Soc. June 1974, 822.
- QUENISSET, J.M., LESTIENNE, B., LAUNAY, J.C. AND NASLAIN, R. "Floating-Zone Melting with Viscous Torque Control" J. Phys. E 13, 771 (1980).
- QUENISSET, J.M., NASLAIN, R. AND HAGENMULLER, P. German Patent DT 2537048 A1 (1972).
- REINERT, R.C. AND YATSKO, M.A. "Crystal Weighing Mechanism for Growth Monitoring of Czochralski Grown Crystals" J. Cryst. Growth 21, 283 (1974).
- RHYNE, J.J. AND CLARK, A.E. "Magnetic Anisotropy of Terbium and Dysprosium" J. Appl. Phys. 38, 1379 (1967).
- RHYNE, J.J., FONER, S., McNIFF, E.J. AND DOCCLO, R. "Rare Earth Metal Single Crystals. I. High Field Properties of Dy, Er, Ho, Tb and Gd" J. Appl. Phys. 39, 892 (1968).
- RHYNE, J.J. AND MCGUIRE, T.R. "Magnetism of Rare-Earth Elements, Alloys and Compounds" IEEE Trans. Magnetics MAG-8, 105 (1972).
- RODE, V.E. AND HERRMANN, R. "Investigation of the Magnetisation of Iron, Cobalt and Nickel at Low Temperatures" Sov. Phys. JETP 19, 1081 (1964).
- RODRIGUES, A.R.D. AND SIDDON, D.P. "Inexpensive Computer-Controlled Experimentation" J. Phys. E 12, 402 (1979).
- ROE, W.C. Ph.D. Thesis, Durham University (1961).
- ROELAND, L.W., COCK, G.J. AND LINDGARD, Per.A. "High Field Magnetisation of Tb Single Crystals" J. Phys. C 8, 3427 (1975).
- REBOUILLAT, J.P. Ph.D. Thesis, Grenoble (1972).

RUDERMAN, M.A. AND KITTEL, C. "Indirect Exchange Coupling of Nuclear Magnetic Moments by Conduction Electrons" Phys. Rev. 96, 99 (1954).

RUMMEL, T. "Apparatus for Pulling Rod-Shaped Crystals of Semiconductor Materials from a Melt in a Crucible" US Patent No 3259467, July 6th 1966.

SATO, H. AND CHANDRASEKHAR, B.S. "Determination of the Magnetic Anisotropy Constant K_2 of Cubic Ferromagnetic Substances" J. Phys. Chem. Solids 1, 228 (1957).

SATO, M. AND TINO, M. "Variation of the Magnetic Anisotropy Energy of Nickel and Ni-Cu Alloys as a Function of Temperature" J. de Phys. et le Rad. 17, 5 (1956).

SATO, T., INUI, J. AND IWAMOTO, H. "Automatic Control System for Czochralski Growth of Large Diameter LiNbO_3 Crystals" Fujitsu Sci. and Tech. J. 12, 93 (1976).

SCHEEL, H.J. AND MULLER-KRUMBHAR, H. "Crystal Pulling Using ACRT" J. Cryst. Growth 49, 291 (1980).

SCHELLENG, J.H. AND RADO, G.T. "Direct Measurements of Anisotropy Energy and Anisotropic Magnetisation in Gallium Iron Oxide" Phys. Rev. 179, 541 (1969).

SEKITO, S. Sci. Rep. Tohoku Univ. 16, 545 (1927).

SEVAST'YANOV Instr. Exp. Tech. 5, 829 (1960).

SHEPHERD, C.H. "Measurements of the Magnetocrystalline Anisotropy Energy of Nickel and Terbium at Low Temperatures" Ph.D. Thesis, University of Salford (1976).

SIEVERT, J.D. AND VOIGT, C. "Influence of Domains on the Magnetic Torque in Cubic Single Crystals" Phys. Stat. Sol. A 37, 205 (1976).

SIEVERT, J.D. AND ZEHLER, V. "On the Measurement of the Magnetic Anisotropy of Cobalt" Z. Angew. Physik 30, 251 (1970).

SMITH, R.L. "Magnetic Anisotropy and Domain Structure in Gadolinium" Ph.D. Thesis, University of Durham (1978).

- SMITH, R.L., CORNER, W.D., TANNER, B.K., JORDAN, R.G. AND JONES, D.W. "The Magnetocrystalline Anisotropy of High-Quality Single-Crystal Gadolinium" Inst. Phys. Conf. Ser. No 37, Chapter 8, pp. 215-221 (1978).
- SMITH, R.L., TANNER, B.K. AND CORNER, W.D. "The Effect of Non-Magnetic Inclusions on the Easy Direction of Gadolinium" J. Phys. F 7, L229-L232 (1977).
- SPLITTGERBER, A.G. AND GILL, S.J. "A Torsion Balance for Magnetic Susceptibility Measurements on Fluids" Rev. Sci. Instrum. 42, 110 (1971).
- STACEY, F.D. "Magnetic Anisotropy of Dispersed Powders" Aust. J. Phys. 13, 196 (1960).
- STEVENS, K.W.H. "Matrix Elements and Operator Equivalents Connected with the Magnetic Properties of Rare-Earth Ions" Proc. Phys. Soc. A 65, 209 (1952).
- STEINBRUEGGE, K.B., HENNINGSEN, T., HOPKINS, R.H., MAZELSKY, R., MELAMED, N.T., RIEDEL, E.P. AND ROLAND, G.W. "Laser Properties of Nd^{+3} and Ho^{+3} Doped Crystals with the Apatite Structure" Appl. Optics 11, 999 (1972).
- STOCKBARGER, D.C. "The Production of Large Single Crystals of Lithium Fluoride" Rev. Sci. Instrum. 7, 137 (1936).
- STUT, H. German Patent DE 2113720 B2 Sept. 28th 1972.
- SUCKSMITH, W. AND THOMPSON, J.E. "The Magnetic Anisotropy of Cobalt" Proc. Roy. Soc. A 225, 362 (1954).
- SUREK, T., CORIELL, S.R. AND CHALMERS, B. "The Growth of Shaped Crystals from the Melt" J. Cryst. Growth 50, 21 (1980).
- SZPUNAR, B. "Magnetic Anisotropy of $SmCo_5$ - A Case of Strong J-Mixing" Acta Physica Polonica A60, 791 (1981).
- SZPUNAR, B. "The Temperature Dependence of the Anisotropy Constants of Cobalt" To be published (1983).
- SZPUNAR, B. AND LINDGARD, Per.A. "On the Origin of the Large Magnetic Anisotropy of Rare Earth - Cobalt Compounds" J. Phys. F 9, L55-L59 (1979).

- TAJIMA, K. "Magnetocrystalline Anisotropy of Rare Earth Impurities Doped in Gadolinium. I. Heavy Rare Earths" J. Phys. Soc. Japan 31, 441 (1971).
- TAJIMA, K. AND CHIKAZUMI, S. "Conventional Torque Magnetometer for Measuring a Large Magnetic Anisotropy" Jap. J. Appl. Phys. 6, 897 (1967 a).
- TAJIMA, K. AND CHIKAZUMI, S. "Magnetocrystalline Anisotropy of Gd-Tb and Gd-Dy Alloys" J. Phys. Soc. Japan 23, 1175 (1967 b).
- TAKAHASHI, M., KADWAKI, S., WAKIYAMA, T., ANAYAMA, T. AND TAKAHASHI, M. "Magnetocrystalline Anisotropy of Co and Co-Ni Alloys" J. Phys. Soc. Japan 44, 825 (1978).
- TAKAHASHI, M. AND SUZUKI, T. "Temperature Dependence of Magnetic Domain Structures in HCP Cobalt Single Crystals" Jap. J. Appl. Phys. 18, 1071 (1979).
- TANNER, B.K. "Dislocation-Free Silver Single Crystals Grown by the Czochralski Method" Z. Naturforsch 28a, 676 (1973).
- TARASOV, L.P. "Dependence of Ferromagnetic Anisotropy on the Field Strength" Phys. Rev. 56, 1224 (1939).
- TARASOV, L.P. AND BITTER, F. "Precise Magnetic Torque Measurements on Single Crystals of Iron" Phys. Rev. 52, 353 (1937).
- TAYLOR, A. J. Inst. Met. 77, 585 (1950).
- TAYLOR, K.N.R. AND DARBY, M.I. "Physics of Rare Earth Solids" Chapman and Hall, London (1972).
- TEAL, G.K. AND LITTLE, J.B. "Growth of Germanium single Crystals" Phys. Rev. 78, 647 (1950).
- TELESNIN, R.V., RYBAK, E.N. AND SARAEVA, I.M. "A Vacuum Magnetometer for Studying Ferromagnetic Films" Prib. I Tekh. Exper. 3, 719 (1965).
- Thermophysical Properties of Matter. Ed. Touloukian, Y.S. Vol. 12, p.70. Plenum, New York (1975).
- TIMAN, B.L. AND BURACHAS, S.F. "Growing Crystals of Constant Diameter by Controlling the Melt Level" Sov. Phys. Crystallogr. 26, 506 (1981).
- TSUKIJI, N. J. Sci. Hiroshima Univ. 33, 23 (1969).

TOHYAMA, K. AND CHIKAZUMI, S. "Magnetocrystalline Anisotropy of Gadolinium-Yttrium Alloys" J. Phys. Soc. Japan 35, 47 (1973).

TRAUBLE, H., BOSER, O., KRONMULLER, H. AND SEEGER, A. "Ferromagnetic Anisotropy in Hexagonal Cobalt Single Crystal" Phys. Stat. Sol. 10, 283 (1965).

TUROV, E.A. AND MITSEK, A.I. "On the Theory of the Temperature Dependence of Ferromagnetic Anisotropy" Sov. Phys. JETP 37, 801 (1960).

TUROVSKII, B.M., SHENDEROVICH, I.L. AND SHUBSKII, G.I. "Growing Single Crystals of Si by the Czochralski Method with Automatic Diameter Control" Inorganic Materials 13, 948 (1977).

TYLER, F. "The Magnetisation Temperature Curves of Iron, Cobalt and Nickel" Phil. Mag. 11, 596 (1931).

VALENTINO, A.J. AND BRANDLE, C.D. "Diameter Control of Czochralski Grown Crystals" J. Cryst. Growth 26, 1 (1974).

Van DIJK, H.J.A., GOORISSEN, J., GROSS, U., KERSTEN, R. AND PISTORIUS, J. "Crystal Diameter Control in Czochralski Growth" Acta Electronica 17, 45 (1974).

Van DIJK, H.J.A., JOCHEM, C.M.G., SCHOLL, G.J. AND Van Der WERF, P. "Diameter Control of LEC Grown GaP Crystals" J. Cryst. Growth 21, 310 (1974).

Van VLECK, J.H. "On the Anisotropy of Cubic Ferromagnetic Materials" Phys. Rev. 52, 1178 (1937).

VANDERKOOY, J. "A Torque Magnetometer for Use in Superconducting Magnets" J. Sci. Instrum. 2, 718 (1969).

VERGE, C., ALTOUNIAN, Z. AND DATARS, W.R. "An Induced Torque Magnetometer" J. Phys. E 10, 16 (1977).

VERHOEVEN, J.D. "Electrotransport as a Means of Purifying Metals" J. Metals 18, 26 (1966).

VOIGT, C. AND FONER, S. "A Simple Compensating Torquemeter for Use in High Field Solenoids" J. Phys. E 5, 126 (1972).

VOIGT, C. AND PELSTER, H.-H. "Torque Curves in the Presence of Domains" Phys. Stat. Sol. A 17, K97 (1973).

- VOJDANI, S., DABIRI, A.E. AND ASHOORI, H. "Diameter of Pulled Germanium Crystals by Means of Peltier Cooling" *J. Cryst. Growth* 24/25, 374 (1974).
- VOLKOV, V.M., KUSTOV, E.F., MAKIETOV, T.K. AND STECZKO, G. "Energy of Magnetic Anisotropy and Reduction Symmetry of Crystals" *Phys. Stat. Sol. B* 104, 649 (1981).
- WAGNER, R.F. AND STANFORD, J.L. "Observation of Magnetoelastic Effects in Terbium Metal by Ferromagnetic Resonance at $\lambda = 2.5 - 3\text{mm}$ " *Phys. Rev.* 184, 505 (1969).
- WARNOCK, R.F. "A Torque Magnetometer Using Strain Gauges as Transducers" M.Sc. Thesis, University of Durham (1975).
- WEISS, P. "Hypothesis of the Molecular Field" *J. de Phys.* 6, 661 (1907).
- WEISS, P. *J. de Phys.* 4, 469 (1905).
-
- WELFORD, J. "The Magnetocrystalline Anisotropy of Dysprosium and Terbium-Scandium Alloys" Ph.D. Thesis, University of Durham (1974).
- WENZL, H., FATTAH, A., GUSTIN, D., MIHELICIC, M. AND UELHOFF, W. "Measurements of the Contact Angle Between Melt and Crystal During Czochralski Growth of Gallium and Germanium" *J. Cryst. Growth* 43, 607 (1978).
- WESTWOOD, W.D., BRIDGER, B. AND MURRAY, E.L. "A Torque Magnetometer with a Permanently Mounted Calibration Coil" *J. Phys. E* 3, 962 (1970).
- WHITE, G.K. "Thermal Expansion of Magnetic Metals at Low Temperatures" *Proc. Phys. Soc.* 86, 159 (1965).
- WILLEY, R.J., LANFEAR, A.R. AND LEAK, D.A. "A Simple Sensitive Torque Magnetometer" *J. Phys. E* 5, 305 (1972).
- WILLIAMS, H.J. "Some Uses of the Torque Magnetometer" *Rev. Sci. Instrum.* 8, 56 (1937).
- WILSON, D., HERON, K., de SA, A. AND O'REILLY, W. "An Automatic Rotating-Head Torque Magnetometer" *J. Phys. E* 10, 1214 (1977).

- WOLF, W.P. "Effect of Crystalline Electric Fields on Ferromagnetic Anisotropy" Phys. Rev. 108, 1152 (1957).
- WYCKOFF, R.W.G. "The Structure of Crystals" Chemical Catalog Co., Inc.: New York, p. 204 (1931).
- YAMAGUCHI, S. "Magnetic Anisotropy of Cobalt as Revealed by Electron Diffraction" J. Appl. Phys. 32, 961 (1961).
- YANG, T.T. "Anisotropy Constants of Gadolinium and Cobalt" Jap. J. Appl. Phys. 15, 279 (1976).
- YANG, T.T., YANG, J.J. AND ROBINSON, L.B. "Temperature Dependence of Ferromagnetic Anisotropy Energy in Cubic Crystals" Solid State Commun. 13, 53 (1973).
- YOSIDA, K. "Magnetic Properties of Cu-Mn Alloys" Phys. Rev. 106, 893 (1957).
- ZASIMCHUK, I.K., FOMIN, A.V. AND OVSIENKO, D.E. "Role of Thermal Stresses in the Formation of Dislocations During Growth from the Melt of Copper Single Crystals" Sov. Phys. Dokl. 24, 55 (1979).
- ZENER, C. "Classical Theory of the Temperature Dependence of Magnetic Anisotropy Energy" Phys. Rev. 96, 1335 (1954).
- ZIJLSTRA, H. "Experimental Methods in Magnetism" Vol. IX of "Selected Topics in Solid State Physics" Ed. Wohlfarth, E.P., North Holland, Amsterdam (1967).
- ZINNES, A.E., NEVIS, B.E. AND BRANDLE, C.D. "Automatic Diameter Control of Czochralski Grown Crystals" J. Cryst. Growth 19, 187 (1973).